REPORT UAG - 55

WORLD DATA CENTER A
for
Solar-Terrestrial Physics

EQUIVALENT IONSPHERIC CURRENT REPRESENTATIONS BY A NEW METHOD, ILLUSTRATED FOR 8-9 NOVEMBER 1969 MAGNETIC DISTURBANCES

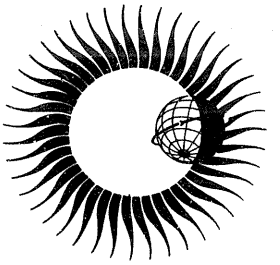

April 1976

WORLD DATA CENTER A

National Academy of Sciences
2101 Constitution Avenue, N. W.
Washington, D. C., U.S.A., 20418

World Data Center A consists of the Coordination Office and seven Subcenters:

World Data Center A
Coordination Office
National Academy of Sciences
2101 Constitution Avenue, N. W.
Washington, D. C., U.S.A. 20418
[Telephone: (202) 389-6478]

Glaciology:

World Data Center A:
Glaciology
U.S. Geological Survey
1305 Tacoma Avenue South
Tacoma, Washington, U.S.A. 98402
[Telephone: (206) 593-6506]

Meteorology (and Nuclear Radiation):

World Data Center A:
Meteorology
National Climatic Center
Federal Building
Asheville, North Carolina, U.S.A. 28801
[Telephone: (704) 258-2850]

Oceanography:

World Data Center A:
Oceanography
National Oceanic and Atmospheric Administration
Washington, D. C., U.S.A. 20235
[Telephone: (202) 634-7249]

Rockets and Satellites:

World Data Center A:
Rockets and Satellites
Goddard Space Flight Center
Code 601
Greenbelt, Maryland, U.S.A. 20771
[Telephone: (301) 982-6695]

Rotation of the Earth:

World Data Center A:
Rotation of the Earth
U.S. Naval Observatory
Washington, D. C., U.S.A. 20390
[Telephone: (202) 254-4023]

Solar-Terrestrial Physics (Solar and Interplanetary Phenomena, Ionospheric Phenomena, Flare-Associated Events, Geomagnetic Variations, Magnetospheric and Interplanetary Magnetic Phenomena, Aurora, Cosmic Rays, Airglow):

World Data Center A
for Solar-Terrestrial Physics
Environmental Data Service, NOAA
Boulder, Colorado, U.S.A. 80302
[Telephone: (303) 499-1000, Ext. 6467]

Solid-Earth Geophysics (Seismology, Tsunamis, Gravimetry, Earth Tides, Recent Movements of the Earth's Crust, Magnetic Measurements, Paleomagnetism and Archeomagnetism, Volcanology, Geothermics):

World Data Center A
for Solid-Earth Geophysics
Environmental Data Service, NOAA
Boulder, Colorado, U.S.A. 83002
[Telephone: (303) 499-1000, Ext. 6521]

Notes:

(1) World Data Centers conduct international exchange of geophysical observations in accordance with the principles set forth by the International Council of Scientific Unions. WDC-A is established in the United States under the auspices of the National Academy of Sciences.

(2) Communications regarding data interchange matters in general and World Data Center A as a whole should be addressed to: World Data Center A, Coordination Office (see address above).

(3) Inquiries and communications concerning data in specific disciplines should be addressed to the appropriate subcenter listed above.

WORLD DATA CENTER A
for
Solar-Terrestrial Physics

REPORT UAG - 55

EQUIVALENT IONSPHERIC CURRENT REPRESENTATIONS BY A NEW METHOD, ILLUSTRATED FOR 8-9 NOVEMBER 1969 MAGNETIC DISTURBANCES

by

Y. Kamide, H. W. Kroehl, M. Kanamitsu, J. H. Allen,
and S. I. Akasofu

April 1976

Published by World Data Center A for
Solar-Terrestrial Physics, NOAA, Boulder, Colorado
and printed by
U.S. DEPARTMENT OF COMMERCE
NATIONAL OCEANIC AND ATMOSPHERIC ADMINISTRATION
ENVIRONMENTAL DATA SERVICE
Asheville, North Carolina, USA 28801

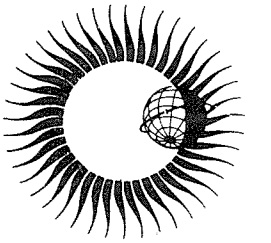

SUBSCRIPTION PRICE: $25.20 a year; $12.00 additional for foreign mailing; single copy price varies.* Checks and money orders should be made payable to the Department of Commerce, NOAA. Remittance and correspondence regarding subscriptions should be sent to the National Climatic Center, Federal Building, Asheville, NC 28801, Attn: Publications.

*PRICE THIS ISSUE $1.60

TABLE OF CONTENTS

EQUIVALENT IONOSPHERIC CURRENT REPRESENTATIONS BY A NEW METHOD

ILLUSTRATED FOR 8-9 NOVEMBER 1969 MAGNETIC DISTURBANCES

by

Y. Kamide[1,2,3], H. W. Kroehl[3], M. Kanamitsu[4],
J. H. Allen[3], and S. -I. Akasofu[2]

PART 1

I. Introduction

This report illustrates a data set of worldwide potential contours for ground magnetic perturbations resulting from a new method described by Kamide *et al.* [1976]. Part 1 contains brief comments on other methods of representing magnetic activity and a discussion of the new method. In Part 2 are plots at 10-minute intervals of magnetic perturbation vectors from 82 northern hemisphere observatories and the corresponding potential contours. Also given are AU and AL index graphs for the 36-hour interval from 1200 UT November 8 to 2400 UT November 9, 1969. Appendices describe in detail the procedures used to determine a potential field from ground magnetic perturbations.

II. Other Methods of Representing Magnetic Activity

Several methods of representing global or regional geomagnetic activity are presently used such as geomagnetic activity indices, spherical harmonic analysis, perturbation vector plots, and equivalent current approximations by equipotential contours.

By design geomagnetic activity indices represent global activity for particular latitudinal regions. This activity in each region may be the result of the same or different ionospheric, magnetospheric or other current systems. For reviews of indices see Lincoln [1967], Siebert [1971], Rostoker [1972], and Allen and Kroehl [1975]. Spherical harmonic analysis is used to define patterns of relatively slowly-varying, symmetric global currents, i.e., Sq-type, where lower harmonics are sufficient [Matsushita and Maeda, 1965]. Appendix 1 discusses spherical harmonic analysis as applied to disturbed conditions.

From vector plots of magnetic perturbations at many locations, hand-drawn equivalent ionospheric current systems are produced (equi-potential contours) which are time consuming and subjective. Equipotential contours were computer generated by Bostrom [1971] for magnetically disturbed times at higher latitudes, but due to the uneven observatory distribution, the resultant contours were somewhat irregular. Each of these methods has inherent limitations which prevent them from accurately describing the intensity and global pattern of magnetic activity for an extended, disturbed time.

III. New Method of Deriving Equipotential Contours

Previous efforts to derive the potential, Φ, from the observed ground magnetic perturbation field were based on solving the three dimensional Laplace's equation in terms of spherical harmonic functions. This new method, developed by Kamide *et al.* [1976], solves the two-dimensional Poisson's equation rewritten as:

$$\sigma = \frac{1}{a^2\sin\theta}\frac{\partial}{\partial\theta}\left(\sin\theta\,\frac{\partial\Phi}{\partial\theta}\right) + \frac{1}{a^2\sin^2\theta}\,\frac{\partial^2\Phi}{\partial\lambda^2} = -\frac{\partial H_\theta \sin\theta}{a\sin\theta\,\partial\theta} - \frac{\partial H_\lambda}{a\sin\theta\,\partial\lambda}. \qquad (1)$$

where θ and λ are geomagnetic colatitude and longitude, H_θ and H_λ are components of the magnetic perturbation and a is the earth's radius. See Appendix 1 for a detailed discussion of this method of potential derivation and related equivalent ionospheric currents. The selection of a suitable grid and proper boundary conditions, the use of observed magnetic variations, and equation (1) are sufficient to determine the potential Φ.

A summary diagram outlining the steps from interval selection through final production of a film of equipotential contour plots is given in Figure 1. The practical procedures for each step once an interval is selected for study are:

(1) Digitization relative to a quiet-time curve of the H and D (X and Y) components from magnetograms from each observatory.

(2) Transformation of these values into geomagnetic north, Xm, and geomagnetic east, Ym, components.

1 CIRES, University of Colorado, Boulder, Colorado
2 Geophysical Institute, University of Alaska, Fairbanks, Alaska
3 Data Studies Division, NOAA/EDS/NGSDC, Boulder, Colorado
4 Advanced Study Program, National Center for Atmospheric Research, Boulder, Colorado

(3a) Interpolation from the observed values at a regular network of grid points assuming the contribution of each of the three nearest observatories is inversely proportional to the distance between the observatory and the grid point. The interpolation formula used is given in Appendix 2.

It has been suggested that the condition, curl $\underline{H}$ = 0, be satisfied in each calculation of the grid point values [Stone, 1969]. However, we correct our $\underline{H}$ values by requiring curl $\underline{H}$ = 0 on a global scale in the next step.

(3b) AU and AL (AE) indices and graphs derived from 12 auroral zone sets of Xm values.

(4) Computation of the magnetic potential at each grid point, representing the associated current system in a thin spherical shell (the ionosphere): This process involves the determination of the best potential field Φ from the interpolated values of $\underline{H}$ (Xm, Ym) perturbations by solving the two-dimensional Poisson's equation (see Appendix 1).

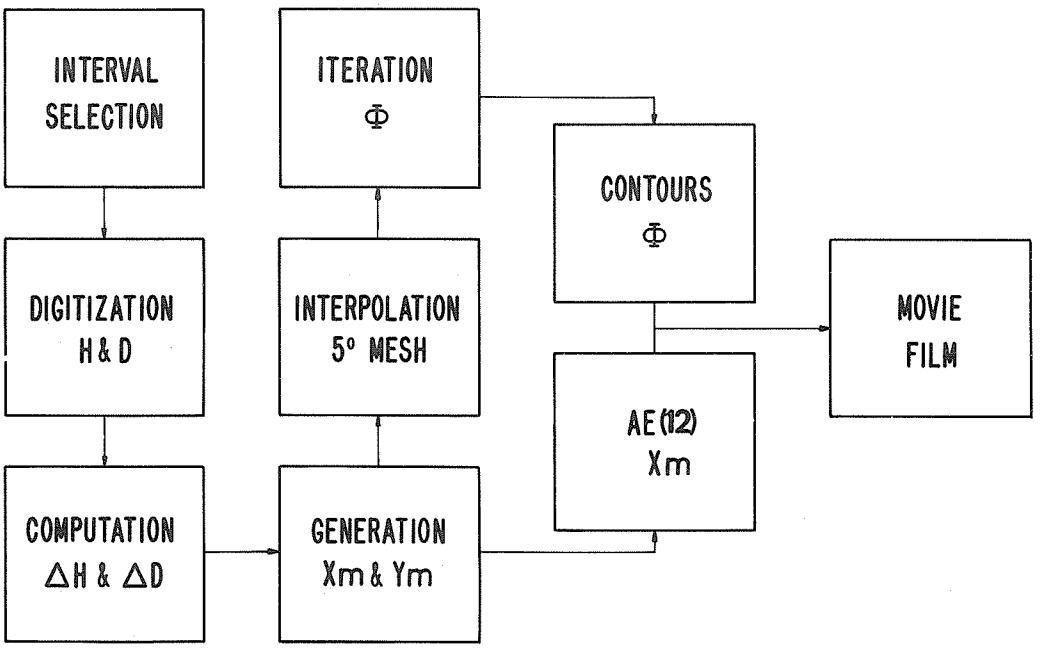

Fig. 1. Flow chart describing the important steps in making the magnetic potential contours.

Our solution used the accelerated Liebmann over-relaxation method of iteration, which is frequently used by meteorologists in dynamic wind analysis. Despite the relatively large number of iteration steps (approximately 250), the over-relaxation method is best adapted to solving elliptic partial differential equations because of simple numerical procedures and less restrictive boundary conditions. For detailed discussion on the boundary conditions and the iteration method, see Appendices 3 and 4.

(5) Plot of equipotential contour lines.

(6) AU and AL index graphs combined with the potential plots and printed on 16 mm cine film.

IV. Discussion of the New Method

Evaluation of the worldwide potential distribution based on vectors of magnetic field perturbations at a worldwide set of observatories is possible by several methods. However, each requires a considerable amount of numerical calculation. Efforts have been directed toward representing the mean Sq field whose pattern is less complicated than the substorm field. Potential for substorm fields have only been obtained for a few epochs including a limited number of substorms, and for strictly limited regions of either high or low latitudes. To do this for all latitudes and over an expanded interval it was necessary to design new comprehensive computer programs.

By our new method, one can produce worldwide potential contours (equivalent ionospheric current systems) from ground magnetic perturbations for any practical time interval. Three major advantages in developing this computer mapping of the potential plots are:

(1) The plot more accurately represents the global extent of geomagnetic activity than do

geomagnetic activity indices. From the plot, we can easily recognize both the global pattern and the intensity of the magnetic perturbations. However, each geomagnetic index is designed to give only the intensity for a specific latitudinal band. As many studies have shown, the space-time distribution of ground magnetic perturbations, especially during the polar magnetic substorm, is so complex that it is impossible to accurately represent it by a single scalar index. Also, most indices are derived from data of a limited observatory network in order to expedite the availability of the index, while the generation of the potential contour plot requires a comprehensive observatory network.

(2) Computer programs plot the worldwide potential contours under consistent assumptions without subjective prejudices.

(3) It is possible to produce successive contours to examine how the disturbance pattern changes before, during, and after different polar magnetic substorms.

In the derivation of magnetic potentials there are both physical and numerical problems. One physical problem is the need to establish a reference level from which the magnetic deviation can be determined. In our examples we used the quiet day curve as the reference level since it was our purpose to calculate the magnetic potential for the substorms. Another is that the actual current system we are attempting to represent does not flow entirely in a thin spherical shell. We are limited to representing as an equivalent ionospheric current system the actual three-dimensional current system producing the magnetic perturbation. Note that in principle it is impossible to infer uniquely the distribution of the external current systems solely from magnetic observations made at the earth's surface. Finally, only data from the northern hemisphere was used due to the uneven distribution and small number of southern hemisphere magnetic observatories. In this sense our results are hemispheric rather than global.

Five important numerical problems in the derivation of the magnetic potential which should be mentioned are:

(1) There may be recording, processing and calibrating errors in the instruments measuring the magnetic field at each observatory. We assume these to be negligible.

(2) Errors may result from the microfilming and subsequent reproduction of the magnetograms due to lenticular distortion. This will affect the timing of a digitized value more than its amplitude. However, if the field is rapidly changing, i.e., the intensity gradient is large, then any timing error can result in a large amplitude error in the value assigned to that time. We have attempted to minimize this problem and consider each value's assigned time to be within three minutes of its actual time.

(3) The largest potential source of numerical error is the linear interpolation of observatory perturbation values to obtain the vector components at each grid point. The interpolation formula uses (Xm, Ym) from the three nearest observatories and calculates the grid point values assuming each observatory's contribution is inversely proportional to its distance from the grid point. For example, in a large area where there are no magnetic observatories, it is impossible to assign a sharp boundary to the auroral electrojets. Conversely, in an area where there are many observatories near a grid point, the interpolation process acts to average the data. The obtained potential distribution cannot exactly reproduce the observed magnetic perturbation, especially if the grid size is larger than the distance between the observatories.

(4) We calculated the forcing term σ of a Poisson's equation (1) using the spatial change in the magnetic components of the perturbation field, see equation A4-2, p. 17, instead of the exact partial solution. This assumption can be another potential source of error.

(5) Errors are generated during the iteration process of the potential calculation. We set the convergence criterion δ to be 10^3 γ·km, which is only 1 to 2% of the contour interval. These errors can be minimized by choosing a smaller value for δ (see Appendix 4). However, by decreasing the convergence criterion (in turn, increasing the number of iteration steps), the accumulated computer error during iteration becomes larger.

Considering all these error sources, it is necessary to compare calculated magnetic field perturbations (from the calculated potential distribution) with the original value at each observatory to determine how accurately the calculated potential can reproduce the observed values. Table 1 shows one comparison for the maximum phase of a substorm (1252 UT, January 12, 1973). The values agree reasonably well, except in and near the region of larger intensity gradients. A better match could be obtained by using a smaller grid size. For such a comparison, the calculated observatory value includes the inherent errors from interpolating and differentiating from the potentials at the grid points. These additional errors are probably as large as the errors discussed in items 3 and 4.

We believe that, despite such limitations, this method of representation of the equivalent current system has significant advantages over magnetic activity indices, magnetic vector plots, hand-drawn ionospheric current systems, etc., due to its ease in calculation, reproducibility, opportunity for

pattern recognition, and intensity representation. (It takes about 4 seconds to produce a potential contour map using the computer at the National Center for Atmospheric Research).

The authors suggest that the generation of such magnetic potential contours for periods during the IMS (International Magnetospheric Study, 1976-1979) would produce a valuable data product for participants. The contour plots could be made for several intervals chosen in conjunction with rocket launches and satellite observations. They would add useful information on ground magnetic perturbations and the responsible currents, a global aspect for conditions during the rocket and satellite observations, and improved understanding of magnetospheric processes.

Table 1.

Comparison between magnetic perturbations observed and those calculated at the locations of the observatories.

Observatory	Observed	Calculated	Change	% Change
Polar cap				
Alert	594γ	500γ	-94γ	-15.8%
Godhavn	306	333	+27	+8.8
Mould Bay	143	150	+7	+4.9
Resolute Bay	224	200	-24	-10.7
Thule	310	313	+2	+0.6
Auroral zone				
Abisko	349	250	-99	-28.4
Baker Lake	359	333	-98	-7.2
Cape Chelyuskin	447	476	+29	+6.4
Cape Wellen	533	555	+22	+4.1
College	878	833	-45	-5.1
Dixon Island	321	300	-21	-6.5
Fort Churchill	573	526	-47	-8.2
Fort Yukon	996	833	-163	-16.4
Great Whale River	417	417	0	0.0
Meanook	375	350	-25	-6.7
Point Barrow	894	909	+15	+1.7
Sitka	335	350	+15	+4.5
Mid- and low-latitudes				
Almeria	55	65	+10	+18.2
Baguio	17	22	+5	+29.4
Bangui	54	58	+4	+7.4
Boulder	82	79	-3	-3.6
Dallas	64	69	+5	+7.8
Dourbes	63	70	+7	+11.1
Eskdalemuir	72	80	+8	+11.1
Fredericksburg	75	64	-11	-14.6
Fuquene	17	20	+3	+17.6
Furstenfeldbruck	46	50	+4	+8.6
Guam	27	30	+3	+11.1
Honolulu	39	50	+11	+28.2
Huancayo	8	8	0	0.0
Hyderbad	33	40	+7	+21.2
Irkutsk	98	110	+12	+12.2
Kakioka	40	50	+10	+25.0
Leningrad	57	60	+3	+5.3
Lunping	33	33	0	0.0
M'Bour	53	54	+1	+1.9
Newport	28	30	+2	+7.1
Niemegk	110	120	+10	+9.1
Odessa	74	80	+6	+8.1
Paramaribo	22	18	-4	-18.2
San Juan	12	10	-2	-16.7
St. John's	97	100	+13	+13.4
Tashkent	72	80	+8	+11.1
Tucson	58	61	+3	+5.2
			Average of % Change is	3.0%
			Average of |% Change| is	10.2%

V. The Disturbance of 8-9 November 1969

In order to apply our new method of equipotential contour plotting to examine the progressive changes during a magnetic storm, we decided to make a movie film, using contour plots each 2-1/2 minutes. The important steps are outlined in Figure 1. Interval selection was made using the AE, Kp and Dst indices from 1969 through 1973 to identify a relatively short magnetic storm preceded by a quiet period and having a variety of substorm characteristics. The disturbed interval chosen was 1200 UT November 8 - 2400 UT November 9, 1969. The quiet interval, which was used as the reference level, was 1800 UT November 5 - 1800 UT November 6, 1969. The Kp values for this interval are 0+, 1, 1-, 1-, 1-, 0+, 0, and 0+.

The next step required the digitizing of the H and D (or X and Y) traces for 82 northern hemisphere observatories for both disturbed and quiet intervals, which were all the data available through the World Data Center A for Solar-Terrestrial Physics. The location of these observatories is shown in Figure 2 in geographic coordinates. Geographic and geomagnetic coordinates are given in Table 2. The disturbed period traces were digitized relative to their baselines every 2.5 minutes with a maximum timing error range of 2.5 minutes, and the quiet-period trace was scaled on the hour with the same accuracy. The 2.5 minute interpolated quiet-time values were subtracted from the 2.5 minute disturbed values to obtain H and D (or X and Y) perturbation values at each observatory. The 2.5 minute perturbation values were then transformed into Xm and Ym.

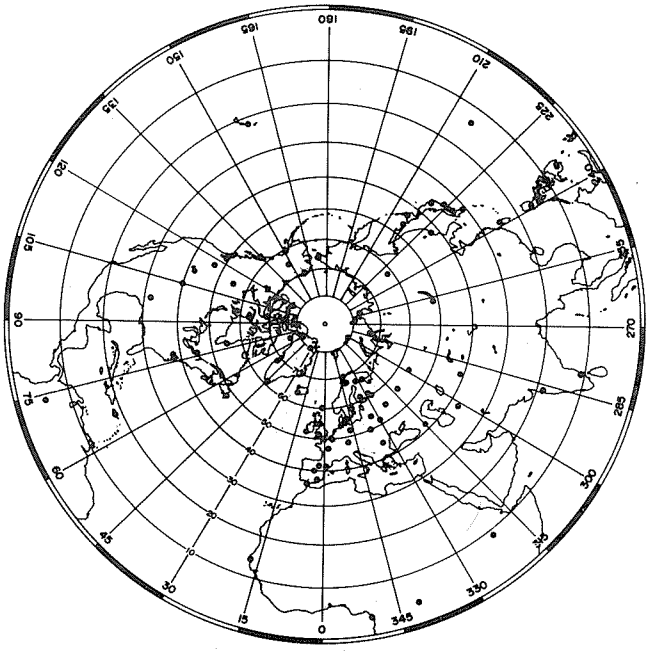

Fig. 2. Observatories in geographical coordinates whose records were used in the derivation of the magnetic potential contours.

Table 2

Observations used for the derivation of the magnetic potential distribution for 8-9 November 1969.

	Observatory	Geographic Latitude N	Geographic Longitude E	Geomagnetic* Latitude N	Geomagnetic* Longitude E
1	Abisko	68.36°	18.82°	65.99°	115.63°
2	Addis Ababa	9.03	38.77	5.26	109.89
3	Alert	82.50	297.50	85.90	166.68
4	Alibag	18.63	72.87	9.43	144.34
5	Almeria	36.85	357.53	40.47	76.01
6	Annamalainagar	11.40	79.68	1.51	150.10
7	Ashkhabad	37.95	58.10	30.45	133.77
8	Baguio	16.42	120.60	5.16	189.98
9	Baker Lake	64.33	263.97	73.83	316.50
10	Bangui	4.43	18.57	4.67	89.25
11	Barrow	71.30	203.25	68.71	241.85
12	Boulder	40.13	254.77	49.04	317.40
13	Cape Chelyuskin	77.72	104.28	66.32	176.85
14	Cape Wellen	66.17	190.17	61.96	237.79
15	Chambon-La-Foret	48.02	2.27	50.31	85.07
16	College	64.87	212.17	64.79	257.33
17	Dallas	32.98	263.25	42.98	328.64
18	Davao	7.08	125.58	-3.95	195.26
19	Dixon Island	73.55	80.57	63.03	162.00
20	Dourbes	50.10	4.60	51.83	88.39
21	Ebro (Tortosa)	40.82	0.50	43.74	80.37
22	Eskdalemuir	55.32	356.80	53.31	83.57
23	Fort Churchill	58.80	265.90	68.74	323.92
24	Fredericksburg	38.20	282.63	49.51	350.78
25	Fuquene	5.47	286.27	16.88	355.87
26	Furstenfeldbruck	48.17	11.28	48.67	93.99
27	Godhavn	69.23	306.48	79.72	33.77
28	Great Whale River	55.27	282.22	66.55	348.48
29	Guam	13.58	144.87	4.10	213.63
30	Hartland	50.98	355.52	54.48	79.70
31	Heiss Island	80.62	58.05	71.30	156.32
32	Honolulu	21.32	202.00	21.23	267.29
33	Huancayo	-12.05	284.67	-0.67	354.55
34	Irkutsk	52.17	104.45	40.78	175.31
35	Kakioka	36.23	140.18	26.15	206.65
36	Kanoya	31.42	130.88	20.65	198.75
37	Kazan	55.83	48.85	49.26	130.94
38	Kiev	50.72	30.30	47.46	112.79
39	Leirvogur	64.18	338.30	70.05	71.77
40	Leningrad	59.95	30.70	56.14	117.90
41	Lerwick	60.13	358.82	62.38	89.22
42	Logrono	42.45	357.50	45.90	77.91
43	Lovo	59.35	17.83	57.94	106.36
44	Lunping	25.00	121.17	13.76	190.19
45	Lvov	49.90	23.75	47.89	106.49
46	M'Bour	14.40	343.02	21.07	55.77
47	Meanook	54.62	246.67	61.93	302.04
48	Memambetsu	43.90	144.20	34.14	209.10
49	Minsk	54.10	26.52	51.37	110.98
50	Moca	3.35	8.67	5.56	79.31
51	Moscow	55.48	37.32	50.77	121.08
52	Mould Bay	76.30	240.60	79.65	258.77
53	Muntinlupa	14.37	121.02	3.13	190.46
54	Murmansk	68.25	33.08	63.39	126.25
55	Narssarssuaq	61.20	314.60	71.06	37.72
56	Newport	48.26	243.01	55.18	301.13
57	Niemegk	52.07	12.68	52.10	97.21
58	Nurmijarvi	60.52	24.65	57.75	113.14
59	Odessa	46.78	30.88	43.57	111.74
60	Ottawa	45.40	284.40	57.76	352.51
61	Resolute Bay	74.70	265.10	83.11	290.94
62	Rude Skov	55.85	12.45	55.74	99.16

* These coordinates based on different model than that used in Report UAG-38.

Table 2 (cont'd.)

	Observatory	Geographic Latitude N	Geographic Longitude E	Geomagnetic* Latitude N	Geomagnetic* Longitude E
63	Sakhalinsk	46.95°	142.72°	37.02°	207.33°
64	San Fernando	36.47	353.80	40.81	72.06
65	San Juan	18.12	293.85	29.79	3.98
66	Simosato	33.57	135.93	23.15	203.13
67	Sitka	57.07	224.67	60.14	276.22
68	Sodankyla	67.37	26.63	63.66	120.47
69	St. John's	47.60	307.30	58.39	22.17
70	Surlari	44.68	26.25	42.41	106.72
71	Sverdlovsk	56.73	61.07	48.45	141.26
72	Tashkent	41.33	69.62	32.30	144.67
73	Tbilisi	42.08	44.70	36.58	122.72
74	Thule	77.48	290.83	88.91	6.74
75	Toledo	39.88	355.93	43.71	75.39
76	Tromso	69.67	18.95	67.02	117.17
77	Tucson	32.25	249.17	40.50	313.06
78	Valentia	51.93	349.75	56.48	74.18
79	Victoria	48.52	236.58	54.31	293.88
80	Vladivostok	43.68	132.17	32.38	198.60
81	Wingst	53.75	9.07	54.27	95.32
82	Yakutsk	62.02	129.72	51.07	194.42

* These coordinates based on different model than that used in Report UAG-38.

From Xm values of 12 auroral zone observatories, we also calculated AU and AL indices. The observatories used were Leirvogur, Narssarssuaq, Great Whale River, Fort Churchill, Meanook, Sitka, College, Barrow, Cape Wellen, Cape Chelyuskin, Dixon Island, and Abisko. These indices were in good agreement with the AU and AL indices prepared by NGSDC [Allen *et al.*, 1974]. The only significant difference was an increase in the substorm value at 1735 UT on November 8, 1969, of approximately 300 γ, or 50%.

Using the method of Section III and appropriate boundary conditions (see Appendix 3), potentials were calculated and contours were plotted on cine film for each 2.5 minutes. Examples of selected frames are described below (Figures 3 through 9) to illustrate the information displayed in Part 2 of this report. Each film frame also shows the AU and AL graphs for the entire interval and for this report they are combined with vector plots of the perturbation values from which the potentials were derived. All the potential contours are plotted in geomagnetic coordinates. The letters H or L appearing in the center of each potential vortex indicate high potential or low potential, respectively, relative to the values surrounding the region. Circulation of ionospheric currents around the high potential (H) is clockwise, around the low potential (L) is counterclockwise. The magnitude of the equivalent ionospheric current is proportional to the number of contour lines and the current density is proportional to the number of lines through a unit area. The contour interval is $5 \times 10^4 \gamma \cdot$km, corresponding to about 5×10^4 amp using a conventional overhead current approximation.

Figure 3 shows an example of the quiet period before auroral electrojet activity has begun. The AU and AL indices and associated horizontal timing bar are on the left side. Both the magnetic vector and the potential contour plots indicate a quiet-time ring current of about -20 γ in mid- and low-latitudes especially in the afternoon sector. In high latitudes, both H and L appear characterizing a weak S_q^P type current system.

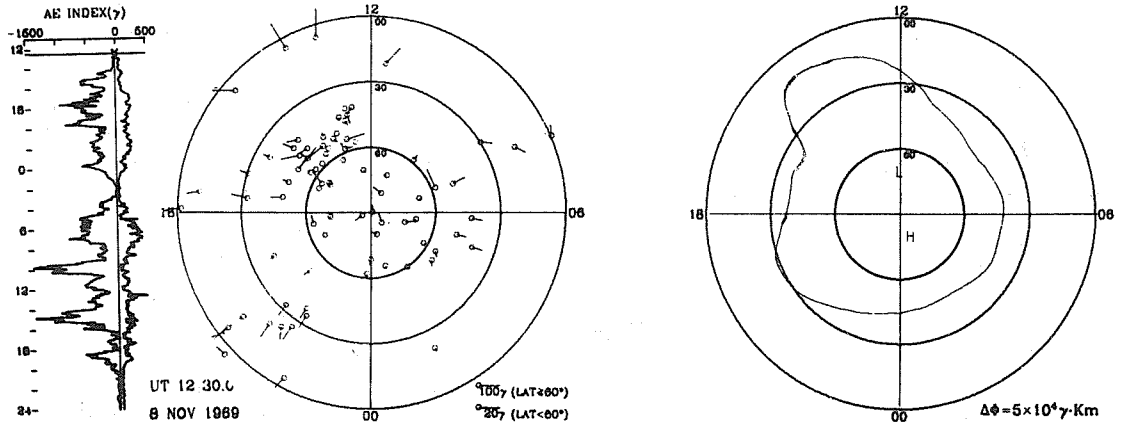

Fig. 3. Distribution of the ground magnetic perturbation vectors and the corresponding magnetic potential contours for a quiet period - 1230 UT on 8 November 1969.

The plots shown in Figure 4 describe the magnetic perturbations 1-1/2 hours after Figure 3 and just before the onset of a weak substorm. Comparing the plots in Figure 4 with those in Figure 3, we notice a change in the polar cap. The magnitude of the disturbance vectors has increased to 100 γ and the direction has changed to a dawn-to-dusk orientation. Also, in the auroral region, +Xm values are seen in the evening sector and -Xm values are seen toward morning. In the potential contour, two vortices can be seen; the low potential vortex is larger and more intense than the high potential vortex. These are essentially the same characteristics as the S_q^P (or DP 2) current system produces [Nishida, 1968; Nishida and Kokubun, 1971].

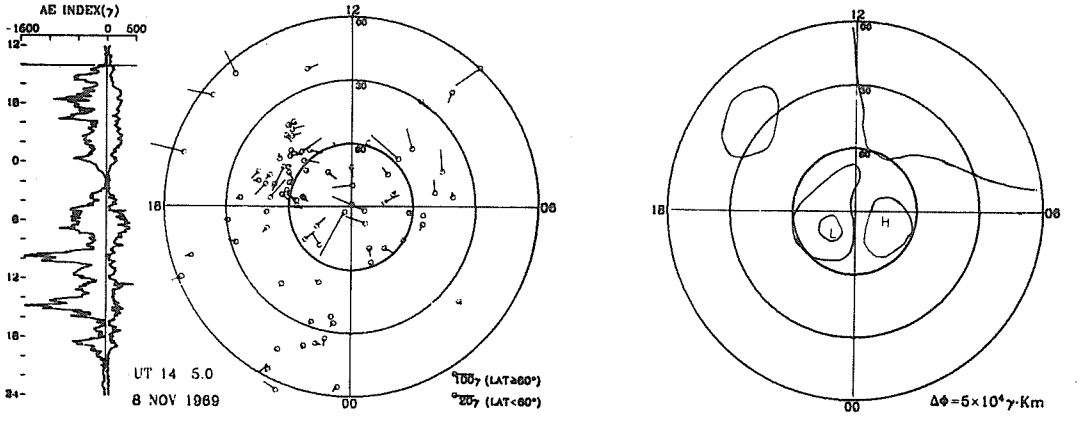

Fig. 4. Distribution of the ground magnetic perturbation vectors and the corresponding magnetic potential contours for the instant just before the onset of a substorm - 1405.0 UT on 8 November 1969.

Figure 5 shows an example of the maximum phase of a typical substorm in which AL = -800γ and AU = 300γ. The most intense -Xm was observed at a Siberian observatory near midnight. Less intense -Xm values were observed in Alaska (06 MLT)*. In mid- and low-latitudes, the -Xm bays appear smaller than expected, perhaps because of the quiet-time level selected. The corresponding potential plots show a global contour pattern concentrated in the nightside auroral zone (region of the westward electrojet). About 1/3 of the contours (current) from this region close in the polar cap, 1/3 close through mid- and low-latitudes of the dayside, and the remaining 1/3 close in the nightside low latitudes. This pattern is a consistent characteristic of our plots and is quite different from the pattern of most proposed substorm current systems. Exceptions are found in the current patterns constructed by Fukushima [1951, 1953], and Kokubun [1965]. The -Xm occurred at only two auroral zone observatories in the evening sector (Leirvogur and Narssarssuaq), and the corresponding eastward electrojet (represented by the poleward portion of the evening H vortex) is not as conspicuous.

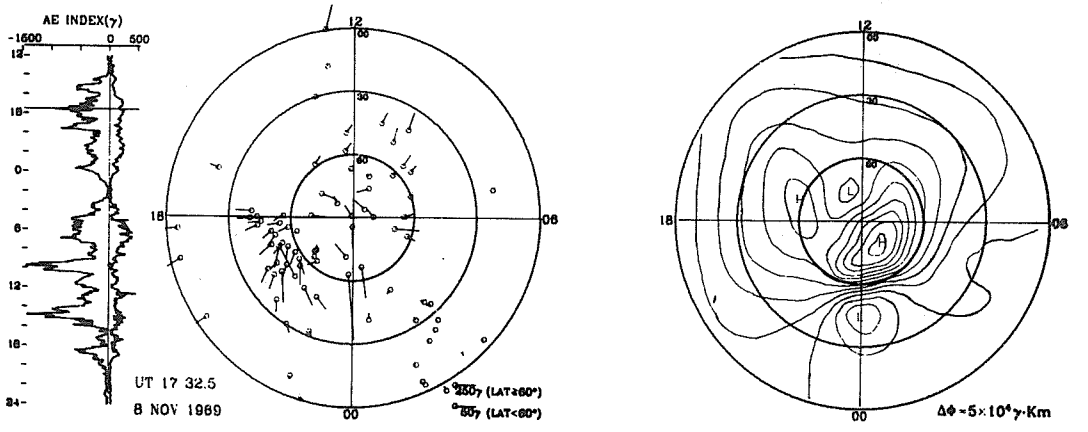

Fig. 5. Distribution of the ground magnetic perturbation vectors and the correspoinding magnetic potential contours for the maximum phase of a typical substorm-1732.5 UT on 8 November 1969.

* MLT = Magnetic Local Time

Figure 6 shows the vector and potential plots resulting from the storm sudden commencement (SSC) at 1836 UT on November 8, 1969. We observe a sudden increase of the Xm component in mid-latitudes. Obayashi and Jacobs [1957] have shown that a typical SSC current system consists of lower latitude zonal eastward current and the DS type current in high latitudes. Our current pattern is similar to their pattern except that the zonal part is disrupted in the evening sector near Huancayo. At Huancayo the Xm measured from the quiet-day level was still negative in this particular example, although it was less negative than the value before the SSC.

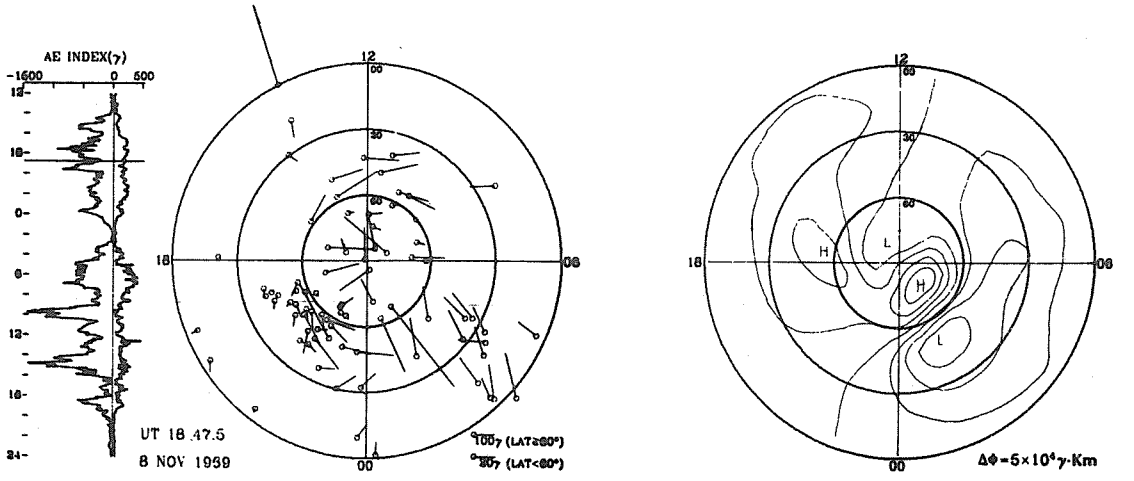

Fig. 6. Distribution of the ground magnetic perturbation vectors and the corresponding magnetic potential contours for the field just after an SSC - 1847.5 UT on 8 November 1969.

Figure 7 shows the pattern of the maximum phase of one substorm which had an intense westward electrojet without an eastward electrojet (see the corresponding AE index). The most intense current is centered in the pre-midnight sector between the two foci. In this particular example, the latitudinal width of the electrojet current is unrealistically large due to poor observatory distribution, i.e., no magnetic observatory between the Alaska stations (where the intense -Xm was observed) and Honolulu (where +Xm was observed). Our simple interpolation method does not define an equatorward boundary of the westward electrojet corresponding to the optical aurora boundary. An intense ring current in the magnetosphere appears as the equivalent return current from the westward electrojet.

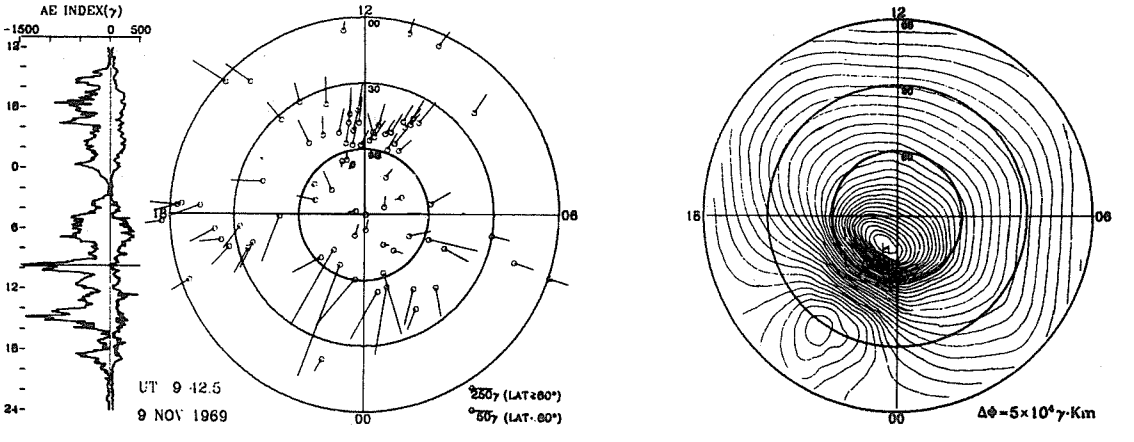

Fig. 7. Distribution of the ground magnetic perturbation vectors and the corresponding magnetic potential contours for the maximum phase of a substorm -0942.5 UT on 9 November 1969.

Figure 8 shows an example of an intense westward electrojet (AL = -1500 γ), with a weak eastward electrojet (AU = 280 γ). This pattern is different from Figure 7 as follows: (1) The westward electrojet spreads over a wider area in the nighttime sector. (2) The current is distorted near 16 MLT as a result of the eastward electrojet in the auroral region.

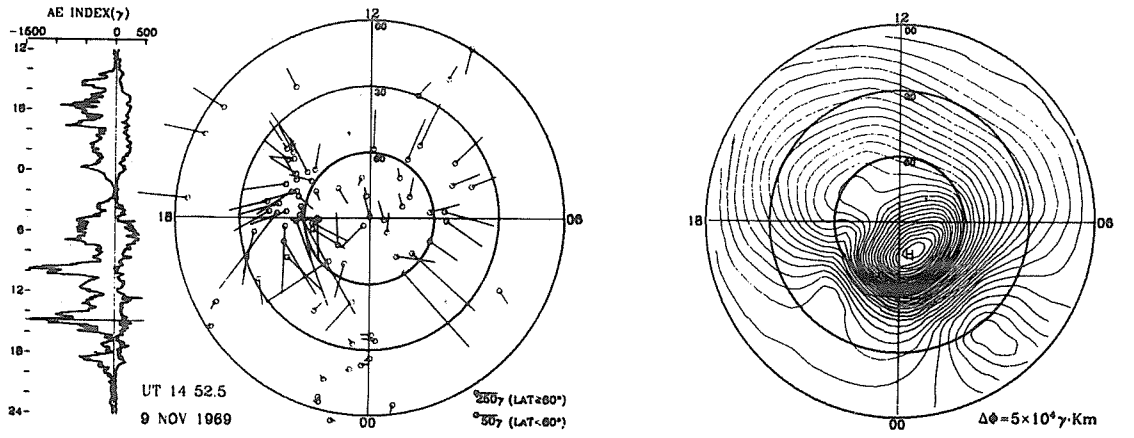

Fig. 8. Distribution of the ground magnetic perturbation vectors and the corresponding magnetic potential contours for the maximum phase of a substorm - 1452.5 UT on 9 November 1969.

Figure 9 shows the recovery phase of the magnetic storm. The vector plot depicts weak activity of the auroral electrojets with perturbations of about the same intensity as those at mid-latitude. The almost circular potential contours suggest a symmetric ring current in the magnetosphere during the recovery phase of the magnetic storm.

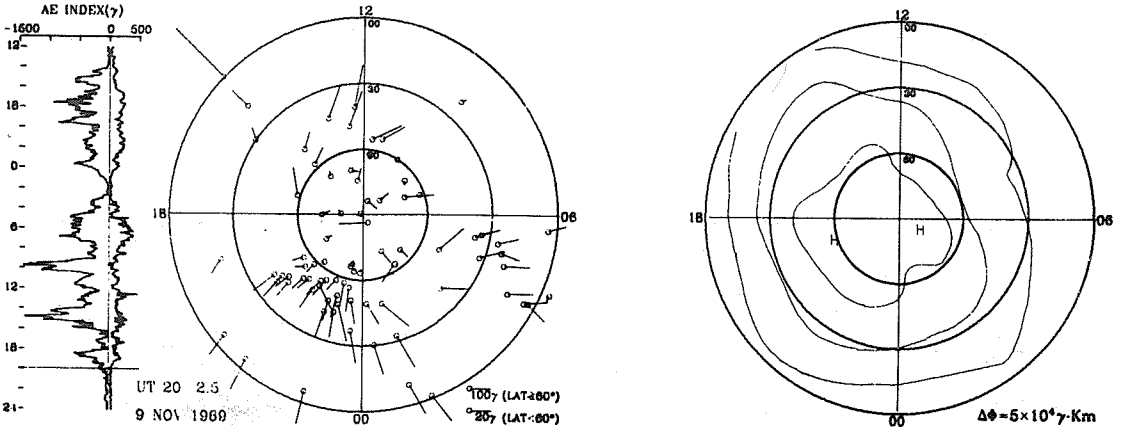

Fig. 9. Distribution of the ground magnetic perturbation vectors and the corresponding magnetic potential contours for the recovery phase of a magnetic storm - 2002.5 UT on 9 November 1969.

VI. Availability of Detailed Data

The complete data set is available on 16 mm cine film. Each frame of the film has the potential contour plot and the AE index graph and is repeated five times, allowing the viewer to follow the progression of contour changes. One film was made showing contour variations for latitudes between 0^{o} and 90^{o} and another between 45^{o} and 90^{o}. Film copies may be obtained from Data Studies Division, NOAA/EDS/NGSDC, Boulder, Colorado 80302, U.S.A., at a cost of $30.00 per film. Copies of magnetograms are available from World Data Center A for Solar-Terrestrial Physics, as described in the Catalog of Geomagnetic Data, Report UAG-49.

Acknowledgements

We are very much obliged to R. Bostrom and N. Fukushima for their useful discussions. We would like to thank M. L. Buhler, T. T. Wetmore, and S. A. Liss for their assistance in computer programming in the early stages of the work, and C. Samora for his patience in digitizing the magnetic records. Encouragement and financial support were provided by A. H. Shapley, P. A. Gilman, and J. R. Herring. Acknowledgement is made to the National Center for Atmospheric Research, which is sponsored by the National Science Foundation, for the computing time used in this project. This work was supported also in part by the National Science Foundation, Atmospheric Science Section, under grant DES74-23832 to the Geophysical Institute of the University of Alaska.

Appendix 1.

Determination of a Potential Field for Ground Magnetic Perturbations

The ground magnetic field perturbation $\underline{H}$ is assumed to be derivable from a magnetic potential Φ, as

$$\underline{H} = -\text{grad}\ \Phi. \tag{A1-1a}$$

The three components of the geomagnetic field (X_m, Y_m, Z) on the earth's surface (radius a) may be expressed as

$$\begin{aligned} X_m &= -H_\theta = \partial\Phi/a\partial\theta, \\ Y_m &= H_\lambda = \partial\Phi/a\sin\theta\partial\lambda, \\ Z &= -H_r = \partial\Phi/\partial r. \end{aligned} \tag{A1-1b}$$

Thus, we have

$$\text{div}\ \underline{H} = \text{div}\ (-\text{grad}\ \Phi) = \nabla^2\Phi. \tag{A1-2}$$

Since div $\underline{H}$ = 0, equation (A1-2) gives the three-dimensional Laplace equation,

$$\nabla^2\Phi = 0. \tag{A1-3}$$

1.1 Spherical harmonic analysis

In the spherical coordinates,

$$\nabla^2 = \frac{1}{r^2}\frac{\partial}{\partial r}\left(r^2\frac{\partial}{\partial r}\right) + \frac{1}{r^2\sin\theta}\frac{\partial}{\partial\theta}\left(\sin\theta\frac{\partial}{\partial\theta}\right) + \frac{1}{r^2\sin^2\theta}\frac{\partial^2}{\partial\lambda^2}.$$

Thus, we can rewrite the equation (A1-3) in terms of a function Sn (θ, λ) as

$$r^{n-2}\left[(1-\mu^2)\frac{\partial^2 Sn}{\partial\mu^2} - 2\mu\frac{\partial Sn}{\partial\mu} + n(n+1)Sn + \frac{1}{1-\mu^2}\frac{\partial^2 Sn}{\partial\lambda^2}\right] = 0, \tag{A1-4}$$

where
$$\Phi(r, \theta, \lambda) = r^2 Sn\ (\theta, \lambda), \tag{A1-5a}$$

and
$$\mu = \cos\theta. \tag{A1-5b}$$

Any function S_n satisfying equation (A1-4) is called a spherical surface harmonic of degree n. The general solution of (A1-4) gives the following form by using the associated Legendre function $P_n^m(\mu)$ [Chapman and Bartels, 1940, p. 620].

$$S_n = \sum_{m=0}^{n} C_n^m P_n^m(\mu)\cos(m\lambda + \varepsilon_n^m), \tag{A1-6}$$

where C_n^m and ε_n^m are arbitrary. It is also possible to separate the internal potential $\Phi^{(i)}$ from the external potential $\Phi^{(e)}$ with respect to the earth's surface, as follows:

$$\Phi = \Phi^{(e)} + \Phi^{(i)}, \tag{A1-7}$$

with
$$\Phi^{(e)} = a\sum_{n=1}^{\infty}\left(\frac{r}{a}\right)^n T_n^{(e)}, \tag{A1-8}$$

$$\Phi^{(i)} = \sum_{n=1}^{\infty}\left(\frac{a}{r}\right)^{n+1} T_n^{(i)}. \tag{A1-9}$$

The function $T_n(\theta,\lambda)$ is given by

$$T_n^{(e,i)} = \sum_{m=0}^{n} \left[g_n^{m(e,i)} \cos m\lambda + h_n^{m(e,i)} \sin m\lambda \right] P_n^m(\mu). \tag{A1-10}$$

Substituting (A1-10) into (A1-1b), we obtain

$$X_m = \sum_{n=1}^{\infty} \sum_{m=0}^{n} \left[(g_n^{m(e)} + g_n^{m(i)}) \cos m\lambda + (h_n^{m(e)} + h_n^{m(i)}) \sin m\lambda \right] \frac{dP_n^m}{d\theta}, \tag{A1-11a}$$

$$Y_m = \sum_{n=1}^{\infty} \sum_{m=0}^{n} \left[m(g_n^{m(e)} + g_n^{m(i)}) \sin m\lambda - m(h_n^{m(e)} + h_n^{m(i)}) \cos m\lambda \right] \frac{P_n^m}{\sin\theta}, \tag{A1-11b}$$

$$Z = \sum_{n=1}^{\infty} \sum_{m=0}^{n} \left[(n g_n^{m(e)} - (n+1) g_n^{m(i)}) \cos m\lambda + (n h_n^{m(e)} - (n+1) h_n^{m(i)}) \sin m\lambda \right] P_n^m. \tag{A1-11c}$$

On the other hand, when the observed geomagnetic field is expressed in terms of spherical harmonics it is possible to calculate all the coefficients $g_n^{m(e,i)}$, and $h_n^{m(e,i)}$ in (A1-11). Thus, the geomagnetic field can be represented by the magnetic potential which is given by the spherical harmonic function.

1.2 A new method to obtain the magnetic potential

As mentioned previously, there are difficulties in calculating all the spherical harmonic coefficients expressed in (A1-11). We develop here a new method to determine numerically the potential values on the earth's surface. In the case of two-dimensional coordinates (θ,λ) on the earth's surface, equation (A1-2) is written as:

$$\sigma = \frac{1}{a^2 \sin\theta} \frac{\partial}{\partial\theta} \left(\sin\theta \frac{\partial\Phi}{\partial\theta} \right) + \frac{1}{a^2 \sin^2\theta} \frac{\partial^2\Phi}{\partial\lambda^2}, \tag{A1-12a}$$

where

$$\sigma = -(\operatorname{div} \underline{H})_{\theta,\lambda} = -\frac{\partial H_\theta \sin\theta}{a \sin\theta \partial\theta} - \frac{\partial H_\lambda}{a \sin\theta \partial\lambda}. \tag{A1-12b}$$

The value on the lefthand side of (A1-12a) is given by observations through a suitable interpolation at each grid point. Therefore, we can obtain Φ by solving the two-dimensional Poisson's equation (A1-12a), which is equivalent to (1), under proper boundary conditions.

We can also obtain equations (1) from (A1-2) as follows:

Rewriting (A1-2), we obtain

$$\frac{1}{r^2 \sin\theta} \frac{\partial}{\partial\theta} \left(\sin\theta \frac{\partial\Phi}{\partial\theta} \right) + \frac{1}{r^2 \sin^2\theta} \frac{\partial^2\Phi}{\partial\lambda^2} = -\frac{1}{r^2} \frac{\partial}{\partial r} \left(r^2 \frac{\partial\Phi}{\partial r} \right). \tag{A1-13}$$

Using (A1-1b), the righthand side of (A1-13) is

$$-\frac{1}{r^2} \frac{\partial}{\partial r} \left(r^2 \frac{\partial\Phi}{\partial r} \right) = \frac{1}{r^2} \frac{\partial}{\partial r} (r^2 H_r). \tag{A1-14}$$

Since div $\underline{H} = 0$, namely

$$\frac{1}{r\sin\theta}\left[\frac{\partial}{\partial\theta}(H_\theta \sin\theta) + \frac{\partial H_\lambda}{\partial\lambda} + \frac{\sin\theta}{r}\frac{\partial}{\partial r}(r^2 H_r)\right] = 0,$$

the righthand side of (A1-14) is expressed as

$$\frac{1}{r^2}\frac{\partial}{\partial r}(r^2 H_r) = -\frac{1}{r\sin\theta}(H_\theta \sin\theta) - \frac{1}{r\sin\theta}\frac{\partial H_\lambda}{\partial\lambda}, \qquad \text{(A1-15)}$$

which is equivalent to (A1-12b), that is the lefthand side of (A1-12a), by setting $r = a$.

1.3 Magnetic potential of a current in a thin spherical shell

If the external origin part of the responsible current, whose current density is $\underline{i}$ (i_θ, i_λ) is assumed to flow in a thin spherical shell of radius R (viz., the ionosphere), a current function J can be introduced by

$$i_\theta = \partial J/R\sin\theta\partial\lambda$$

$$i_\lambda = -\partial J/R\partial\theta. \qquad \text{(A1-16)}$$

If the current function is expanded into spherical harmonics

$$J = \sum_n Jn\ (\theta,\lambda),$$

then

$$Jn = -\frac{10}{4\pi}\frac{2n+1}{n+1}\left(\frac{R}{a}\right)^n \Phi_n(e). \qquad \text{(A1-17)}$$

In this way, the ground magnetic perturbations can be represented by the ionospheric current. Iso-intensity contours of the magnetic potential are referred to as the equivalent ionospheric current system, since a purely horizontal ionospheric current would produce a similar magnetic perturbation as the one observed.

Appendix 2.

Interpolation Formula

The interpolation formula to obtain the field values at a regular network of point is

$$T_{i,j} = D\,(T_A/d_A + T_B/d_B + T_C/d_C), \text{ if } d_A, d_B, \text{ or } d_C \neq 0, \tag{A2-1}$$

$$T_{i,j} = T_A, T_B, \text{ or } T_C, \text{ if } d_A, d_B, \text{ or } d_C = 0,$$

where

$$D = d_A d_B d_C/(d_A d_B + d_B d_C + d_C d_A), \tag{A2-2}$$

and

$$T_{i,j} = X_{m\ i,j} \text{ or } Y_{m\ i,j}.$$

Here d_A, d_B, and d_C denote the distances between the grid point (i,j) and the observatories A, B, and C, respectively. The grid point values $T_{i,j}$ would not satisfy a potential, due to errors introduced during data processing.

Appendix 3.

Boundary Conditions for the Poisson's Equation

Two different boundary conditions are set: First, we set the potential values equal to 0 at $\xi = \pm \pi\alpha$ and $\eta = \pm \pi\alpha$, which is near the magnetic equator. ξ and η describe a rectangular coordinate system in the azimuthal equidistance projection of the earth's surface where η and ξ are directed toward the sun and the dawn-side, respectively. Second, we used the potential values calculated along the same rectangular boundary curve s constructed by $\xi = \pm \pi\alpha$ and $\eta = \pm \pi\alpha$ through the following procedures: (i) Correction was made for the interpolated value H_s (H_s is the tangential component to the boundary curve s) so that the value

$$\oint H_s^c ds = \int_{\xi=\pi\alpha} H_s^c ds + \int_{\eta=\pi\alpha} H_s^c ds + \int_{\eta=-\pi\alpha} H_s^c ds + \int_{\xi=-\pi\alpha} H_s^c ds = 0 \tag{A3-1}$$

This is accomplished by substituting H_s at each grid point by corrected H_s^c, which is given by

$$H_s^c = H_s - \oint H_s ds \Big/ \oint ds. \tag{A3-2}$$

(ii) Using these corrected field values, we calculate further the potential values along the boundary s.

Thus, the calculations may be inaccurate at latitudes near the equator. However, we show that these two different boundary conditons made no significant difference in the finally-obtained contour pattern. This means that the effect of the forcing factor σ in (A1-12a) is more important than the boundary condition effects.

In Figure A1, we show our calculated equipotential contour plots for the magnetic polar substorm, which occurred on January 12, 1973. We used data from 73 magnetic observatories in the northern hemisphere, which were all the available data at the time through NGSDC (National Geophysical and Solar-Terrestrial Data Center). We used the first boundary condition, that is, we set the potential values equal to 0 near the equator.

Figure A2 shows the equi-potential contour plots for the same event calculated based on the second boundary condition, which requires significantly more calculation. Although there are slight differences between features in Figures A1 and A2 in the equatorial region, the change in the boundary condition did not significantly change the global pattern.

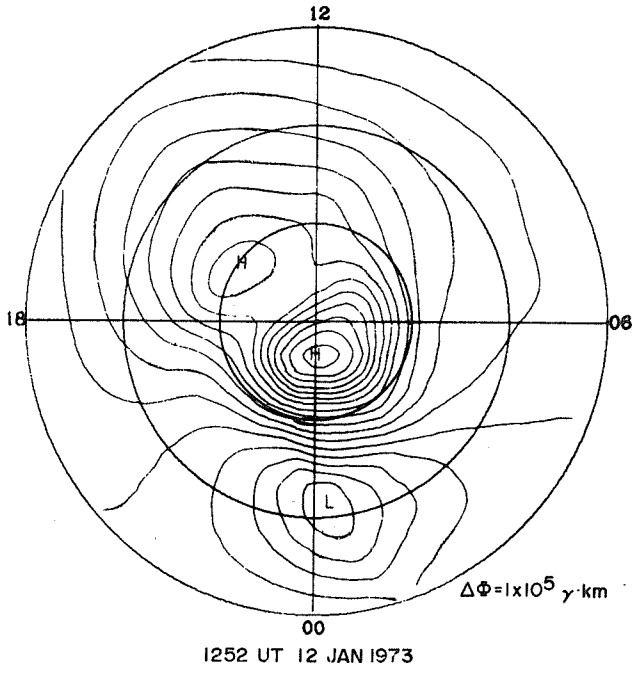

Fig. A1. Computed equipotential contour lines for the magnetic perturbation distribution at 1252 UT January 12, 1973, on the basis of the first boundary condition $\Phi = 0$ near the magnetic equator.

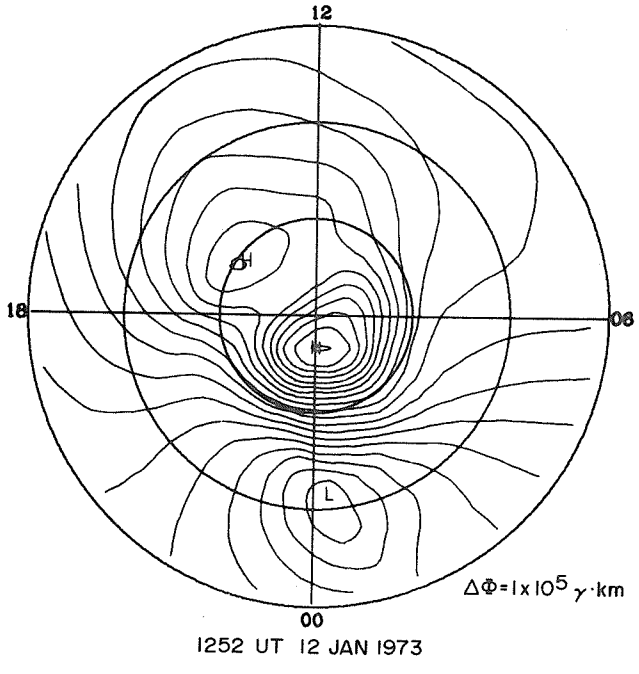

Fig. A2. Computed equipotential contour lines for the magnetic perturbation distribution at 1252 UT January 12, 1973, on the basis of the second boundary condition.

Appendix 4.

Iteration Procedure to Obtain the Global Potential Field

The residual $R_{i,j}^{(m)}$ at a grid point (i,j) at the m-th iteration step is written as

$$R_{i,j}^{(m)} = \nabla^2 \Phi_{i,j}^{(m)} - \sigma_{i,j}$$

$$= \tfrac{1}{4} \left(\Phi_{i-1,j}^{(m+1)} + \Phi_{i,j-1}^{(m+1)} + \Phi_{i+1,j}^{(m)} + \Phi_{i,j-1}^{(m)}\right) - \Phi_{i,j}^{(m)} - \frac{\Delta s^2 \sigma_{i,j}}{4} \qquad \text{(A4-1)}$$

where

$$\sigma_{i,j} = - (\text{div } \underline{H})_{i,j}$$

$$= \frac{H\xi_{i+1,j} - H\xi_{i-1,j}}{2\Delta s} - \frac{H\eta_{i,j+1} - H\eta_{i,j-1}}{2\Delta s} \qquad \text{(A4-2)}$$

and Δs is the grid distance. By using (A4-1) and

$$\Phi_{i,j}^{(m+1)} = \Phi_{i,j}^{(m)} + \alpha \cdot R_{i,j}^{(m)}, \qquad \text{(A4-3)}$$

We repeat the correction procedure until $|R_{i,j}|$ reaches the convergence criterion δ at all the grid points. Here, α is the over-relaxation parameter, which is determined from the number of grid points to maximize the convergence rate [Gary, 1969]. In these calculations, we set $\delta = 10^3$ γ.km and $\alpha = 1.6$.

REFERENCES

ALLEN, J. H. and H. W. KROEHL — 1975 — Spatial and temporal distributions of magnetic effects of auroral electrojets as derived from AE indices, *J. Geophys. Res., 80,* 3667.

ALLEN, J. H., C. C. ABSTON, and L. D. MORRIS — 1974 — Auroral electrojet magnetic activity indices AE (11) for 1969, *Report UAG-31,* World Data Center-A for Solar-Terrestrial Physics, NOAA, Boulder, Colorado, 80302.

BOSTRÖM, R. — 1971 — Polar magnetic substorms, in *The Radiating Atmosphere,* B. M. McCormac (ed.), D. Reidel Pub. Co., Dordrecht-Holland, pp. 357-365.

CHAPMAN, S. and J. BARTELS — 1940 — *Geomagnetism, Vol. 1,* Clarendon, Oxford.

FUKUSHIMA, N. — 1951 — Development and decay processes of the bay disturbances in geomagnetic field, *Rep. Ionos. Res. Jap. 5,* 59.

FUKUSHIMA, N. — 1953 — Polar magnetic storms and geomagnetic bays, *J. Fac. Sci. Univ. Tokyo, Sect. II, 8,* 293.

GARY, J. — 1969 — The numerical solution of partial differential equations, *NCAR Manuscript No. 69-54,* National Center for Atmospheric Research, Boulder, Colorado.

KAMIDE, Y., M. KANAMITSU, and S.-I. AKASOFU — 1976 — A new method of mapping worldwide potential contours for ground magnetic perturbations -Equivalent ionospheric current representations-, *J. Geophys. Res., 81,* in press.

KOKUBUN, S. — 1965 — Dynamic behaviour and north-south conjugacy of geomagnetic bays, *Rep. Ionos. Space Res. Jap., 19,* 177.

LINCOLN, J.V. — 1967 — Geomagnetic indices, in *Physics of Geomagnetic Phenomena, Vol. 1,* edited by S. Matsushita and W. H. Campbell, pp. 67-100, Academic, New York.

MATSUSHITA, S. and H. MAEDA — 1965 — On the geomagnetic solar quiet daily variation field during the IGY, *J. Geophys. Res. 70,* 2535.

NISHIDA, A. — 1968 — Geomagnetic D_p 2 fluctuations and associated magnetospheric phenomena, *J. Geophys, Res., 73,* 1795.

NISHIDA, A. and S. KOKUBUN — 1971 — New polar magnetic disturbances; S_q^P, SP, DPC and DP 2, *Rev. Geophys. Space Phys., 9,* 417.

OBAYASHI, T. and J. A. JACOBS — 1957 — Sudden commencements of magnetic storm and atmospheric dynamo action, *J. Geophys. Res., 62,* 589.

ROSTOKER, G. — 1972 — Geomagnetic indices, *Rev. Geophys. Space Phys., 10,* 935.

SIEBERT, M. — 1971 — Masszahlen der erdmagnetischen Aktivitat, in *Encyclopedia of Physics, Vol. 49, No. 3,* edited by S. Flugge, pp. 206-276, Springer, New York.

STONE, D. J. — 1969 — Automatic evaluation of ionospheric current system, *Planet. Space Sci., 17,* 491.

PART 2

The 10-Minute Plots for 8-9 November 1969 Disturbances

The magnetic vector plot and the corresponding potential contour are shown for every 10 minutes with the AU (12) and AL (12) indices plotted for the entire 36-hour interval. Time is identified along the lefthand edge, 2 hours per tick mark. The frame time is denoted by the timing bar which moves from top to bottom of the AU, AL graph as time increases. Universal time, date, vector scale, geomagnetic latitude and geomagnetic local time are identified for each vector plot. The vector, determined from Xm and Ym perturbations, is plotted for each of the 82 observatory locations using geomagnetic coordinates. The magnitude of the vectors varies with latitude and with amplitude of $|AL|$. For less disturbed periods, i.e., $|AL| < 500\gamma$, the labeled vector for latitudes 60° to 90° is 100 γ and for latitudes below 60° is 20 γ. For $|AL| \geq 500\ \gamma$, the labeled vector for latitudes 60° and above is 250 γ and for latitudes below 60° is 50 γ. The magnetic potential contour plots are identified by Universal Time, date, $\Delta\Phi$, geomagnetic latitude and magnetic local time. We use two different contour intervals,

$$\Delta\Phi = 5 \times 10^{4}\ \gamma \cdot \text{km} \text{ if } |AL| \geq 500\gamma, \text{ and}$$

$$\Delta\Phi = 3 \times 10^{4}\ \gamma \cdot \text{km} \text{ if } |AL| < 500\gamma.$$

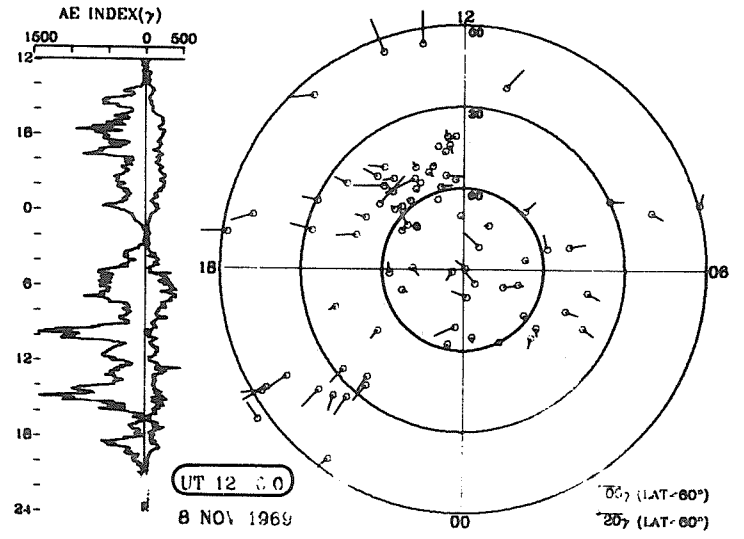
AE INDEX(γ)
1600
0
500
12
18
0
6
12
18
24
UT 12 0.0
8 NOV 1969
12
18
06
00
100γ (LAT≥60°)
20γ (LAT<60°)

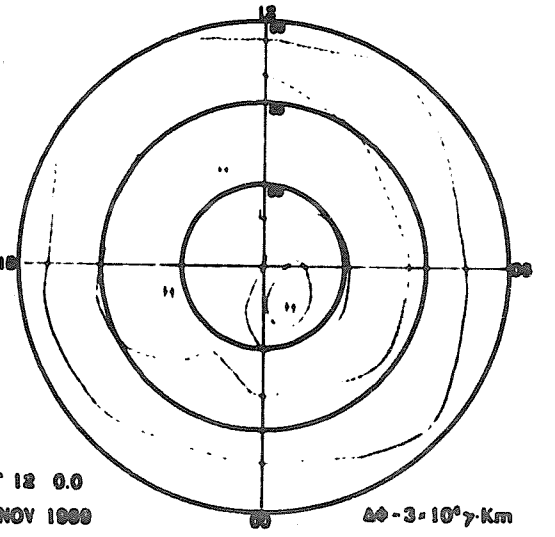
UT 12 0.0
8 NOV 1969
Δφ=3×10⁴γ·Km

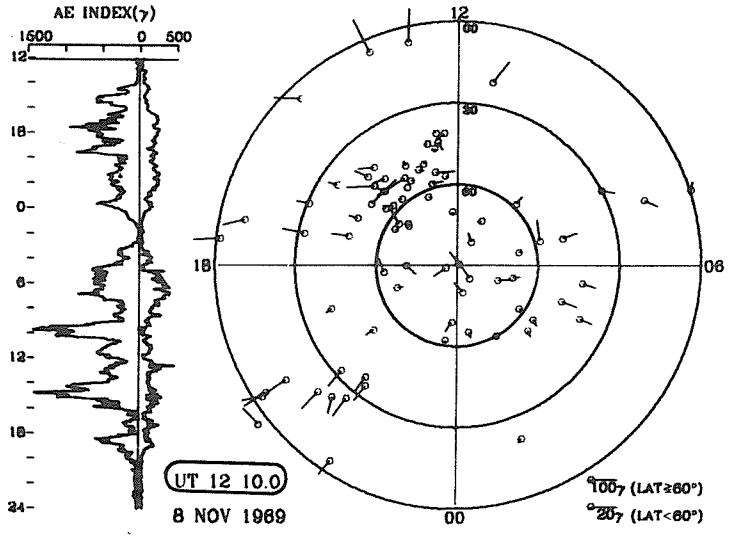
AE INDEX(γ)
1600
0
500
12
18
0
6
12
18
24
UT 12 10.0
8 NOV 1969
12
18
06
00
100γ (LAT≥60°)
20γ (LAT<60°)

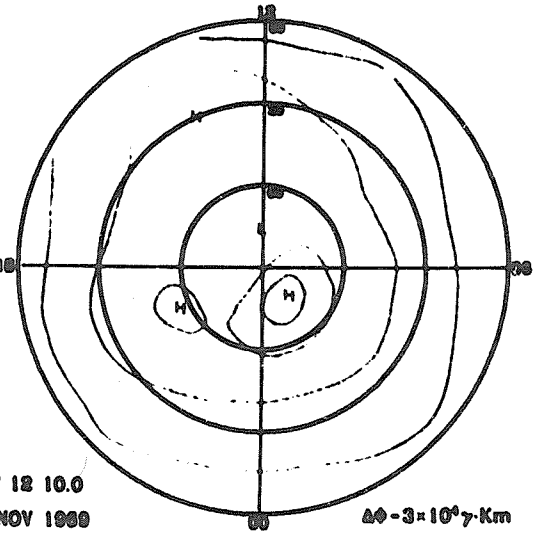
UT 12 10.0
8 NOV 1969
Δφ=3×10⁴γ·Km

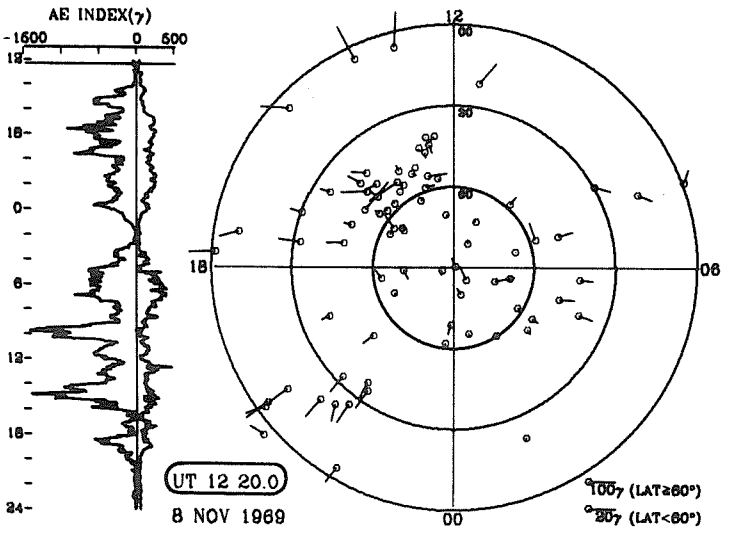
AE INDEX(γ)
1600
0
500
12
18
0
6
12
18
24
UT 12 20.0
8 NOV 1969
12
18
06
00
100γ (LAT≥60°)
20γ (LAT<60°)

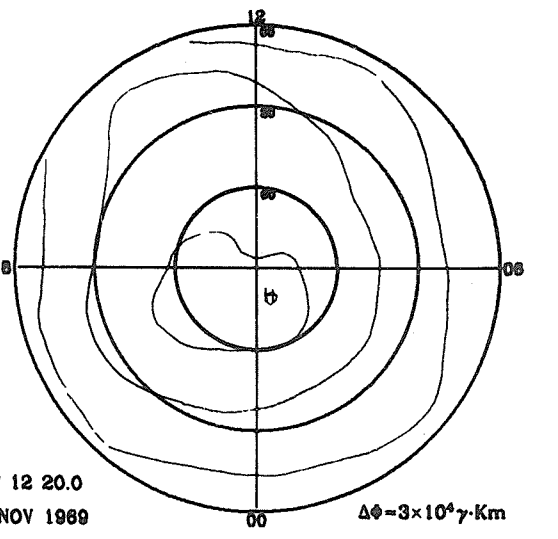
UT 12 20.0
8 NOV 1969
Δφ=3×10⁴γ·Km

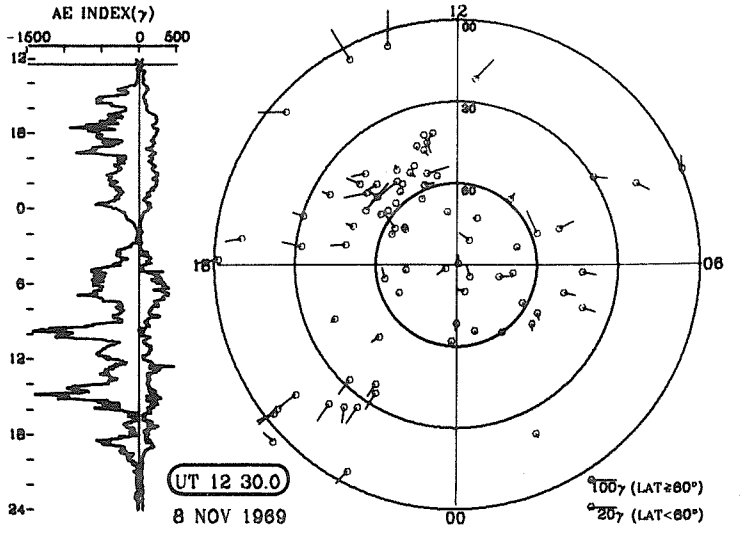
AE INDEX(γ)
-1500
0
500
12
18
0
6
12
18
24
12
00
30
60
18
06
00
UT 12 30.0
8 NOV 1969
100γ (LAT≥60°)
20γ (LAT<60°)

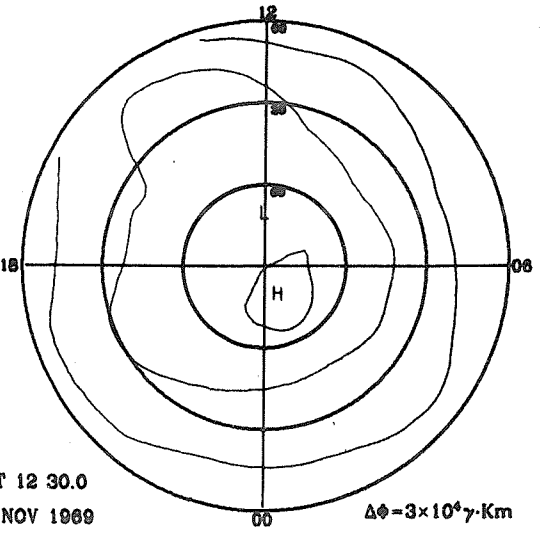
12
00
30
60
18
06
00
L
H
UT 12 30.0
8 NOV 1969
Δφ=3×10⁴γ·Km

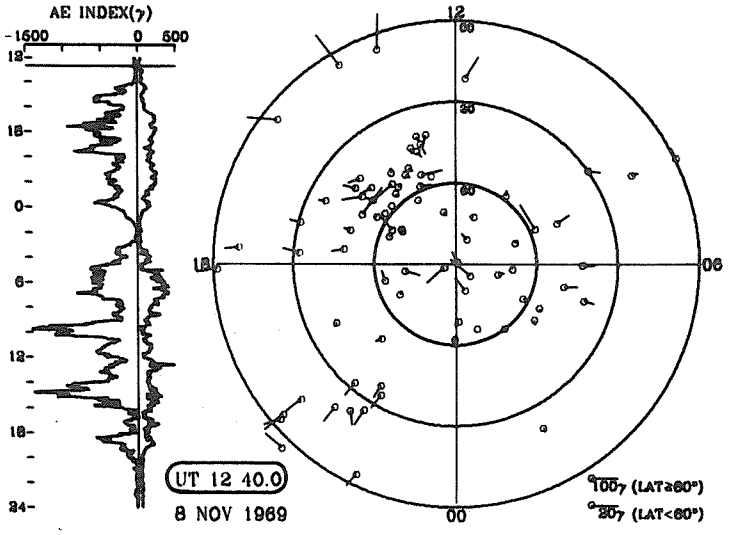
AE INDEX(γ)
-1500
0
500
12
18
0
6
12
18
24
12
00
30
60
18
06
00
UT 12 40.0
8 NOV 1969
100γ (LAT≥60°)
20γ (LAT<60°)

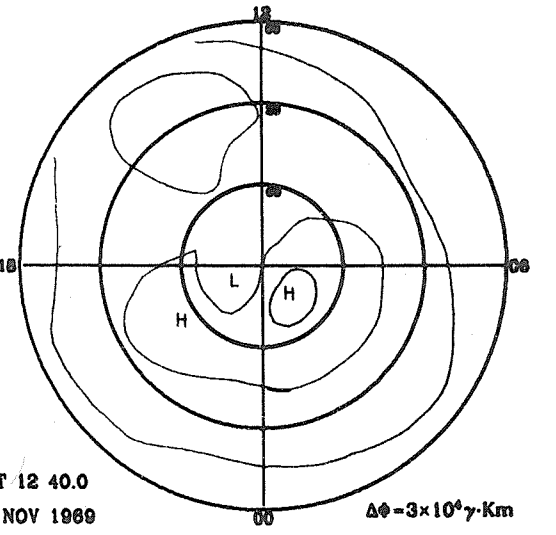
12
00
30
60
18
06
00
L
H
H
UT 12 40.0
8 NOV 1969
Δφ=3×10⁴γ·Km

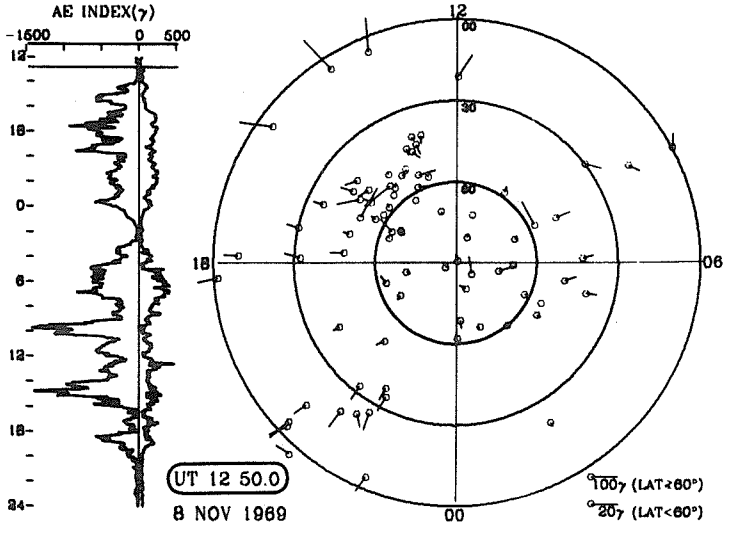
AE INDEX(γ)
-1500
0
500
12
18
0
6
12
18
24
12
00
30
60
18
06
00
UT 12 50.0
8 NOV 1969
100γ (LAT≥60°)
20γ (LAT<60°)

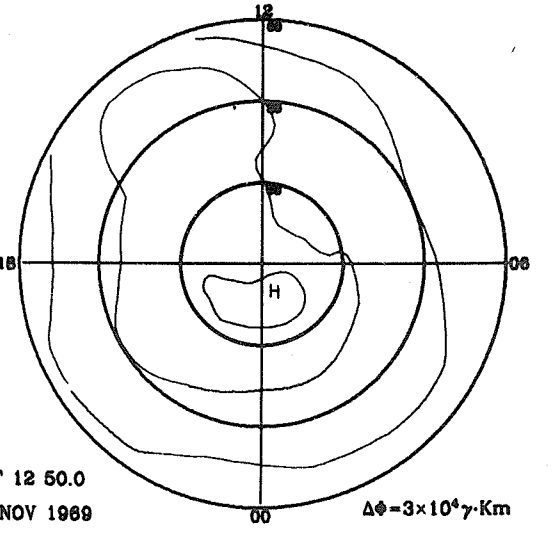
12
00
30
60
18
06
00
H
UT 12 50.0
8 NOV 1969
Δφ=3×10⁴γ·Km

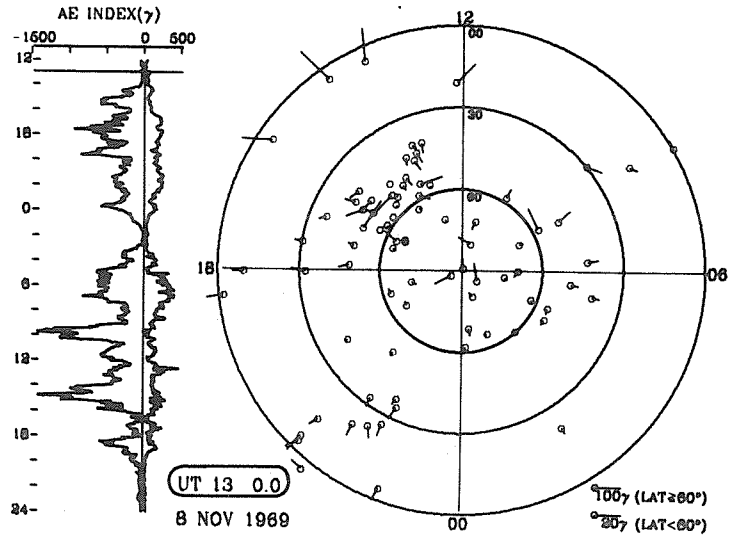
AE INDEX(γ)
-1600
0
600
12
18
0
6
12
18
24
12
00
30
60
18
06
UT 13 0.0
8 NOV 1969
100γ (LAT≥60°)
20γ (LAT<60°)

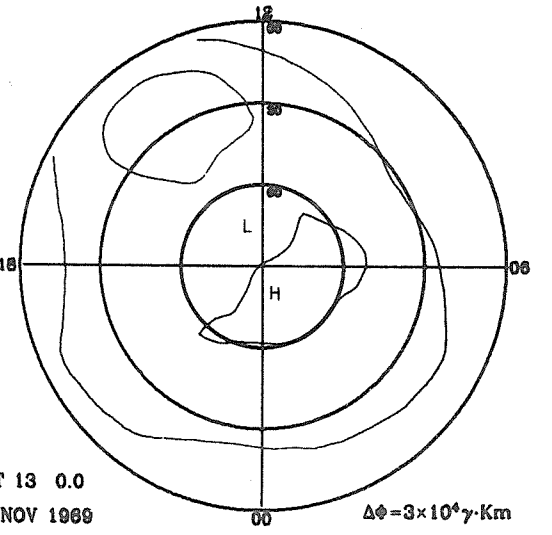
12
00
30
60
18
06
L
H
UT 13 0.0
8 NOV 1969
Δφ=3×10⁴γ·Km

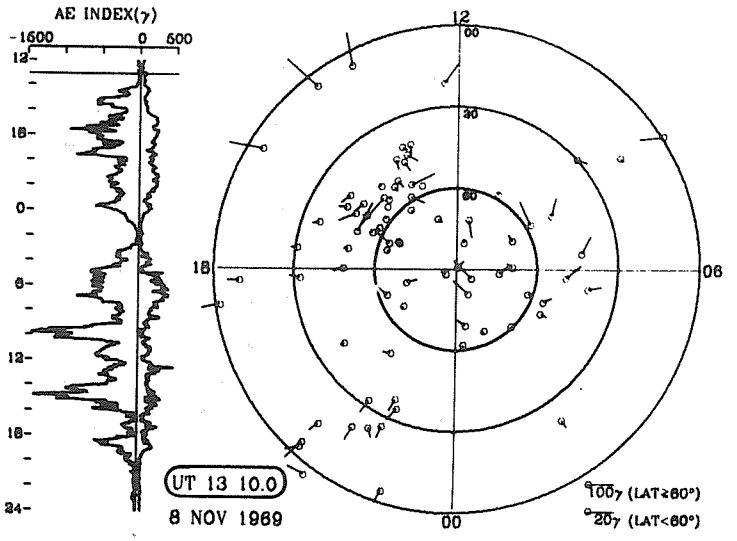
AE INDEX(γ)
-1600
0
600
12
18
0
6
12
18
24
12
00
30
60
18
06
UT 13 10.0
8 NOV 1969
100γ (LAT≥60°)
20γ (LAT<60°)

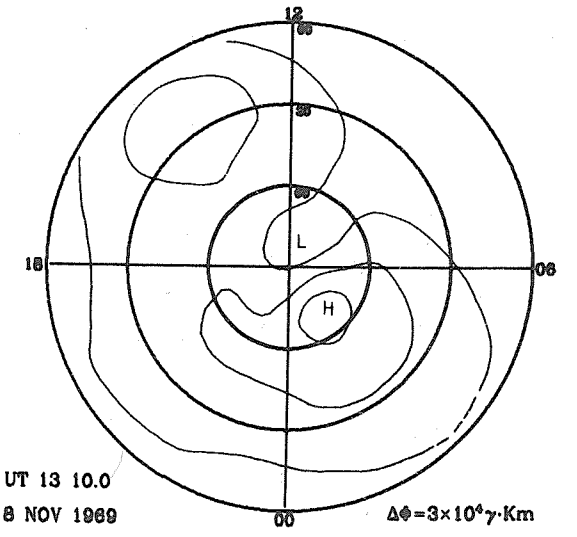
12
00
30
60
18
06
L
H
UT 13 10.0
8 NOV 1969
Δφ=3×10⁴γ·Km

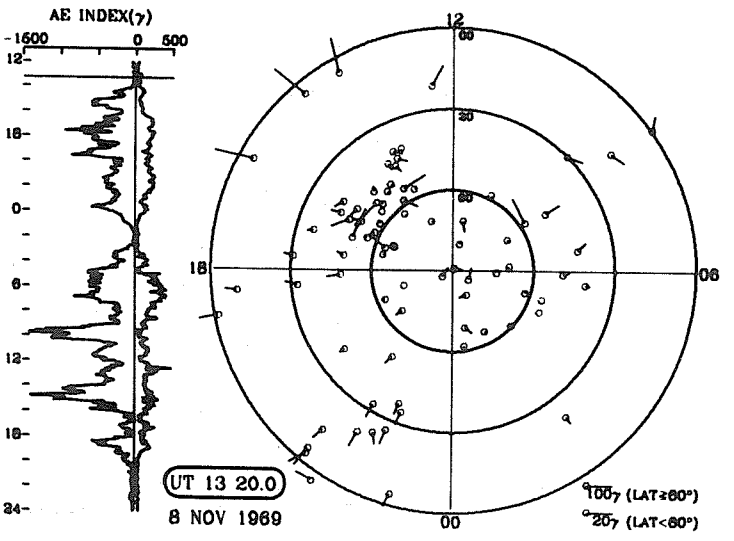
AE INDEX(γ)
-1600
0
500
12
18
0
6
12
18
24
12
00
30
60
18
06
UT 13 20.0
8 NOV 1969
100γ (LAT≥60°)
20γ (LAT<60°)

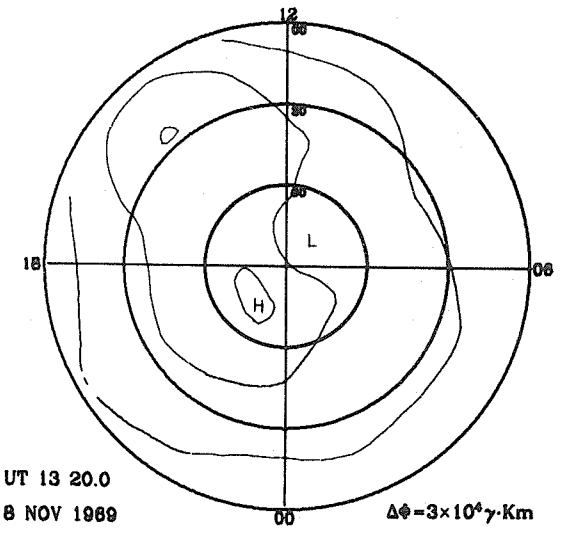
12
00
30
60
18
06
L
H
UT 13 20.0
8 NOV 1969
Δφ=3×10⁴γ·Km

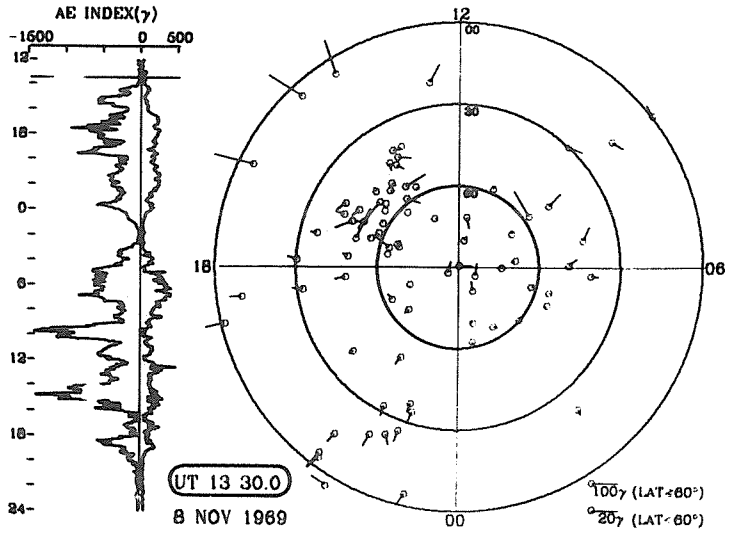
AE INDEX(γ)
-1600
0
600
12
18
0
6
12
18
24
12
00
30
60
18
06
00
UT 13 30.0
8 NOV 1969
100γ (LAT≥60°)
20γ (LAT<60°)

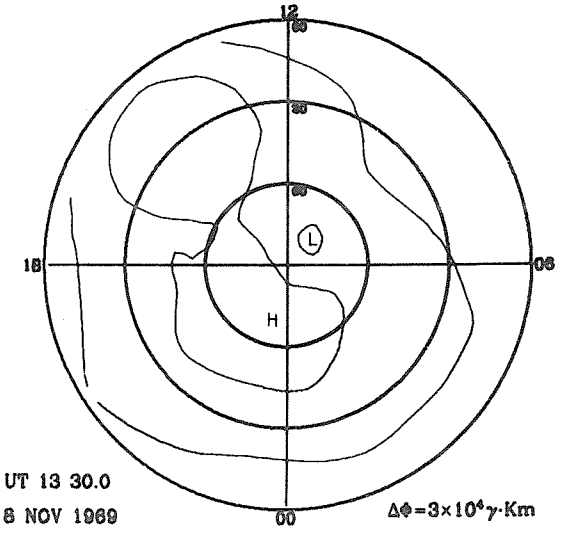
12
00
30
60
18
06
00
L
H
UT 13 30.0
8 NOV 1969
Δφ=3×10⁴γ·Km

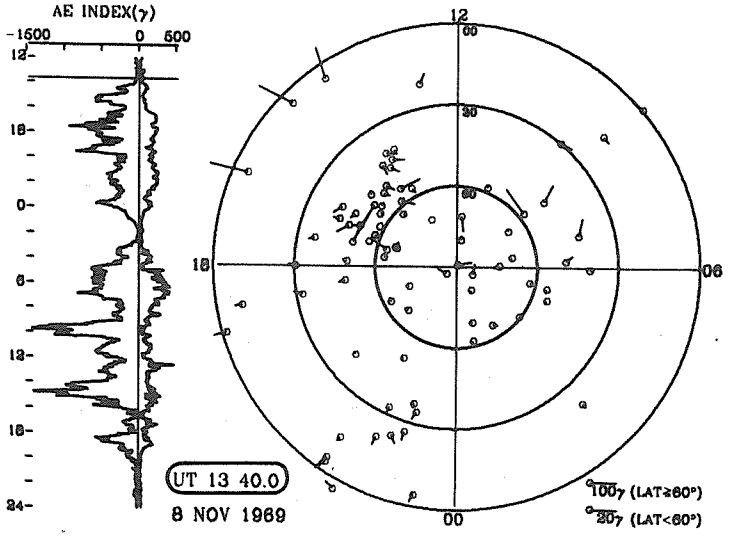
AE INDEX(γ)
-1600
0
600
12
18
0
6
12
18
24
12
00
30
60
18
06
00
UT 13 40.0
8 NOV 1969
100γ (LAT≥60°)
20γ (LAT<60°)

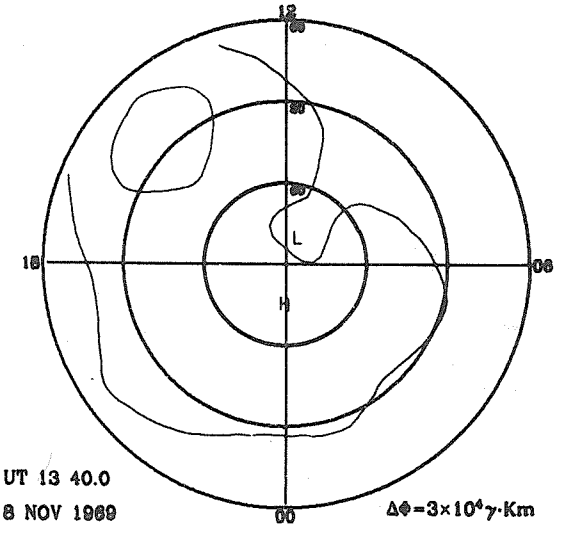
12
00
30
60
18
06
00
L
H
UT 13 40.0
8 NOV 1969
Δφ=3×10⁴γ·Km

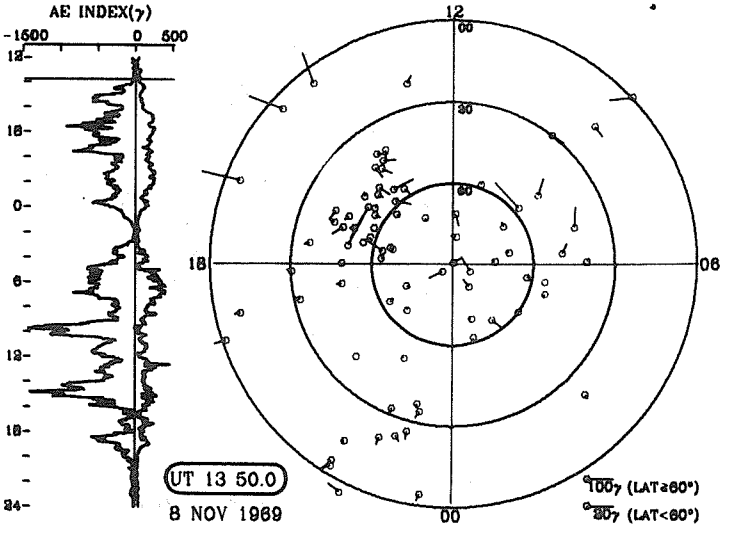
AE INDEX(γ)
-1600
0
600
12
18
0
6
12
18
24
12
00
30
60
18
06
00
UT 13 50.0
8 NOV 1969
100γ (LAT≥60°)
20γ (LAT<60°)

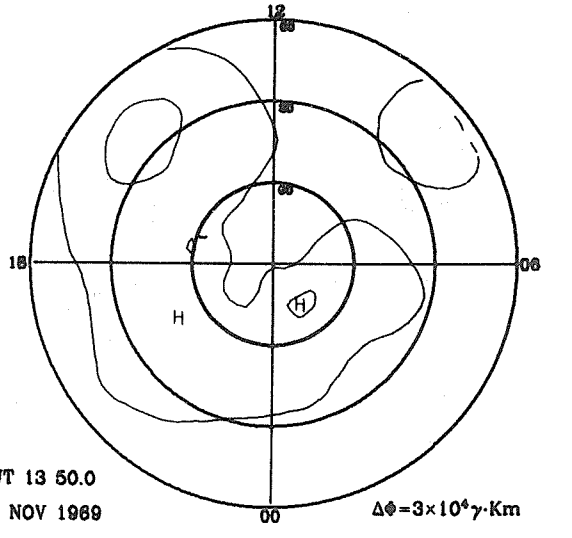
12
00
30
60
18
06
00
H
H
UT 13 50.0
8 NOV 1969
Δφ=3×10⁴γ·Km

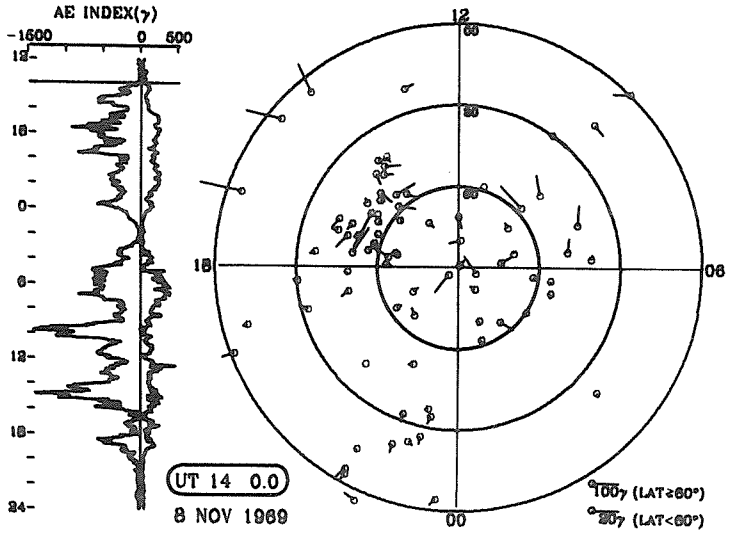
AE INDEX(γ)
-1600
0
600
12
18
0
6
12
18
24
12
18
06
00
30
60
UT 14 0.0
8 NOV 1969
100γ (LAT≥60°)
20γ (LAT<60°)

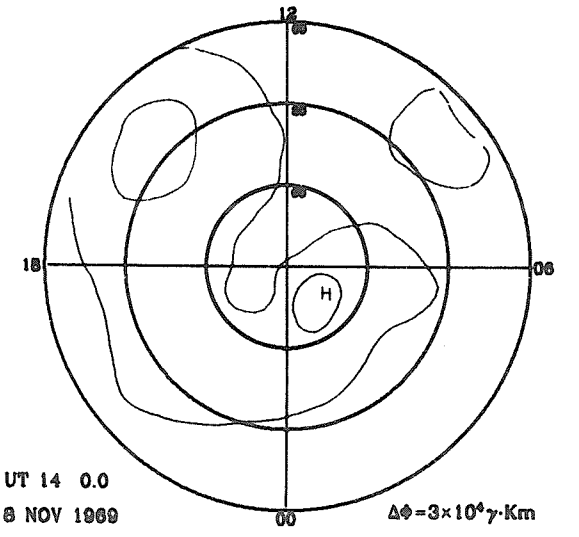
12
18
06
00
30
60
H
UT 14 0.0
8 NOV 1969
Δφ=3×10⁴γ·Km

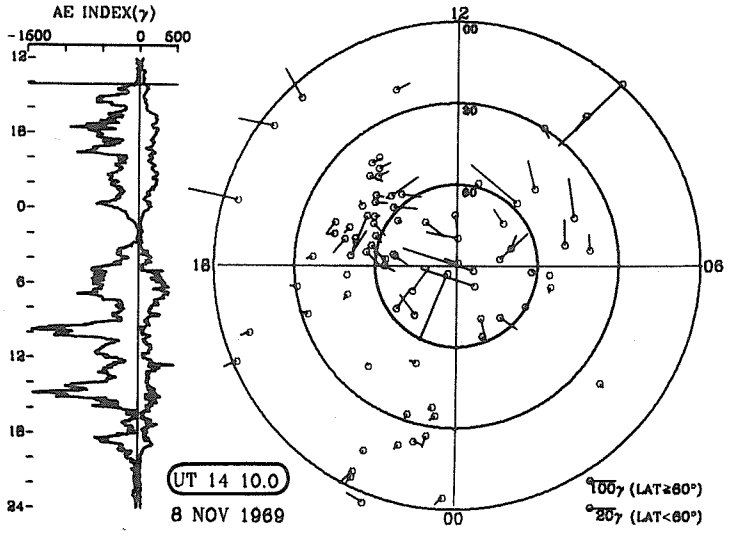
AE INDEX(γ)
-1600
0
600
12
18
0
6
12
18
24
12
18
06
00
30
60
UT 14 10.0
8 NOV 1969
100γ (LAT≥60°)
20γ (LAT<60°)

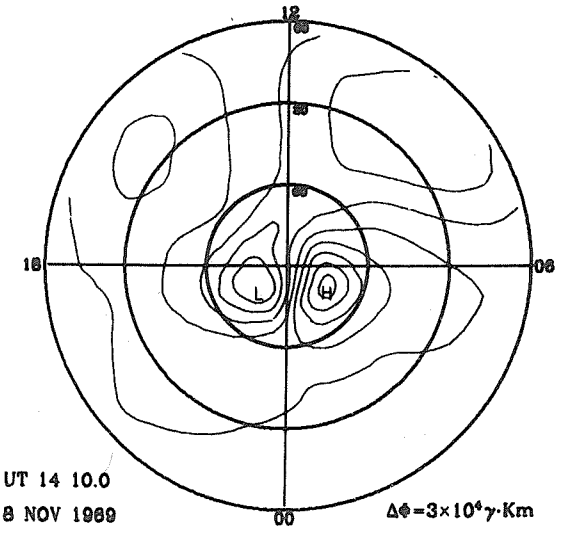
12
18
06
00
30
60
L
H
UT 14 10.0
8 NOV 1969
Δφ=3×10⁴γ·Km

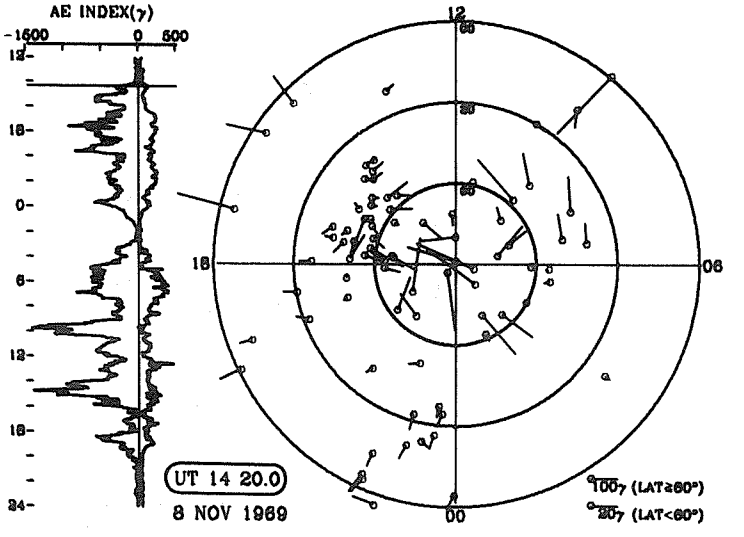
AE INDEX(γ)
-1600
0
600
12
18
0
6
12
18
24
12
18
06
00
30
60
UT 14 20.0
8 NOV 1969
100γ (LAT≥60°)
20γ (LAT<60°)

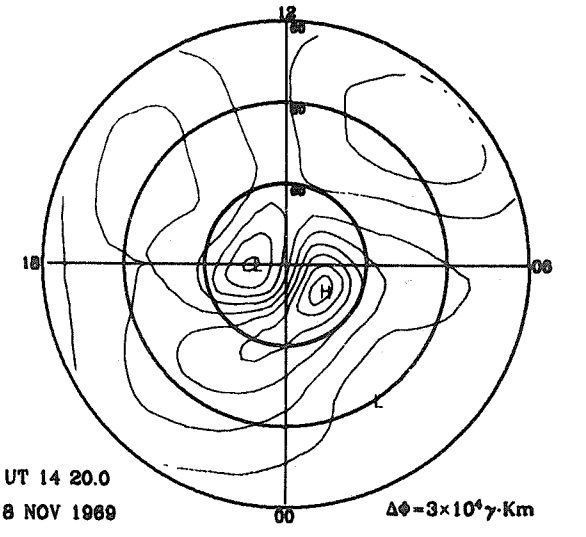
12
18
06
00
30
60
L
H
L
UT 14 20.0
8 NOV 1969
Δφ=3×10⁴γ·Km

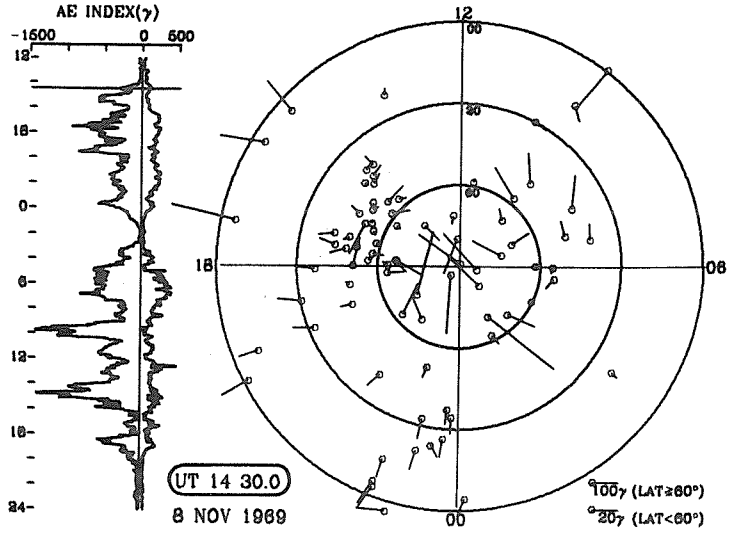
AE INDEX(γ)
-1500
0
500
12
18
0
6
12
18
24
12
00
30
60
18
06
UT 14 30.0
8 NOV 1969
100γ (LAT≥60°)
20γ (LAT<60°)

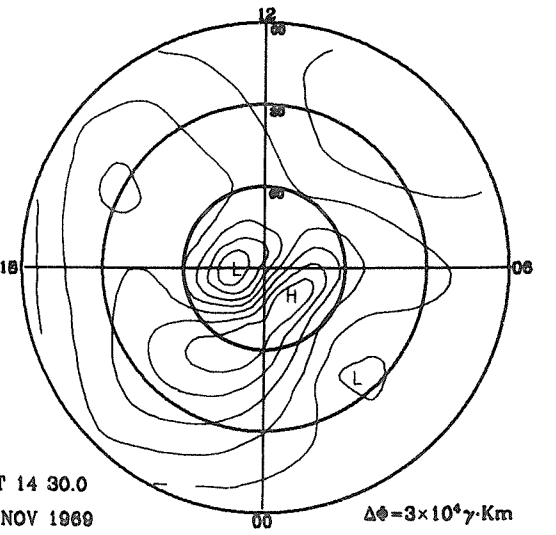
12
00
30
60
18
06
L
H
L
UT 14 30.0
8 NOV 1969
Δφ=3×10⁴γ·Km

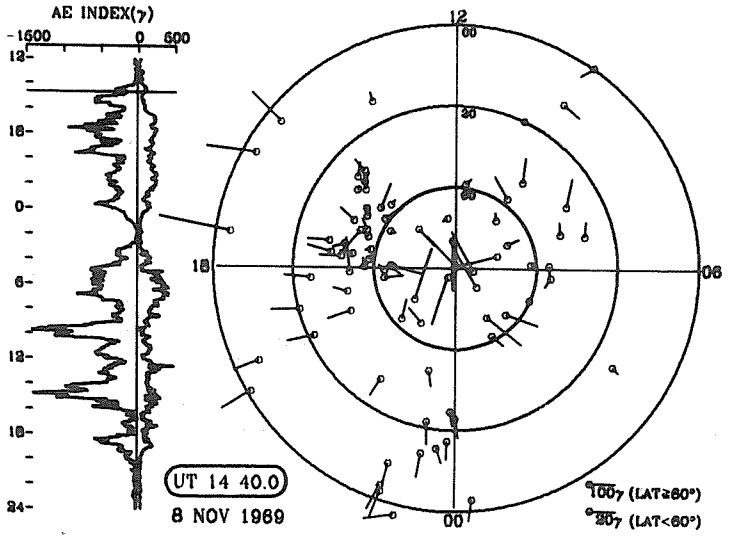
AE INDEX(γ)
-1500
0
500
12
18
0
6
12
18
24
12
00
30
60
18
06
UT 14 40.0
8 NOV 1969
100γ (LAT≥60°)
20γ (LAT<60°)

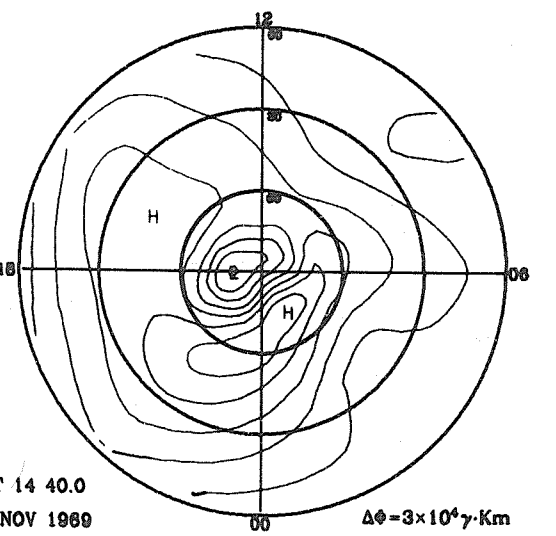
12
00
30
60
18
06
H
L
H
UT 14 40.0
8 NOV 1969
Δφ=3×10⁴γ·Km

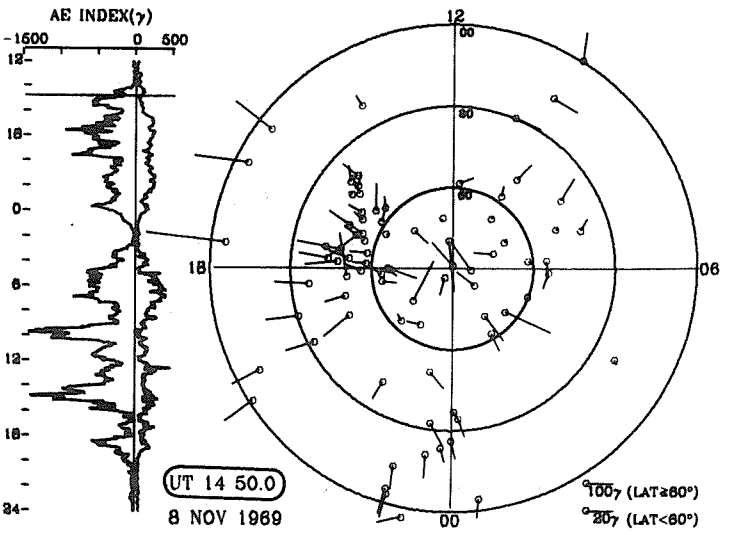
AE INDEX(γ)
-1500
0
500
12
18
0
6
12
18
24
12
00
30
60
18
06
UT 14 50.0
8 NOV 1969
100γ (LAT≥60°)
20γ (LAT<60°)

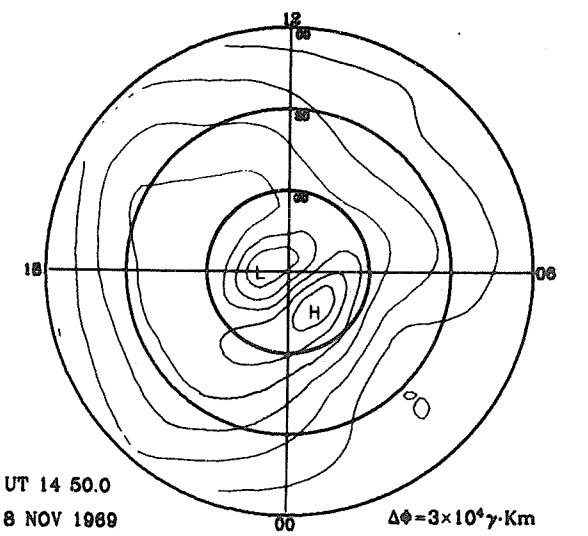
12
00
30
60
18
06
L
H
UT 14 50.0
8 NOV 1969
Δφ=3×10⁴γ·Km

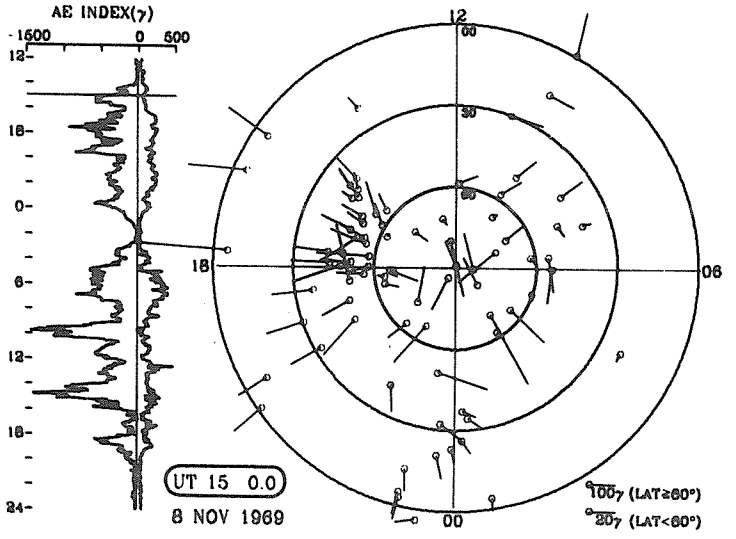
AE INDEX(γ)
-1500
0
500
12
18
0
6
12
18
24
12
00
30
60
18
06
00
UT 15 0.0
8 NOV 1969
100γ (LAT≥60°)
20γ (LAT<60°)

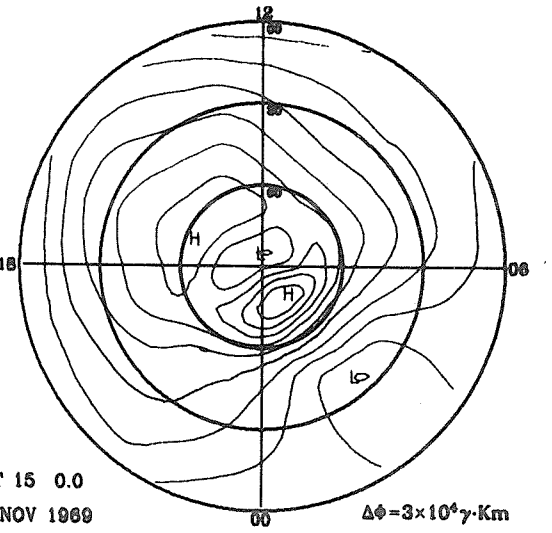
12
00
30
60
18
06
00
H
H
L
UT 15 0.0
8 NOV 1969
Δφ=3×10⁴γ·Km

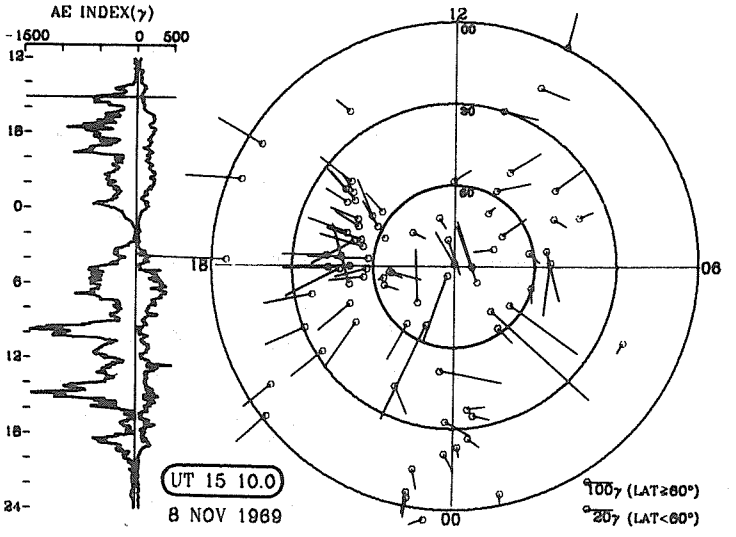
AE INDEX(γ)
-1500
0
500
12
18
0
6
12
18
24
12
00
30
60
18
06
00
UT 15 10.0
8 NOV 1969
100γ (LAT≥60°)
20γ (LAT<60°)

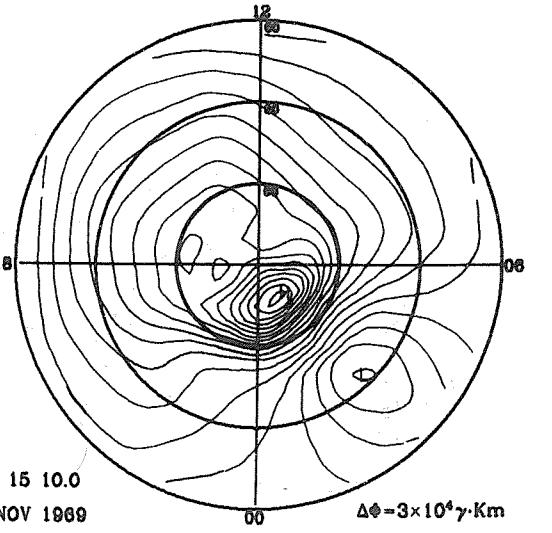
12
00
30
60
18
06
00
UT 15 10.0
8 NOV 1969
Δφ=3×10⁴γ·Km

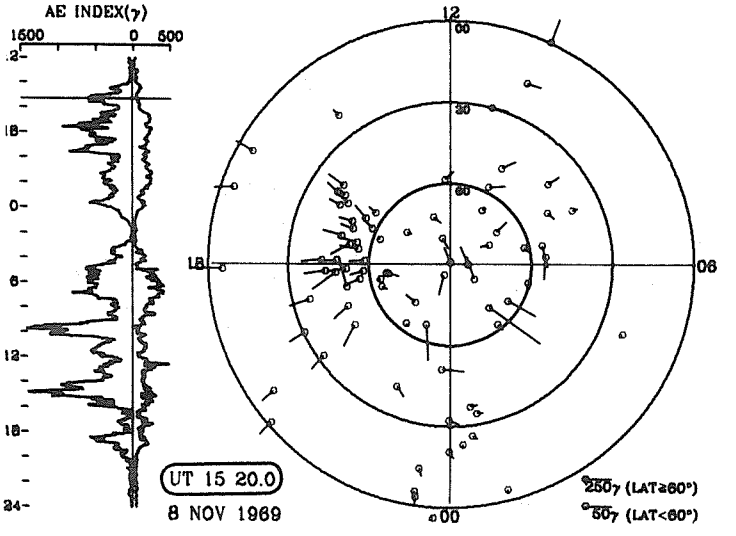
AE INDEX(γ)
1500
0
500
12
18
0
6
12
18
24
12
00
30
60
18
06
00
UT 15 20.0
8 NOV 1969
250γ (LAT≥60°)
50γ (LAT<60°)

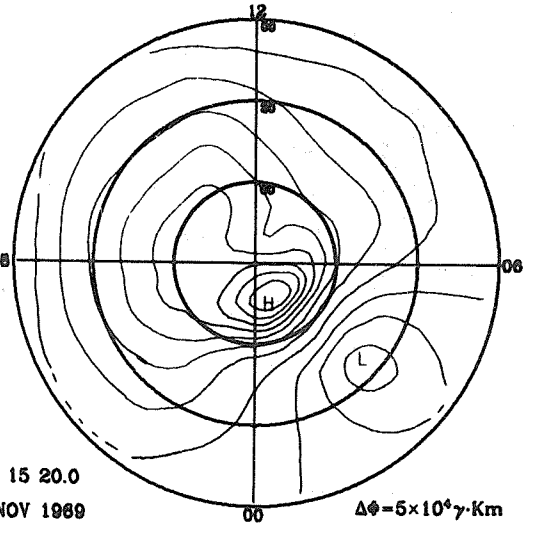
12
00
30
60
18
06
00
H
L
UT 15 20.0
8 NOV 1969
Δφ=5×10⁴γ·Km

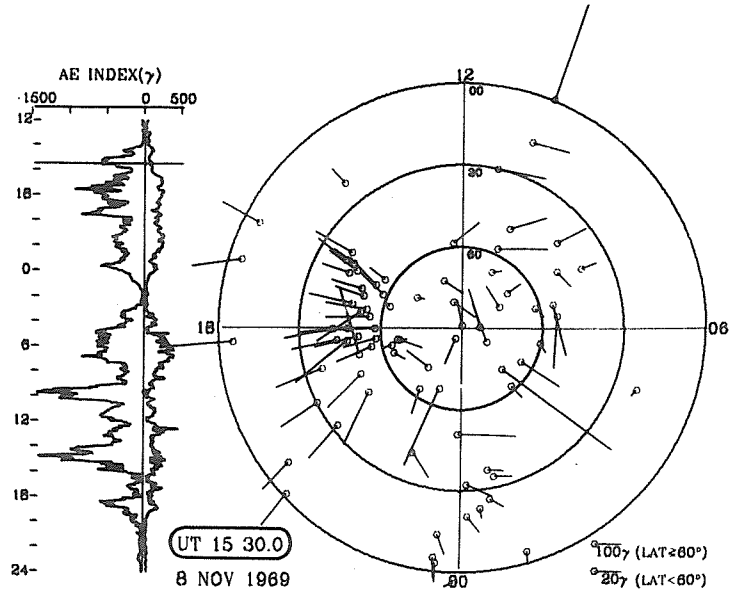
AE INDEX(γ)
-1600
0
500
12
18
0
6
12
18
24
12
00
30
60
18
06
00
UT 15 30.0
8 NOV 1969
100γ (LAT≥60°)
20γ (LAT<60°)

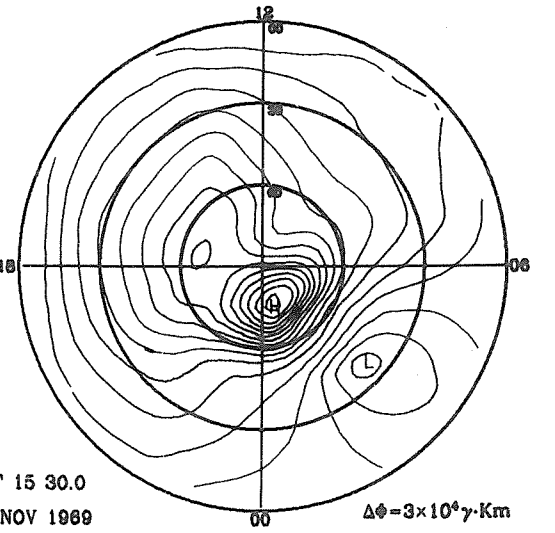
12
00
30
60
18
06
00
H
L
UT 15 30.0
8 NOV 1969
Δ∅=3×10⁴γ·Km

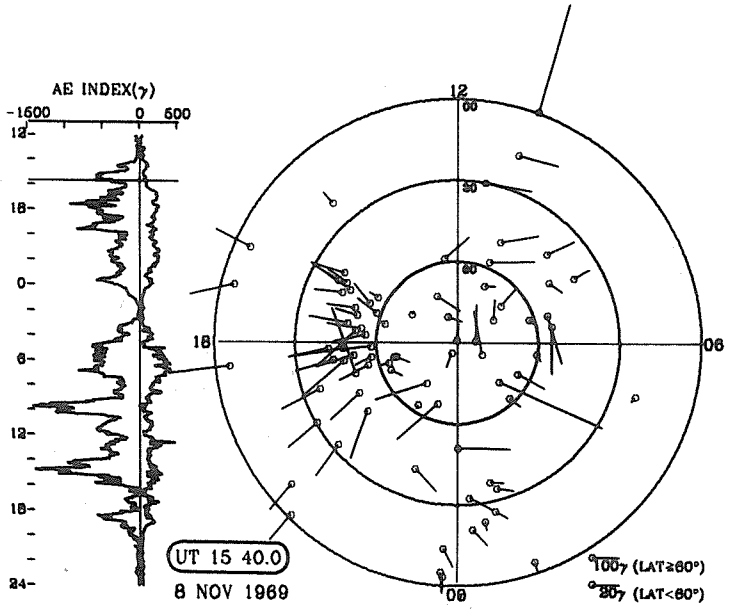
AE INDEX(γ)
-1600
0
500
12
18
0
6
12
18
24
12
00
30
60
18
06
00
UT 15 40.0
8 NOV 1969
100γ (LAT≥60°)
20γ (LAT<60°)

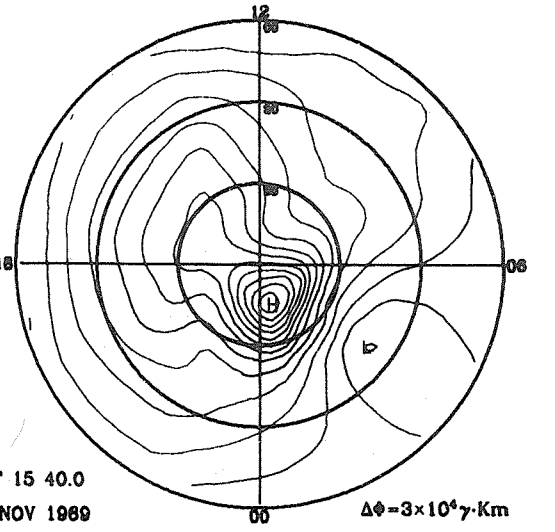
12
00
30
60
18
06
00
H
L
UT 15 40.0
8 NOV 1969
Δ∅=3×10⁴γ·Km

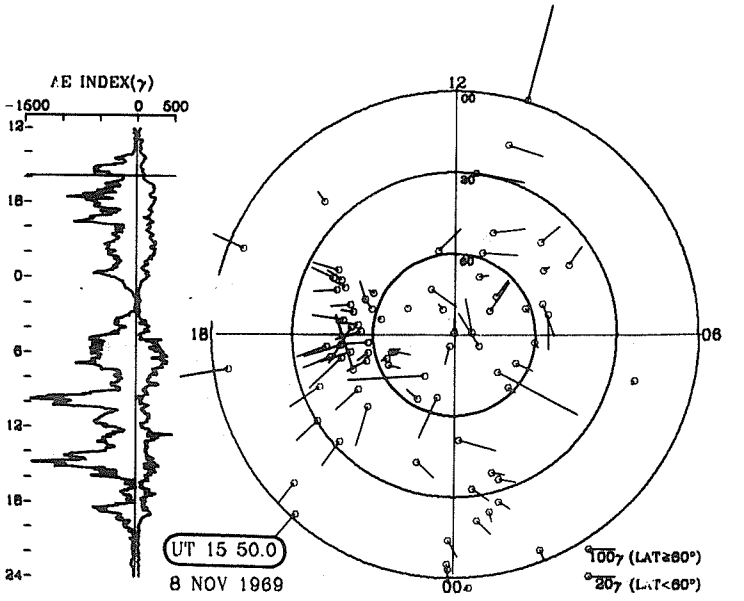
AE INDEX(γ)
-1600
0
500
12
18
0
6
12
18
24
12
00
30
60
18
06
00
UT 15 50.0
8 NOV 1969
100γ (LAT≥60°)
20γ (LAT<60°)

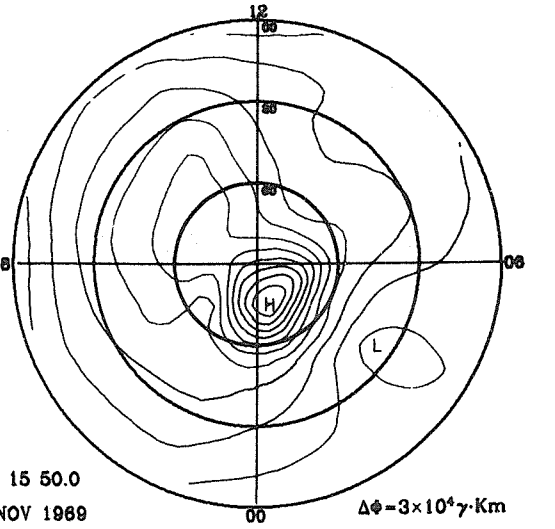
12
00
30
60
18
06
00
H
L
UT 15 50.0
8 NOV 1969
Δ∅=3×10⁴γ·Km

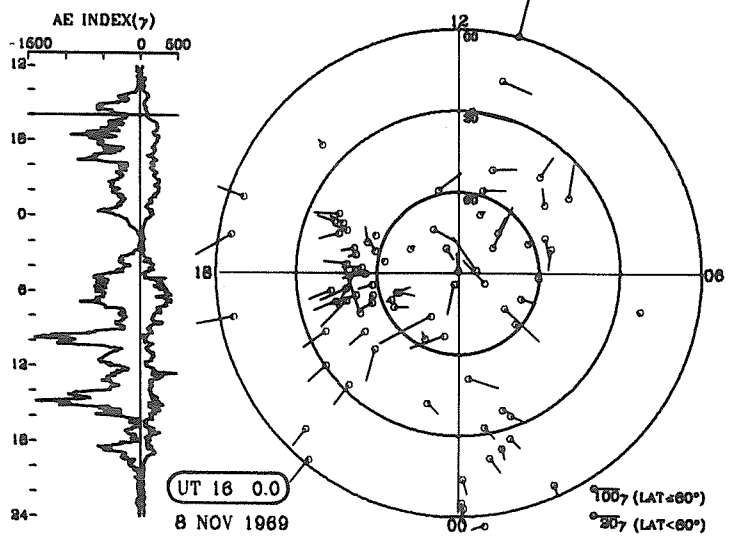
AE INDEX(γ)
-1600
0
500
12
18
0
6
12
18
24
12
60
30
60
18
06
00
UT 16 0.0
8 NOV 1969
100γ (LAT≥60°)
20γ (LAT<60°)

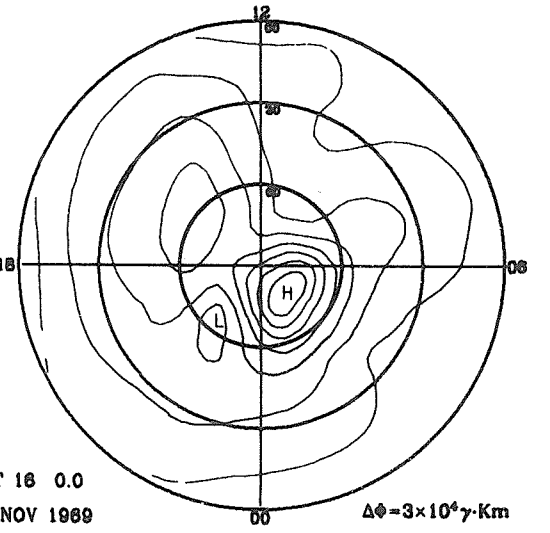
12
60
30
60
18
06
00
H
L
UT 16 0.0
8 NOV 1969
Δφ=3×10⁴γ·Km

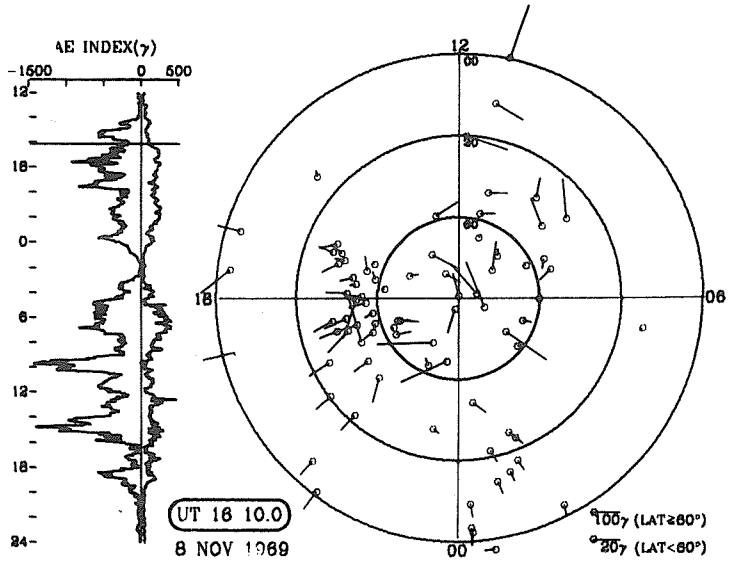
AE INDEX(γ)
-1600
0
500
12
18
0
6
12
18
24
12
60
30
60
18
06
00
UT 16 10.0
8 NOV 1969
100γ (LAT≥60°)
20γ (LAT<60°)

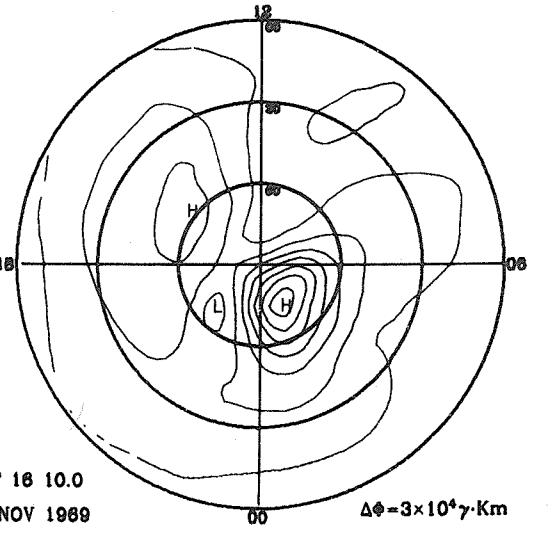
12
60
30
60
18
06
00
H
L
H
UT 16 10.0
8 NOV 1969
Δφ=3×10⁴γ·Km

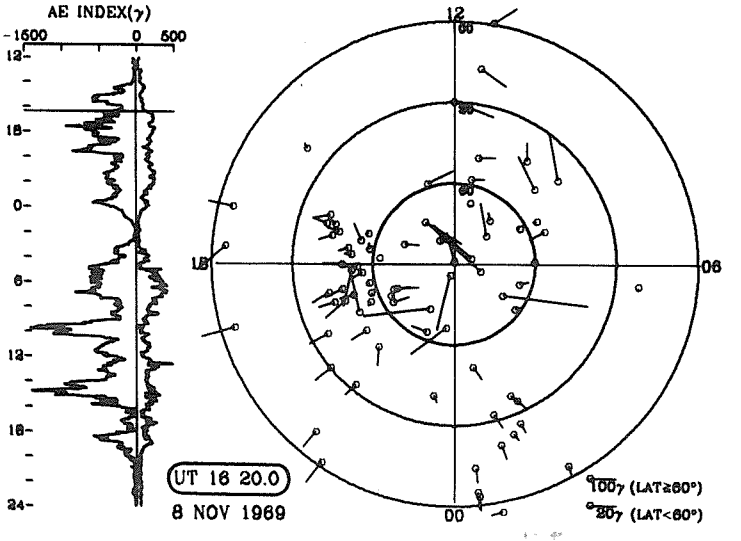
AE INDEX(γ)
-1600
0
500
12
18
0
6
12
18
24
12
60
30
60
18
06
00
UT 16 20.0
8 NOV 1969
100γ (LAT≥60°)
20γ (LAT<60°)

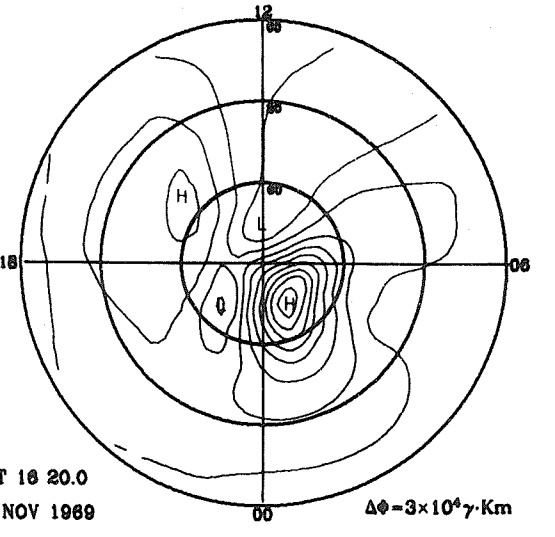
12
60
30
60
18
06
00
H
L
H
UT 16 20.0
8 NOV 1969
Δφ=3×10⁴γ·Km

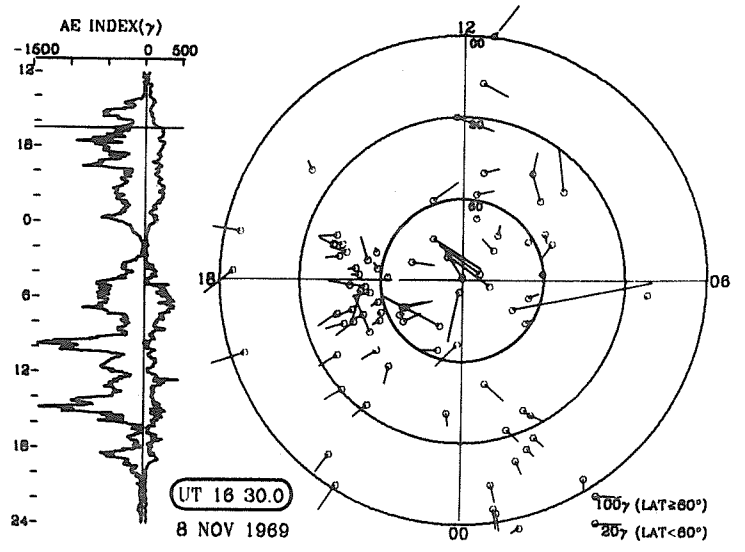
AE INDEX(γ)
-1600
0
500
12
18
0
6
12
18
24
12
00
18
06
UT 16 30.0
8 NOV 1969
100γ (LAT≥60°)
20γ (LAT<60°)

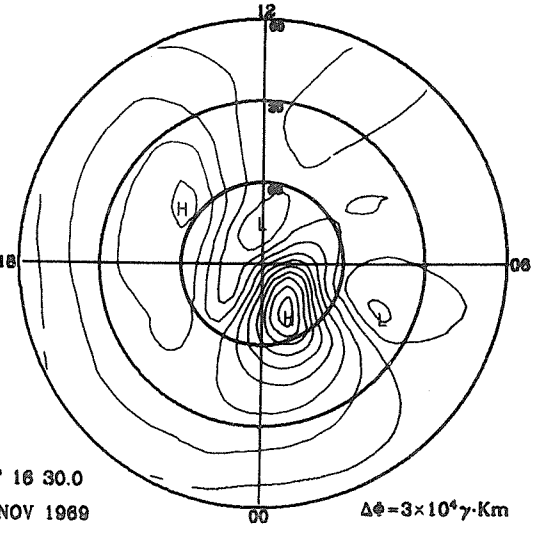
12
00
18
06
H
L
UT 16 30.0
8 NOV 1969
Δφ=3×10⁴γ·Km

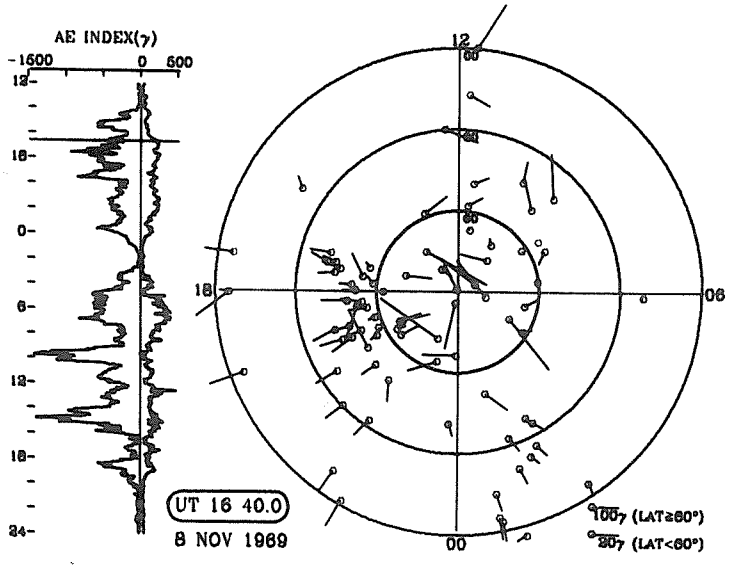
AE INDEX(γ)
-1600
0
500
12
18
0
6
12
18
24
12
00
18
06
UT 16 40.0
8 NOV 1969
100γ (LAT≥60°)
20γ (LAT<60°)

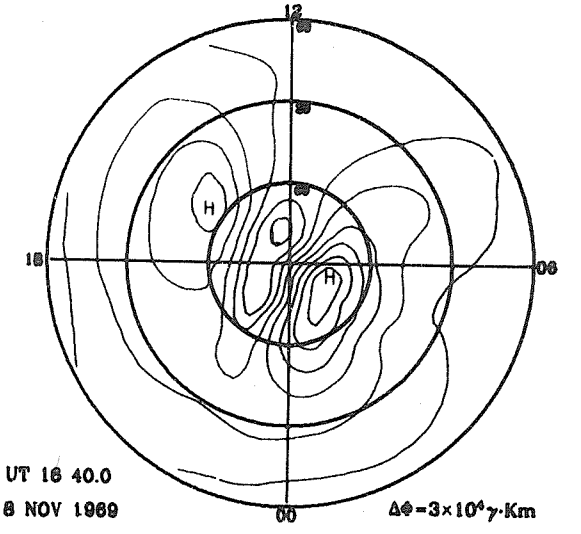
12
00
18
06
H
UT 16 40.0
8 NOV 1969
Δφ=3×10⁴γ·Km

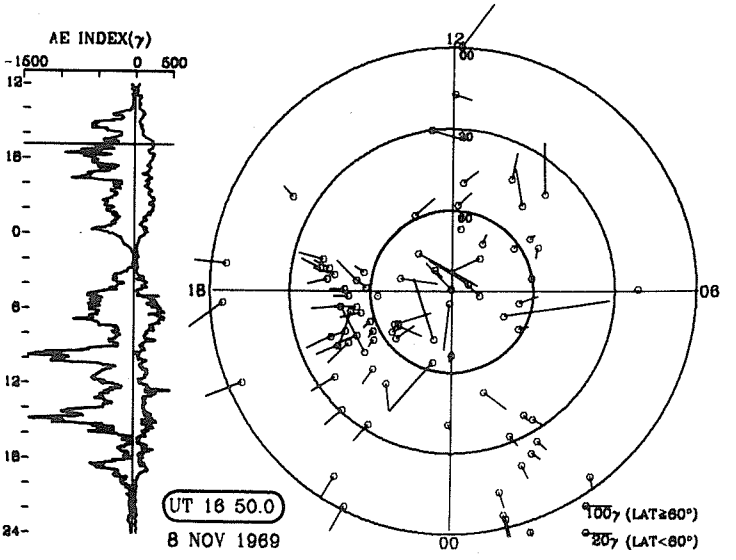
AE INDEX(γ)
-1600
0
500
12
18
0
6
12
18
24
12
00
18
06
UT 16 50.0
8 NOV 1969
100γ (LAT≥60°)
20γ (LAT<60°)

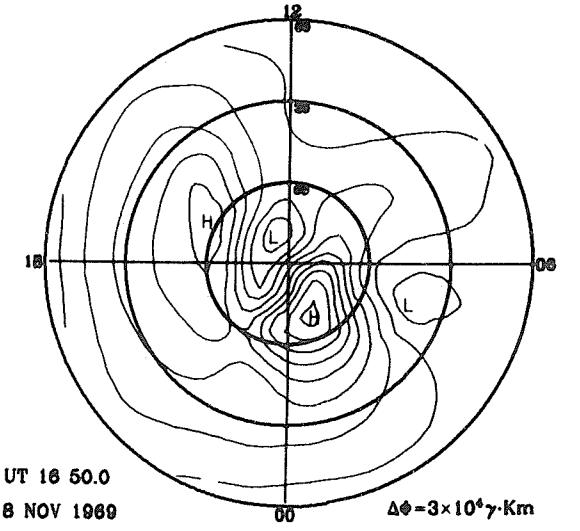
12
00
18
06
H
L
UT 16 50.0
8 NOV 1969
Δφ=3×10⁴γ·Km

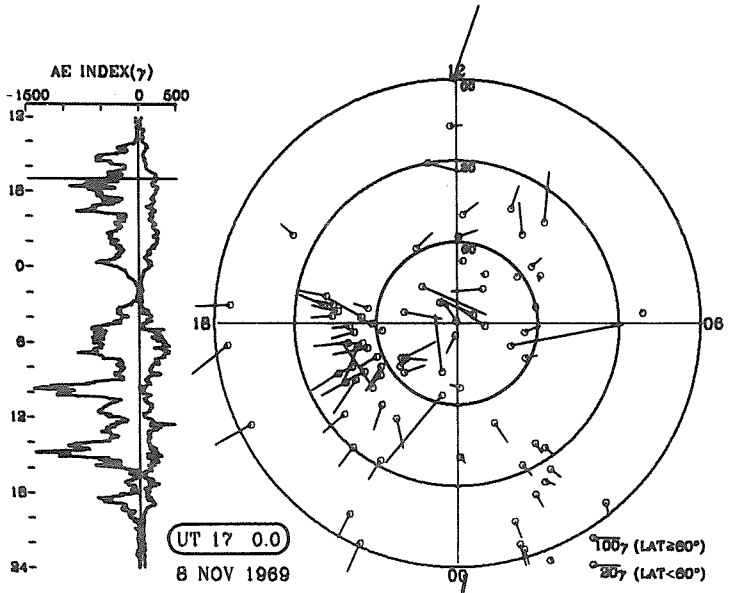
AE INDEX(γ)
-1500
0
500
12
18
0
6
12
18
24
12
18
06
00
UT 17 0.0
8 NOV 1969
100γ (LAT≥60°)
20γ (LAT<60°)

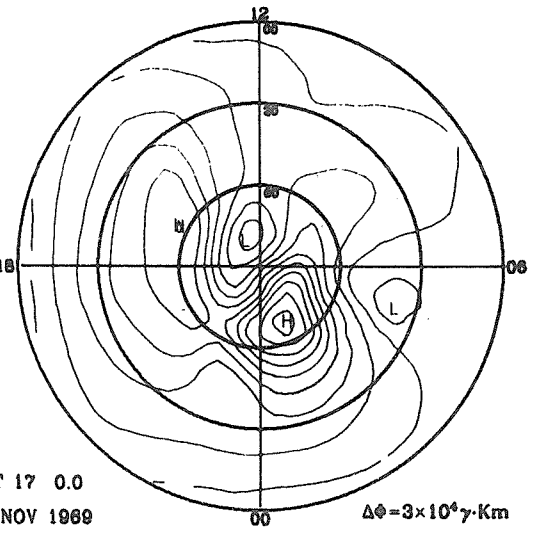
12
18
06
00
H
L
UT 17 0.0
8 NOV 1969
Δ∅=3×10⁴γ·Km

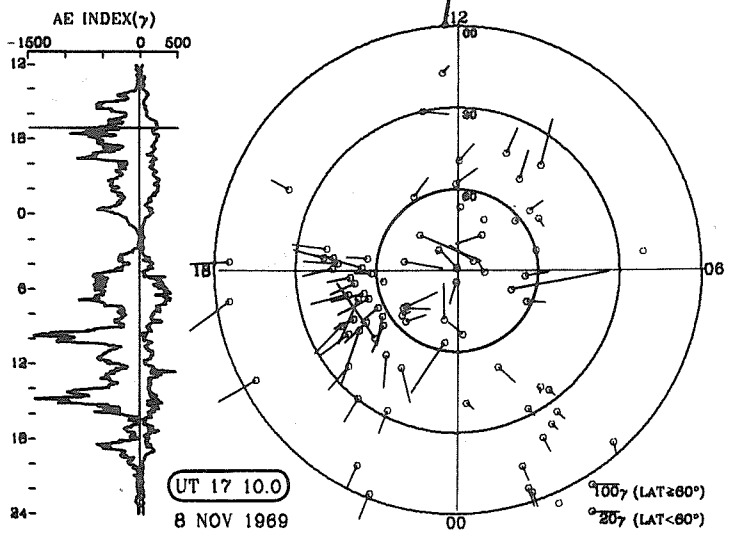
AE INDEX(γ)
-1500
0
500
12
18
0
6
12
18
24
12
18
06
00
UT 17 10.0
8 NOV 1969
100γ (LAT≥60°)
20γ (LAT<60°)

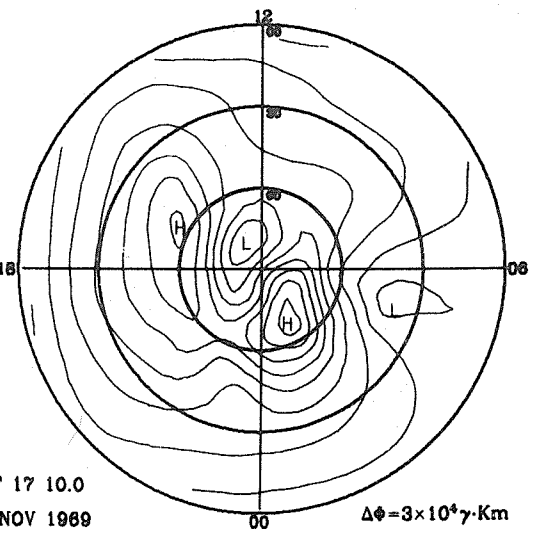
12
18
06
00
H
L
UT 17 10.0
8 NOV 1969
Δ∅=3×10⁴γ·Km

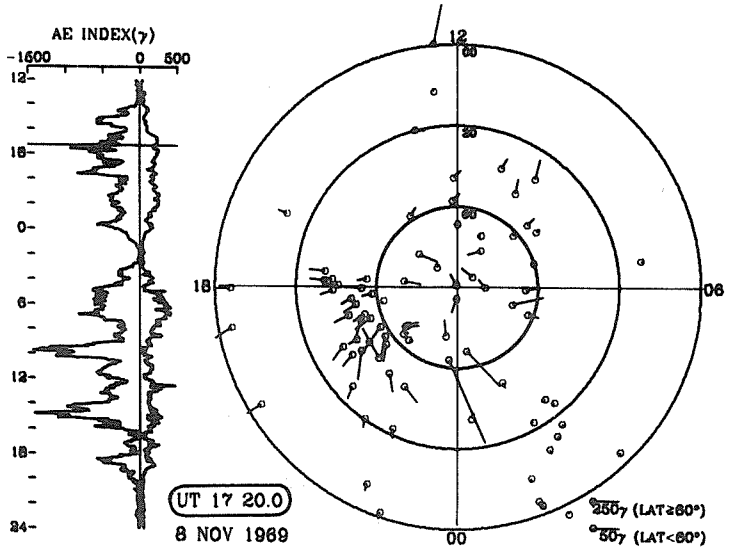
AE INDEX(γ)
-1500
0
500
12
18
0
6
12
18
24
12
18
06
00
UT 17 20.0
8 NOV 1969
250γ (LAT≥60°)
50γ (LAT<60°)

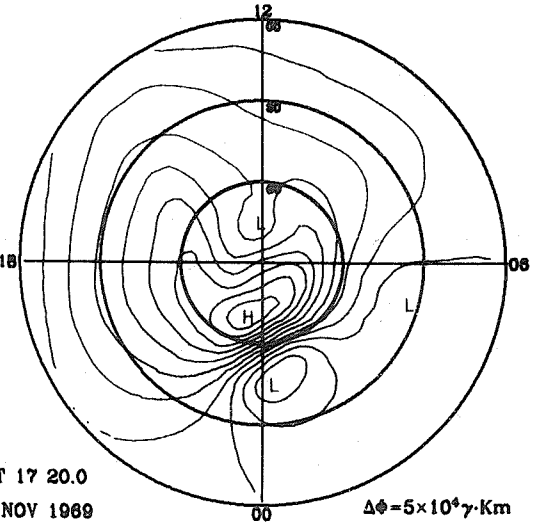
12
18
06
00
H
L
UT 17 20.0
8 NOV 1969
Δ∅=5×10⁴γ·Km

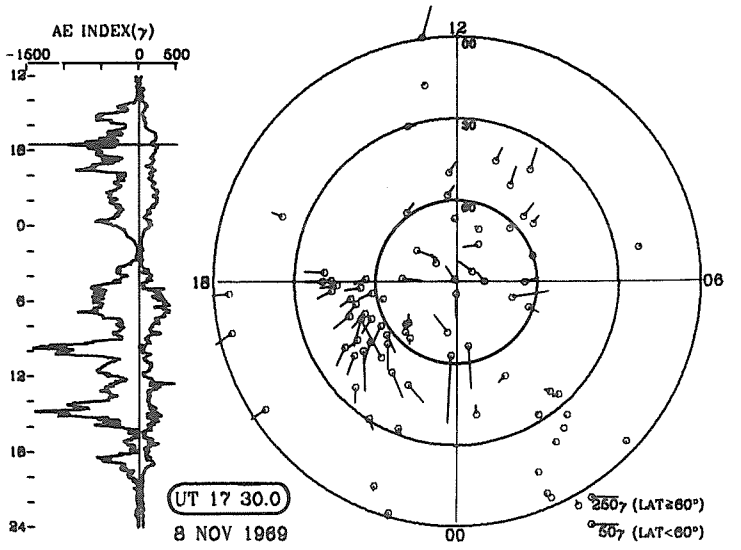
AE INDEX(γ)
-1600
0
500
12
18
0
6
12
18
24
12
60
30
60
18
06
00
UT 17 30.0
8 NOV 1969
250γ (LAT≥60°)
50γ (LAT<60°)

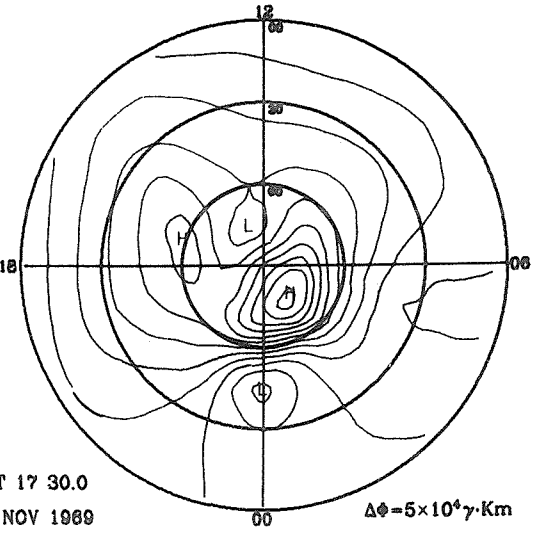
12
60
30
60
18
06
00
H
L
H
L
UT 17 30.0
8 NOV 1969
Δφ=5×10⁴γ·Km

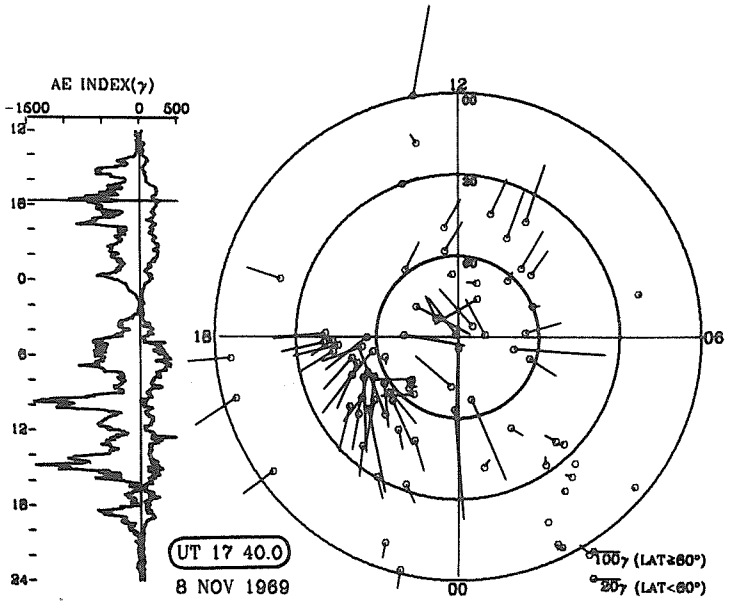
AE INDEX(γ)
-1600
0
500
12
18
0
6
12
18
24
12
60
30
60
18
06
00
UT 17 40.0
8 NOV 1969
100γ (LAT≥60°)
20γ (LAT<60°)

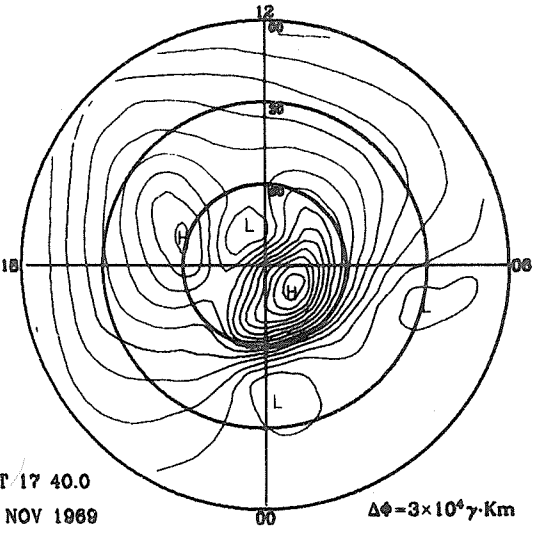
12
60
30
60
18
06
00
H
L
H
L
L
UT 17 40.0
8 NOV 1969
Δφ=3×10⁴γ·Km

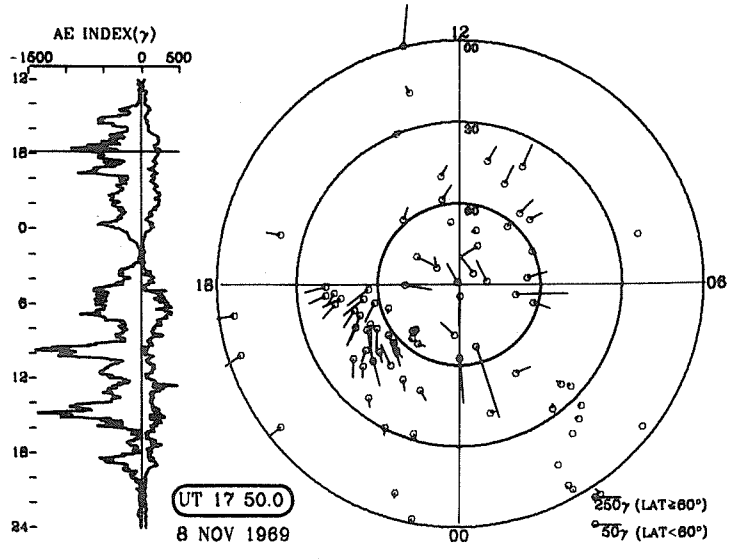
AE INDEX(γ)
-1600
0
500
12
18
0
6
12
18
24
12
60
30
60
18
06
00
UT 17 50.0
8 NOV 1969
250γ (LAT≥60°)
50γ (LAT<60°)

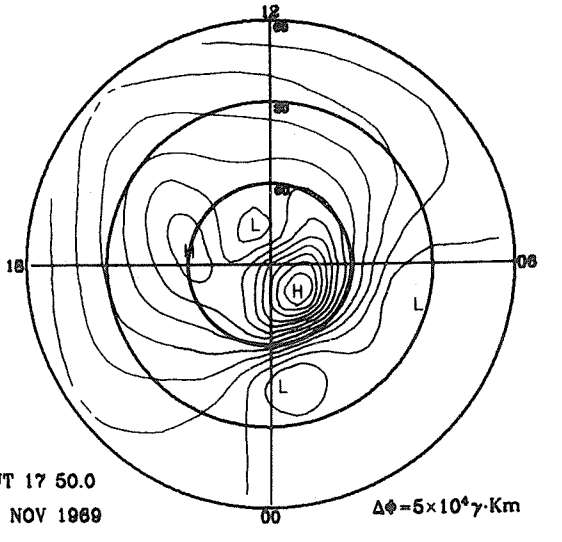
12
60
30
60
18
06
00
H
L
H
L
L
UT 17 50.0
8 NOV 1969
Δφ=5×10⁴γ·Km

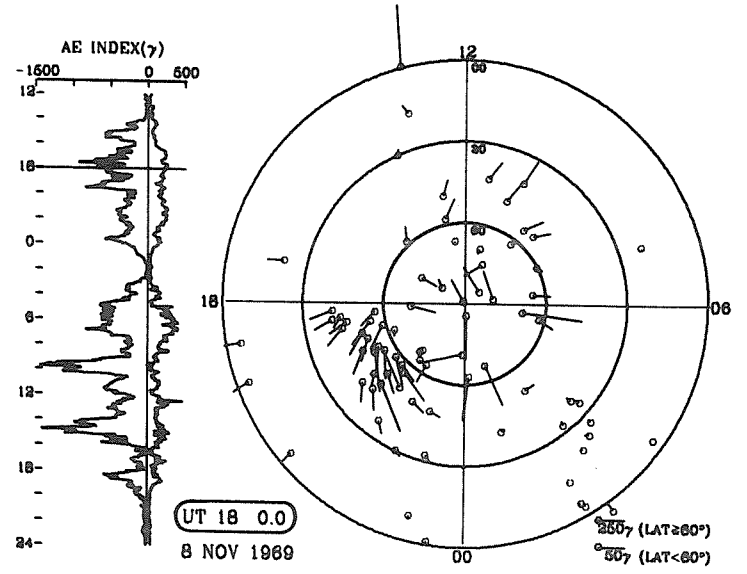
AE INDEX(γ)
-1600
0
600
12
18
0
6
12
18
24
12
00
30
60
18
06
UT 18 0.0
8 NOV 1969
250γ (LAT≥60°)
50γ (LAT<60°)

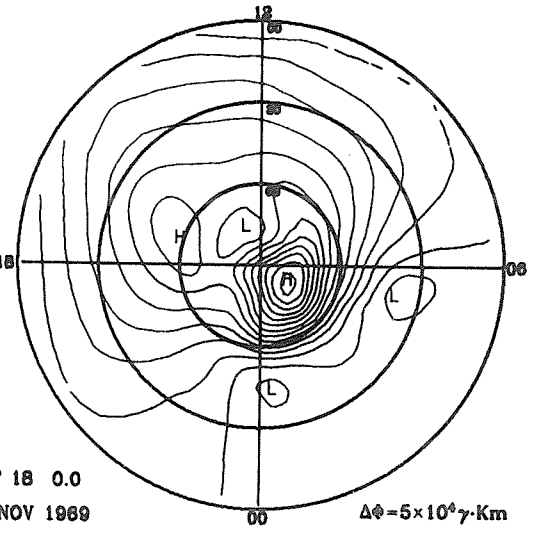
12
00
30
60
18
06
H
L
UT 18 0.0
8 NOV 1969
Δφ=5×10⁴γ·Km

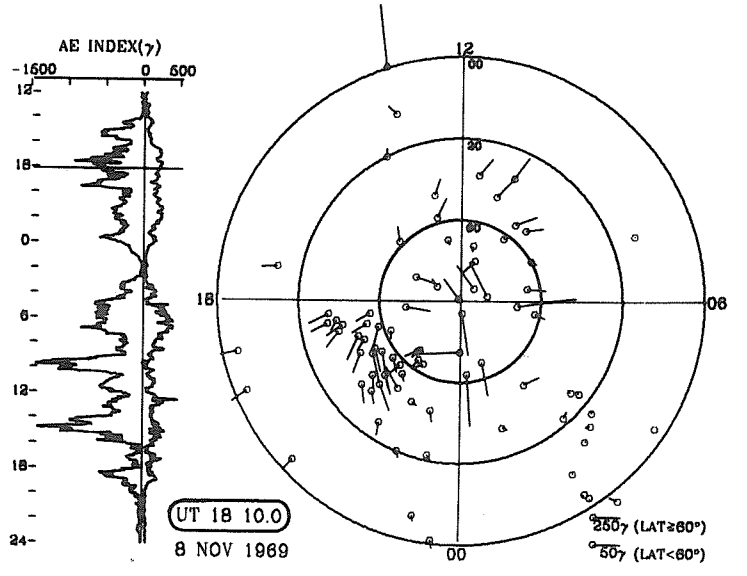
AE INDEX(γ)
-1600
0
600
12
18
0
6
12
18
24
12
00
30
60
18
06
UT 18 10.0
8 NOV 1969
250γ (LAT≥60°)
50γ (LAT<60°)

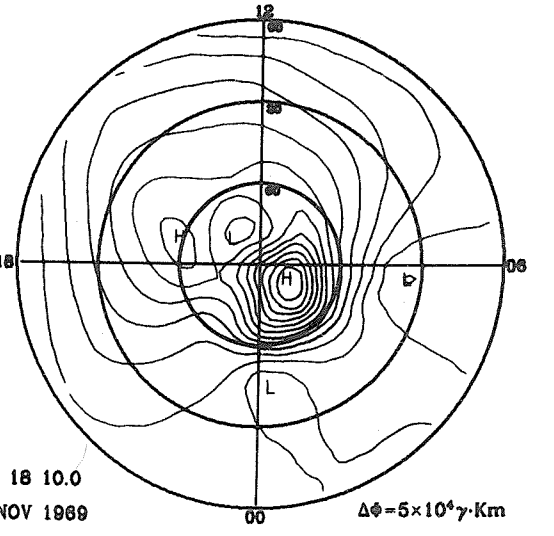
12
00
30
60
18
06
H
L
UT 18 10.0
8 NOV 1969
Δφ=5×10⁴γ·Km

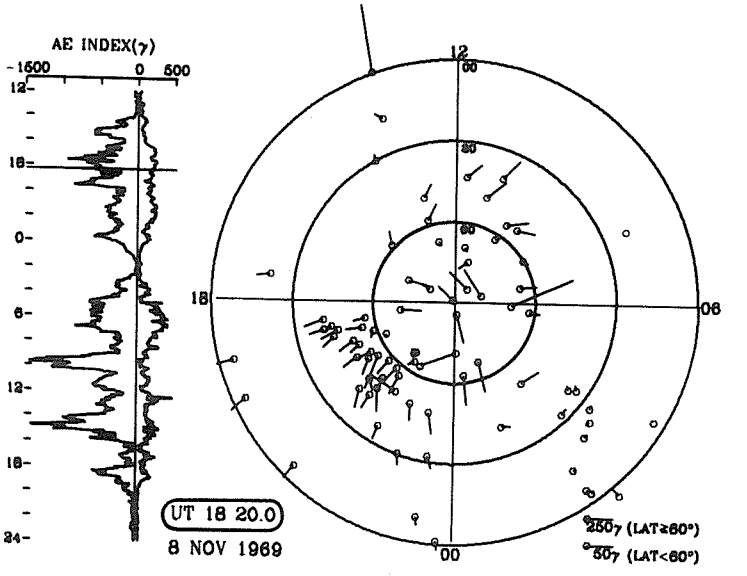
AE INDEX(γ)
-1600
0
600
12
18
0
6
12
18
24
12
00
30
60
18
06
UT 18 20.0
8 NOV 1969
250γ (LAT≥60°)
50γ (LAT<60°)

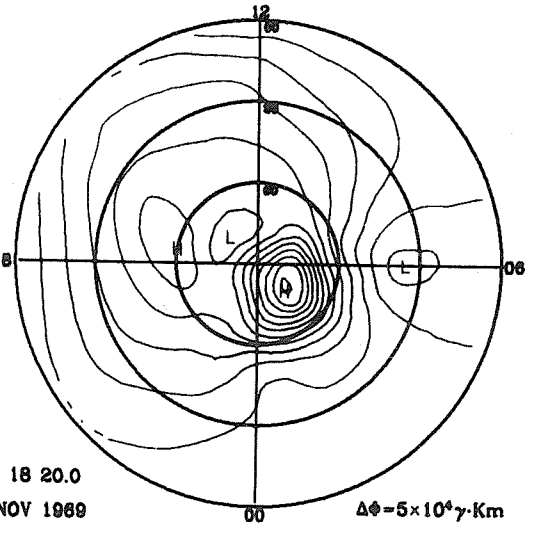
12
00
30
60
18
06
H
L
UT 18 20.0
8 NOV 1969
Δφ=5×10⁴γ·Km

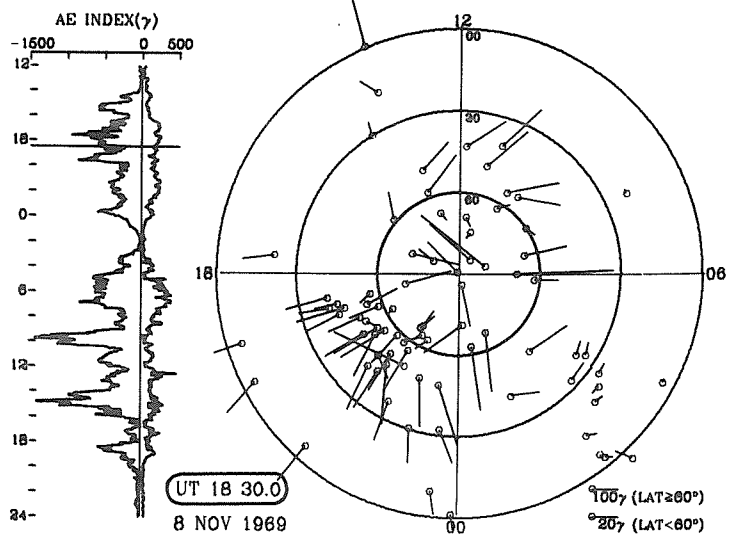
AE INDEX(γ)
-1600
0
500
12
18
0
6
12
18
24
12
00
30
60
18
06
UT 18 30.0
8 NOV 1969
100γ (LAT≥60°)
20γ (LAT<60°)

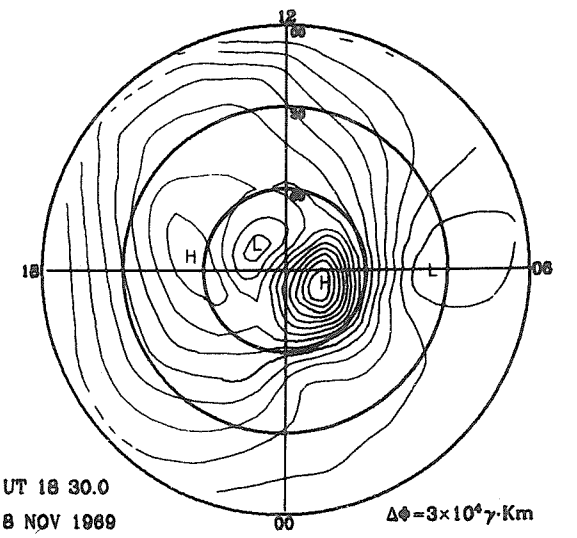
12
00
30
60
18
06
H
L
UT 18 30.0
8 NOV 1969
Δφ=3×10⁴γ·Km

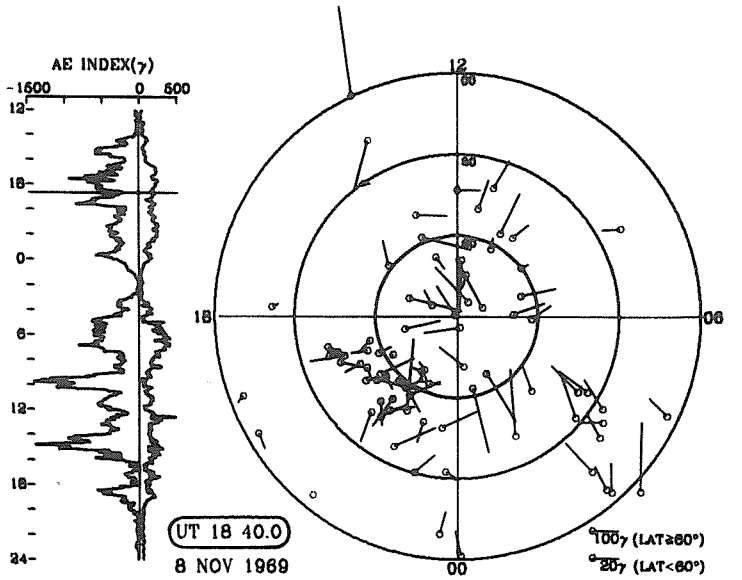
AE INDEX(γ)
-1600
0
500
12
18
0
6
12
18
24
12
00
30
60
18
06
UT 18 40.0
8 NOV 1969
100γ (LAT≥60°)
20γ (LAT<60°)

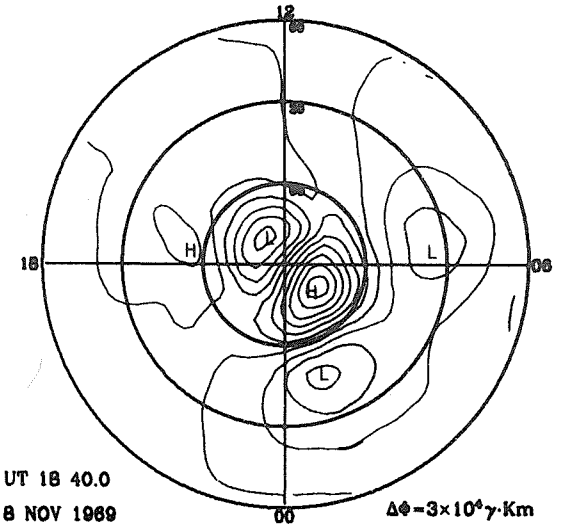
12
00
30
60
18
06
H
L
UT 18 40.0
8 NOV 1969
Δφ=3×10⁴γ·Km

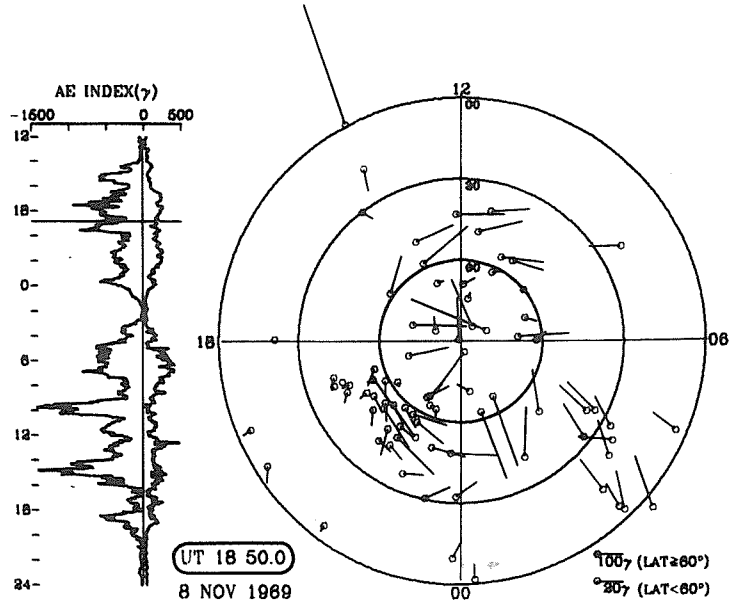
AE INDEX(γ)
-1600
0
500
12
18
0
6
12
18
24
12
00
30
60
18
06
UT 18 50.0
8 NOV 1969
100γ (LAT≥60°)
20γ (LAT<60°)

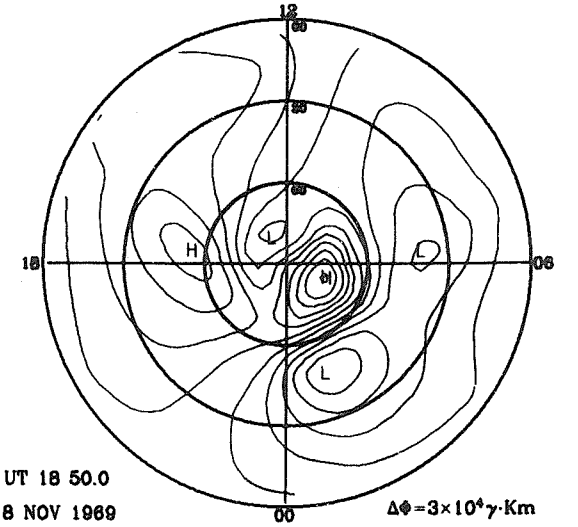
12
00
30
60
18
06
H
L
UT 18 50.0
8 NOV 1969
Δφ=3×10⁴γ·Km

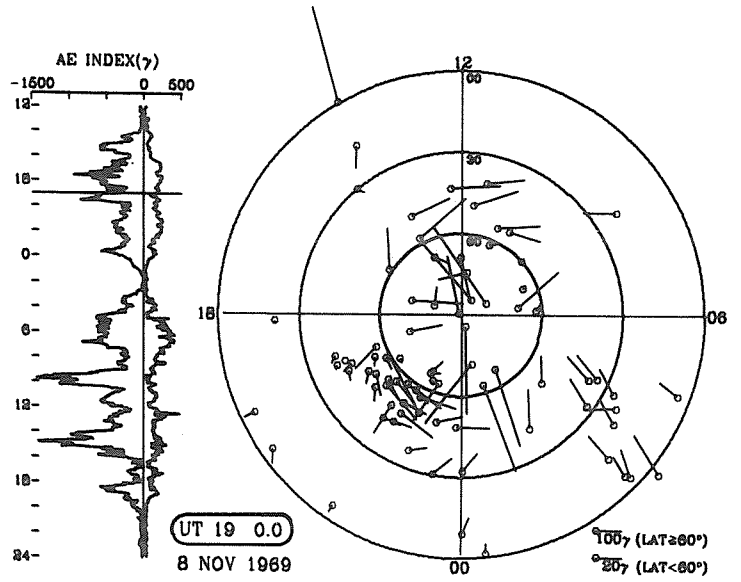
AE INDEX(γ)
-1600
0
500
12
18
0
6
12
18
24
12
00
30
60
18
06
UT 19 0.0
8 NOV 1969
100γ (LAT≥60°)
20γ (LAT<60°)

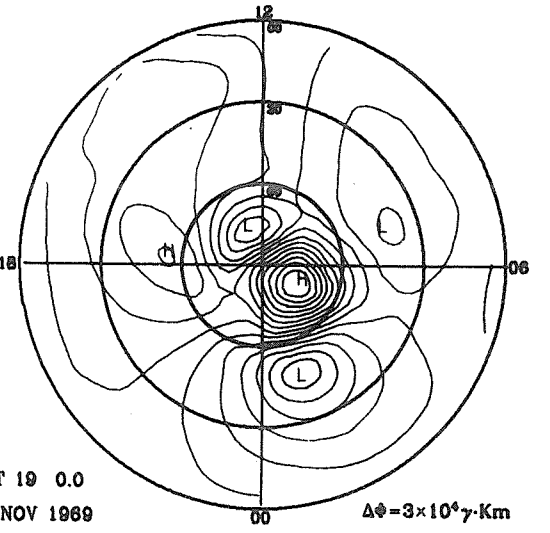
12
00
30
60
18
06
H
L
L
UT 19 0.0
8 NOV 1969
Δφ=3×10⁴γ·Km

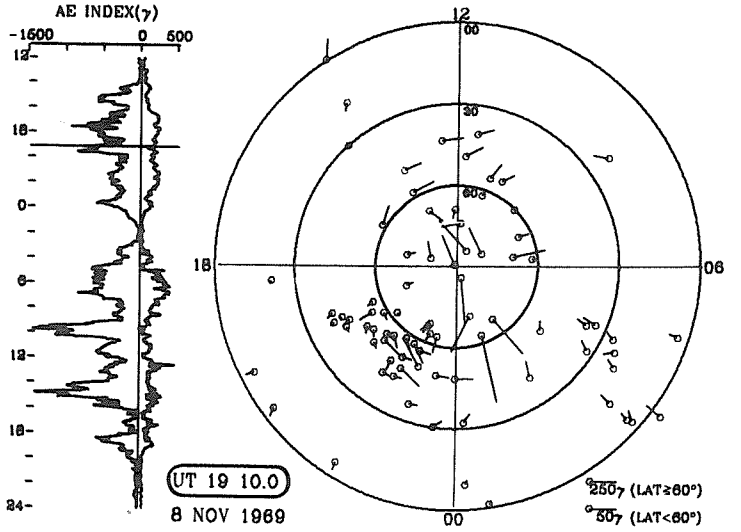
AE INDEX(γ)
-1600
0
500
12
18
0
6
12
18
24
12
00
30
60
18
06
UT 19 10.0
8 NOV 1969
250γ (LAT≥60°)
50γ (LAT<60°)

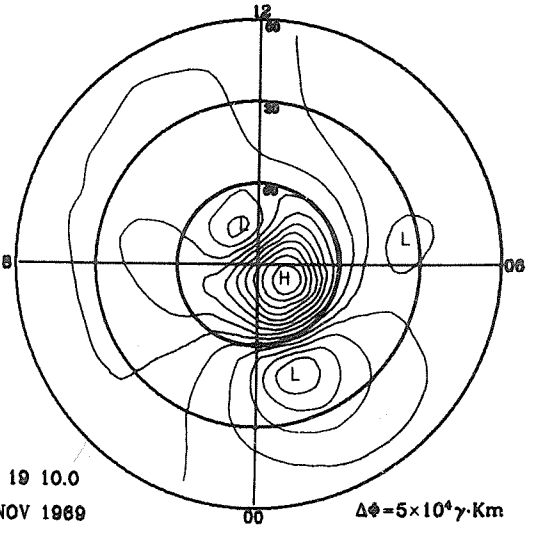
12
00
30
60
18
06
H
L
L
UT 19 10.0
8 NOV 1969
Δφ=5×10⁴γ·Km

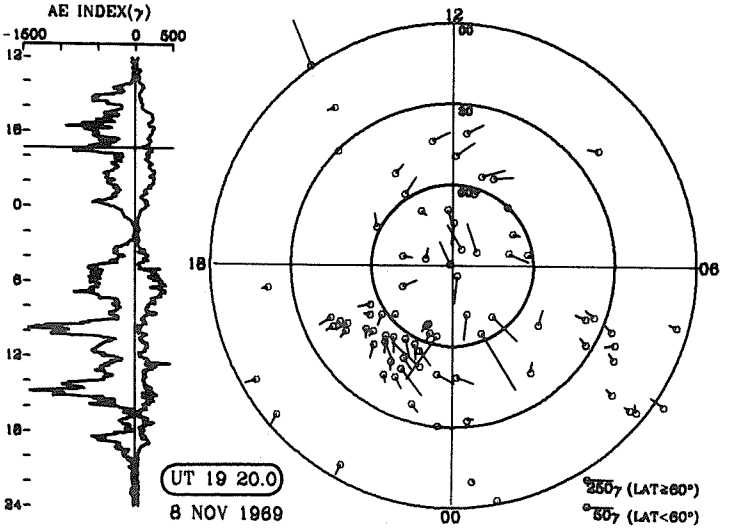
AE INDEX(γ)
-1600
0
500
12
18
0
6
12
18
24
12
00
30
60
18
06
UT 19 20.0
8 NOV 1969
250γ (LAT≥60°)
50γ (LAT<60°)

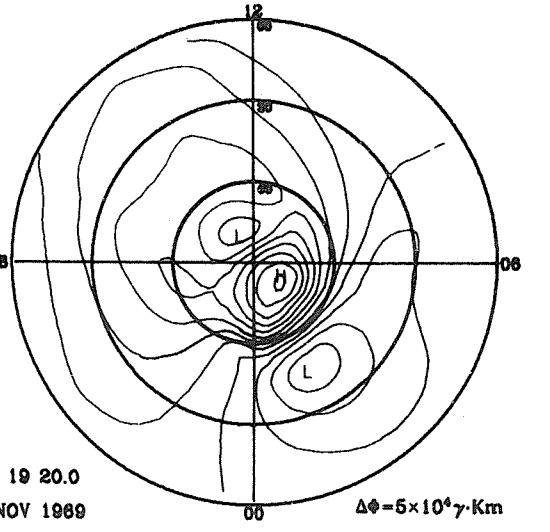
12
00
30
60
18
06
H
L
L
UT 19 20.0
8 NOV 1969
Δφ=5×10⁴γ·Km

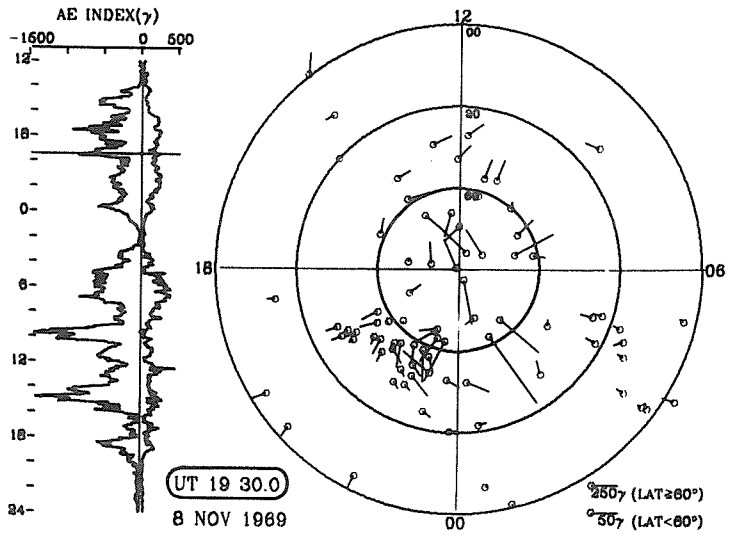
AE INDEX(γ)
-1600
0
500
12
18
0
6
12
18
24
12
00
18
06
UT 19 30.0
8 NOV 1969
250γ (LAT≥60°)
50γ (LAT<60°)

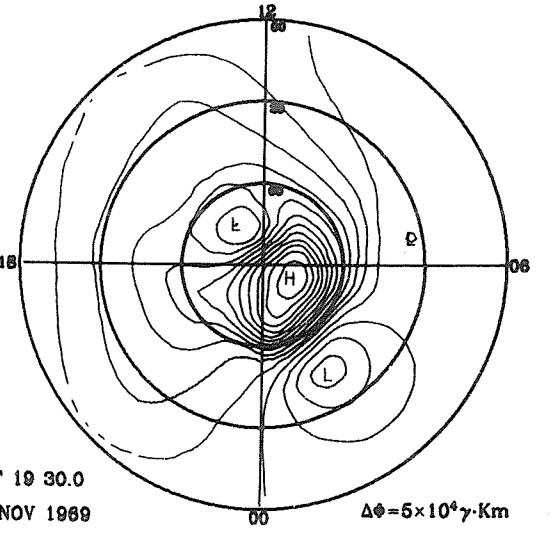
12
00
18
06
H
L
L
UT 19 30.0
8 NOV 1969
Δφ=5×10⁴γ·Km

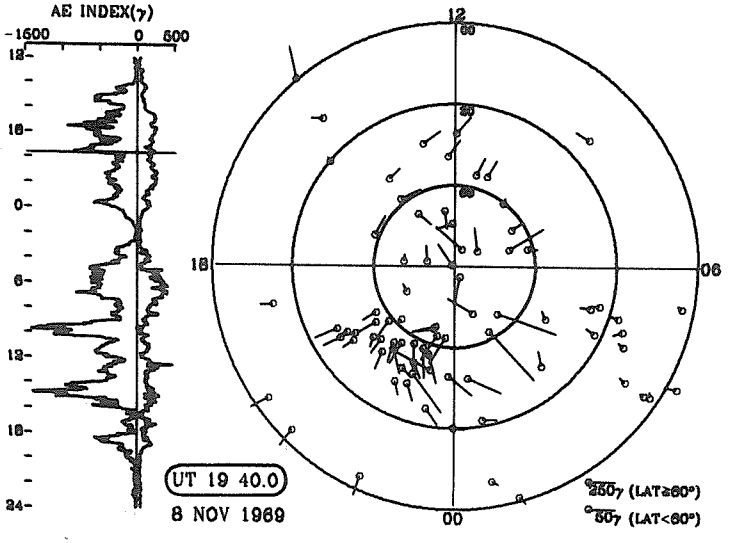
AE INDEX(γ)
-1600
0
500
12
18
0
6
12
18
24
12
00
18
06
UT 19 40.0
8 NOV 1969
250γ (LAT≥60°)
50γ (LAT<60°)

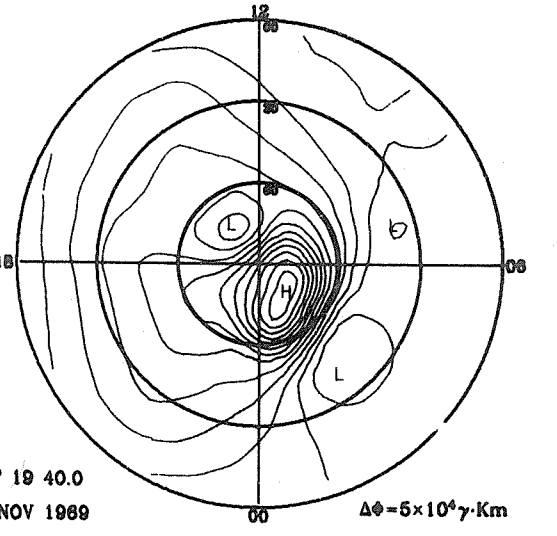
12
00
18
06
L
H
L
UT 19 40.0
8 NOV 1969
Δφ=5×10⁴γ·Km

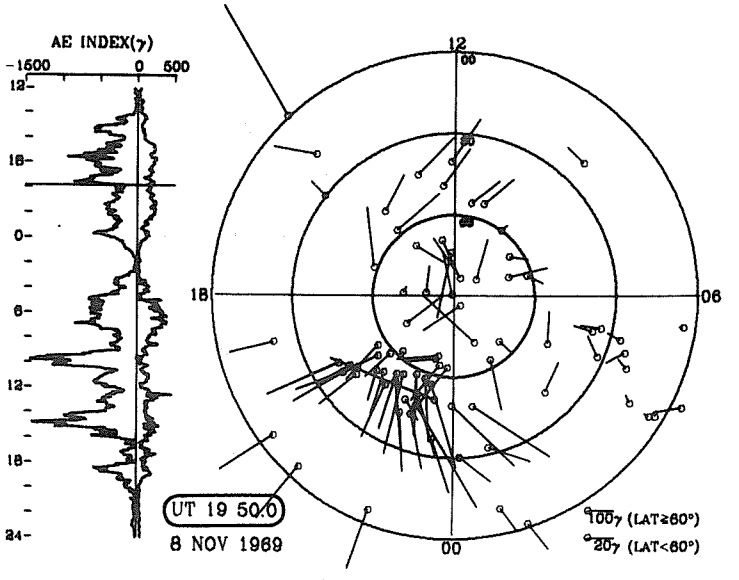
AE INDEX(γ)
-1600
0
500
12
18
0
6
12
18
24
12
00
18
06
UT 19 50.0
8 NOV 1969
100γ (LAT≥60°)
20γ (LAT<60°)

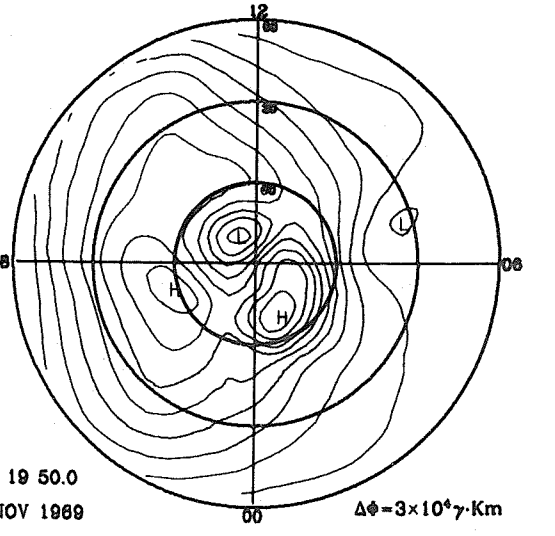
12
00
18
06
H
H
UT 19 50.0
8 NOV 1969
Δφ=3×10⁴γ·Km

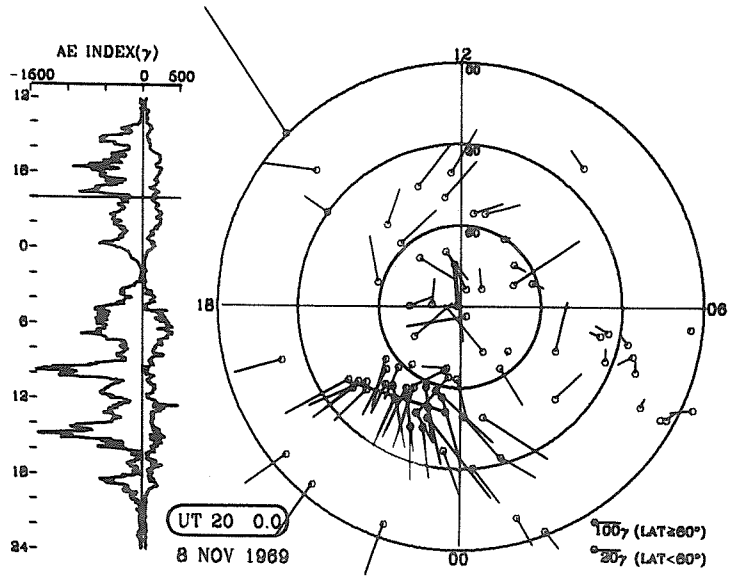
AE INDEX(γ)
-1600
0
500
12
18
0
6
12
18
24
12
00
06
18
30
60
UT 20 0.0
8 NOV 1969
100γ (LAT≥60°)
20γ (LAT<60°)

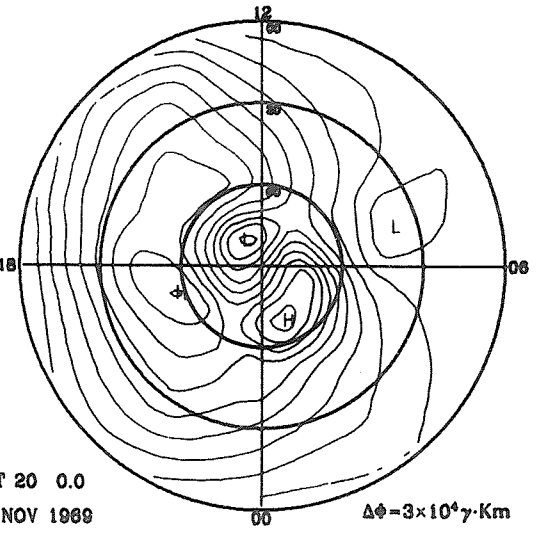
12
00
06
18
30
60
H
L
UT 20 0.0
8 NOV 1969
Δφ=3×10⁴γ·Km

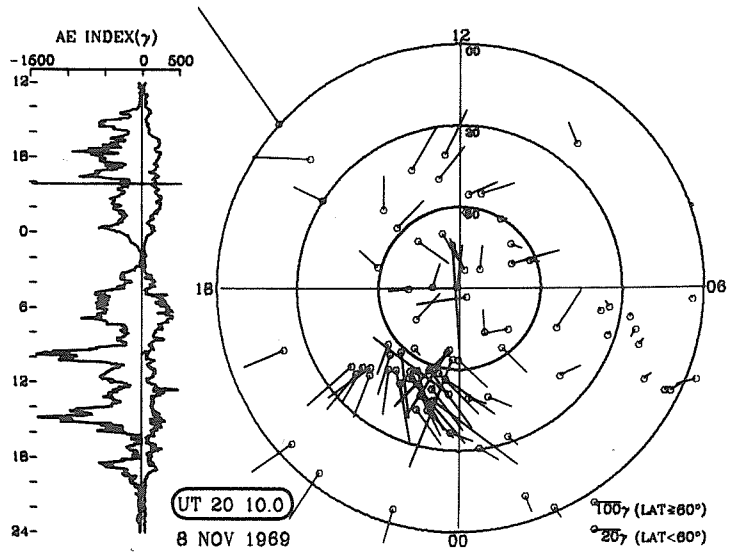
AE INDEX(γ)
-1600
0
500
12
18
0
6
12
18
24
12
00
06
18
30
60
UT 20 10.0
8 NOV 1969
100γ (LAT≥60°)
20γ (LAT<60°)

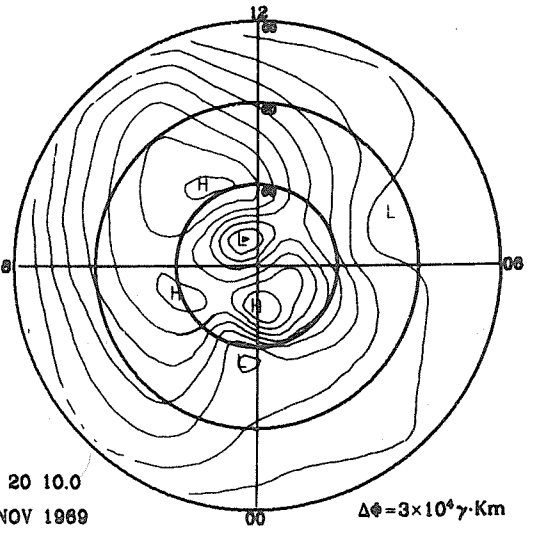
12
00
06
18
30
60
H
L
UT 20 10.0
8 NOV 1969
Δφ=3×10⁴γ·Km

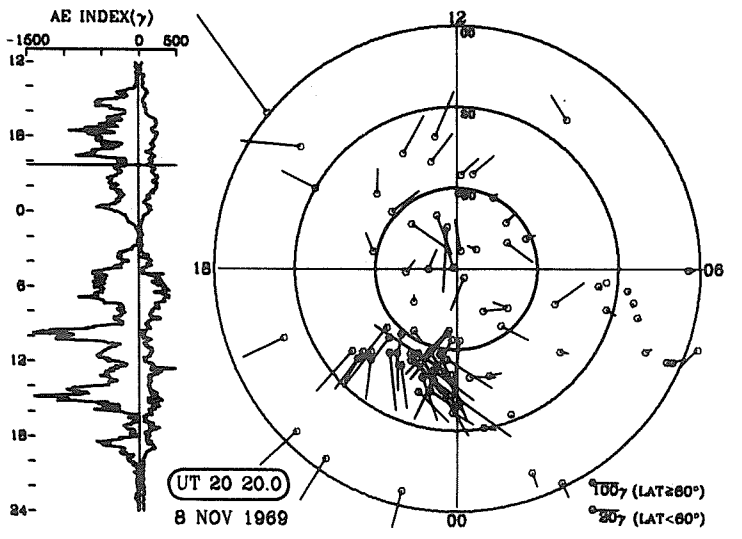
AE INDEX(γ)
-1600
0
500
12
18
0
6
12
18
24
12
00
06
18
30
60
UT 20 20.0
8 NOV 1969
100γ (LAT≥60°)
20γ (LAT<60°)

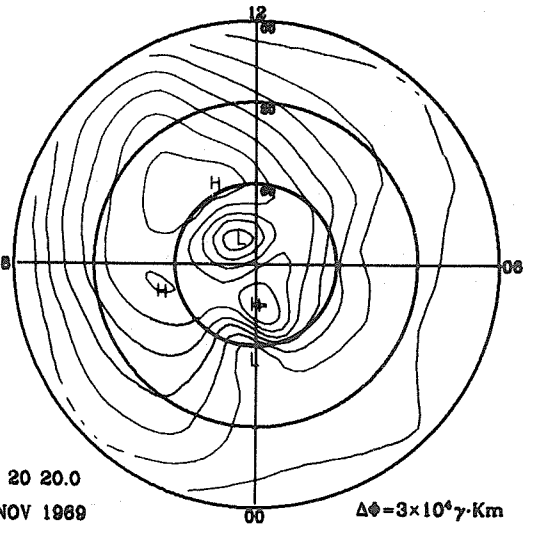
12
00
06
18
30
60
H
L
UT 20 20.0
8 NOV 1969
Δφ=3×10⁴γ·Km

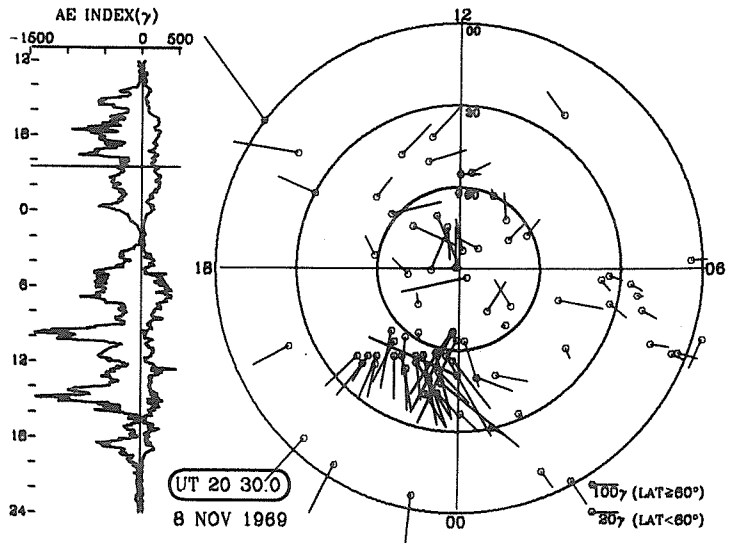
AE INDEX(γ)
-1600
0
500
12
18
0
6
12
18
24
12
00
30
60
18
06
00
UT 20 30.0
8 NOV 1969
100γ (LAT≥60°)
20γ (LAT<60°)

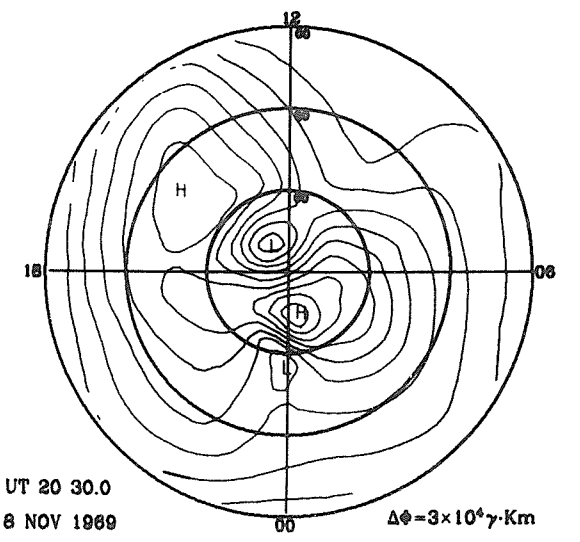
12
00
30
60
18
06
00
H
L
UT 20 30.0
8 NOV 1969
Δφ=3×10⁴γ·Km

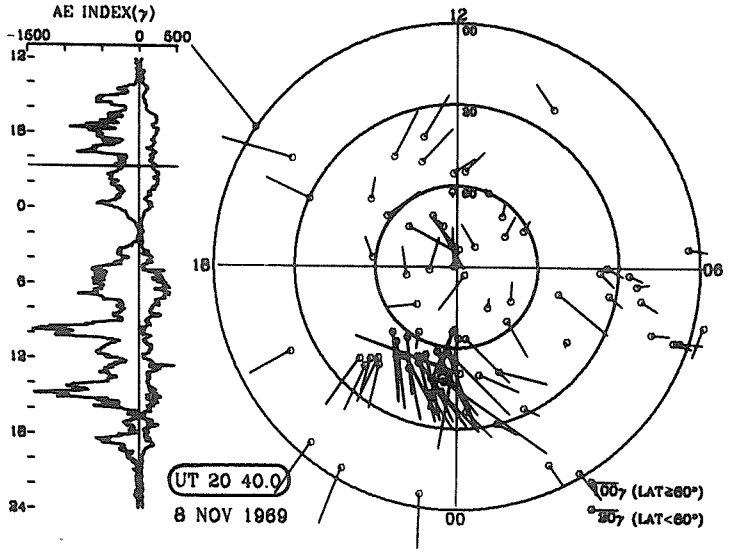
AE INDEX(γ)
-1600
0
500
12
18
0
6
12
18
24
12
00
30
60
18
06
00
UT 20 40.0
8 NOV 1969
100γ (LAT≥60°)
20γ (LAT<60°)

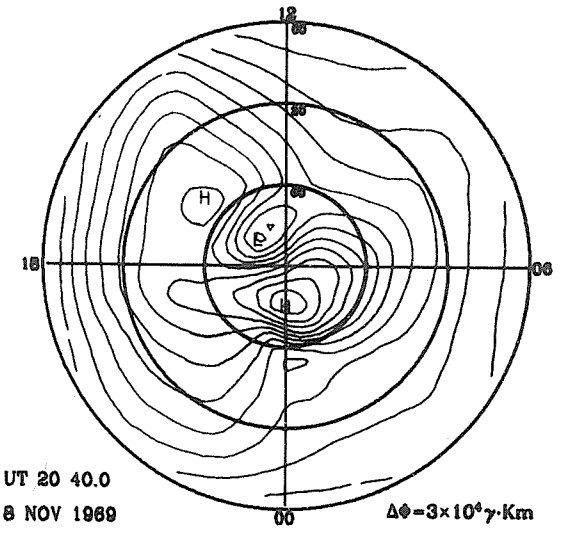
12
00
30
60
18
06
00
H
L
UT 20 40.0
8 NOV 1969
Δφ=3×10⁴γ·Km

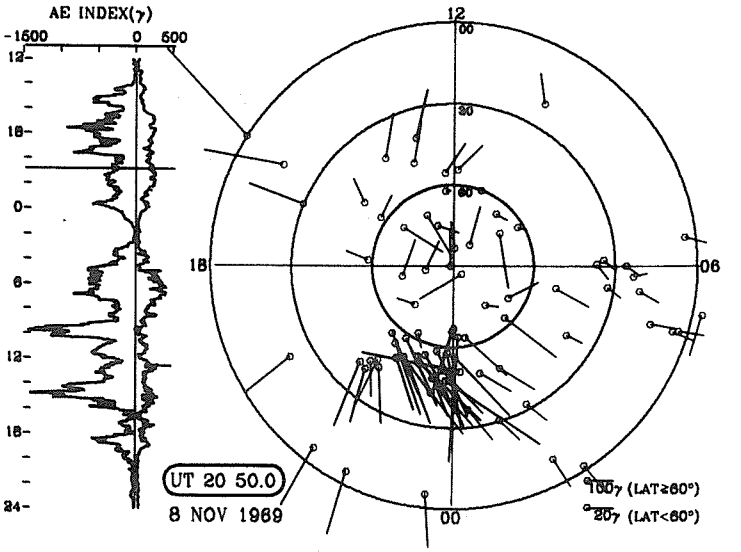
AE INDEX(γ)
-1600
0
500
12
18
0
6
12
18
24
12
00
30
60
18
06
00
UT 20 50.0
8 NOV 1969
100γ (LAT≥60°)
20γ (LAT<60°)

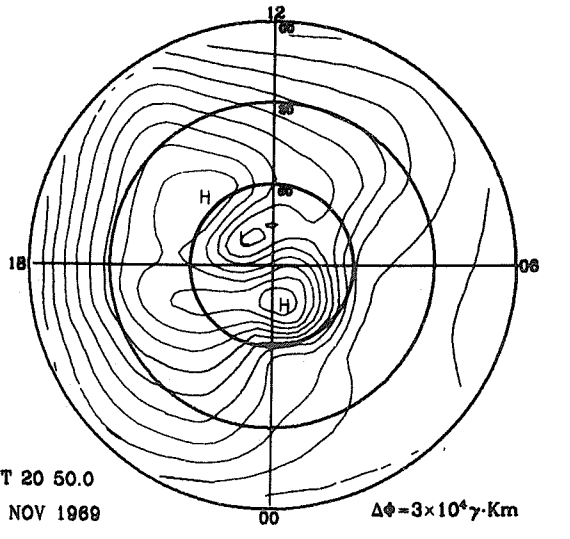
12
00
30
60
18
06
00
H
L
UT 20 50.0
8 NOV 1969
Δφ=3×10⁴γ·Km

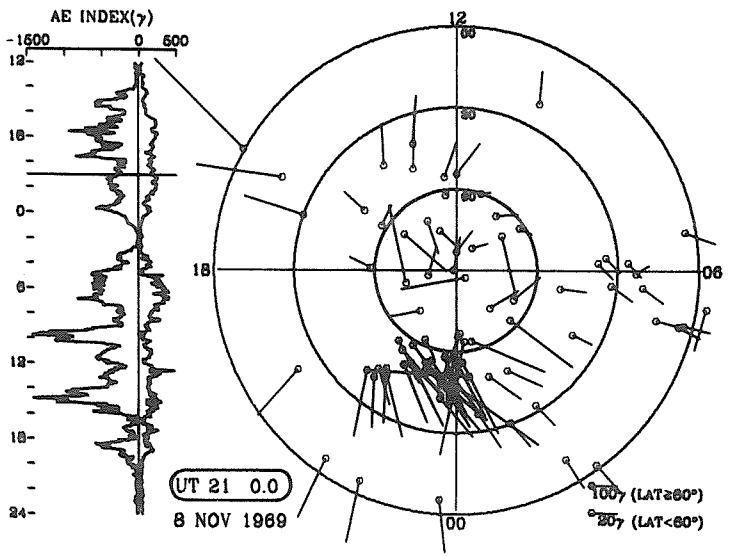
AE INDEX(γ)
-1500
0
500
12
18
0
6
12
18
24
12
60
30
60
18
06
00
UT 21 0.0
8 NOV 1969
100γ (LAT≥60°)
20γ (LAT<60°)

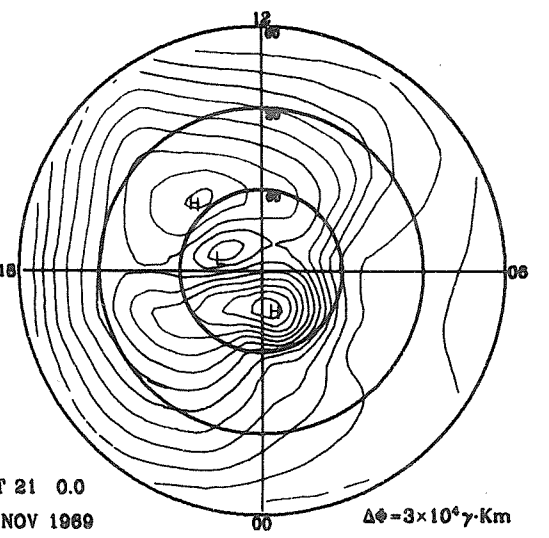
12
60
30
60
18
06
00
H
L
H
UT 21 0.0
8 NOV 1969
Δ♦=3×10⁴γ·Km

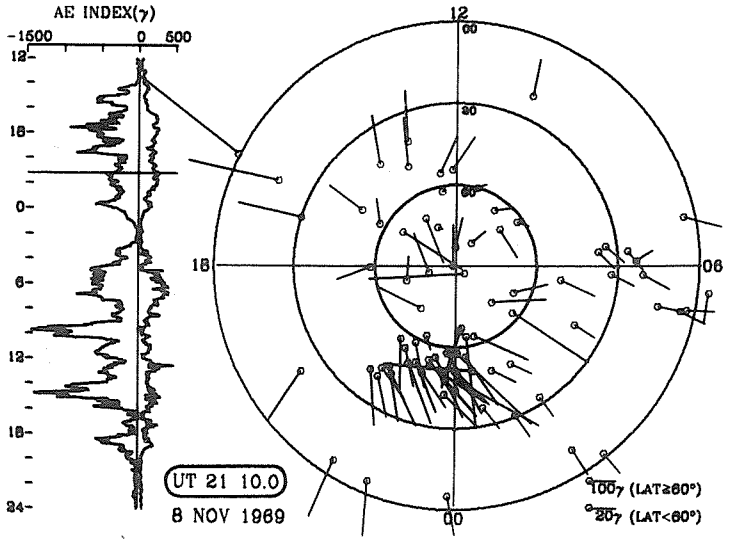
AE INDEX(γ)
-1500
0
500
12
18
0
6
12
18
24
12
60
30
60
18
06
00
UT 21 10.0
8 NOV 1969
100γ (LAT≥60°)
20γ (LAT<60°)

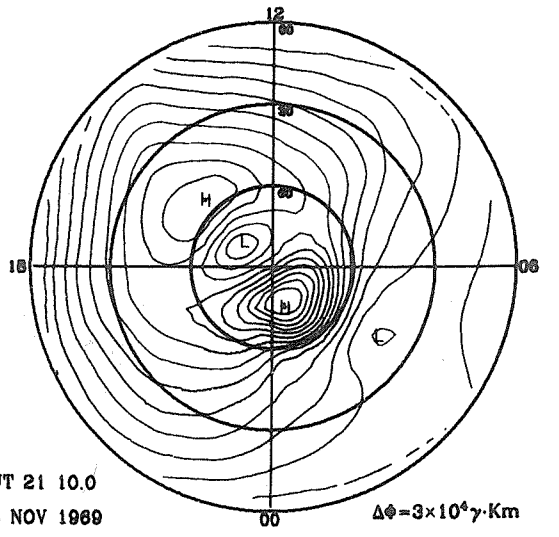
12
60
30
60
18
06
00
H
L
H
L
UT 21 10.0
8 NOV 1969
Δ♦=3×10⁴γ·Km

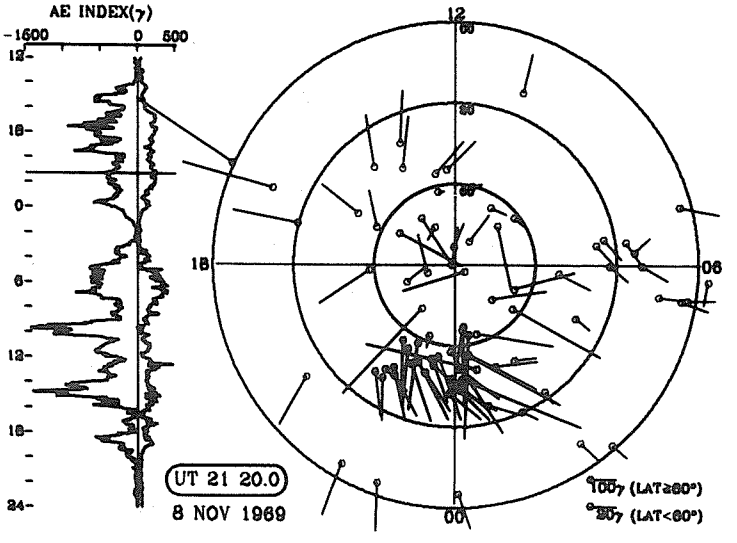
AE INDEX(γ)
-1500
0
500
12
18
0
6
12
18
24
12
60
30
60
18
06
00
UT 21 20.0
8 NOV 1969
100γ (LAT≥60°)
20γ (LAT<60°)

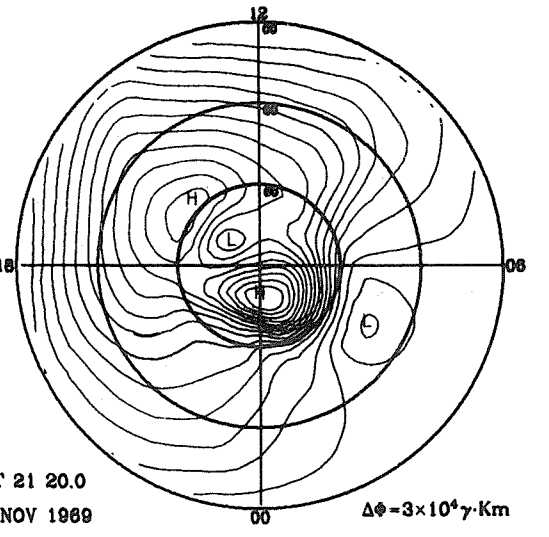
12
60
30
60
18
06
00
H
L
H
L
UT 21 20.0
8 NOV 1969
Δ♦=3×10⁴γ·Km

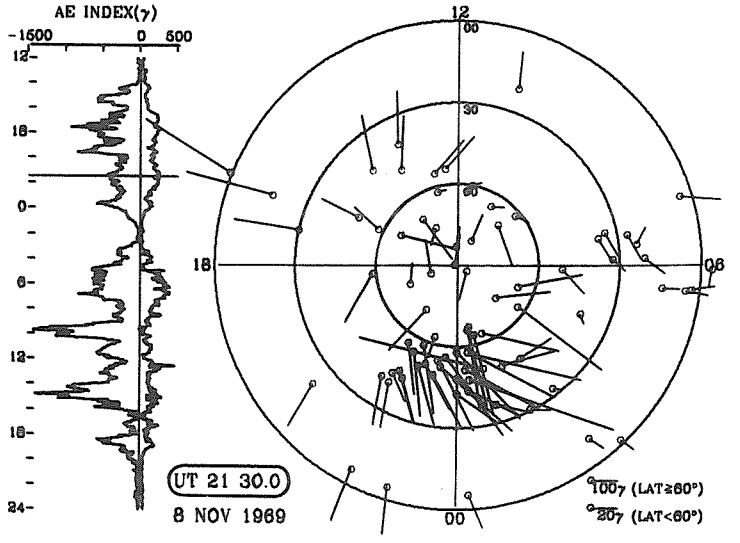
AE INDEX(γ)
-1600
0
500
12
18
0
6
12
18
24
12
00
30
60
18
06
00
UT 21 30.0
8 NOV 1969
100γ (LAT≥60°)
20γ (LAT<60°)

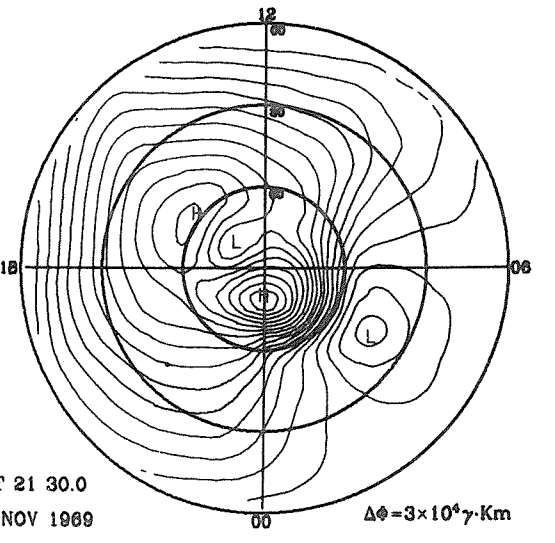
12
00
30
60
18
06
00
H
L
H
L
UT 21 30.0
8 NOV 1969
Δφ=3×10⁴γ·Km

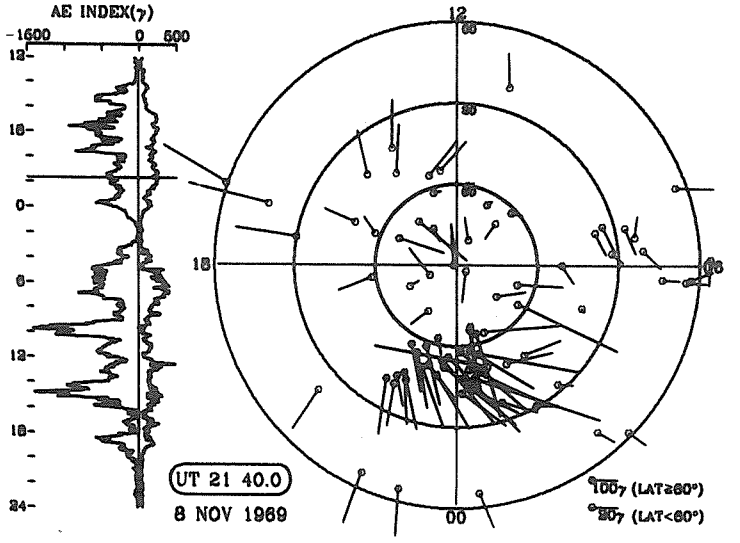
AE INDEX(γ)
-1600
0
500
12
18
0
6
12
18
24
12
00
30
60
18
06
00
UT 21 40.0
8 NOV 1969
100γ (LAT≥60°)
20γ (LAT<60°)

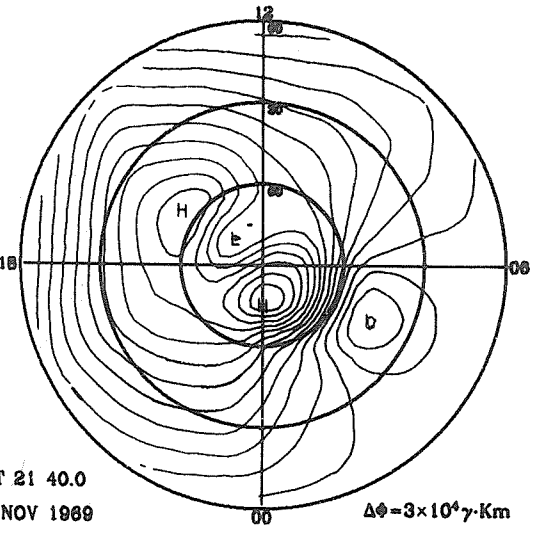
12
00
30
60
18
06
00
H
L
H
L
UT 21 40.0
8 NOV 1969
Δφ=3×10⁴γ·Km

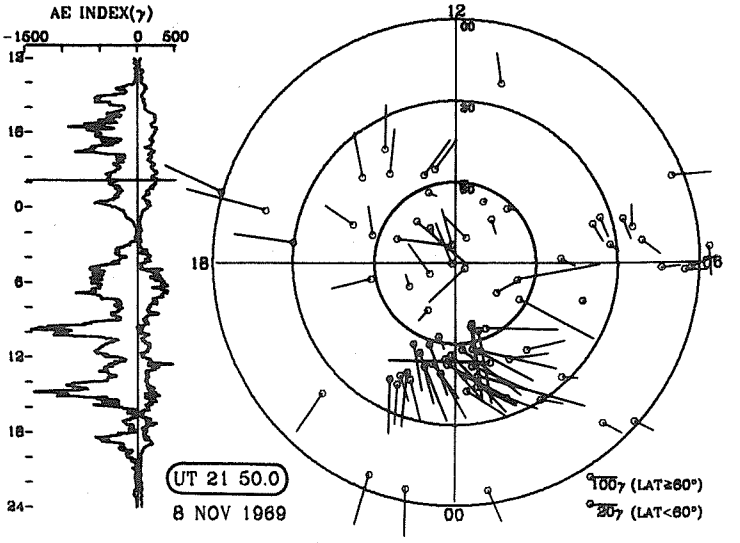
AE INDEX(γ)
-1600
0
500
12
18
0
6
12
18
24
12
00
30
60
18
06
00
UT 21 50.0
8 NOV 1969
100γ (LAT≥60°)
20γ (LAT<60°)

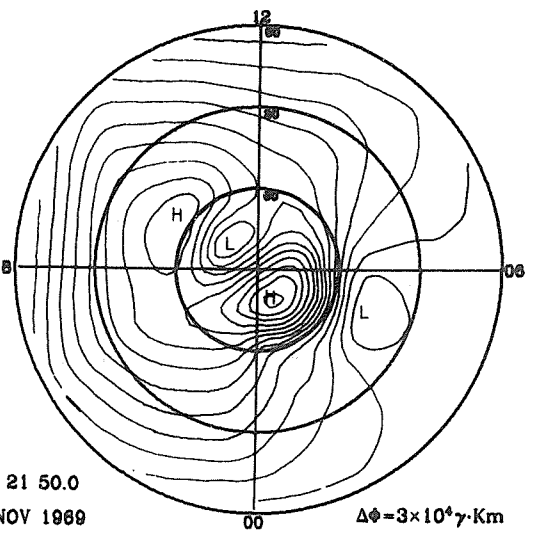
12
00
30
60
18
06
00
H
L
H
L
UT 21 50.0
8 NOV 1969
Δφ=3×10⁴γ·Km

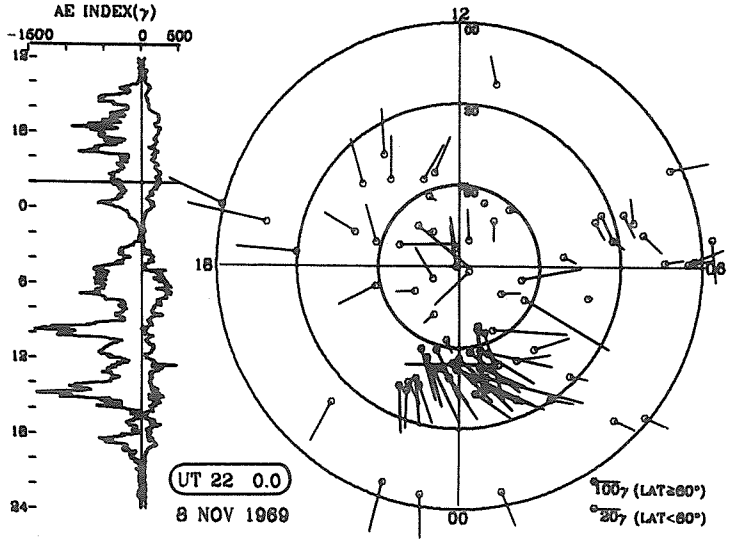
AE INDEX(γ)
-1600
0
600
12
18
0
6
12
18
24
12
60
30
18
06
00
UT 22 0.0
8 NOV 1969
100γ (LAT≥60°)
20γ (LAT<60°)

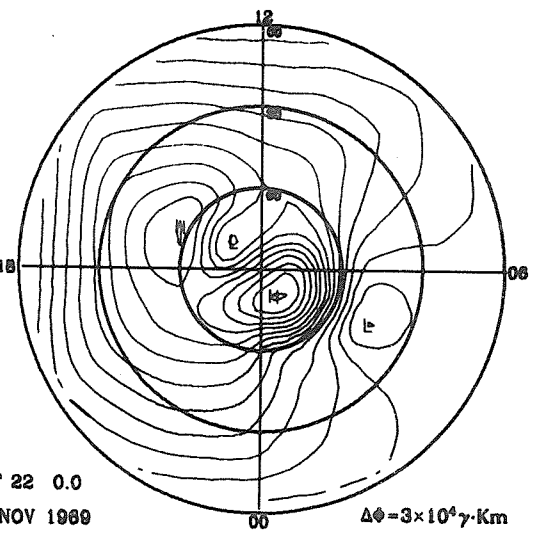
12
60
30
18
06
00
UT 22 0.0
8 NOV 1969
Δ=3×10⁴γ·Km

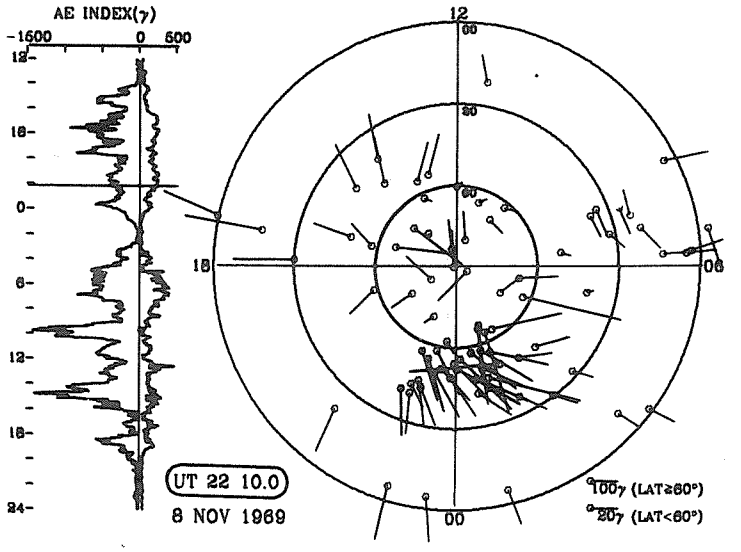
AE INDEX(γ)
-1600
0
600
12
18
0
6
12
18
24
12
60
30
18
06
00
UT 22 10.0
8 NOV 1969
100γ (LAT≥60°)
20γ (LAT<60°)

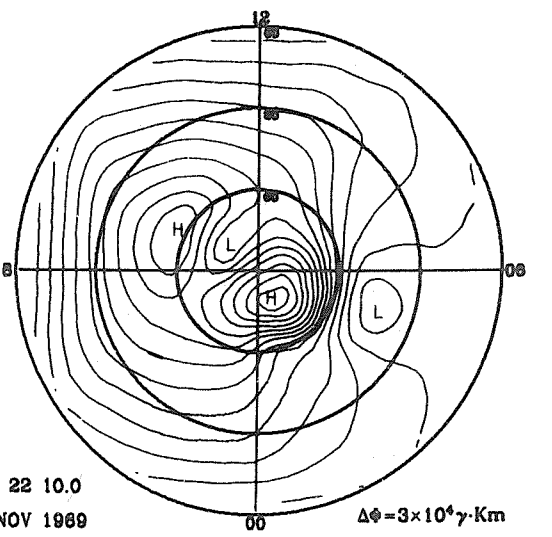
12
60
30
18
06
00
H
L
H
L
UT 22 10.0
8 NOV 1969
Δ=3×10⁴γ·Km

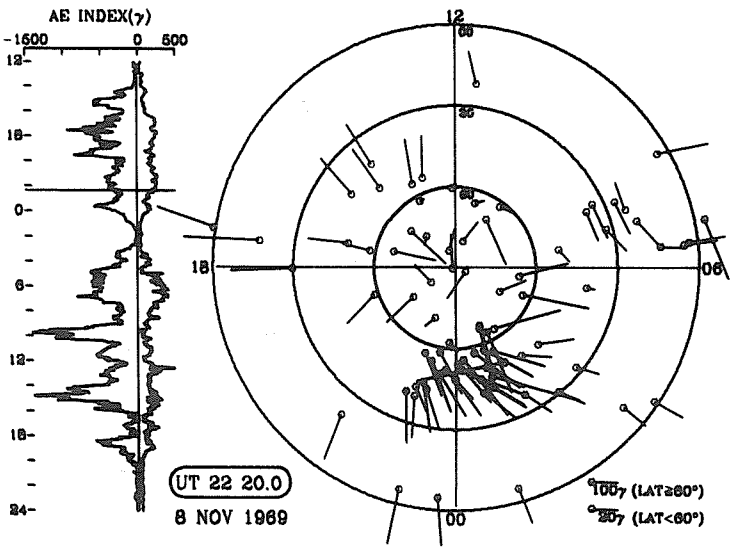
AE INDEX(γ)
-1600
0
600
12
18
0
6
12
18
24
12
60
30
18
06
00
UT 22 20.0
8 NOV 1969
100γ (LAT≥60°)
20γ (LAT<60°)

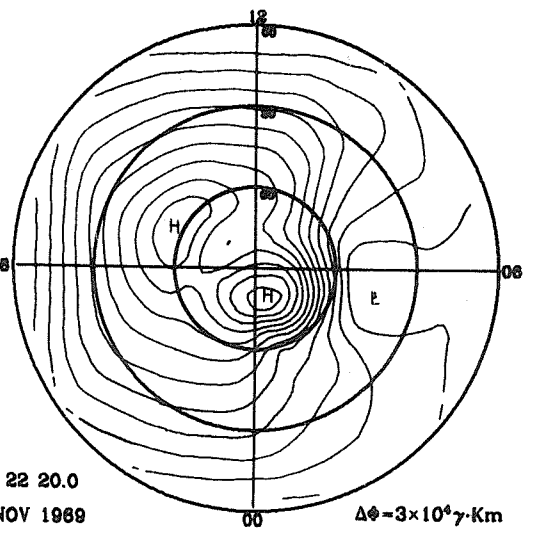
12
60
30
18
06
00
H
H
UT 22 20.0
8 NOV 1969
Δ=3×10⁴γ·Km

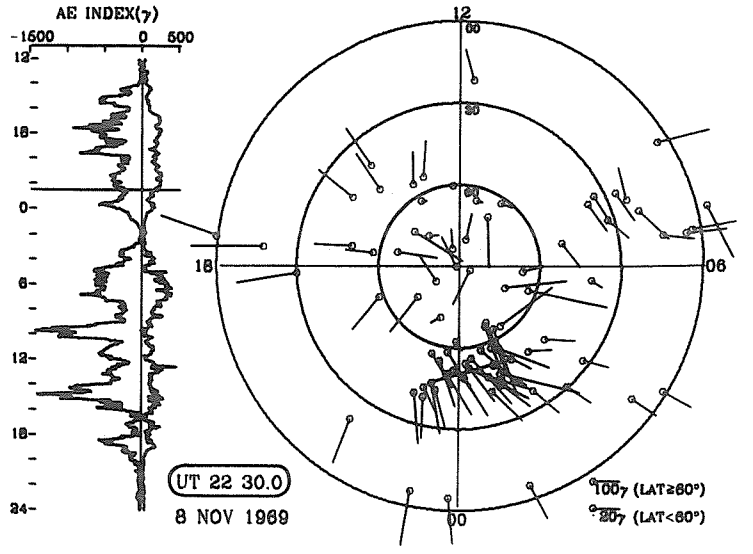
AE INDEX(γ)
-1600
0
500
12
18
0
6
12
18
24
12
00
18
06
30
60
UT 22 30.0
8 NOV 1969
100γ (LAT≥60°)
20γ (LAT<60°)

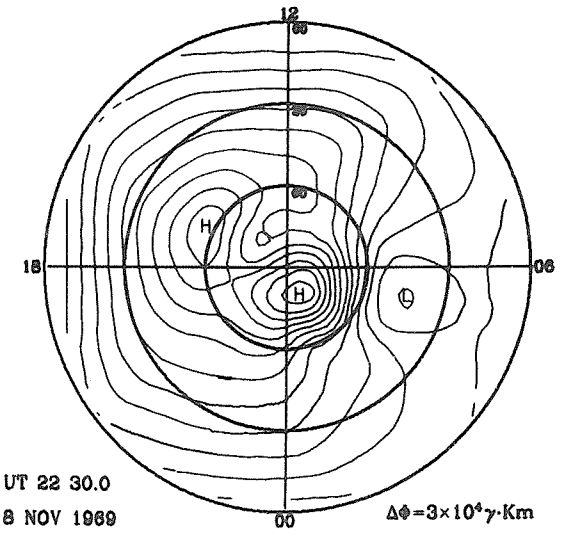
12
00
18
06
30
60
H
H
L
UT 22 30.0
8 NOV 1969
Δφ=3×10⁴γ·Km

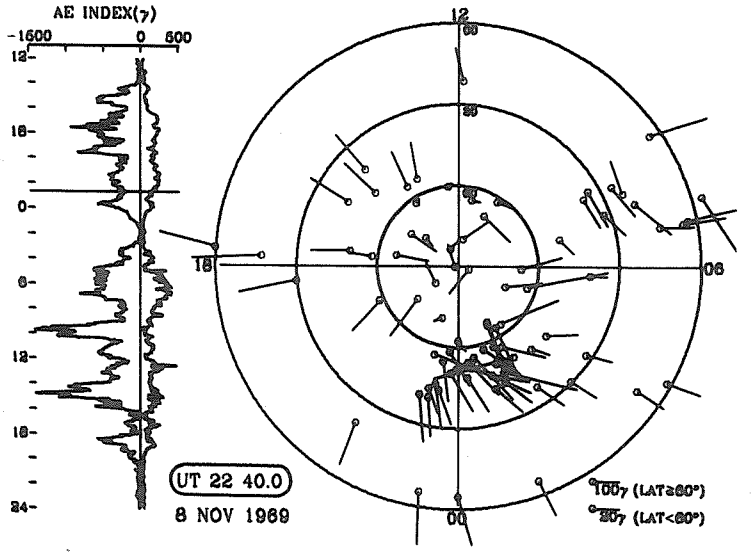
AE INDEX(γ)
-1600
0
500
12
18
0
6
12
18
24
12
00
18
06
30
60
UT 22 40.0
8 NOV 1969
100γ (LAT≥60°)
20γ (LAT<60°)

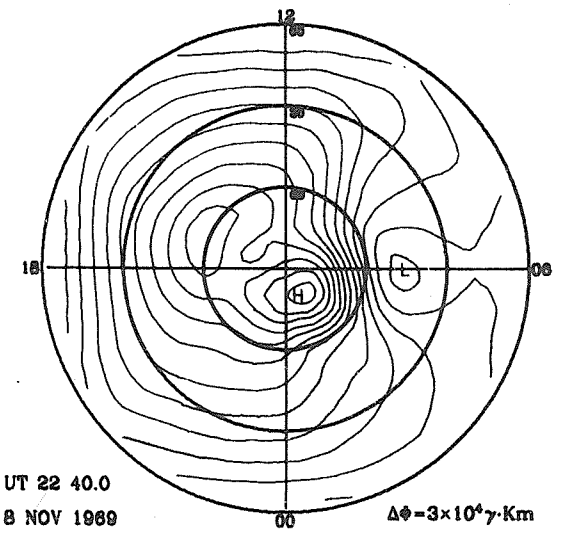
12
00
18
06
30
60
H
H
L
UT 22 40.0
8 NOV 1969
Δφ=3×10⁴γ·Km

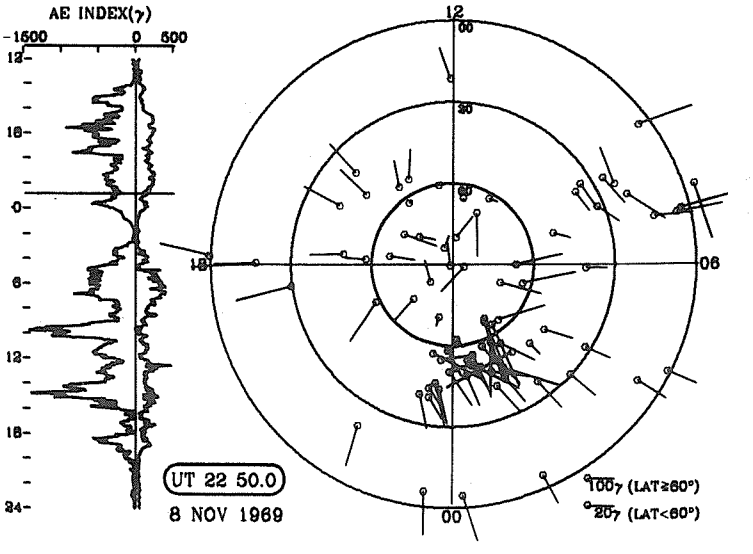
AE INDEX(γ)
-1600
0
500
12
18
0
6
12
18
24
12
00
18
06
30
60
UT 22 50.0
8 NOV 1969
100γ (LAT≥60°)
20γ (LAT<60°)

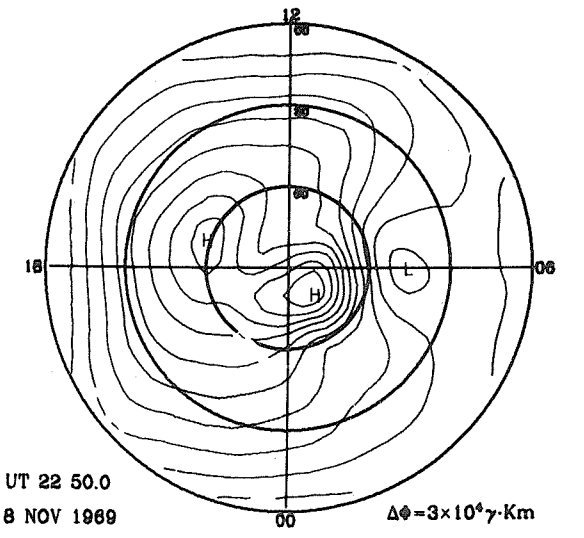
12
00
18
06
30
60
H
H
L
UT 22 50.0
8 NOV 1969
Δφ=3×10⁴γ·Km

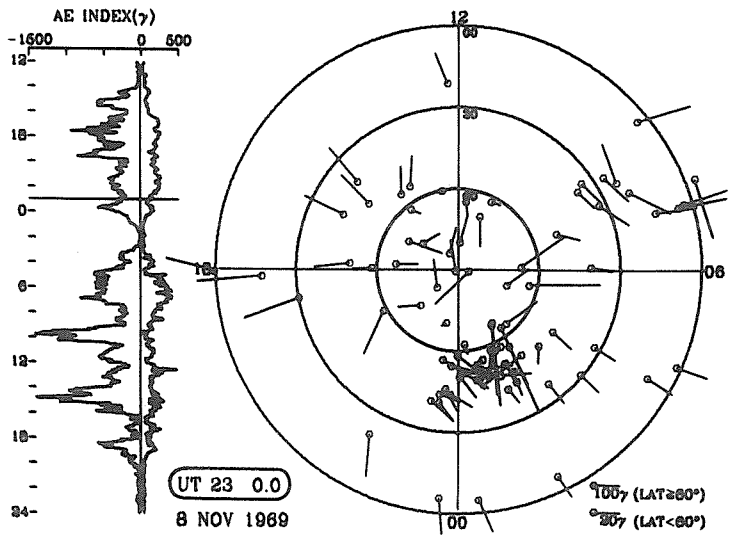
AE INDEX(γ)
-1600
0
500
12
18
0
6
12
18
24
12
60
30
18
06
00
UT 23 0.0
8 NOV 1969
100γ (LAT≥60°)
20γ (LAT<60°)

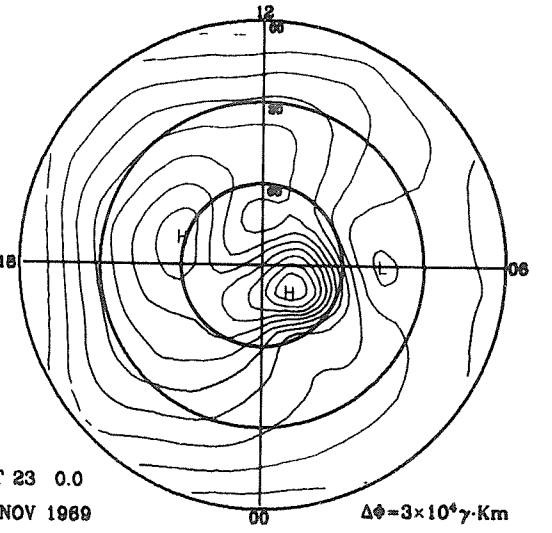
12
60
30
18
06
00
H
L
UT 23 0.0
8 NOV 1969
Δφ=3×10⁴γ·Km

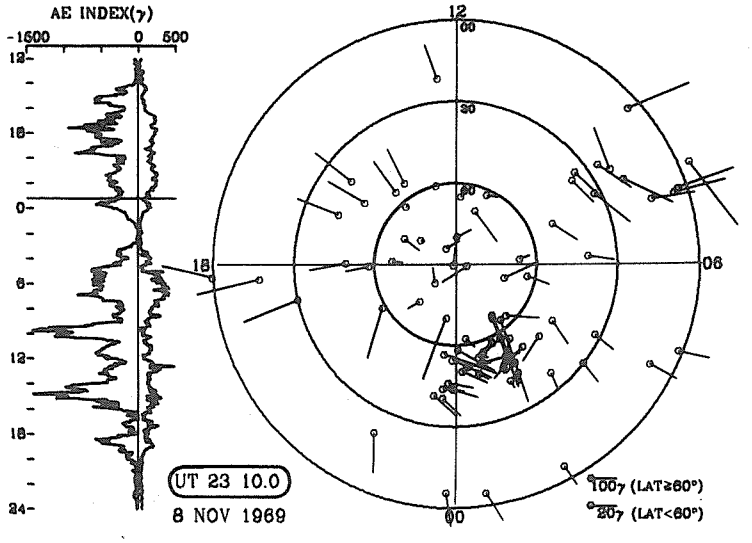
AE INDEX(γ)
-1600
0
500
12
18
0
6
12
18
24
12
60
30
18
06
00
UT 23 10.0
8 NOV 1969
100γ (LAT≥60°)
20γ (LAT<60°)

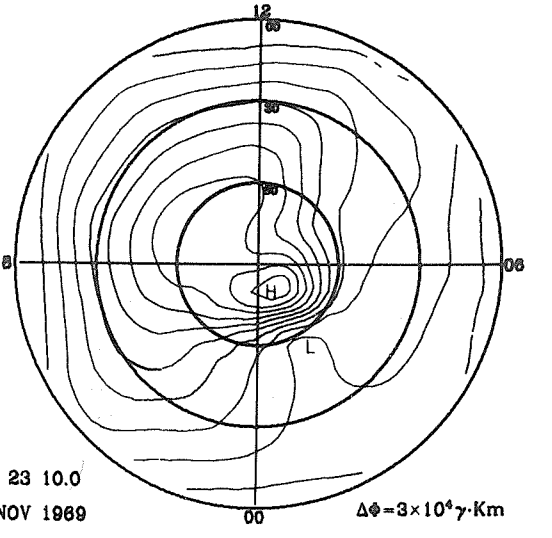
12
60
30
18
06
00
H
L
UT 23 10.0
8 NOV 1969
Δφ=3×10⁴γ·Km

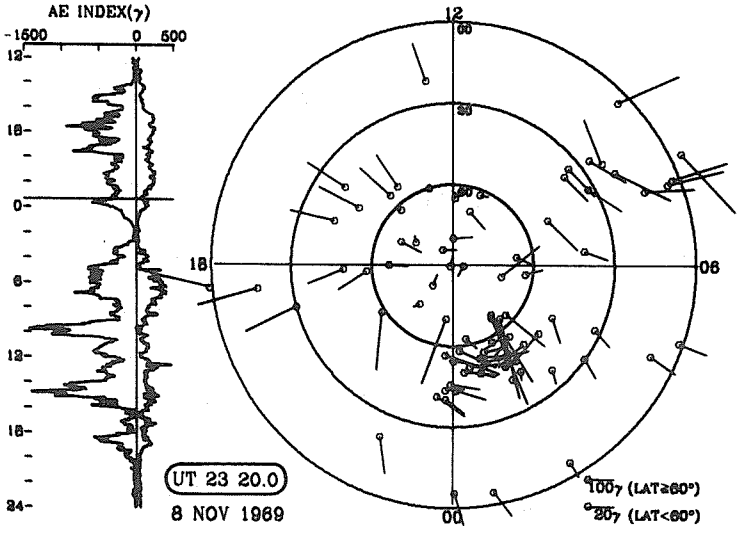
AE INDEX(γ)
-1600
0
500
12
18
0
6
12
18
24
12
60
30
18
06
00
UT 23 20.0
8 NOV 1969
100γ (LAT≥60°)
20γ (LAT<60°)

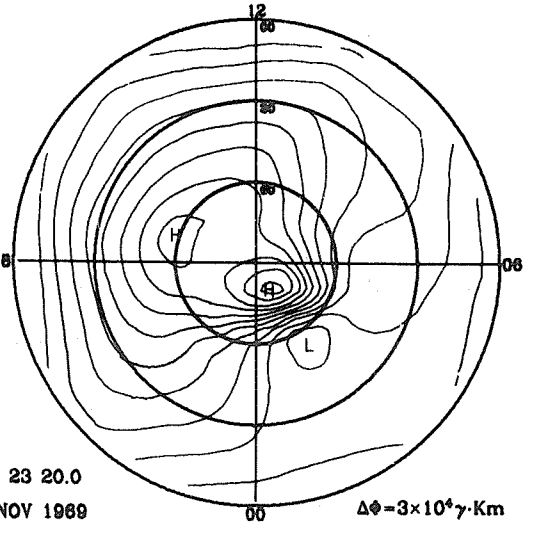
12
60
30
18
06
00
H
L
UT 23 20.0
8 NOV 1969
Δφ=3×10⁴γ·Km

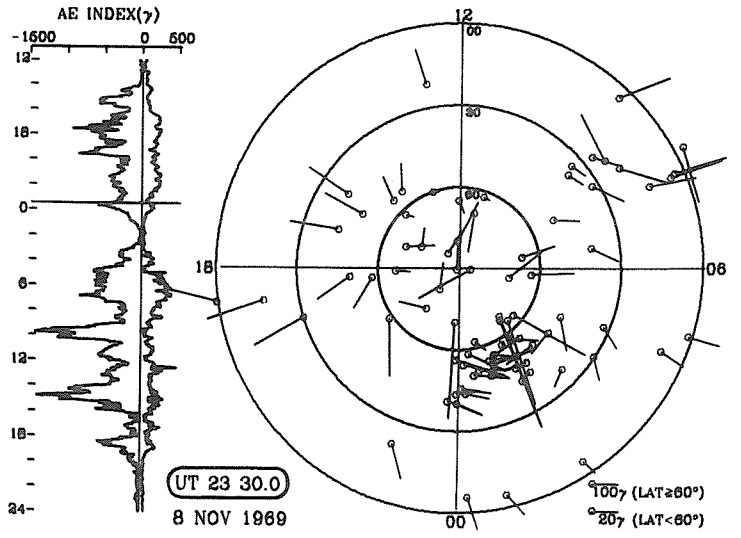
AE INDEX(γ)
-1600
0
500
12
18
0
6
12
18
24
12
00
30
60
18
06
00
UT 23 30.0
8 NOV 1969
100γ (LAT≥60°)
20γ (LAT<60°)

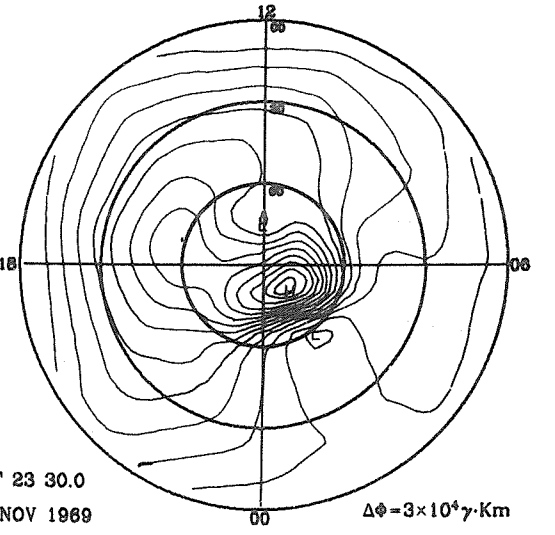
12
00
30
60
18
06
00
H
L
UT 23 30.0
8 NOV 1969
Δφ=3×10⁴γ·Km

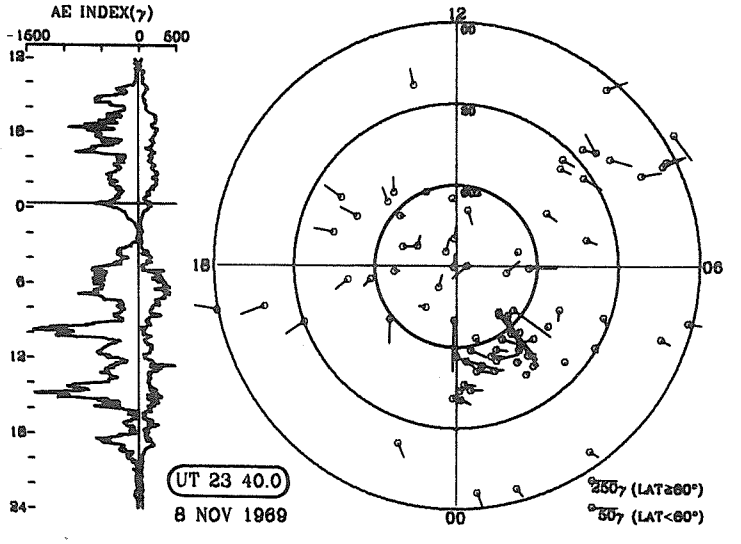
AE INDEX(γ)
-1600
0
500
12
18
0
6
12
18
24
12
00
30
60
18
06
00
UT 23 40.0
8 NOV 1969
250γ (LAT≥60°)
50γ (LAT<60°)

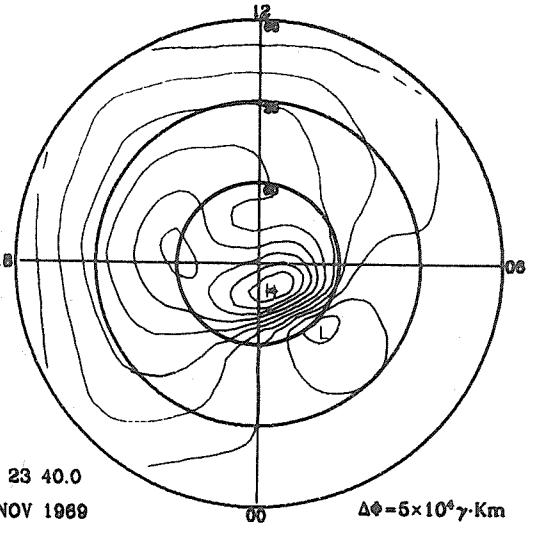
12
00
30
60
18
06
00
H
L
UT 23 40.0
8 NOV 1969
Δφ=5×10⁴γ·Km

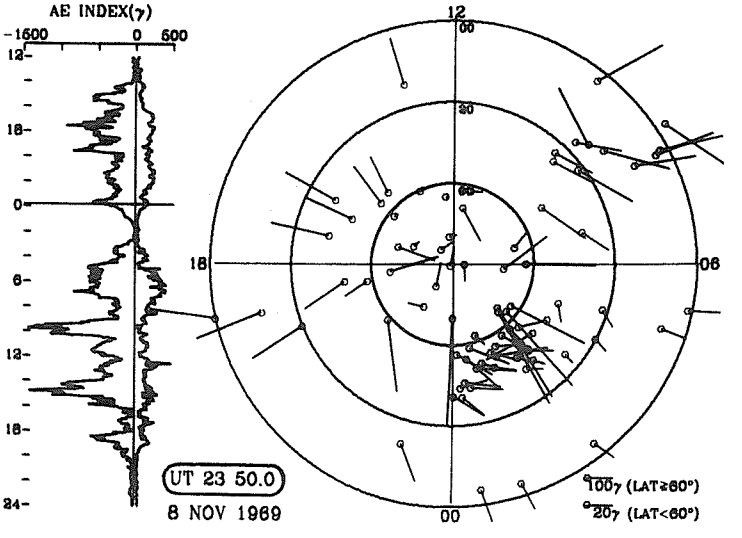
AE INDEX(γ)
-1600
0
500
12
18
0
6
12
18
24
12
00
30
60
18
06
00
UT 23 50.0
8 NOV 1969
100γ (LAT≥60°)
20γ (LAT<60°)

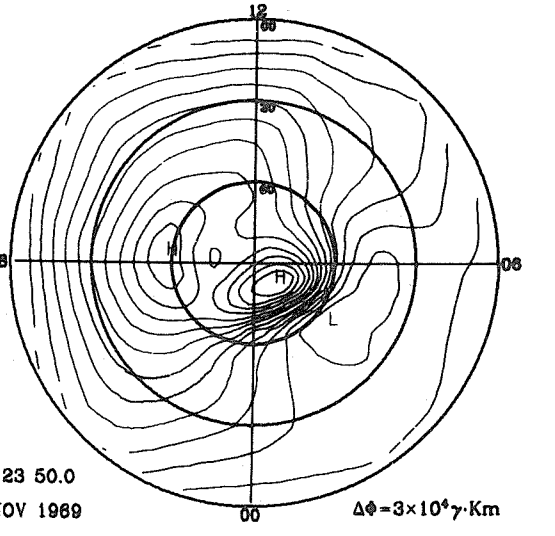
12
00
30
60
18
06
00
H
L
UT 23 50.0
8 NOV 1969
Δφ=3×10⁴γ·Km

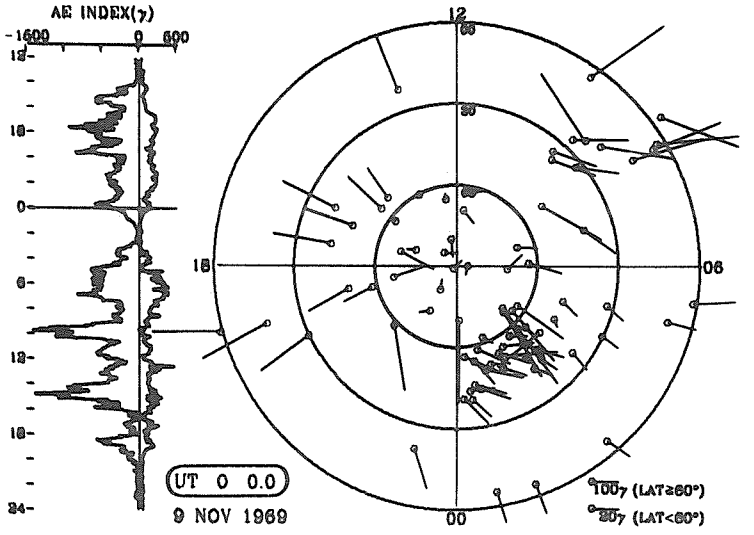
AE INDEX(γ)
-1600
0
600
12
18
0
6
12
18
24
12
60
30
60
18
06
00
UT 0 0.0
9 NOV 1969
100γ (LAT≥60°)
20γ (LAT<60°)

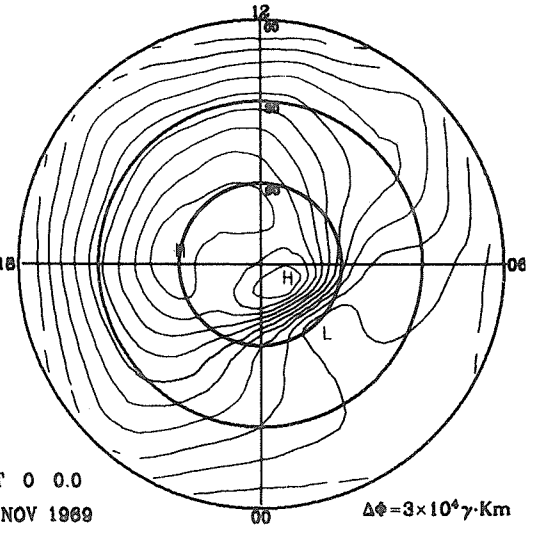
12
60
30
60
18
06
00
H
L
UT 0 0.0
9 NOV 1969
Δ Φ=3×10⁴γ·Km

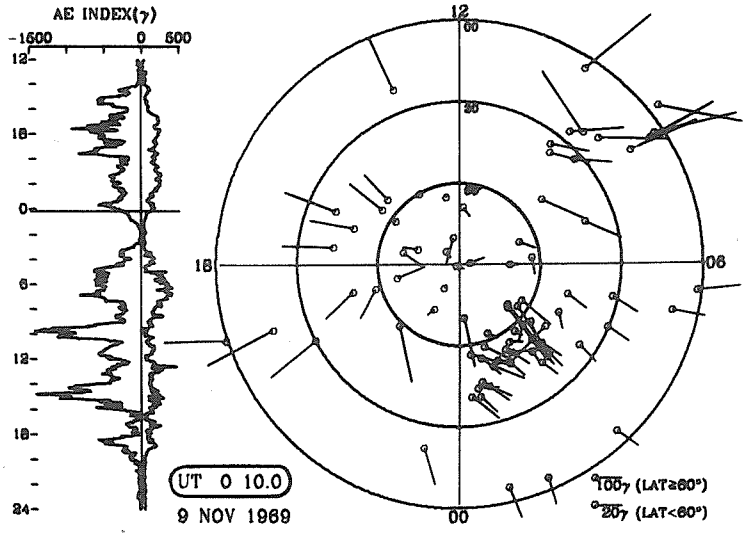
AE INDEX(γ)
-1600
0
600
12
18
0
6
12
18
24
12
60
30
60
18
06
00
UT 0 10.0
9 NOV 1969
100γ (LAT≥60°)
20γ (LAT<60°)

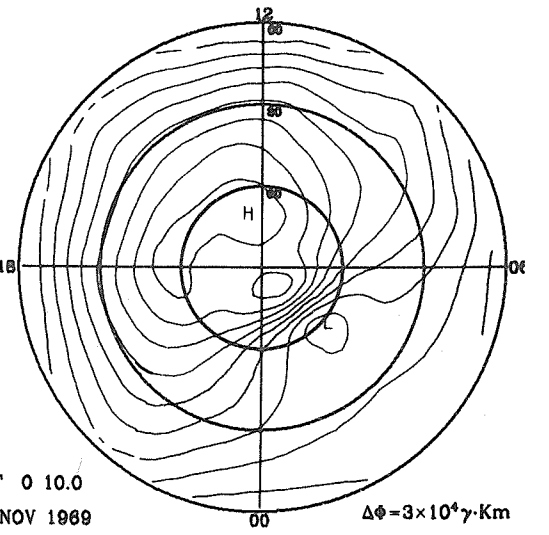
12
60
30
60
18
00
H
L
UT 0 10.0
9 NOV 1969
Δ Φ=3×10⁴γ·Km

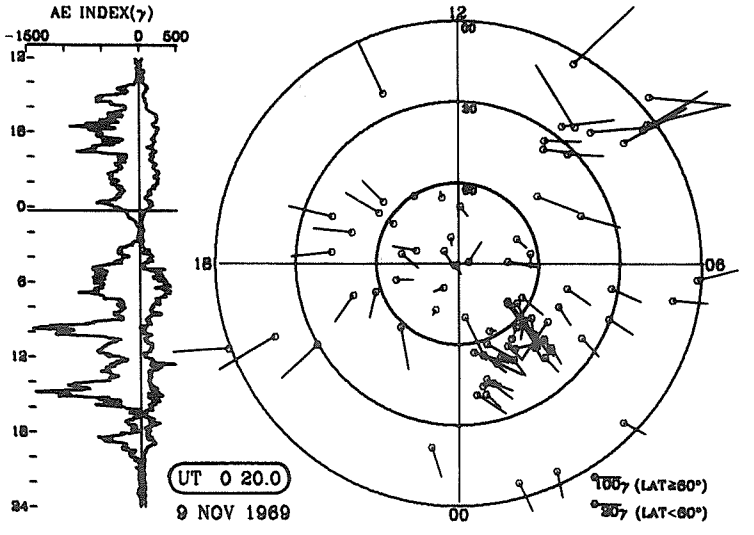
AE INDEX(γ)
-1600
0
600
12
18
0
6
12
18
24
12
60
30
60
18
06
00
UT 0 20.0
9 NOV 1969
100γ (LAT≥60°)
20γ (LAT<60°)

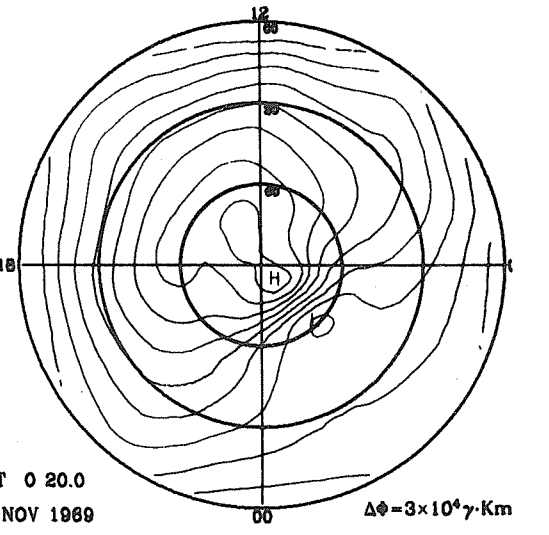
12
60
30
60
18
00
H
UT 0 20.0
9 NOV 1969
Δ Φ=3×10⁴γ·Km

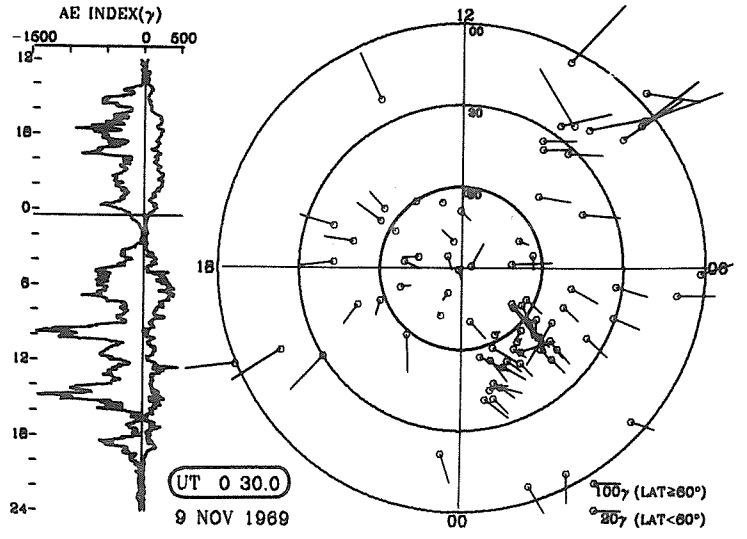
AE INDEX(γ)
-1600
0
500
12
18
0
6
12
18
24
12
00
30
60
18
06
00
UT 0 30.0
9 NOV 1969
100γ (LAT≥60°)
20γ (LAT<60°)

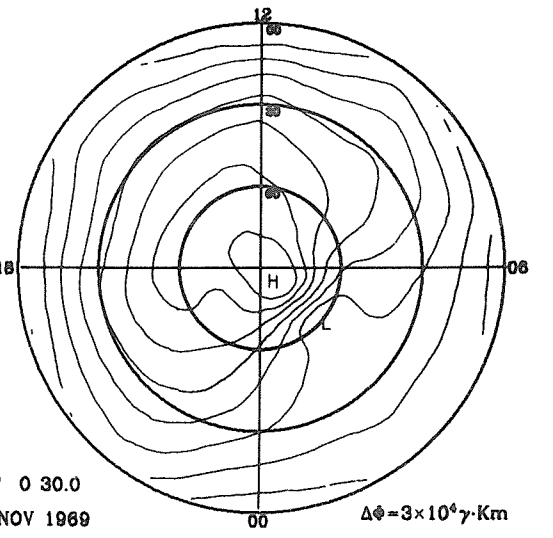
12
00
30
60
18
06
H
L
00
UT 0 30.0
9 NOV 1969
Δφ=3×10⁴γ·Km

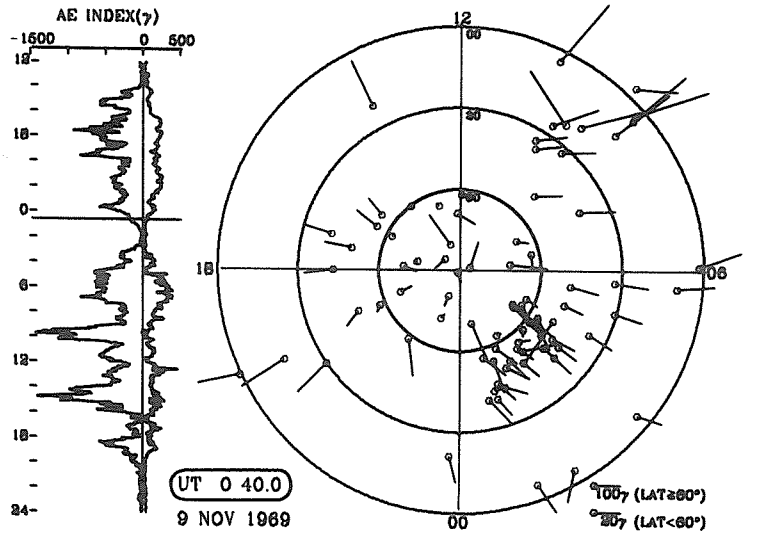
AE INDEX(γ)
-1600
0
500
12
18
0
6
12
18
24
12
00
30
60
18
06
00
UT 0 40.0
9 NOV 1969
100γ (LAT≥60°)
20γ (LAT<60°)

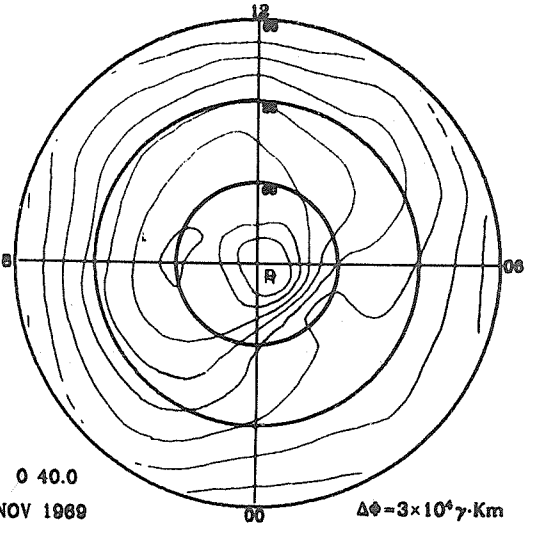
12
00
30
60
18
06
R
00
UT 0 40.0
9 NOV 1969
Δφ=3×10⁴γ·Km

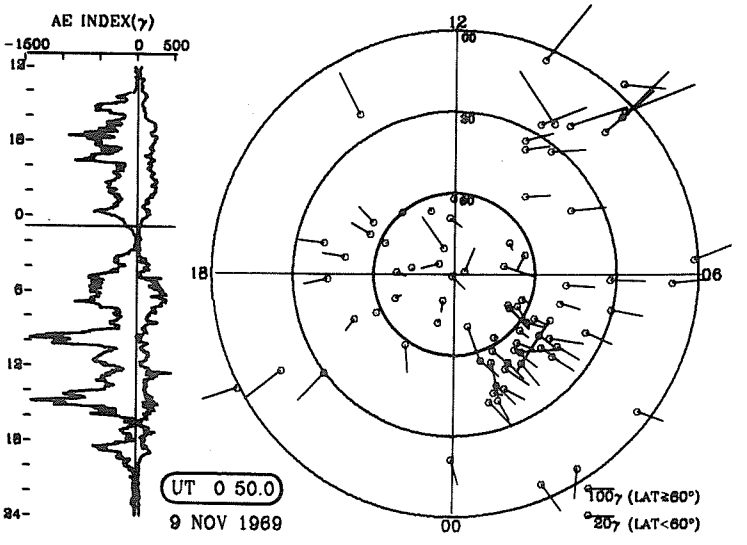
AE INDEX(γ)
-1600
0
500
12
18
0
6
12
18
24
12
00
30
60
18
06
00
UT 0 50.0
9 NOV 1969
100γ (LAT≥60°)
20γ (LAT<60°)

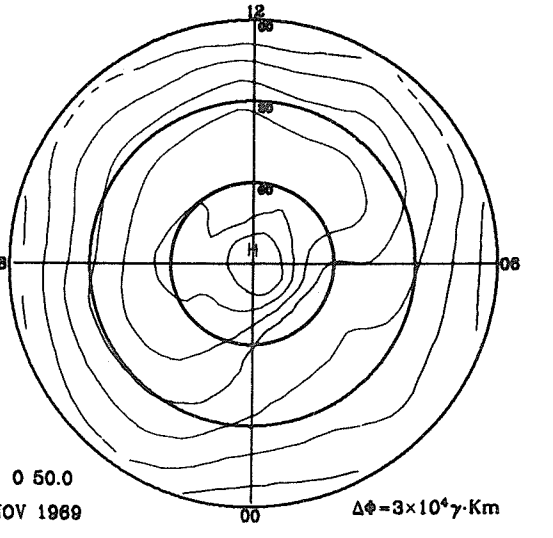
12
00
30
60
18
06
H
00
UT 0 50.0
9 NOV 1969
Δφ=3×10⁴γ·Km

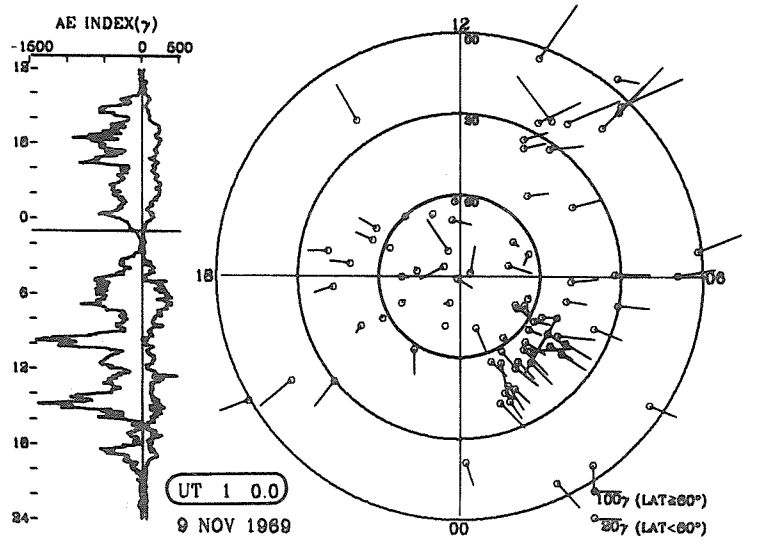
AE INDEX(γ)
-1600
0
600
12
18
0
6
12
18
24
12
60
30
60
18
06
00
UT 1 0.0
9 NOV 1969
100γ (LAT≥60°)
20γ (LAT<60°)

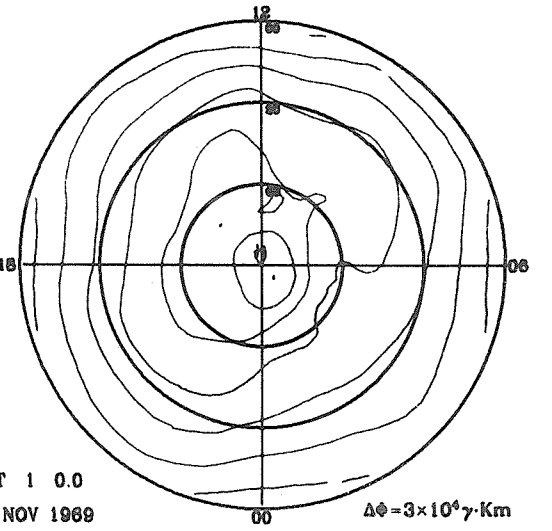
12
60
30
60
18
06
00
UT 1 0.0
9 NOV 1969
Δ∅=3×10⁴γ·Km

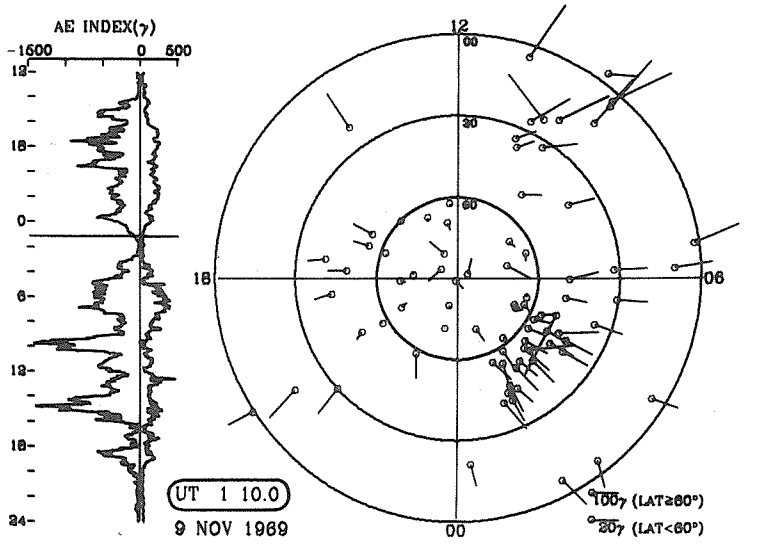
AE INDEX(γ)
-1600
0
600
12
18
0
6
12
18
24
12
60
30
60
18
06
00
UT 1 10.0
9 NOV 1969
100γ (LAT≥60°)
20γ (LAT<60°)

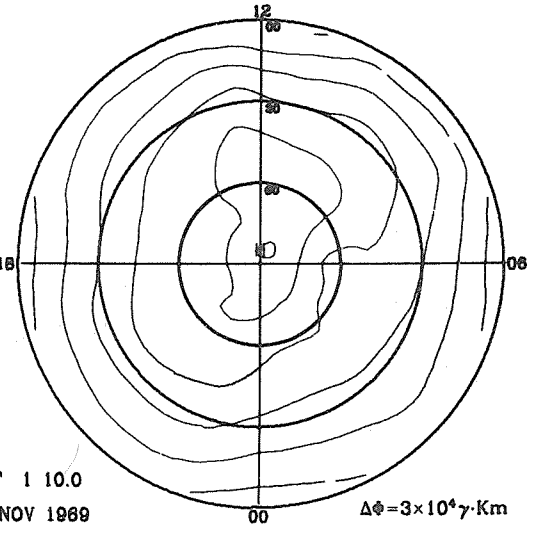
12
60
30
60
18
06
00
UT 1 10.0
9 NOV 1969
Δ∅=3×10⁴γ·Km

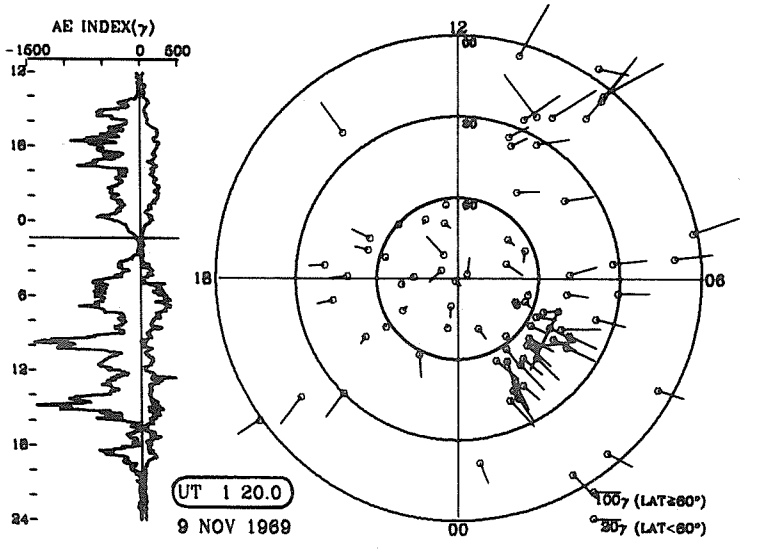
AE INDEX(γ)
-1600
0
600
12
18
0
6
12
18
24
12
60
30
60
18
06
00
UT 1 20.0
9 NOV 1969
100γ (LAT≥60°)
20γ (LAT<60°)

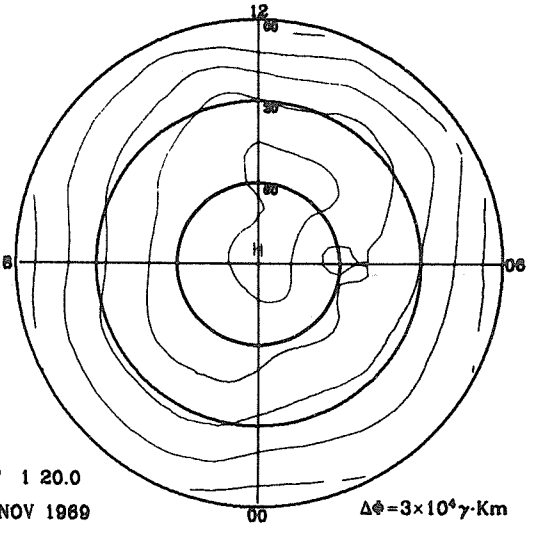
12
60
30
60
18
06
00
UT 1 20.0
9 NOV 1969
Δ∅=3×10⁴γ·Km

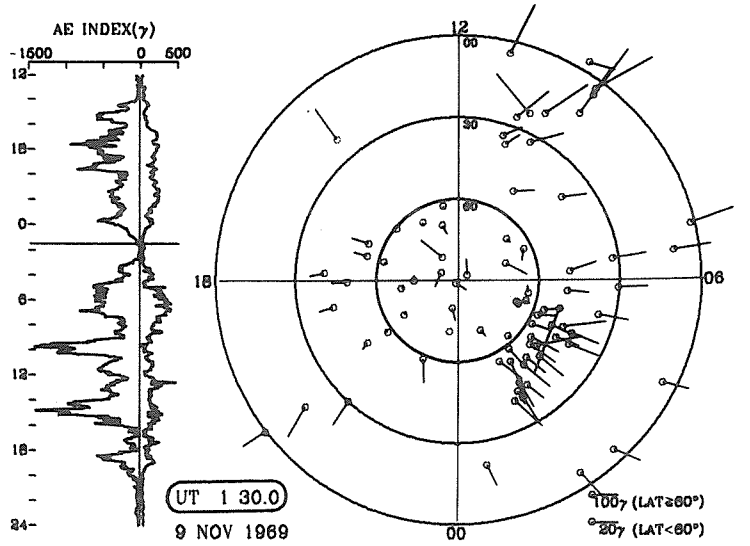
AE INDEX(γ)
-1600
0
500
12
18
0
6
12
18
24
12
00
30
60
18
06
00
UT 1 30.0
9 NOV 1969
100γ (LAT≥60°)
30γ (LAT<60°)

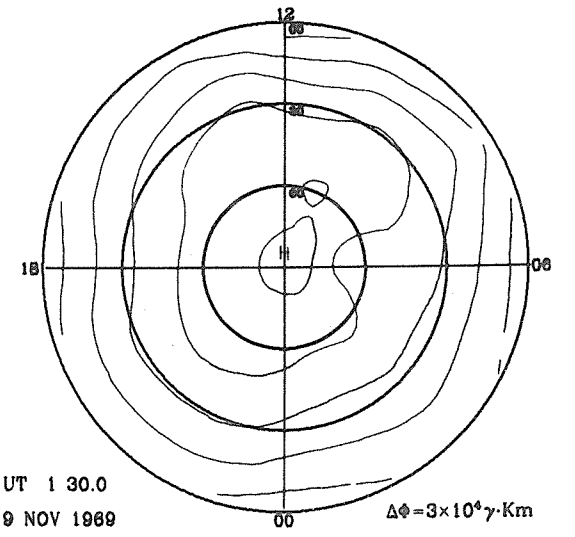
12
00
30
60
18
06
00
UT 1 30.0
9 NOV 1969
Δφ=3×10⁴γ·Km

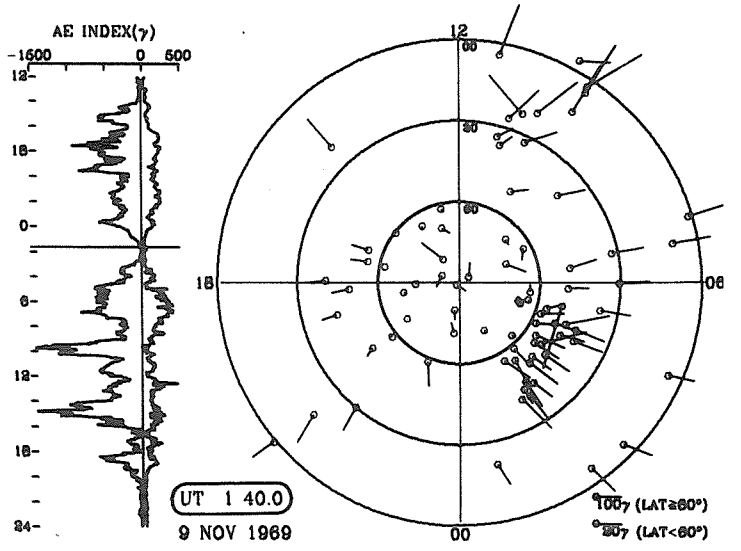
AE INDEX(γ)
-1600
0
500
12
18
0
6
12
18
24
12
00
30
60
18
06
00
UT 1 40.0
9 NOV 1969
100γ (LAT≥60°)
30γ (LAT<60°)

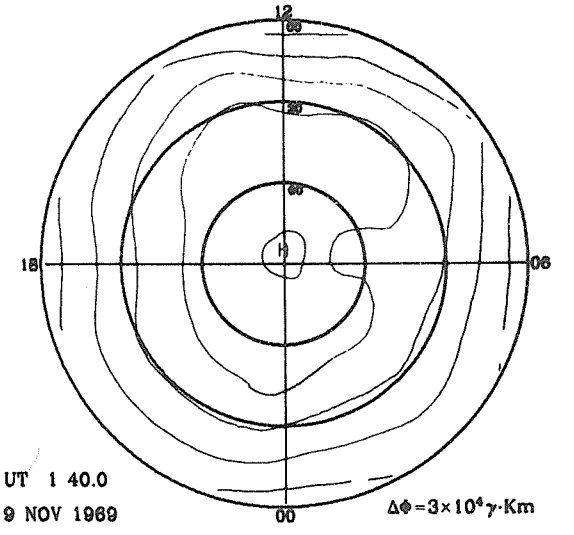
12
00
30
60
18
06
00
UT 1 40.0
9 NOV 1969
Δφ=3×10⁴γ·Km

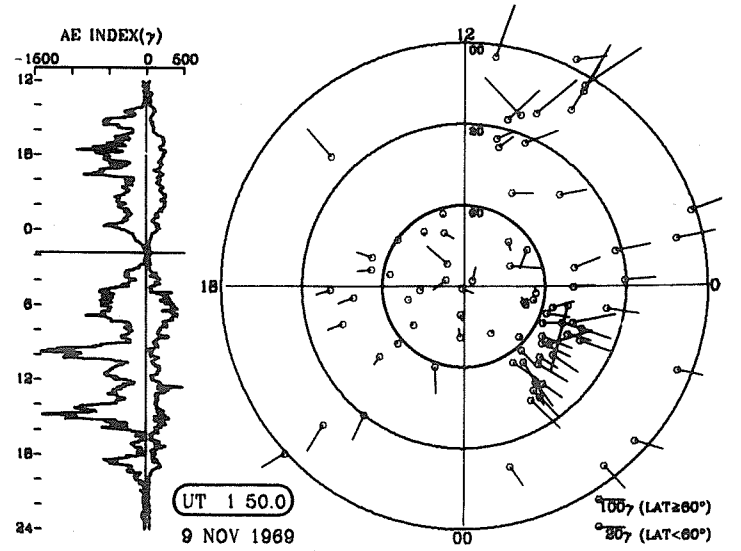
AE INDEX(γ)
-1600
0
500
12
18
0
6
12
18
24
12
00
30
60
18
0
00
UT 1 50.0
9 NOV 1969
100γ (LAT≥60°)
30γ (LAT<60°)

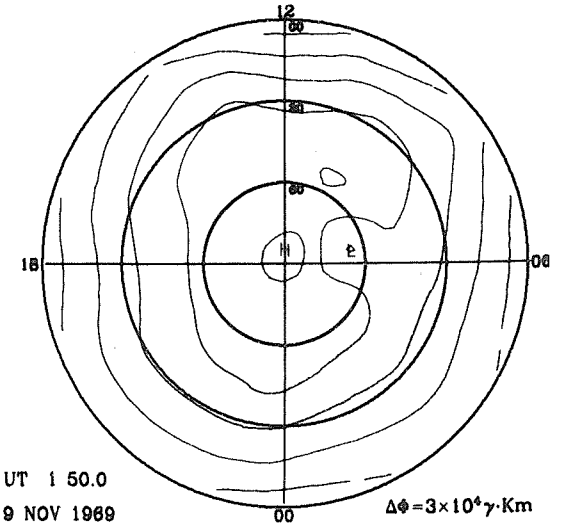
12
00
30
60
18
06
00
UT 1 50.0
9 NOV 1969
Δφ=3×10⁴γ·Km

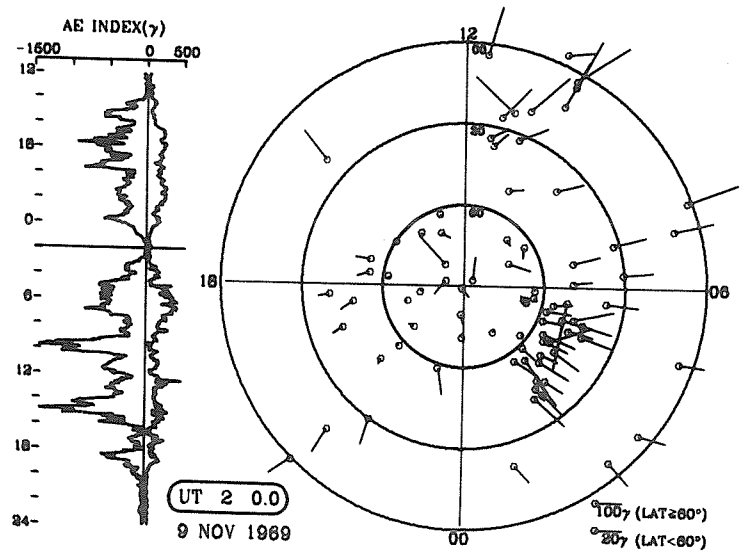
AE INDEX(γ)
-1600
0
500
12
18
0
6
12
18
24
12
60
30
60
18
06
00
UT 2 0.0
9 NOV 1969
100γ (LAT≥60°)
20γ (LAT<60°)

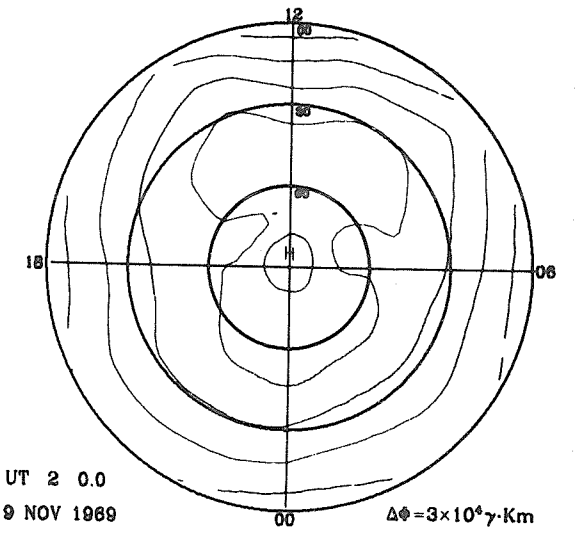
12
60
30
60
18
06
H
00
UT 2 0.0
9 NOV 1969
Δφ=3×10⁴γ·Km

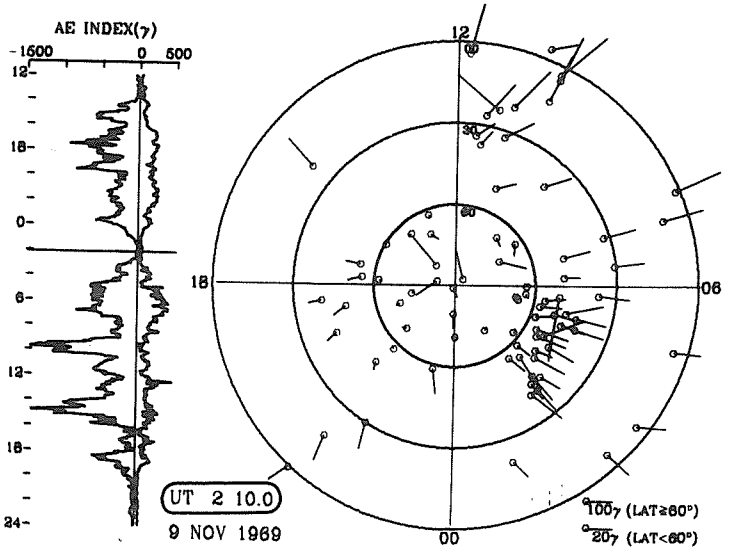
AE INDEX(γ)
-1600
0
500
12
18
0
6
12
18
24
12
60
30
60
18
06
00
UT 2 10.0
9 NOV 1969
100γ (LAT≥60°)
20γ (LAT<60°)

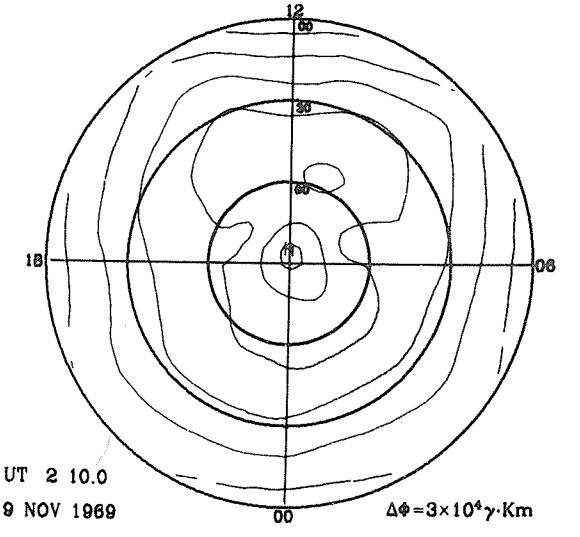
12
60
30
60
18
06
H
00
UT 2 10.0
9 NOV 1969
Δφ=3×10⁴γ·Km

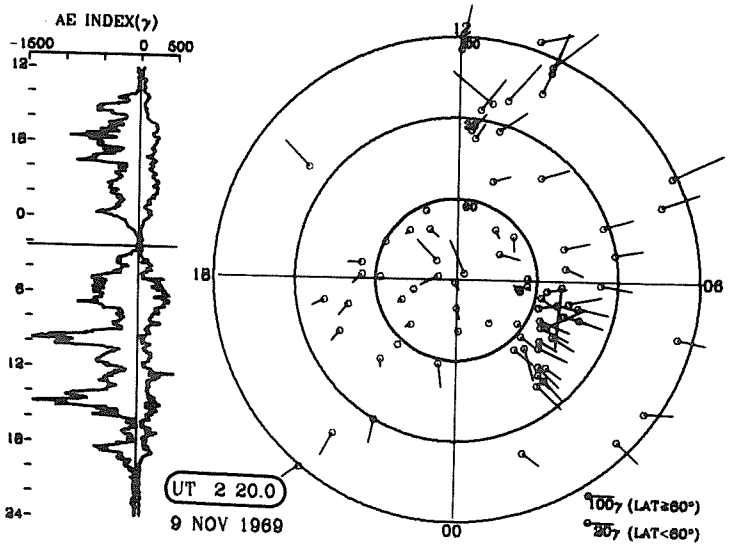
AE INDEX(γ)
-1600
0
500
12
18
0
6
12
18
24
12
60
30
60
18
06
00
UT 2 20.0
9 NOV 1969
100γ (LAT≥60°)
20γ (LAT<60°)

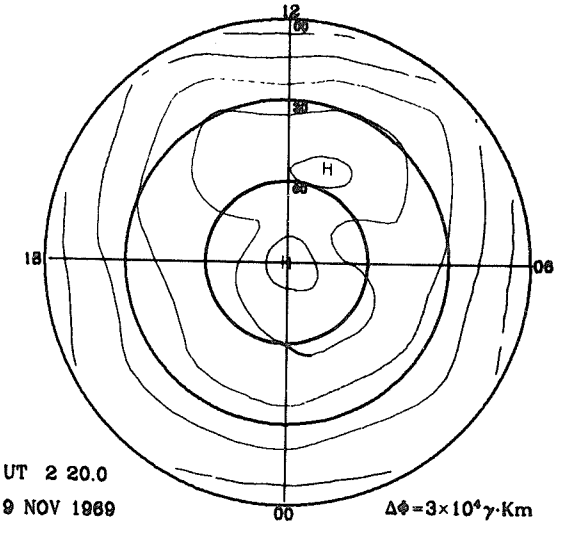
12
60
30
H
60
18
06
H
00
UT 2 20.0
9 NOV 1969
Δφ=3×10⁴γ·Km

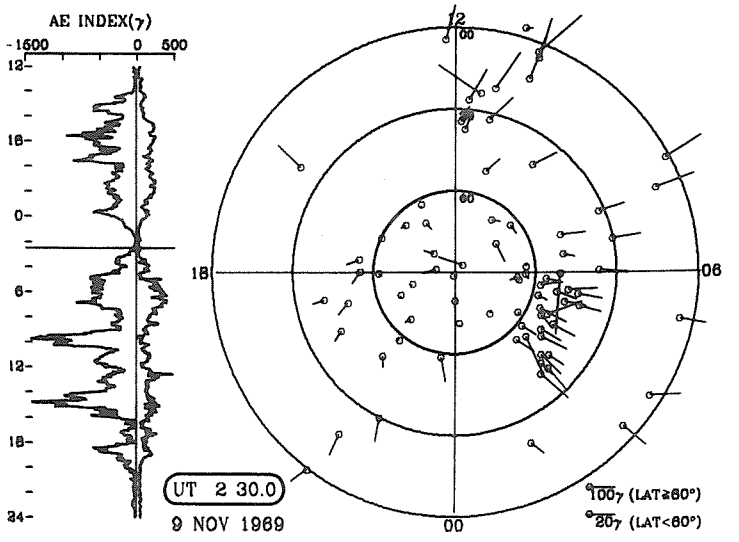
AE INDEX(γ)
-1500
0
500
12
18
0
6
12
18
24
12
60
30
60
18
06
00
UT 2 30.0
9 NOV 1969
100γ (LAT≥60°)
20γ (LAT<60°)

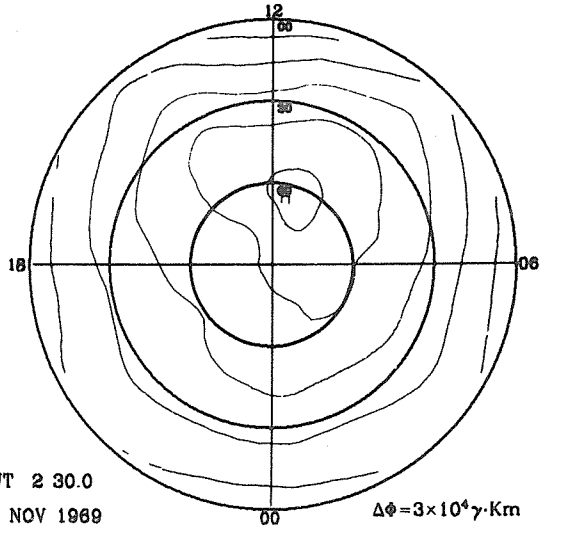
12
60
30
60
H
18
06
00
UT 2 30.0
9 NOV 1969
Δφ=3×10⁴γ·Km

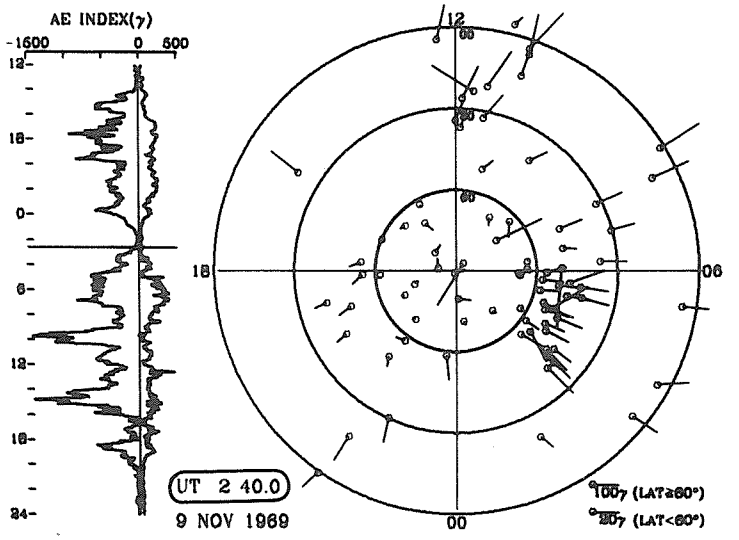
AE INDEX(γ)
-1500
0
500
12
18
0
6
12
18
24
12
60
30
60
18
06
00
UT 2 40.0
9 NOV 1969
100γ (LAT≥60°)
20γ (LAT<60°)

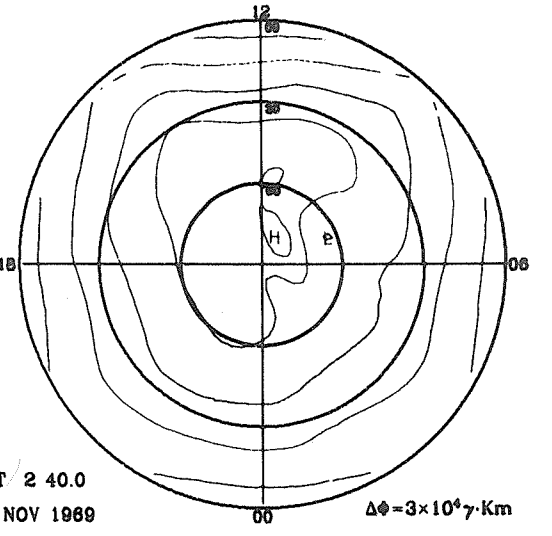
12
60
30
60
H
P
18
06
00
UT 2 40.0
9 NOV 1969
Δφ=3×10⁴γ·Km

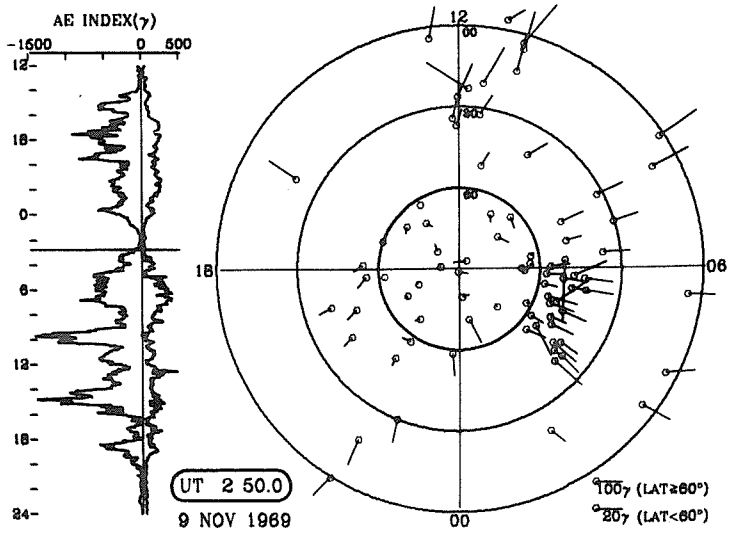
AE INDEX(γ)
-1500
0
500
12
18
0
6
12
18
24
12
60
30
60
18
06
00
UT 2 50.0
9 NOV 1969
100γ (LAT≥60°)
20γ (LAT<60°)

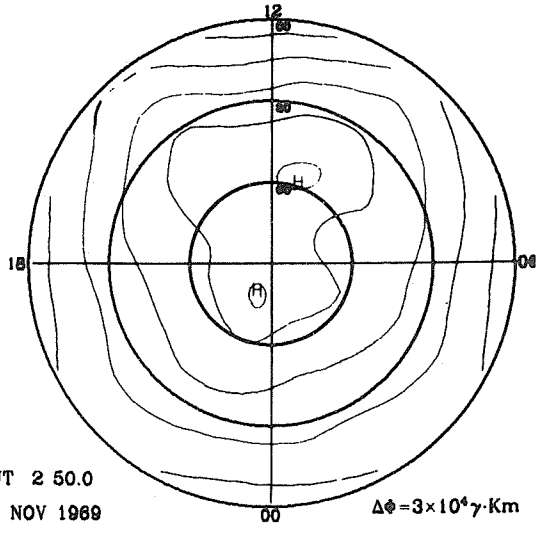
12
60
30
60
H
H
18
06
00
UT 2 50.0
9 NOV 1969
Δφ=3×10⁴γ·Km

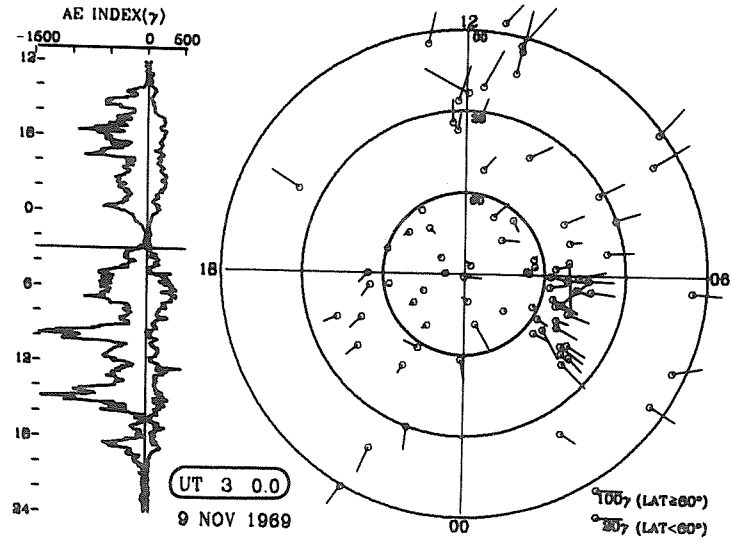
AE INDEX(γ)
-1600
0
600
12
18
0
6
12
18
24
UT 3 0.0
9 NOV 1969
12
18
06
00
100γ (LAT≥60°)
30γ (LAT<60°)

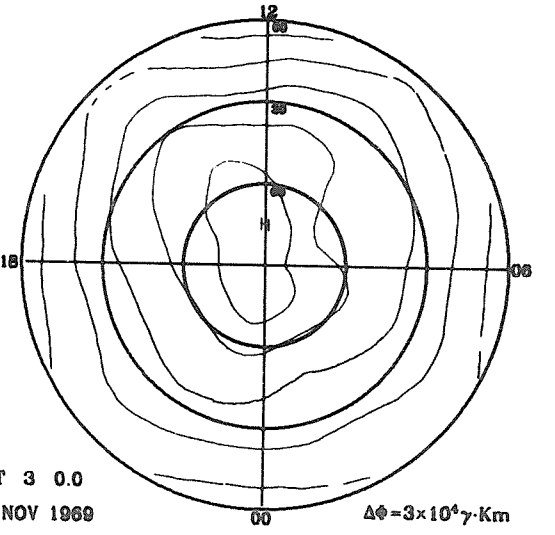
12
18
06
00
H
UT 3 0.0
9 NOV 1969
Δφ=3×10⁴γ·Km

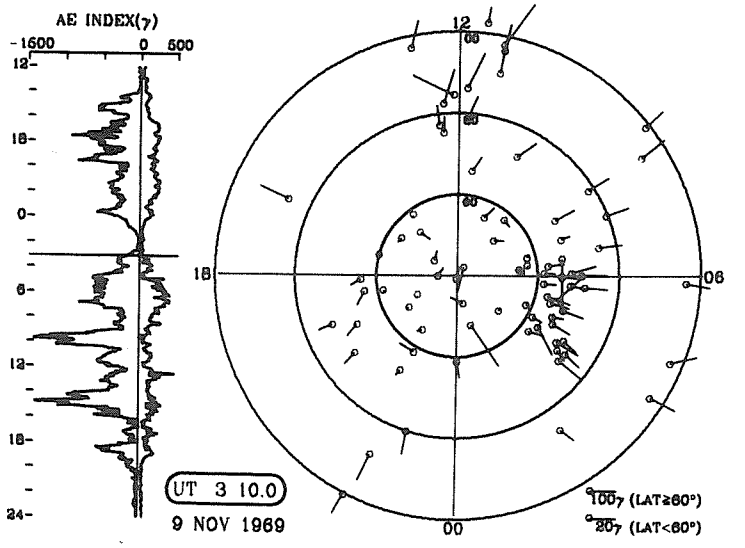
AE INDEX(γ)
-1600
0
600
12
18
0
6
12
18
24
UT 3 10.0
9 NOV 1969
12
18
06
00
100γ (LAT≥60°)
30γ (LAT<60°)

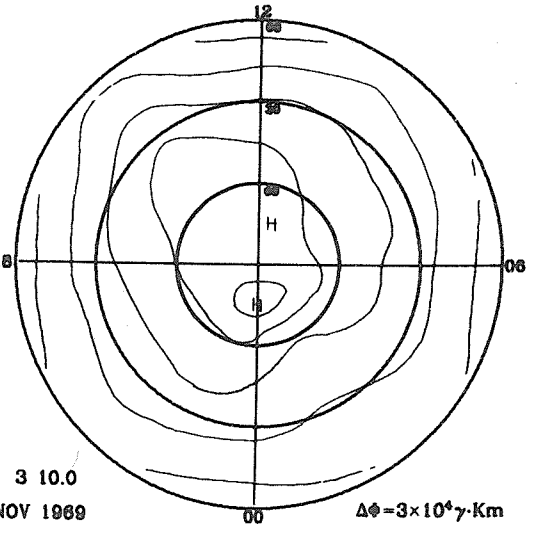
12
18
06
00
H
H
UT 3 10.0
9 NOV 1969
Δφ=3×10⁴γ·Km

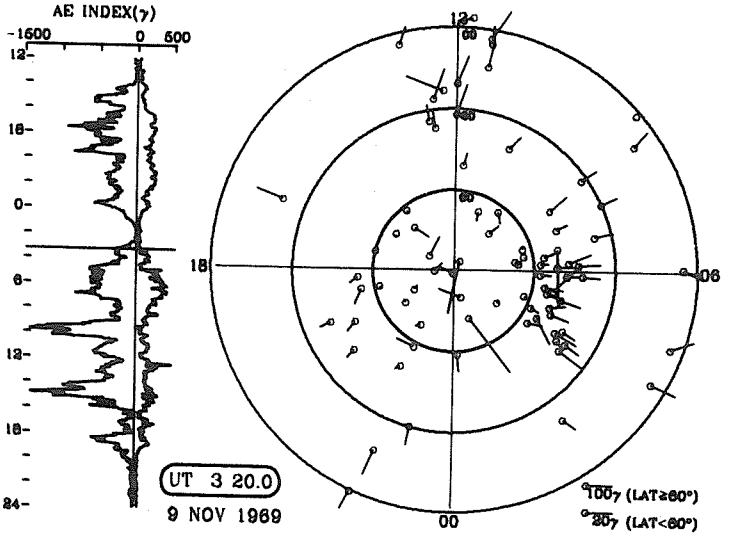
AE INDEX(γ)
-1600
0
600
12
18
0
6
12
18
24
UT 3 20.0
9 NOV 1969
12
18
06
00
100γ (LAT≥60°)
30γ (LAT<60°)

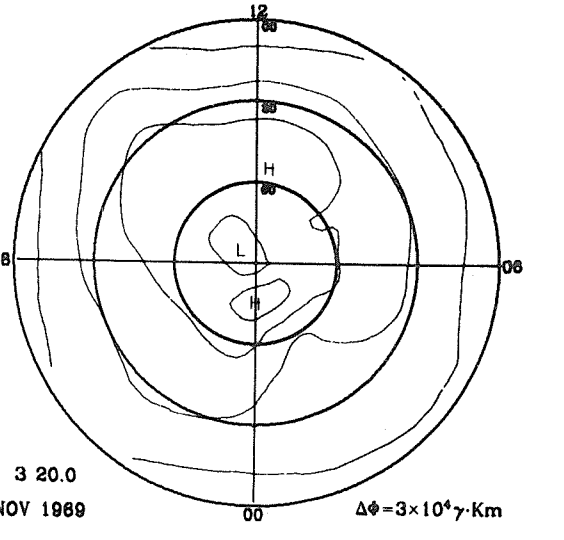
12
18
06
00
H
L
H
UT 3 20.0
9 NOV 1969
Δφ=3×10⁴γ·Km

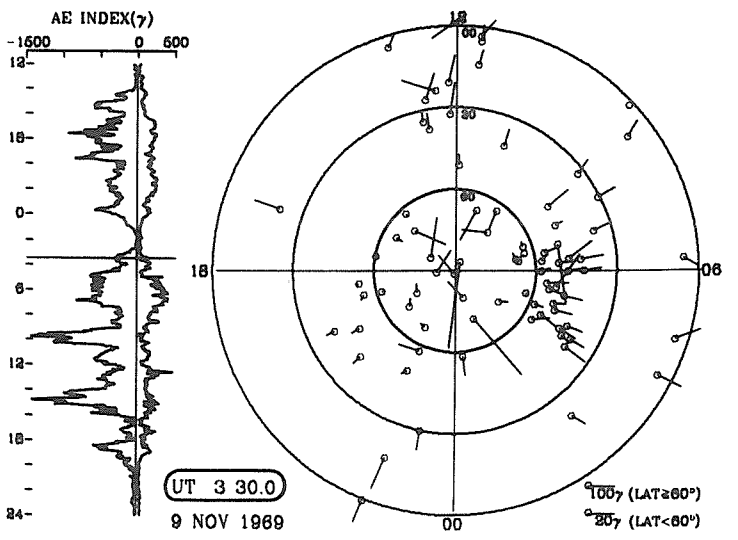
AE INDEX(γ)
-1600
0
600
12
18
0
6
12
18
24
12
00
30
60
18
06
UT 3 30.0
9 NOV 1969
100γ (LAT≥60°)
20γ (LAT<60°)

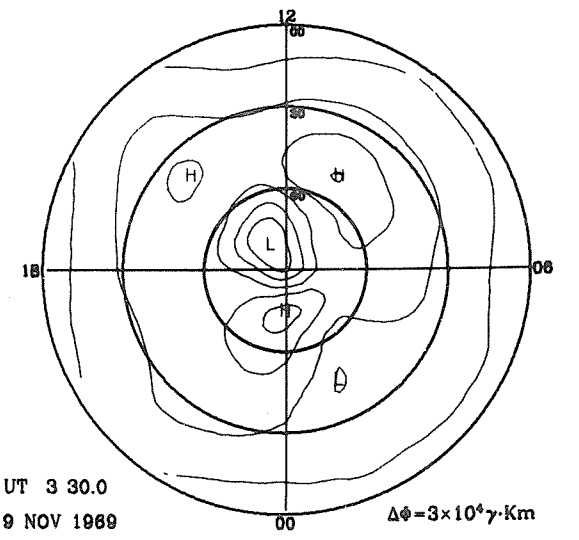
12
00
30
60
18
06
H
L
UT 3 30.0
9 NOV 1969
Δφ=3×10⁴γ·Km

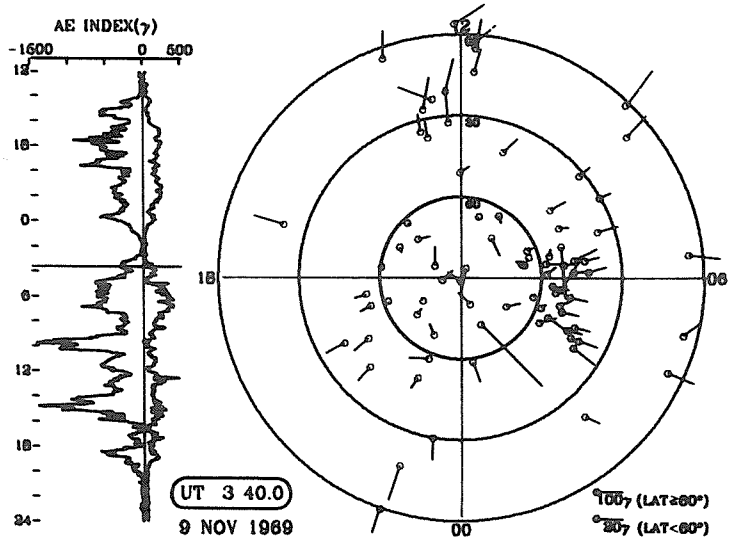
AE INDEX(γ)
-1600
0
600
12
18
0
6
12
18
24
12
00
30
60
18
06
UT 3 40.0
9 NOV 1969
100γ (LAT≥60°)
20γ (LAT<60°)

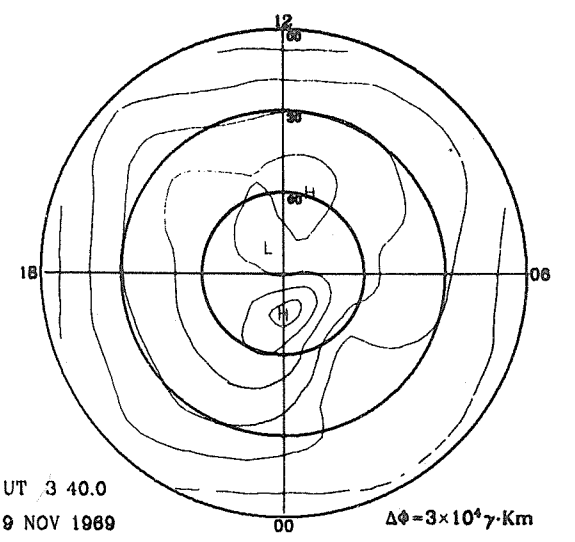
12
00
30
60
18
06
H
L
UT 3 40.0
9 NOV 1969
Δφ=3×10⁴γ·Km

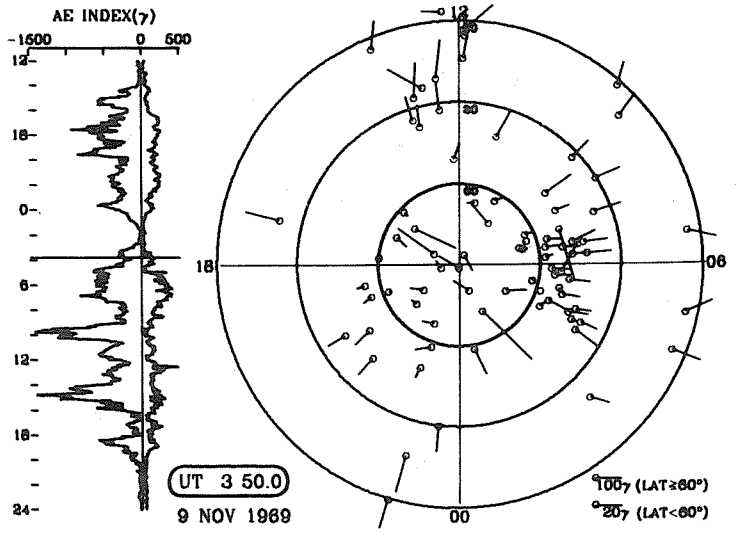
AE INDEX(γ)
-1600
0
600
12
18
0
6
12
18
24
12
00
30
60
18
06
UT 3 50.0
9 NOV 1969
100γ (LAT≥60°)
20γ (LAT<60°)

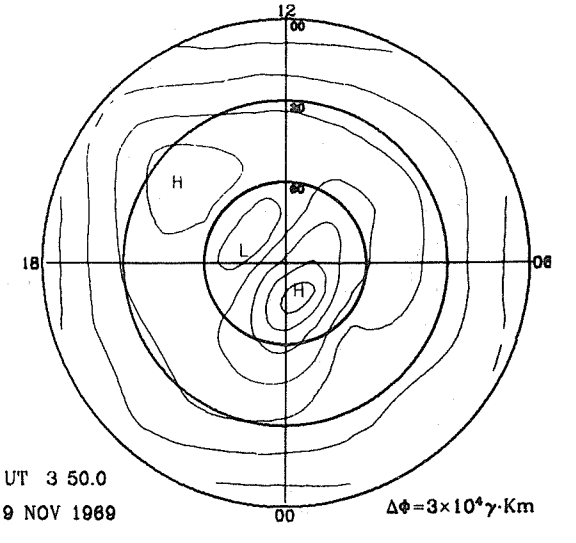
12
00
30
60
18
06
H
L
UT 3 50.0
9 NOV 1969
Δφ=3×10⁴γ·Km

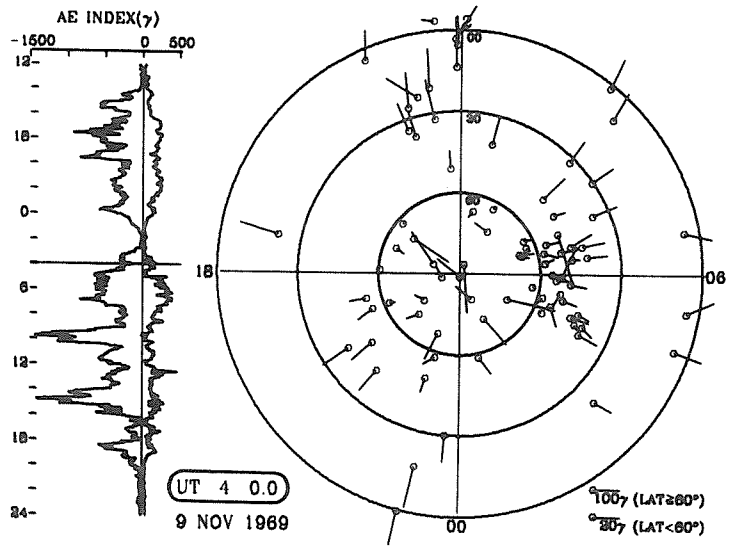
AE INDEX(γ)
-1500
0
500
12
18
0
6
12
18
24
12
00
30
60
18
06
00
UT 4 0.0
9 NOV 1969
100γ (LAT≥60°)
30γ (LAT<60°)

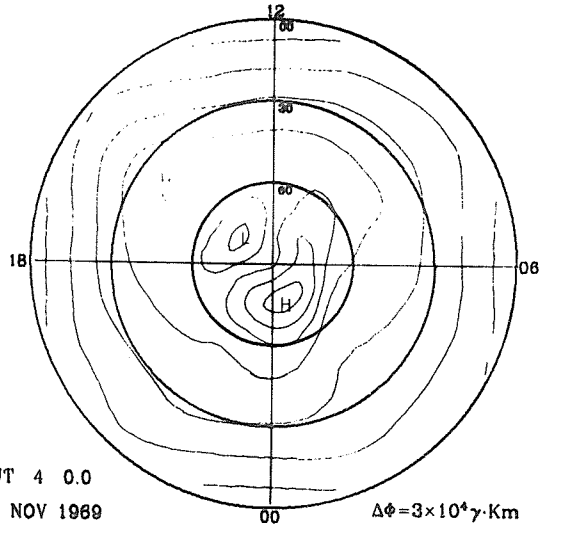
12
00
30
60
18
06
00
H
L
UT 4 0.0
9 NOV 1969
Δφ=3×10⁴γ·Km

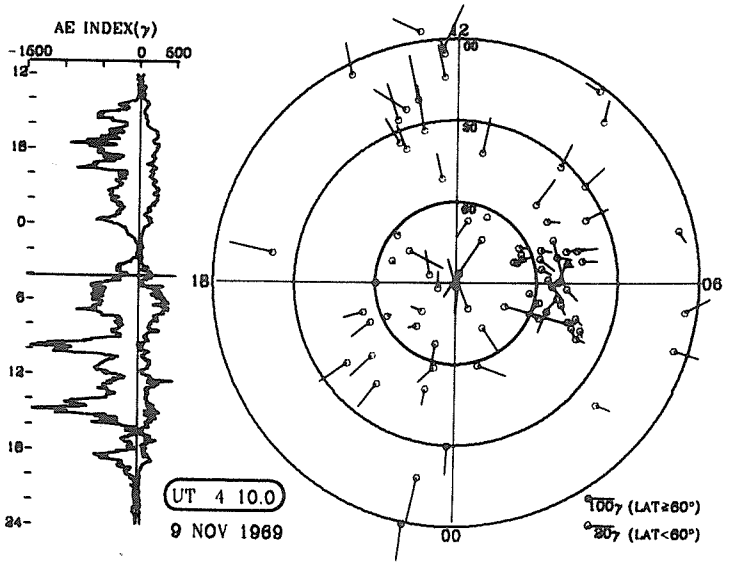
AE INDEX(γ)
-1500
0
500
12
18
0
6
12
18
24
12
00
30
60
18
06
00
UT 4 10.0
9 NOV 1969
100γ (LAT≥60°)
30γ (LAT<60°)

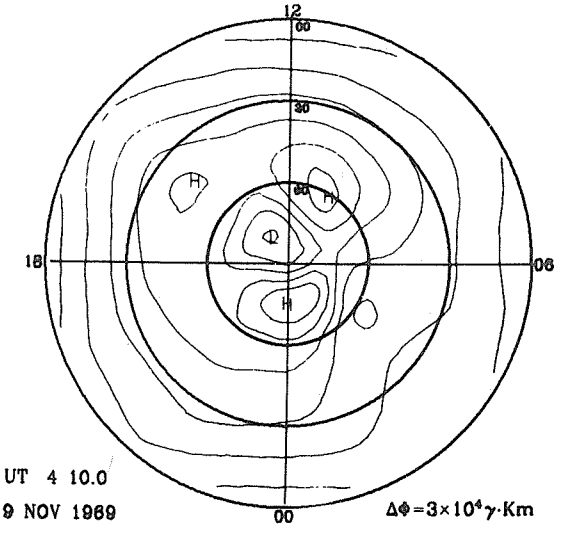
12
00
30
60
18
06
00
H
L
UT 4 10.0
9 NOV 1969
Δφ=3×10⁴γ·Km

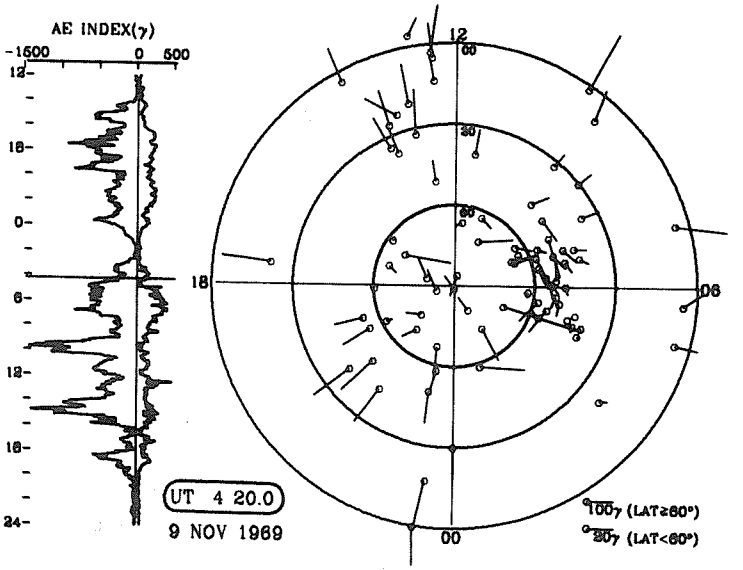
AE INDEX(γ)
-1500
0
500
12
18
0
6
12
18
24
12
00
30
60
18
06
00
UT 4 20.0
9 NOV 1969
100γ (LAT≥60°)
30γ (LAT<60°)

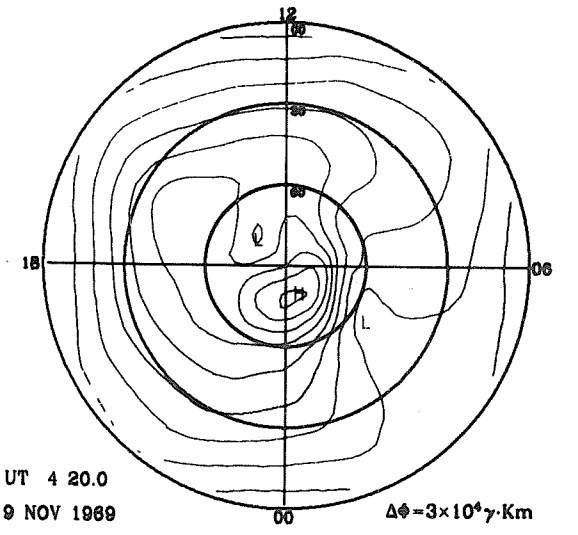
12
00
30
60
18
06
00
H
L
UT 4 20.0
9 NOV 1969
Δφ=3×10⁴γ·Km

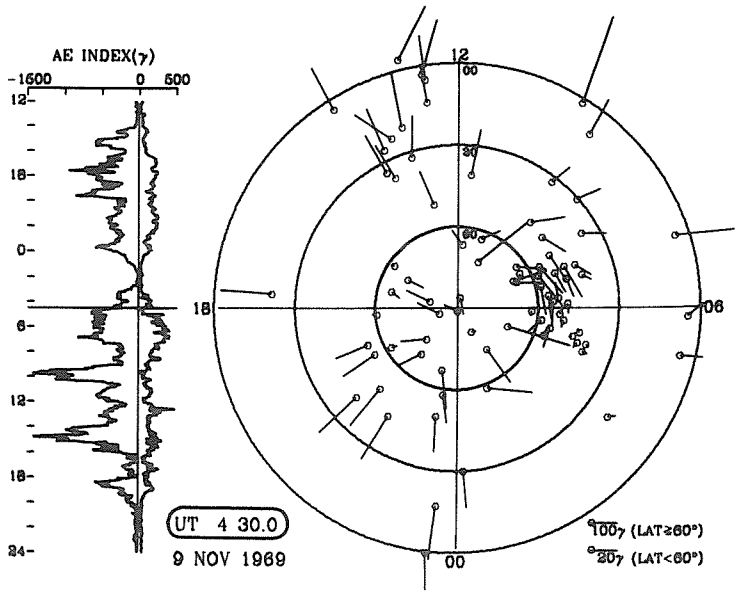
AE INDEX(γ)
-1600
0
500
12
18
0
6
12
18
24
12
00
30
60
18
06
00
UT 4 30.0
9 NOV 1969
100γ (LAT≥60°)
20γ (LAT<60°)

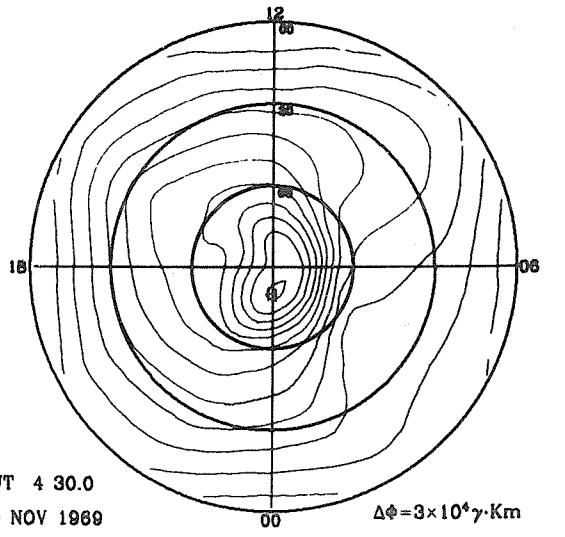
12
00
30
60
18
06
00
UT 4 30.0
9 NOV 1969
Δφ=3×10⁴γ·Km

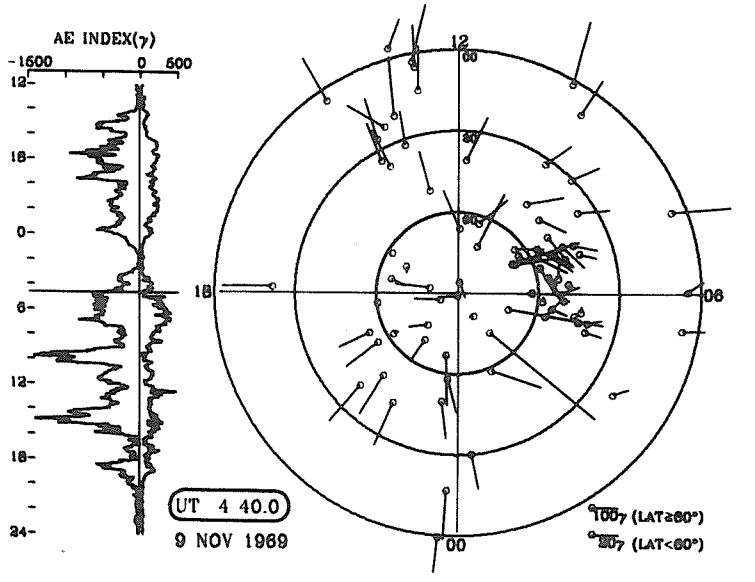
AE INDEX(γ)
-1600
0
500
12
18
0
6
12
18
24
12
00
30
60
18
06
00
UT 4 40.0
9 NOV 1969
100γ (LAT≥60°)
20γ (LAT<60°)

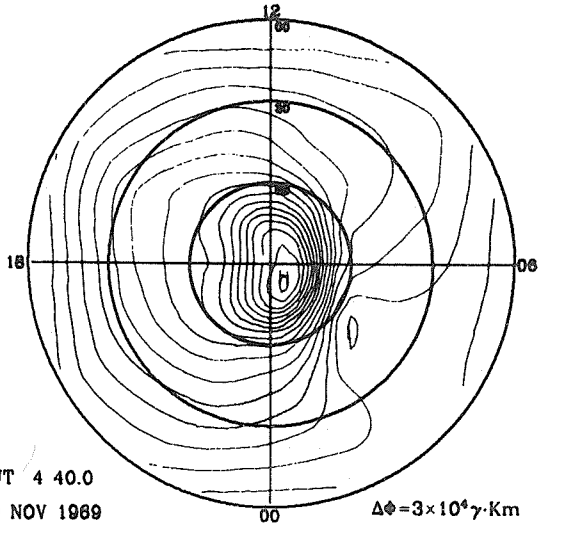
12
00
30
60
18
06
00
UT 4 40.0
9 NOV 1969
Δφ=3×10⁴γ·Km

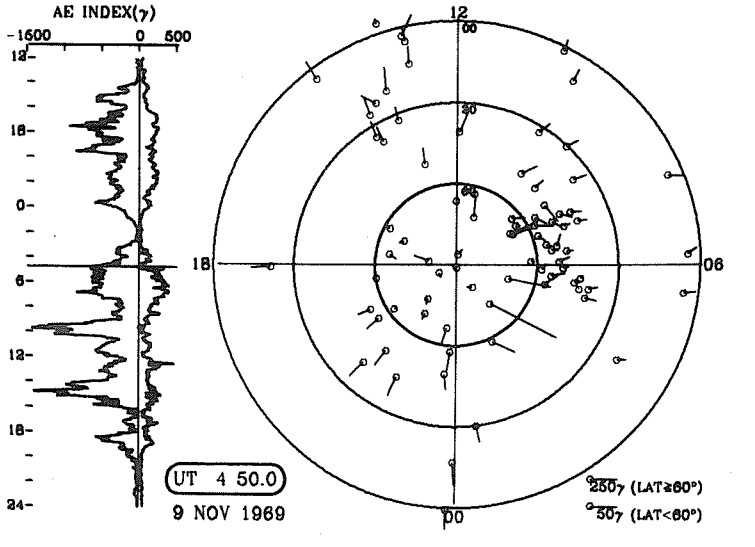
AE INDEX(γ)
-1600
0
500
12
18
0
6
12
18
24
12
00
30
60
18
06
00
UT 4 50.0
9 NOV 1969
250γ (LAT≥60°)
50γ (LAT<60°)

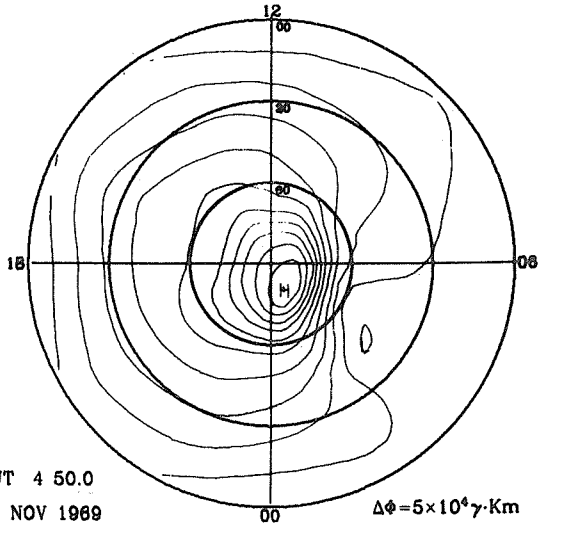
12
00
30
60
18
06
00
UT 4 50.0
9 NOV 1969
Δφ=5×10⁴γ·Km

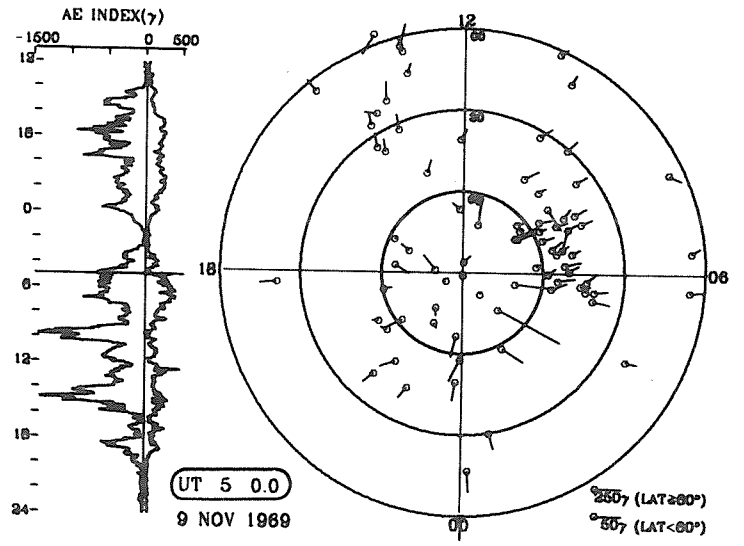
AE INDEX(γ)
-1500
0
600
12
18
0
6
12
18
24
12
60
30
60
18
06
00
UT 5 0.0
9 NOV 1969
250γ (LAT≥60°)
50γ (LAT<60°)

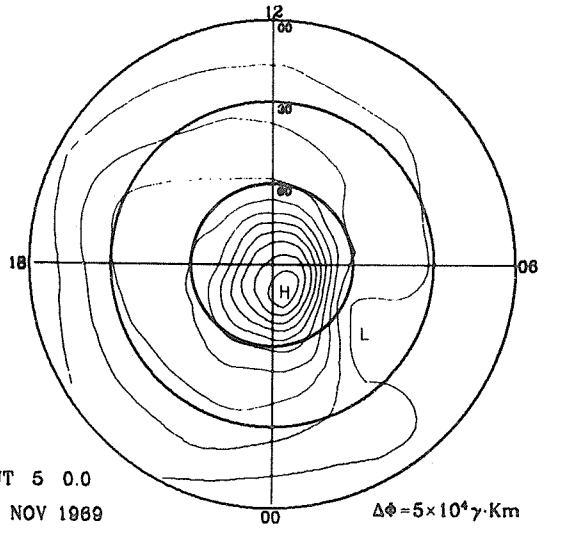
12
00
30
60
18
06
00
H
L
UT 5 0.0
9 NOV 1969
Δφ=5×10⁴γ·Km

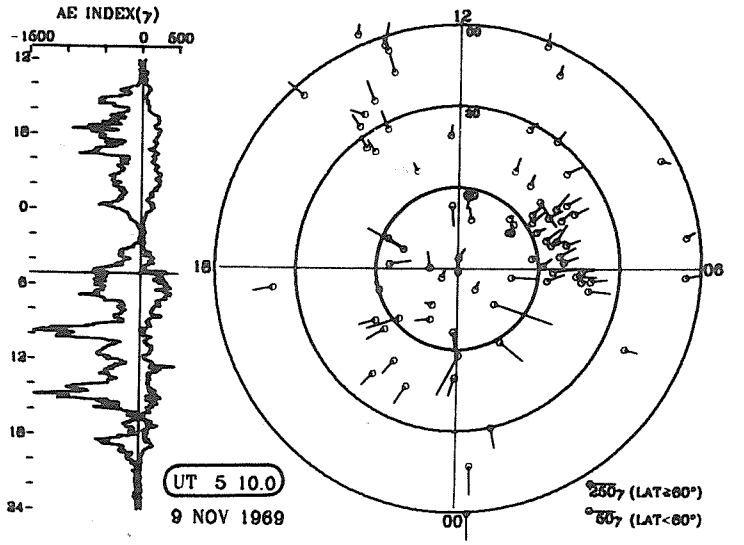
AE INDEX(γ)
-1500
0
600
12
18
0
6
12
18
24
12
60
30
60
18
06
00
UT 5 10.0
9 NOV 1969
250γ (LAT≥60°)
50γ (LAT<60°)

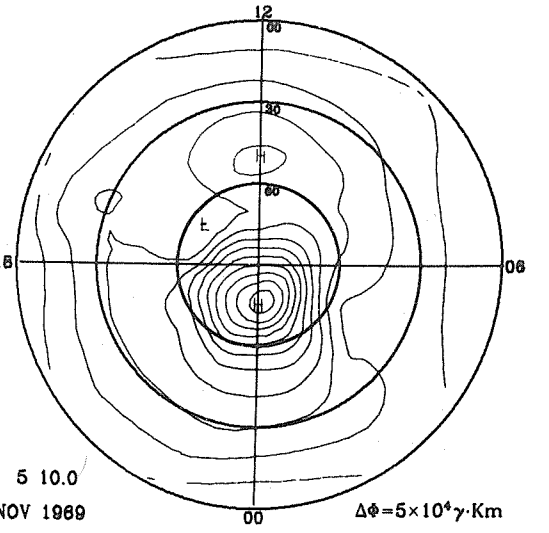
12
00
30
60
18
06
00
H
L
UT 5 10.0
9 NOV 1969
Δφ=5×10⁴γ·Km

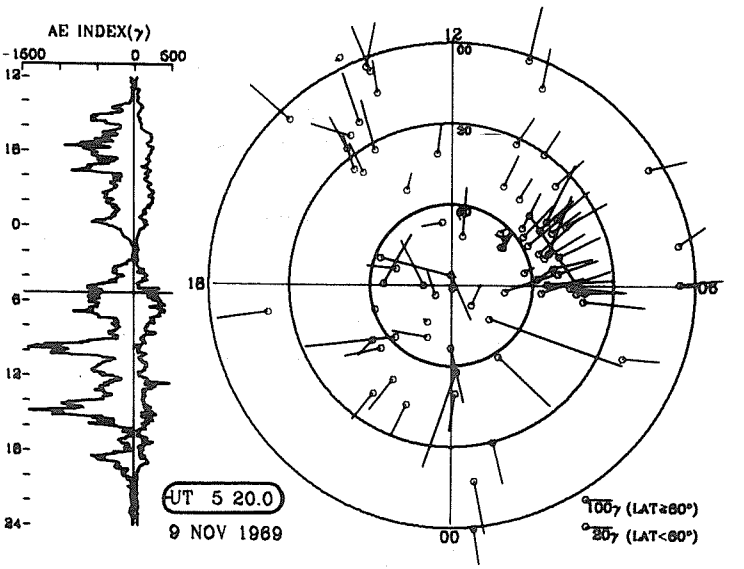
AE INDEX(γ)
-1500
0
600
12
18
0
6
12
18
24
12
60
30
60
18
06
00
UT 5 20.0
9 NOV 1969
100γ (LAT≥60°)
20γ (LAT<60°)

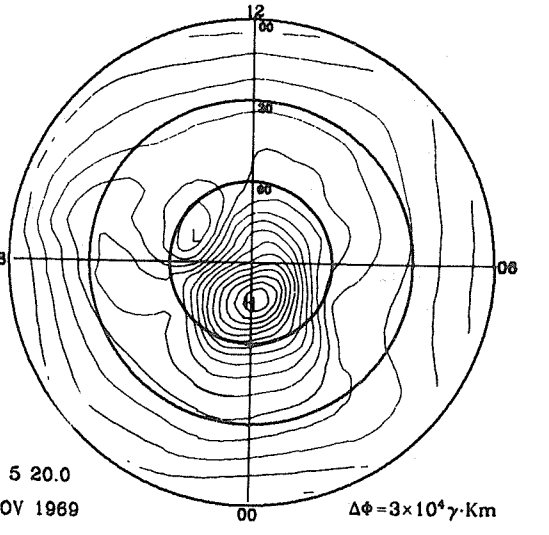
12
00
30
60
18
06
00
L
UT 5 20.0
9 NOV 1969
Δφ=3×10⁴γ·Km

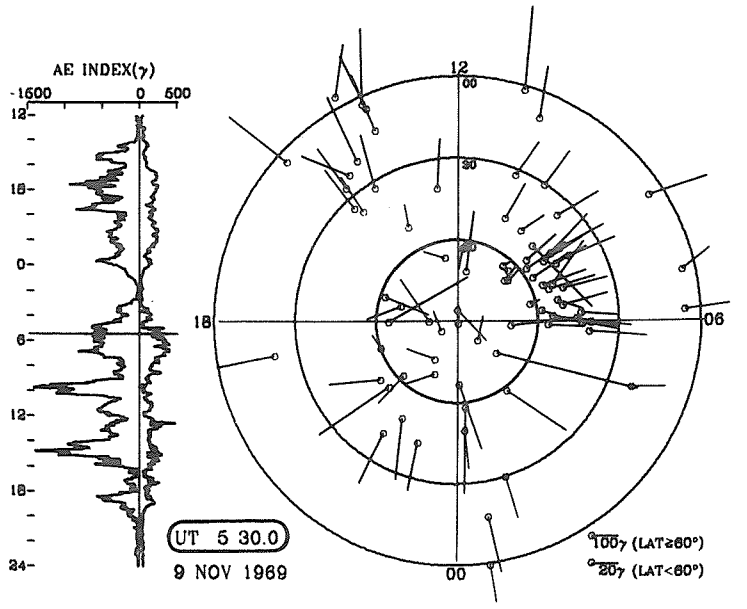
AE INDEX(γ)
-1600
0
500
12
18
0
6
12
18
24
12
00
30
60
18
06
00
UT 5 30.0
9 NOV 1969
100γ (LAT≥60°)
20γ (LAT<60°)

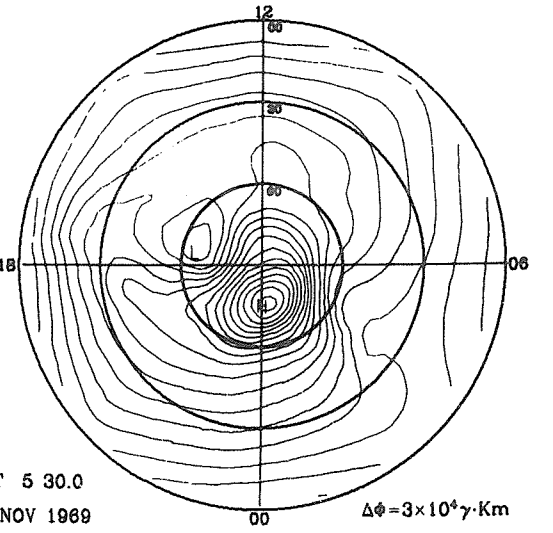
12
00
30
60
18
06
00
L
H
UT 5 30.0
9 NOV 1969
Δφ=3×10⁴γ·Km

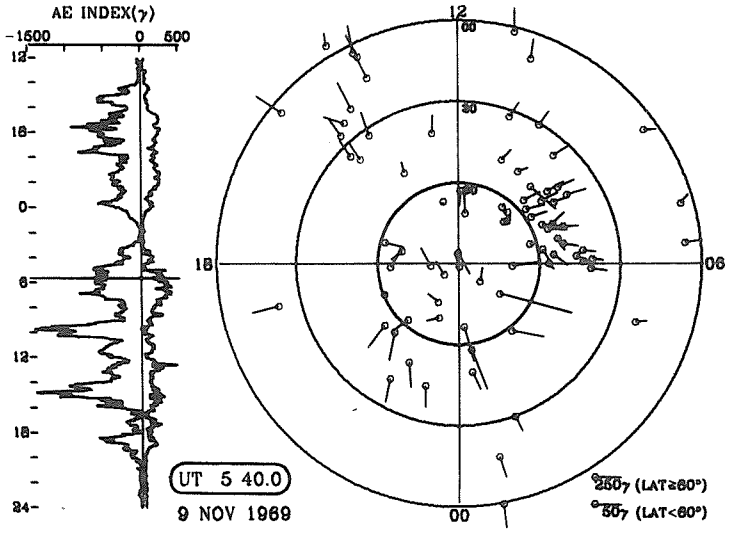
AE INDEX(γ)
-1600
0
500
12
18
0
6
12
18
24
12
00
30
60
18
06
00
UT 5 40.0
9 NOV 1969
250γ (LAT≥60°)
50γ (LAT<60°)

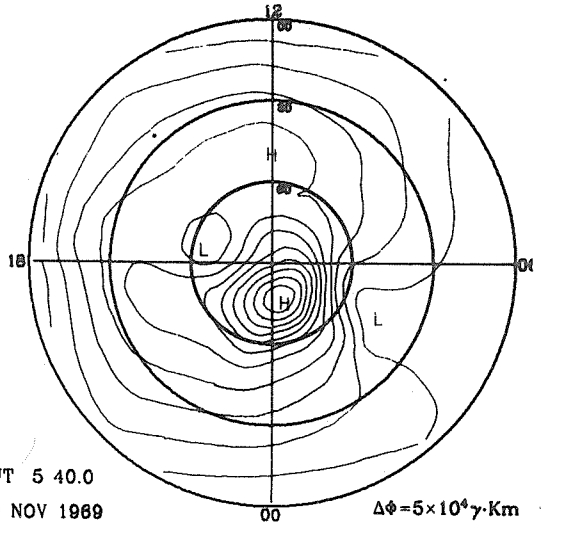
12
00
30
60
18
06
00
H
L
H
L
UT 5 40.0
9 NOV 1969
Δφ=5×10⁴γ·Km

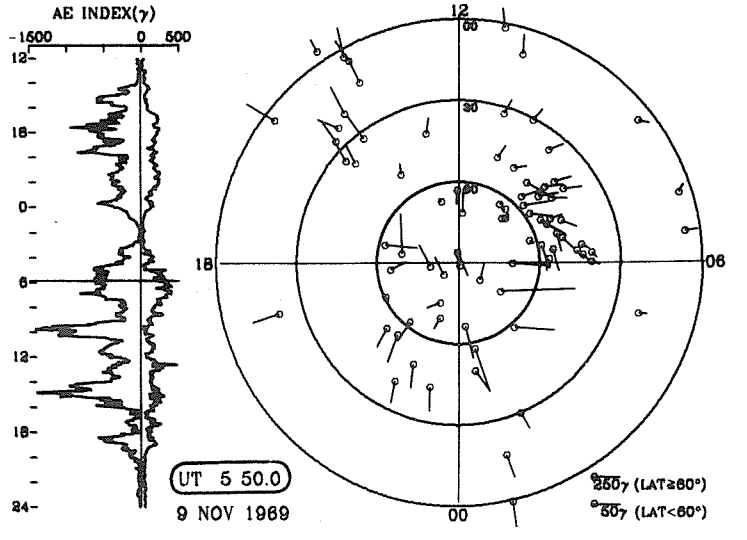
AE INDEX(γ)
-1600
0
500
12
18
0
6
12
18
24
12
00
30
60
18
06
00
UT 5 50.0
9 NOV 1969
250γ (LAT≥60°)
50γ (LAT<60°)

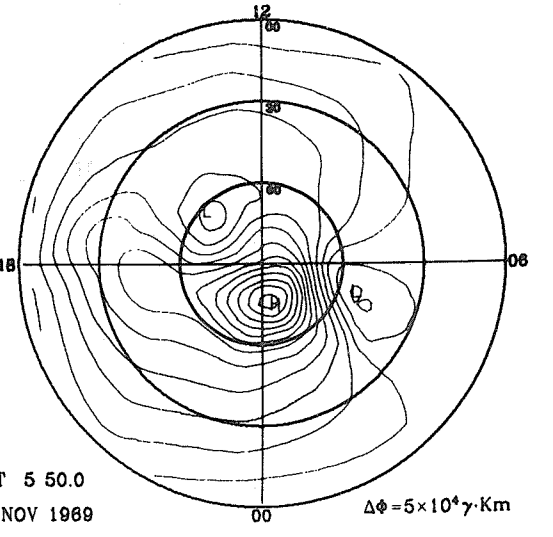
12
00
30
60
18
06
00
L
H
UT 5 50.0
9 NOV 1969
Δφ=5×10⁴γ·Km

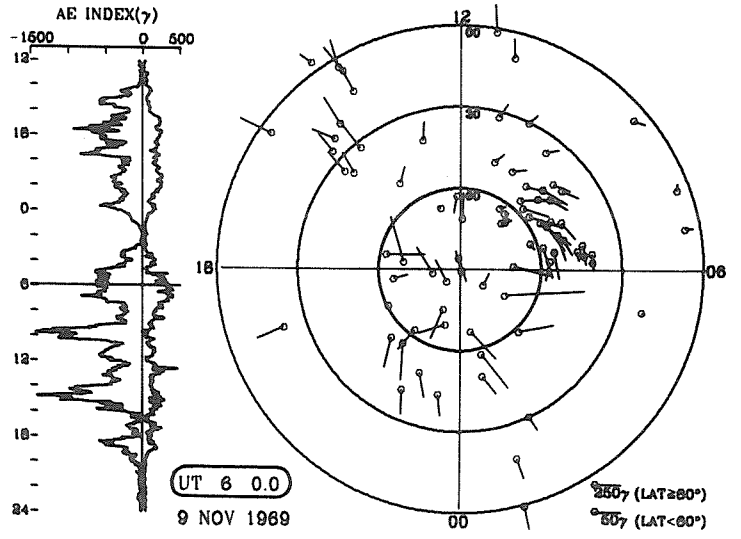
AE INDEX(γ)
-1500
0
500
12
18
0
6
12
18
24
12
00
30
60
18
06
00
UT 6 0.0
9 NOV 1969
250γ (LAT≥60°)
50γ (LAT<60°)

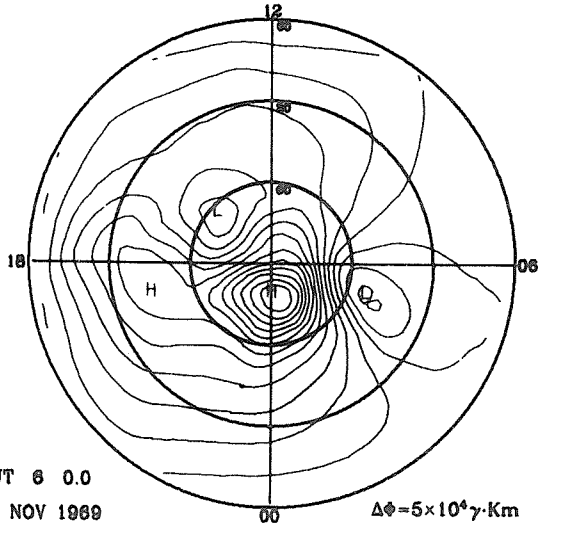
12
00
30
60
18
06
00
L
H
UT 6 0.0
9 NOV 1969
Δφ=5×10⁴γ·Km

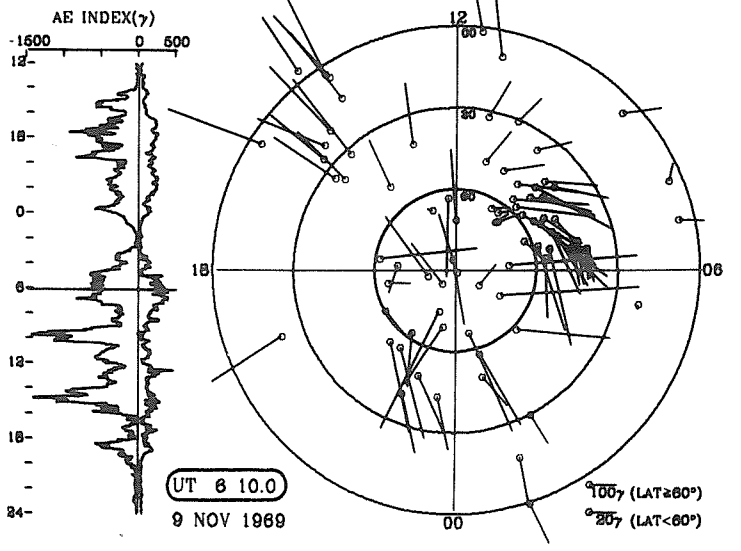
AE INDEX(γ)
-1500
0
500
12
18
0
6
12
18
24
12
00
30
60
18
06
00
UT 6 10.0
9 NOV 1969
100γ (LAT≥60°)
20γ (LAT<60°)

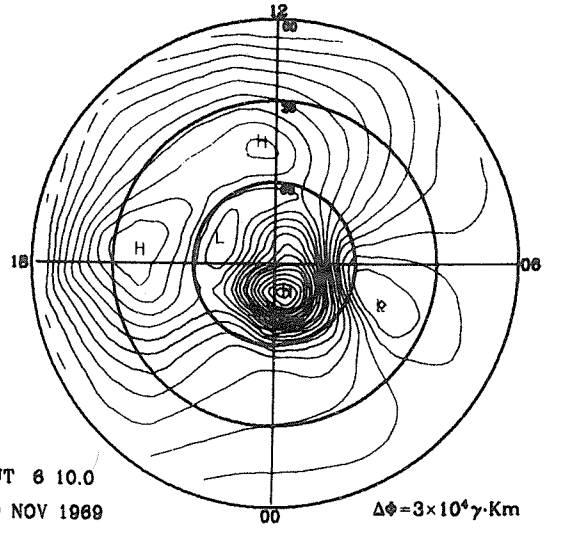
12
00
30
60
18
06
00
H
L
UT 6 10.0
9 NOV 1969
Δφ=3×10⁴γ·Km

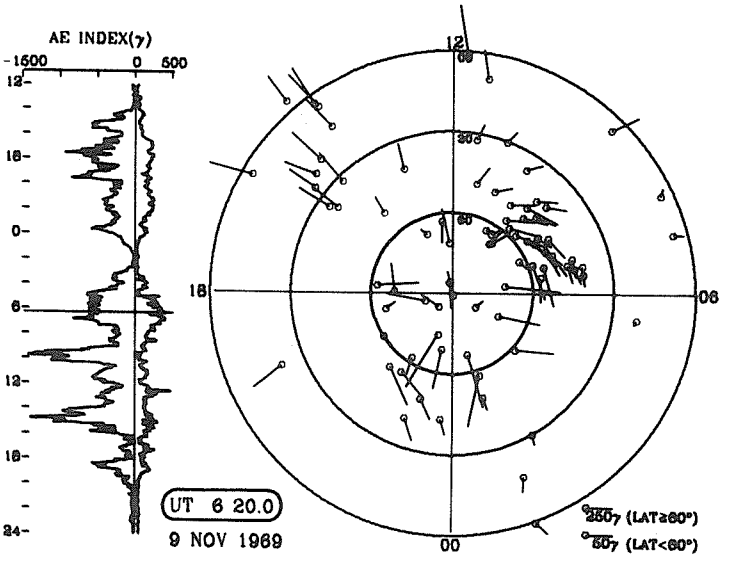
AE INDEX(γ)
-1500
0
500
12
18
0
6
12
18
24
12
00
30
60
18
06
00
UT 6 20.0
9 NOV 1969
250γ (LAT≥60°)
50γ (LAT<60°)

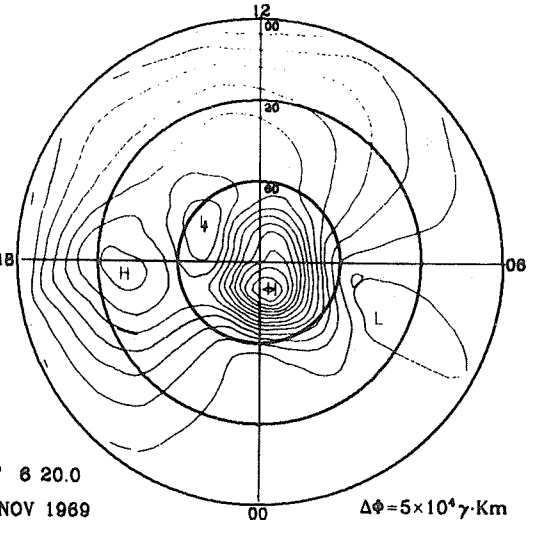
12
00
30
60
18
06
00
H
L
UT 6 20.0
9 NOV 1969
Δφ=5×10⁴γ·Km

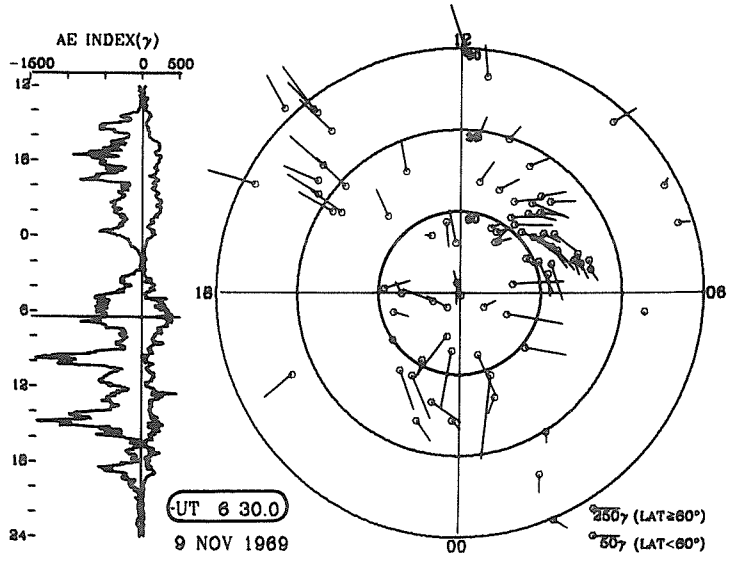
AE INDEX(γ)
-1600
0
500
12
18
0
6
12
18
24
12
30
60
18
06
00
UT 6 30.0
9 NOV 1969
250γ (LAT≥60°)
50γ (LAT<60°)

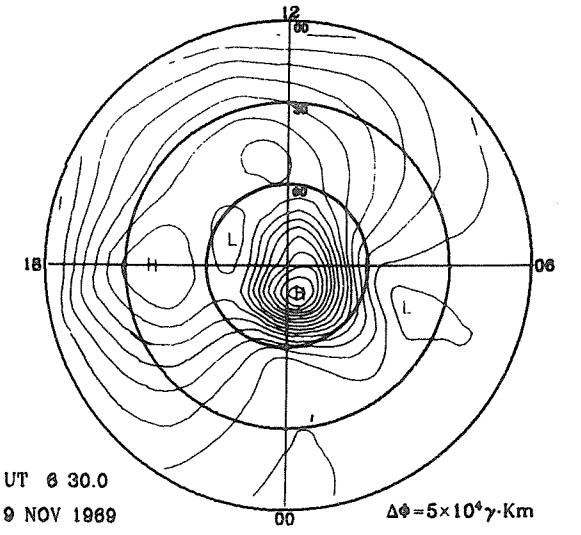
12
00
30
60
18
06
H
L
L
UT 6 30.0
9 NOV 1969
Δφ=5×10⁴γ·Km

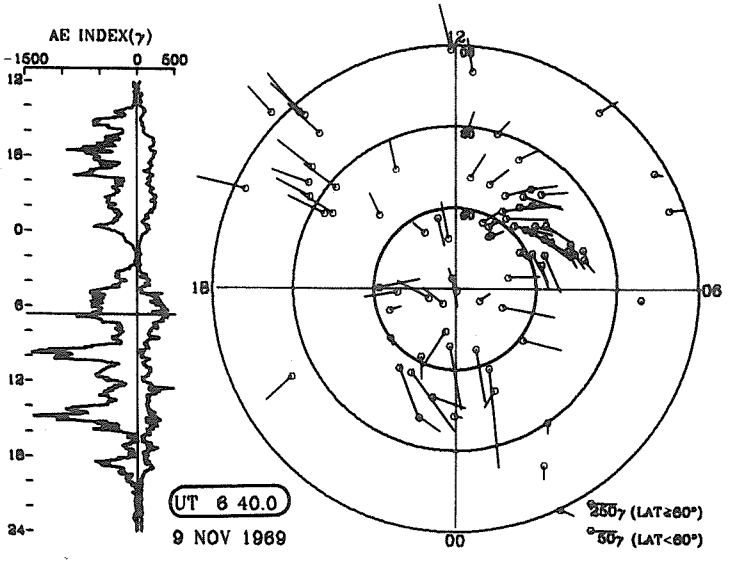
AE INDEX(γ)
-1600
0
500
12
18
0
6
12
18
24
12
30
60
18
06
00
UT 6 40.0
9 NOV 1969
250γ (LAT≥60°)
50γ (LAT<60°)

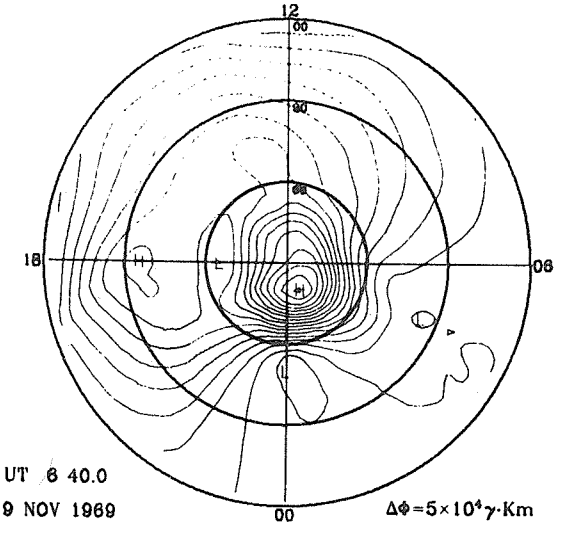
12
00
30
60
18
06
H
L
H
L
UT 6 40.0
9 NOV 1969
Δφ=5×10⁴γ·Km

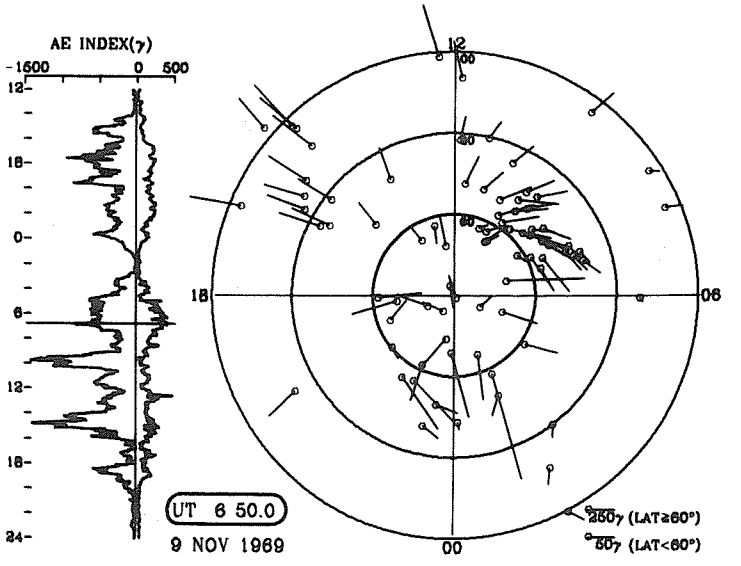
AE INDEX(γ)
-1600
0
500
12
18
0
6
12
18
24
12
30
60
18
06
00
UT 6 50.0
9 NOV 1969
250γ (LAT≥60°)
50γ (LAT<60°)

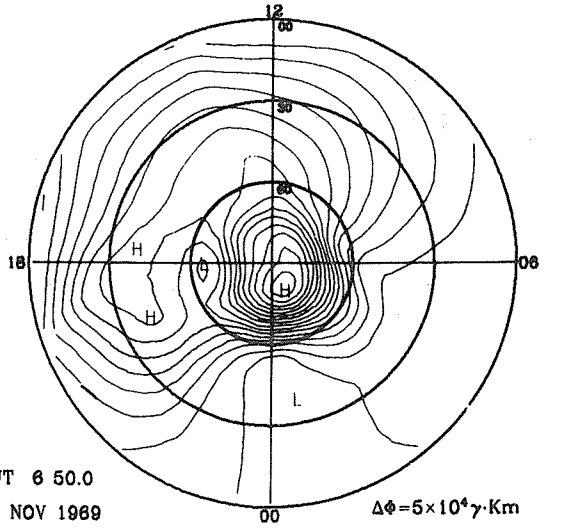
12
00
30
60
18
06
H
H
H
L
UT 6 50.0
9 NOV 1969
Δφ=5×10⁴γ·Km

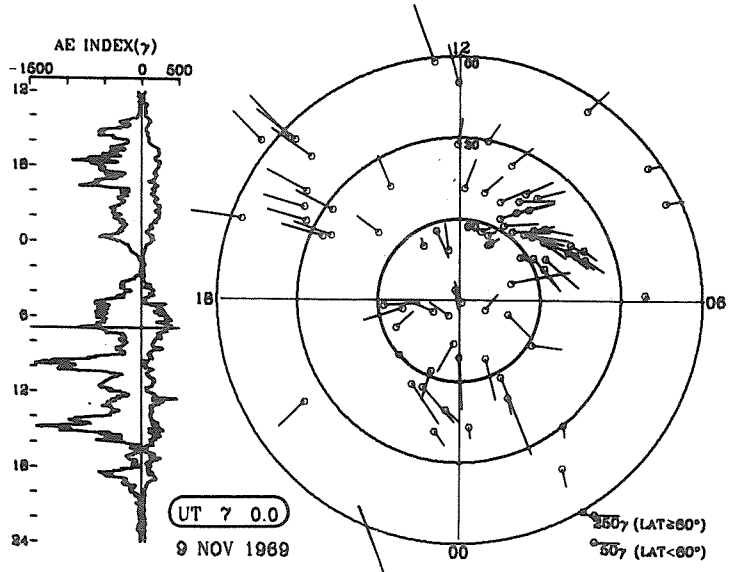
AE INDEX(γ)
-1600
0
500
12
18
0
6
12
18
24
12
60
30
18
06
00
UT 7 0.0
9 NOV 1969
250γ (LAT≥60°)
50γ (LAT<60°)

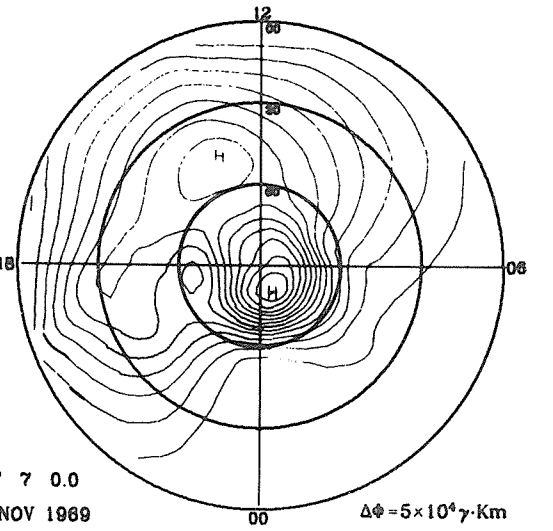
12
60
30
18
06
00
H
UT 7 0.0
9 NOV 1969
Δ𝛷=5×10⁴γ·Km

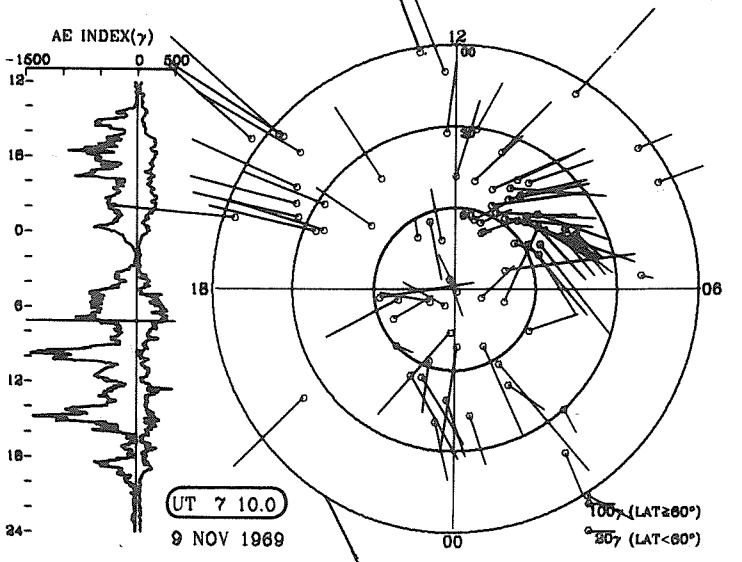
AE INDEX(γ)
-1600
0
500
12
18
0
6
12
18
24
12
60
30
18
06
00
UT 7 10.0
9 NOV 1969
100γ (LAT≥60°)
20γ (LAT<60°)

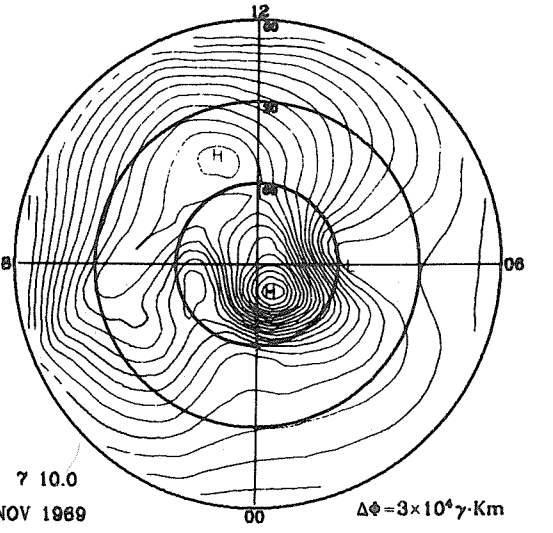
12
60
30
18
06
00
H
UT 7 10.0
9 NOV 1969
Δ𝛷=3×10⁴γ·Km

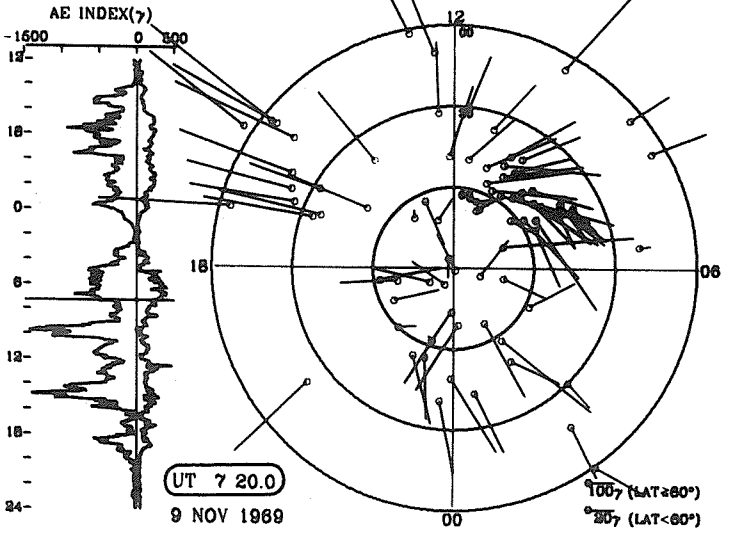
AE INDEX(γ)
-1600
0
500
12
18
0
6
12
18
24
12
60
30
18
06
00
UT 7 20.0
9 NOV 1969
100γ (LAT≥60°)
20γ (LAT<60°)

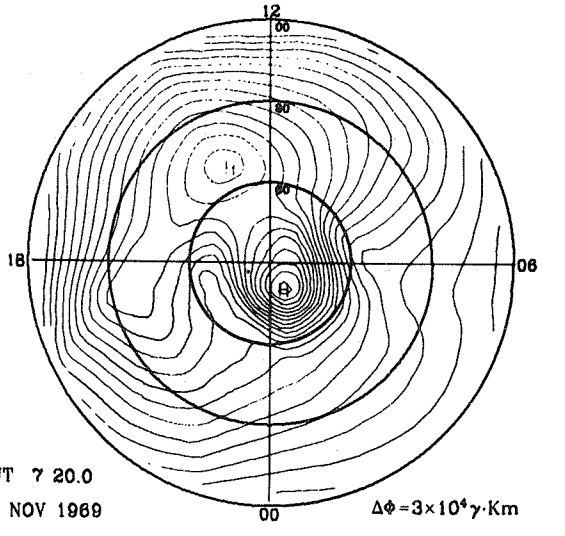
12
60
30
18
06
00
H
UT 7 20.0
9 NOV 1969
Δ𝛷=3×10⁴γ·Km

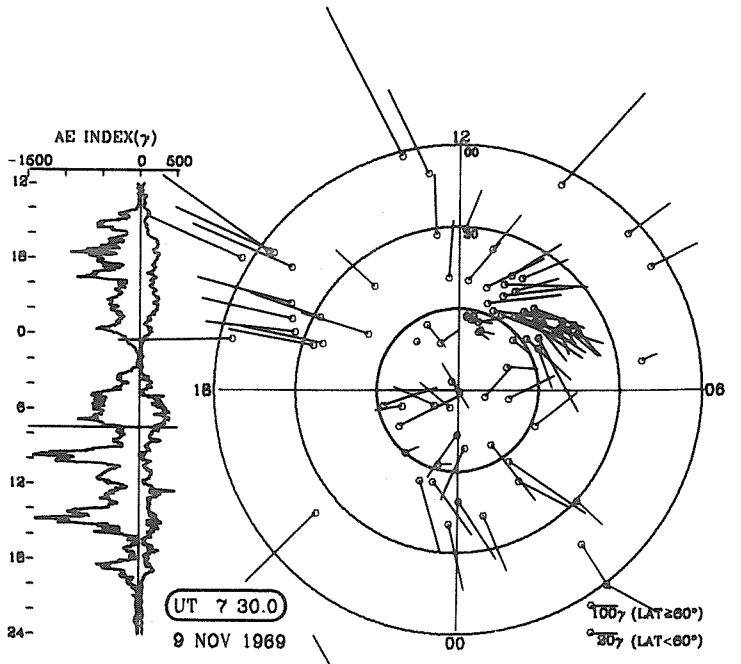
AE INDEX(γ)
-1500
0
500
12
18
0
6
12
18
24
12
00
30
60
18
06
00
UT 7 30.0
9 NOV 1969
100γ (LAT≥60°)
20γ (LAT<60°)

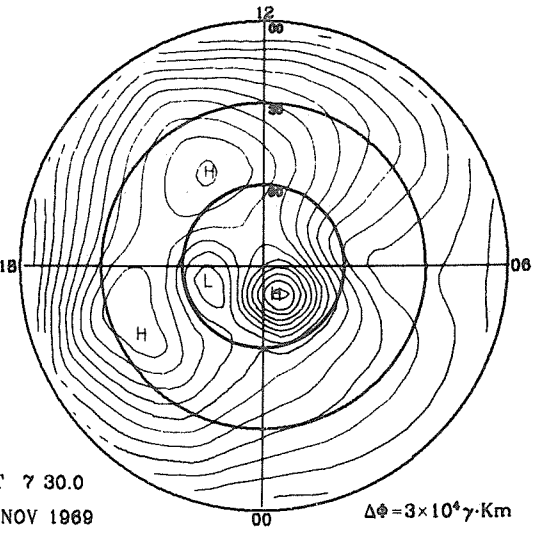
12
00
30
60
18
06
00
H
L
H
UT 7 30.0
9 NOV 1969
Δφ=3×10⁴γ·Km

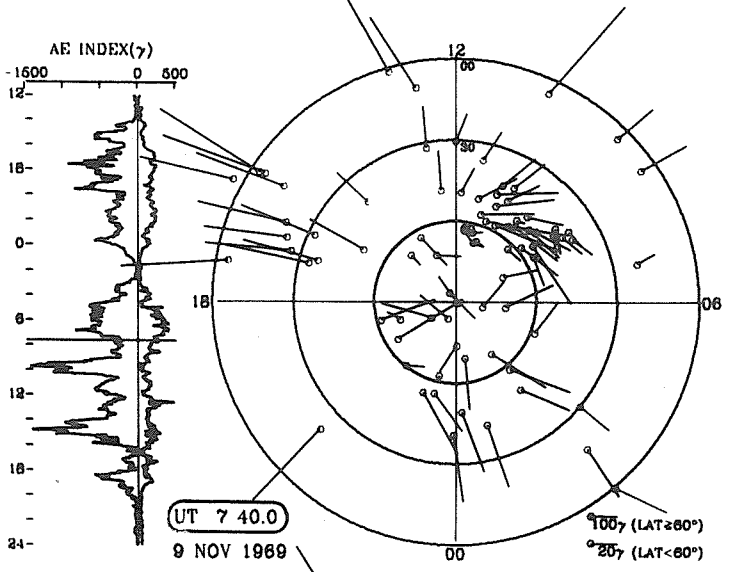
AE INDEX(γ)
-1500
0
500
12
18
0
6
12
18
24
12
00
30
60
18
06
00
UT 7 40.0
9 NOV 1969
100γ (LAT≥60°)
20γ (LAT<60°)

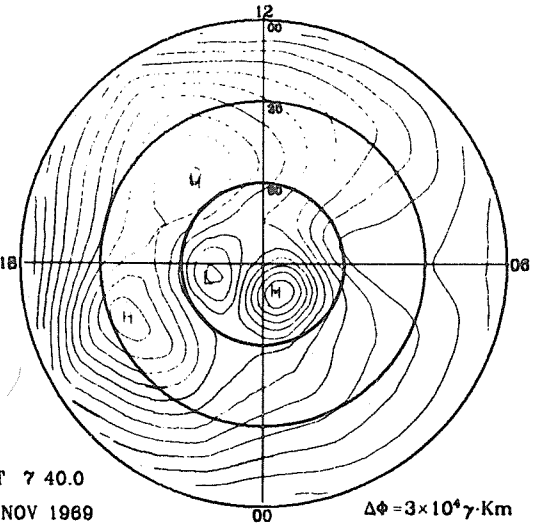
12
00
30
60
18
06
00
H
L
H
H
UT 7 40.0
9 NOV 1969
Δφ=3×10⁴γ·Km

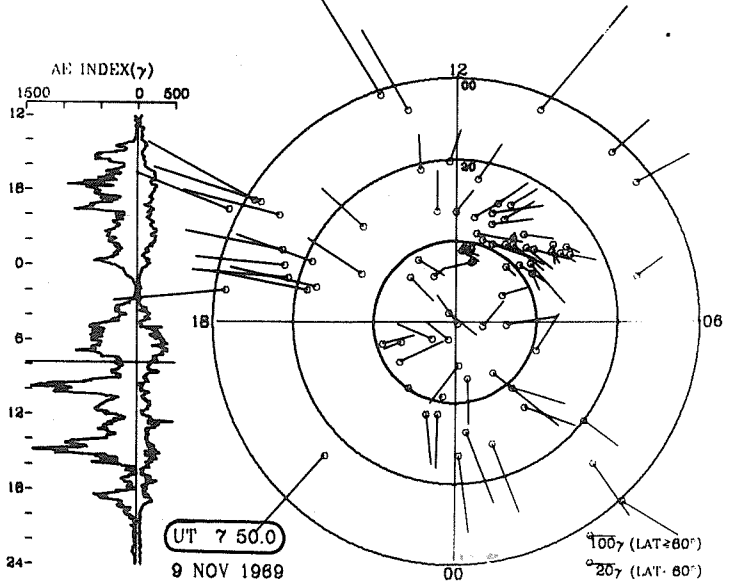
AE INDEX(γ)
1500
0
500
12
18
0
6
12
18
24
12
00
30
60
18
06
00
UT 7 50.0
9 NOV 1969
100γ (LAT≥60°)
20γ (LAT< 60°)

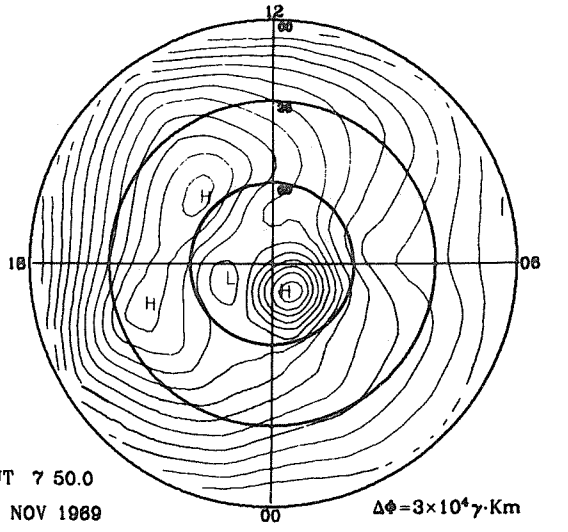
12
00
30
60
18
06
00
H
L
H
H
UT 7 50.0
9 NOV 1969
Δφ=3×10⁴γ·Km

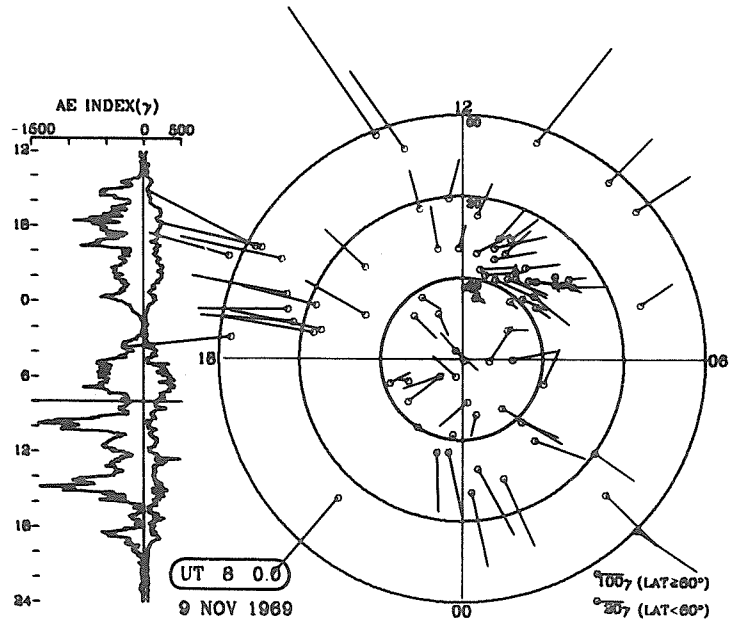
AE INDEX(γ)
-1600
0
500
12
18
0
6
12
18
24
12
00
30
60
18
06
00
UT 8 0.0
9 NOV 1969
100γ (LAT≥60°)
20γ (LAT<60°)

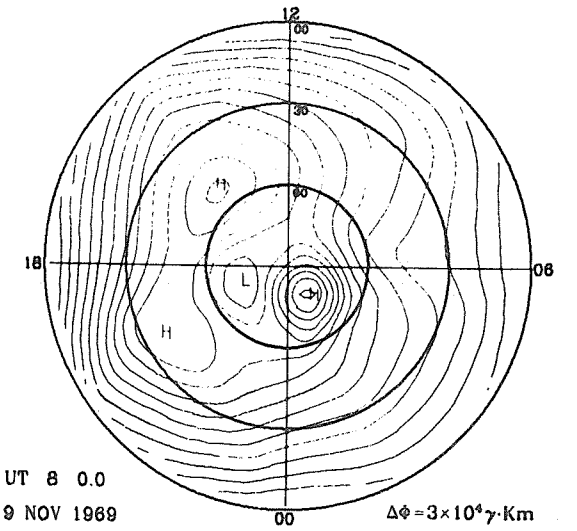
12
00
30
60
18
06
00
H
L
H
UT 8 0.0
9 NOV 1969
Δφ=3×10⁴γ·Km

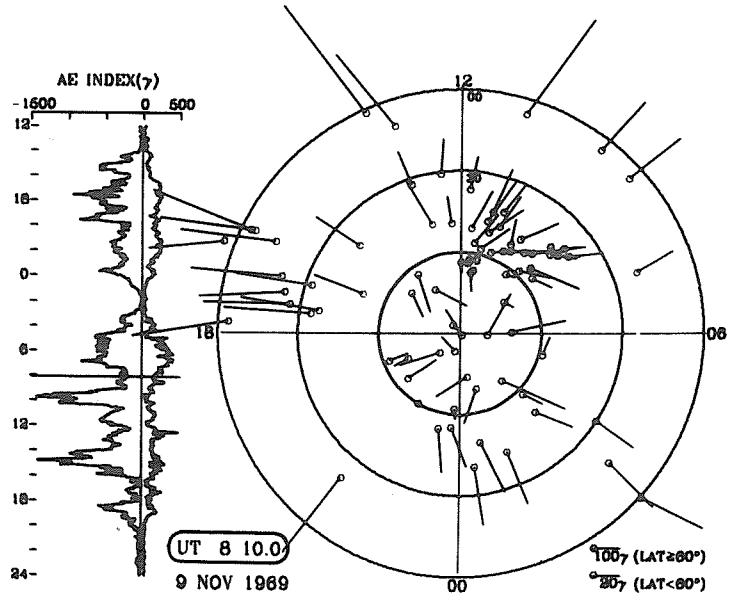
AE INDEX(γ)
-1600
0
500
12
18
0
6
12
18
24
12
00
30
60
18
06
00
UT 8 10.0
9 NOV 1969
100γ (LAT≥60°)
20γ (LAT<60°)

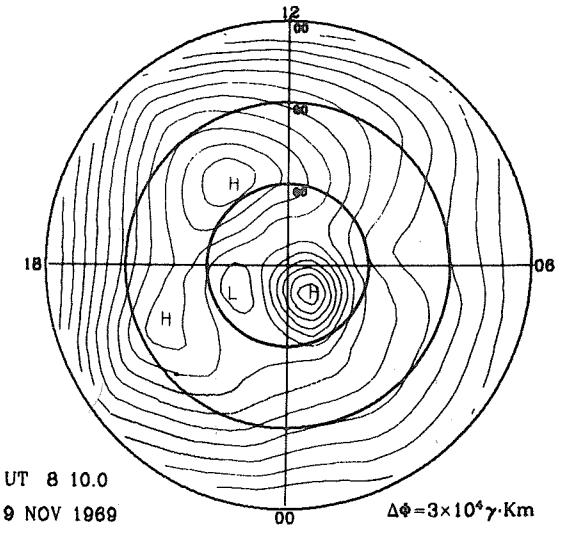
12
00
60
60
60
18
06
00
H
L
H
H
UT 8 10.0
9 NOV 1969
Δφ=3×10⁴γ·Km

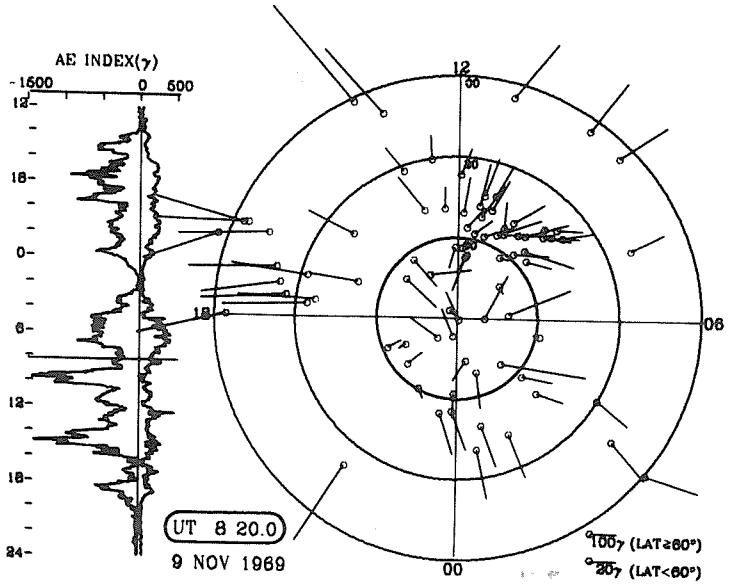
AE INDEX(γ)
-1600
0
500
12
18
0
6
12
18
24
12
00
30
60
18
06
00
UT 8 20.0
9 NOV 1969
100γ (LAT≥60°)
20γ (LAT<60°)

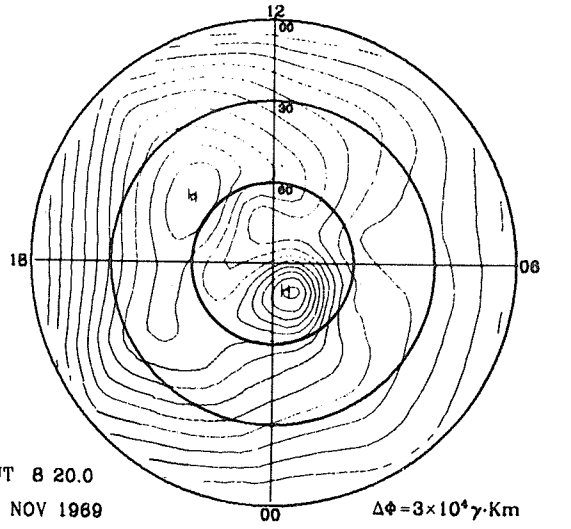
12
00
30
60
18
06
00
H
H
UT 8 20.0
9 NOV 1969
Δφ=3×10⁴γ·Km

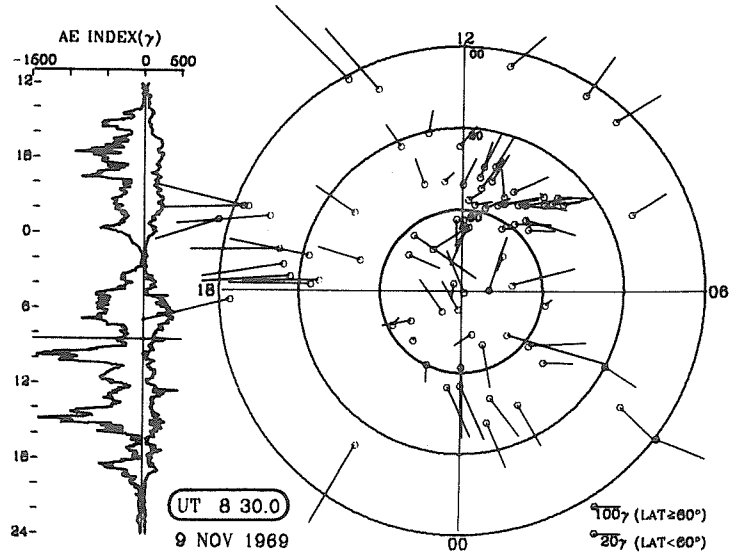
AE INDEX(γ)
-1600
0
500
12
18
0
6
12
18
24
12
00
30
60
18
06
00
UT 8 30.0
9 NOV 1969
100γ (LAT≥60°)
20γ (LAT<60°)

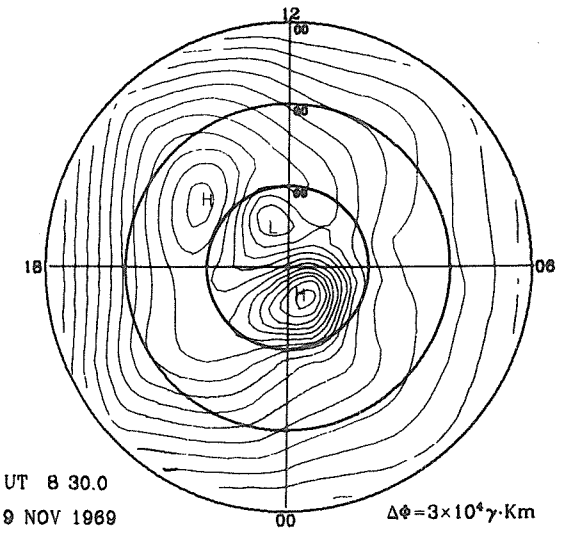
12
00
30
60
18
06
00
H
L
UT 8 30.0
9 NOV 1969
Δφ=3×10⁴γ·Km

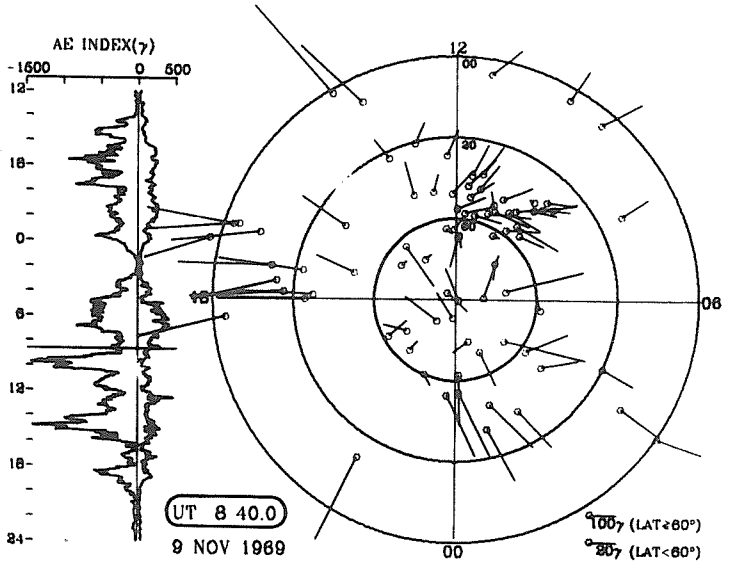
AE INDEX(γ)
-1600
0
500
12
18
0
6
12
18
24
12
00
30
60
18
06
00
UT 8 40.0
9 NOV 1969
100γ (LAT≥60°)
20γ (LAT<60°)

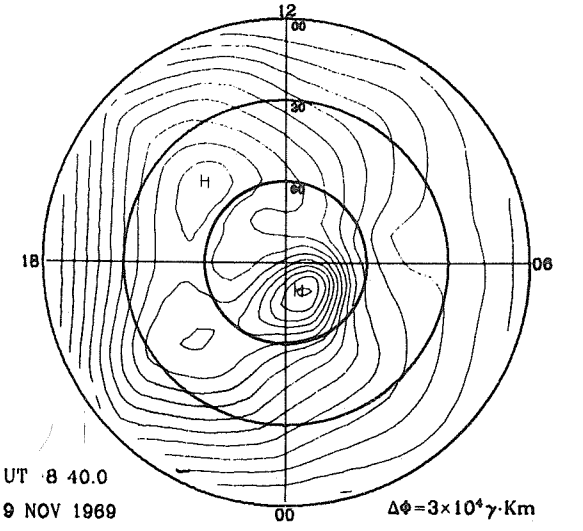
12
00
30
60
18
06
00
H
UT 8 40.0
9 NOV 1969
Δφ=3×10⁴γ·Km

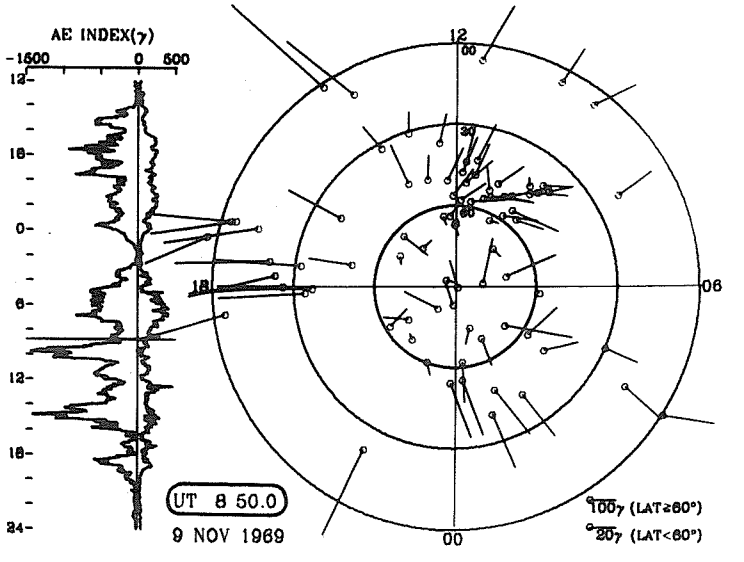
AE INDEX(γ)
-1600
0
500
12
18
0
6
12
18
24
12
00
30
60
18
06
00
UT 8 50.0
9 NOV 1969
100γ (LAT≥60°)
20γ (LAT<60°)

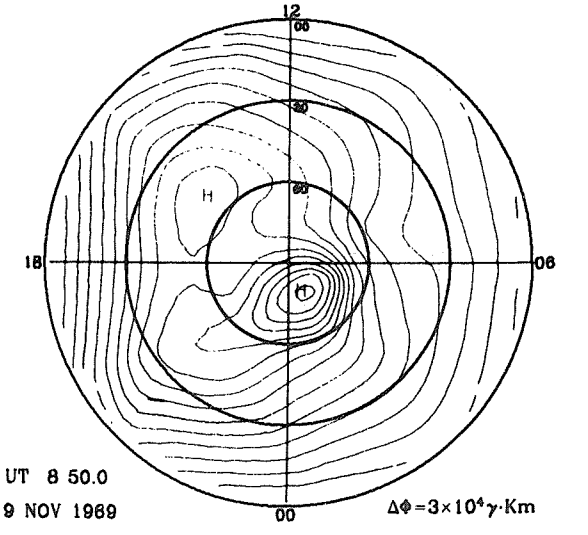
12
00
30
60
18
06
00
H
UT 8 50.0
9 NOV 1969
Δφ=3×10⁴γ·Km

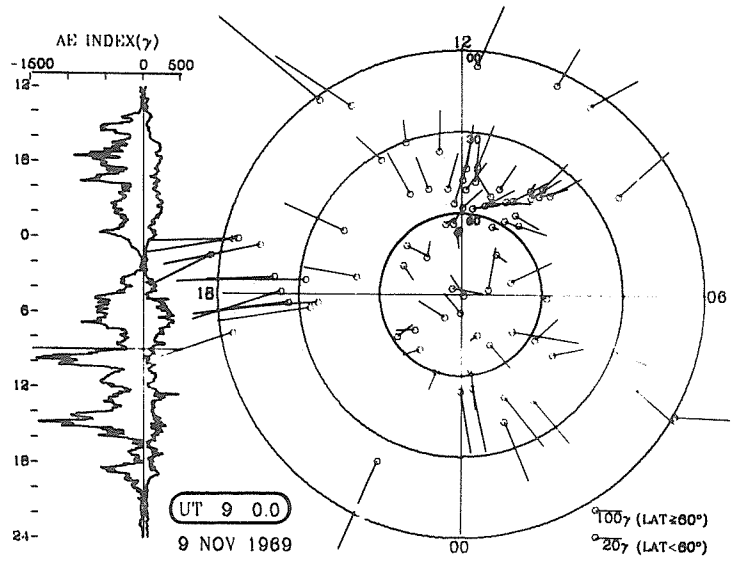
AE INDEX(γ)
-1600
0
500
12
18
0
6
12
18
24
12
00
30
60
18
06
00
UT 9 0.0
9 NOV 1969
100γ (LAT≥60°)
20γ (LAT<60°)

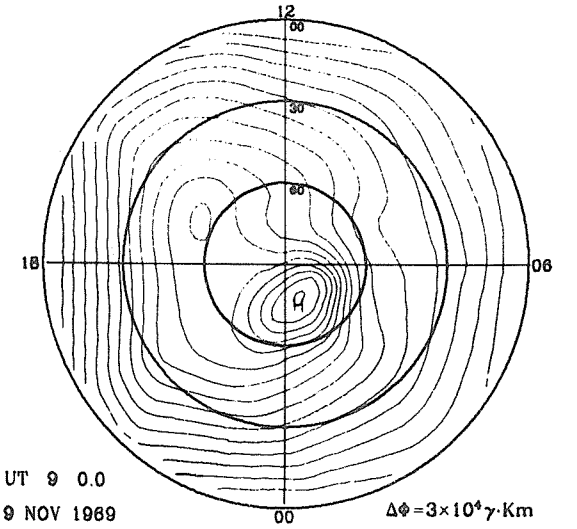
12
00
30
60
18
06
00
A
UT 9 0.0
9 NOV 1969
Δφ=3×10⁴γ·Km

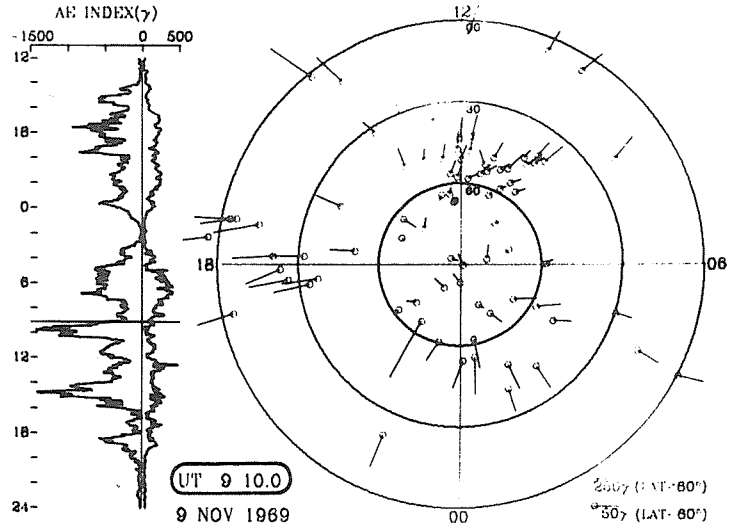
AE INDEX(γ)
-1600
0
500
12
18
0
6
12
18
24
12
00
30
60
18
06
00
UT 9 10.0
9 NOV 1969
250γ (LAT≥60°)
50γ (LAT<60°)

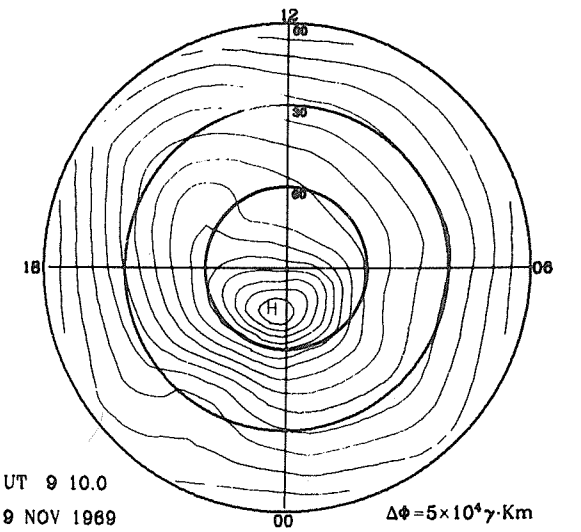
12
00
30
60
18
06
00
H
UT 9 10.0
9 NOV 1969
Δφ=5×10⁴γ·Km

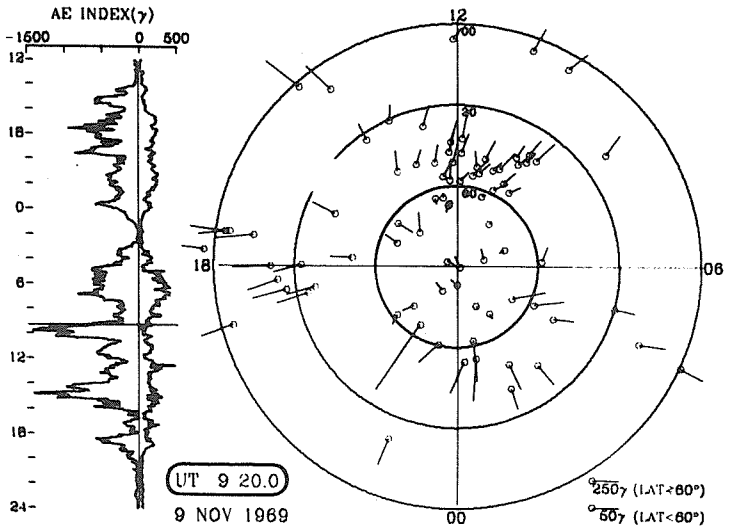
AE INDEX(γ)
-1600
0
500
12
18
0
6
12
18
24
12
00
30
60
18
06
00
UT 9 20.0
9 NOV 1969
250γ (LAT≥60°)
50γ (LAT<60°)

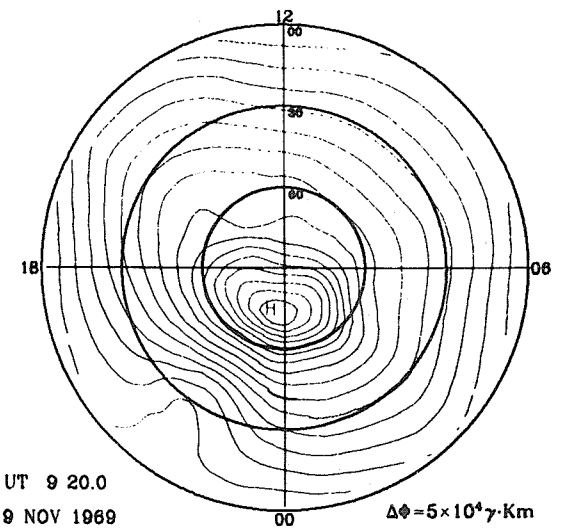
12
00
30
60
18
06
00
H
UT 9 20.0
9 NOV 1969
Δφ=5×10⁴γ·Km

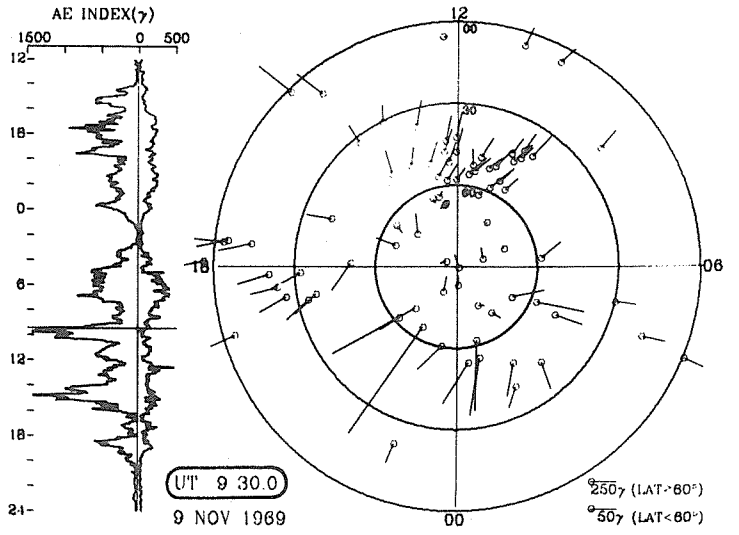
AE INDEX(γ)
1500
0
500
12
18
0
6
12
18
24
12
00
30
60
18
06
UT 9 30.0
9 NOV 1969
250γ (LAT>60°)
50γ (LAT<60°)

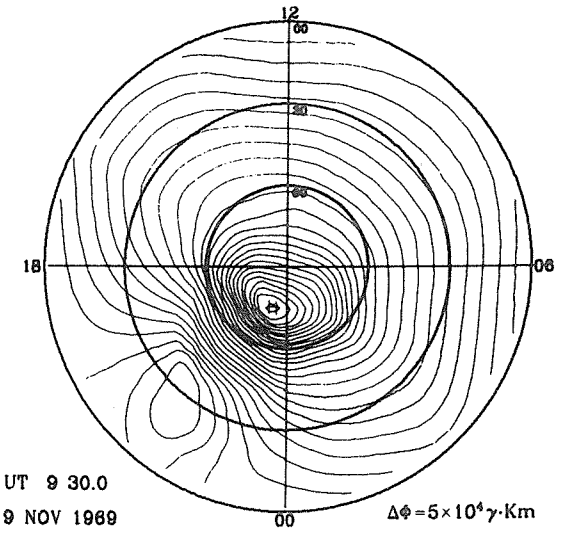
12
00
30
60
18
06
UT 9 30.0
9 NOV 1969
Δφ=5×10⁴γ·Km

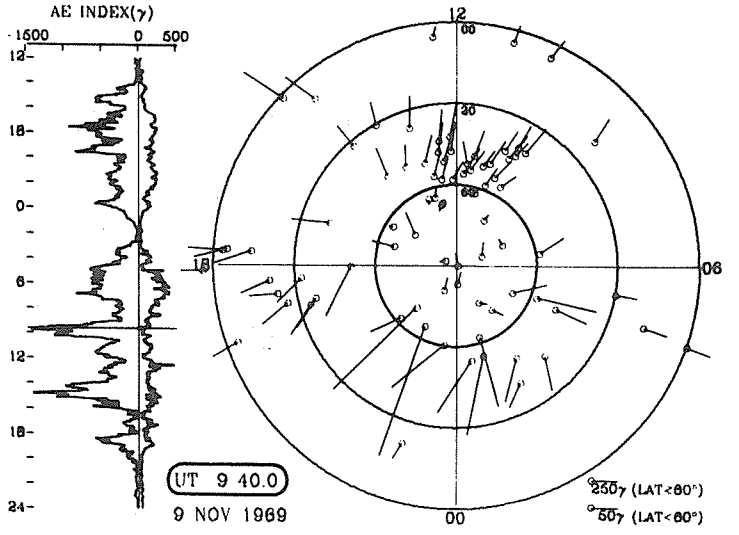
AE INDEX(γ)
1500
0
500
12
18
0
6
12
18
24
12
00
30
60
18
06
UT 9 40.0
9 NOV 1969
250γ (LAT>60°)
50γ (LAT<60°)

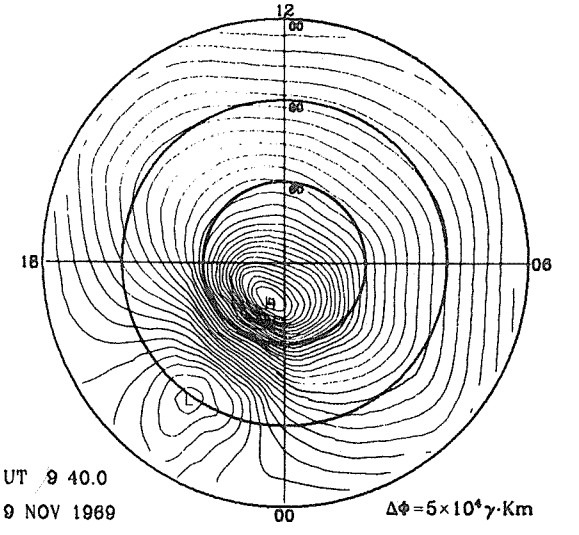
12
00
30
60
18
06
UT 9 40.0
9 NOV 1969
Δφ=5×10⁴γ·Km

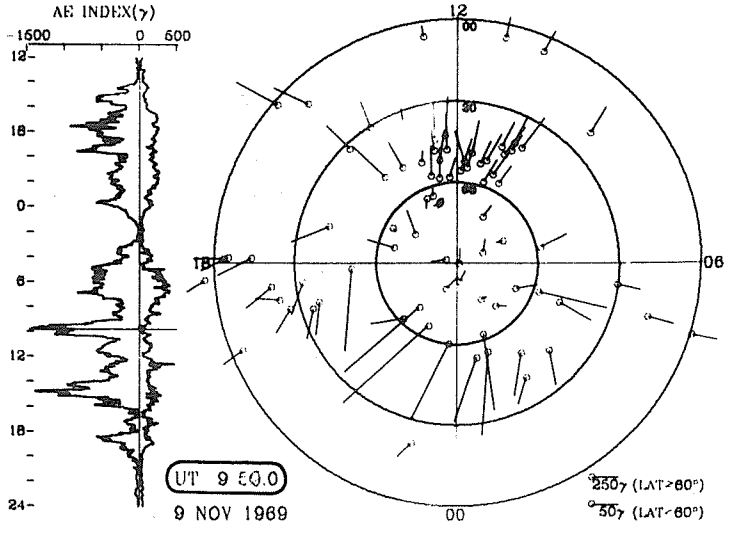
AE INDEX(γ)
1500
0
500
12
18
0
6
12
18
24
12
00
30
60
18
06
UT 9 50.0
9 NOV 1969
250γ (LAT>60°)
50γ (LAT<60°)

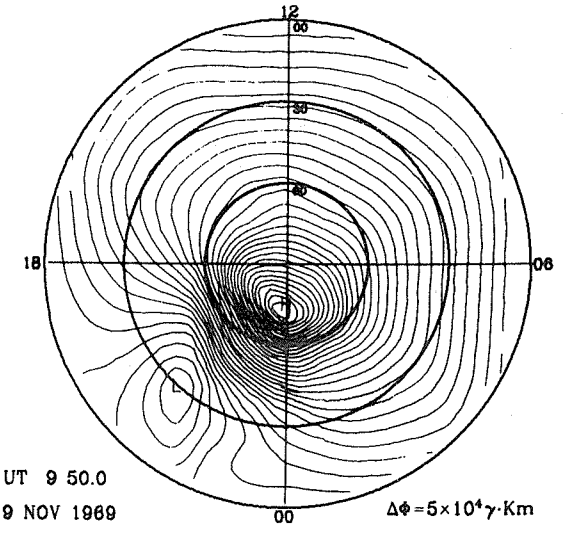
12
00
30
60
18
06
UT 9 50.0
9 NOV 1969
Δφ=5×10⁴γ·Km

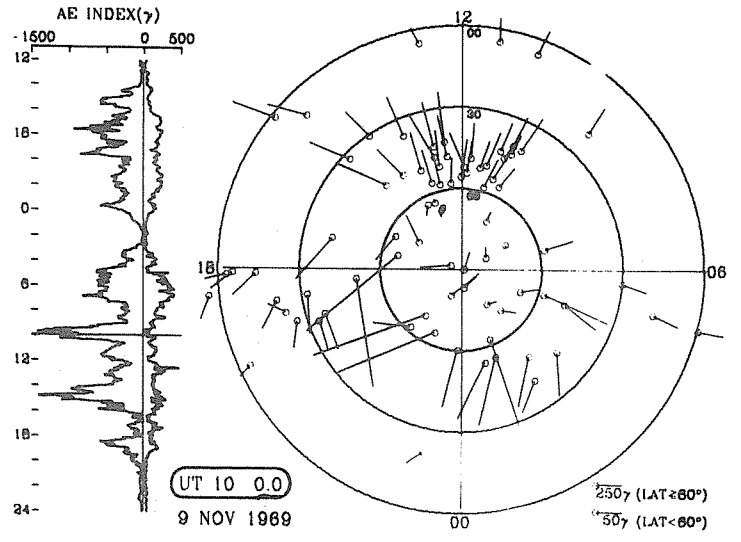
AE INDEX(γ)
-1500
0
500
12
18
0
6
12
18
24
12
00
30
60
18
06
00
UT 10 0.0
9 NOV 1969
250γ (LAT≥60°)
50γ (LAT<60°)

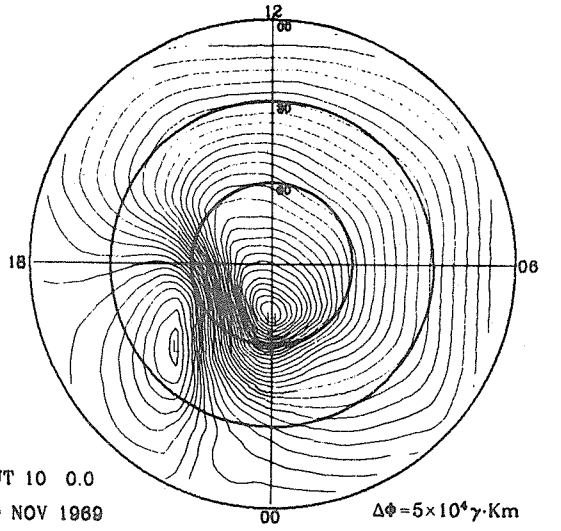
12
00
30
60
18
06
00
UT 10 0.0
9 NOV 1969
ΔΦ=5×10⁴γ·Km

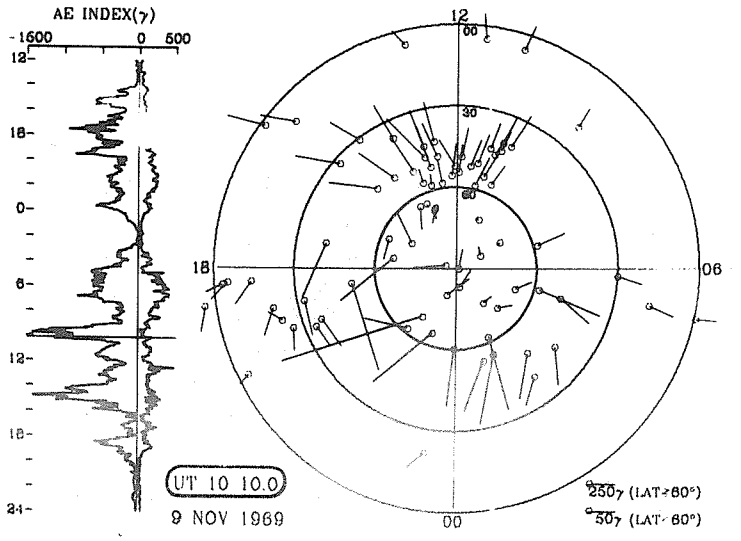
AE INDEX(γ)
-1600
0
500
12
18
0
6
12
18
24
12
00
30
60
18
06
00
UT 10 10.0
9 NOV 1969
250γ (LAT≥60°)
50γ (LAT<60°)

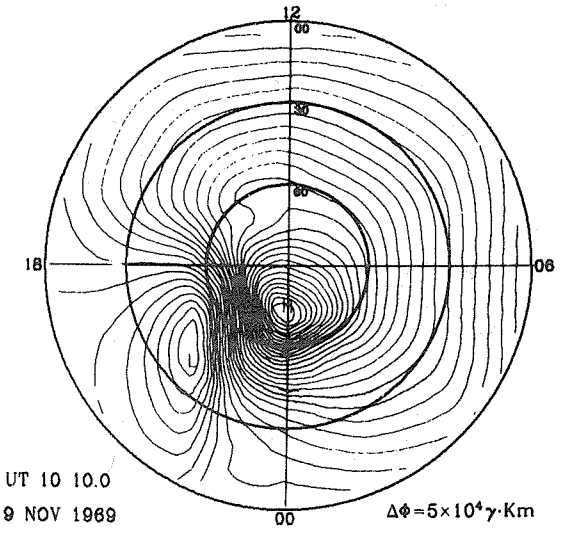
12
00
30
60
18
06
00
UT 10 10.0
9 NOV 1969
ΔΦ=5×10⁴γ·Km

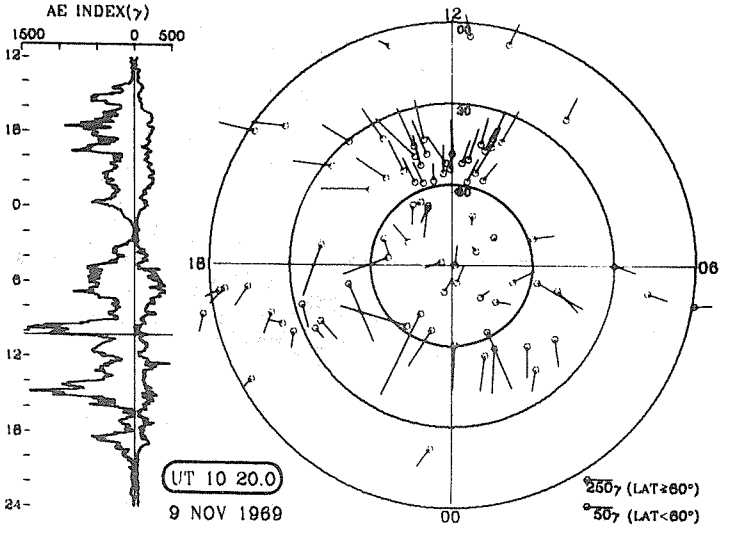
AE INDEX(γ)
1500
0
500
12
18
0
6
12
18
24
12
00
30
60
18
06
00
UT 10 20.0
9 NOV 1969
250γ (LAT≥60°)
50γ (LAT<60°)

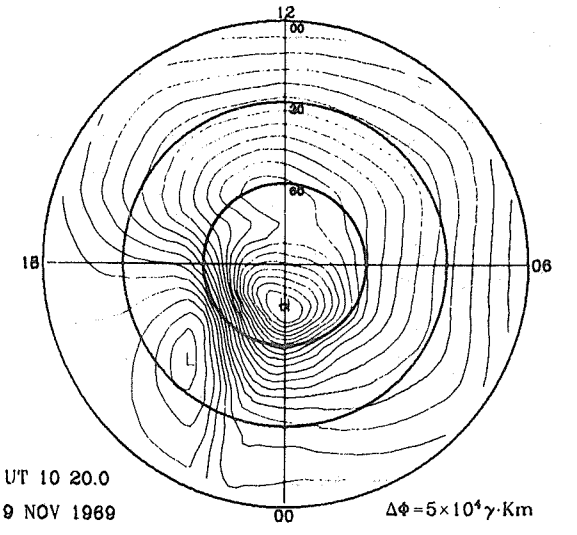
12
00
30
60
18
06
00
UT 10 20.0
9 NOV 1969
ΔΦ=5×10⁴γ·Km

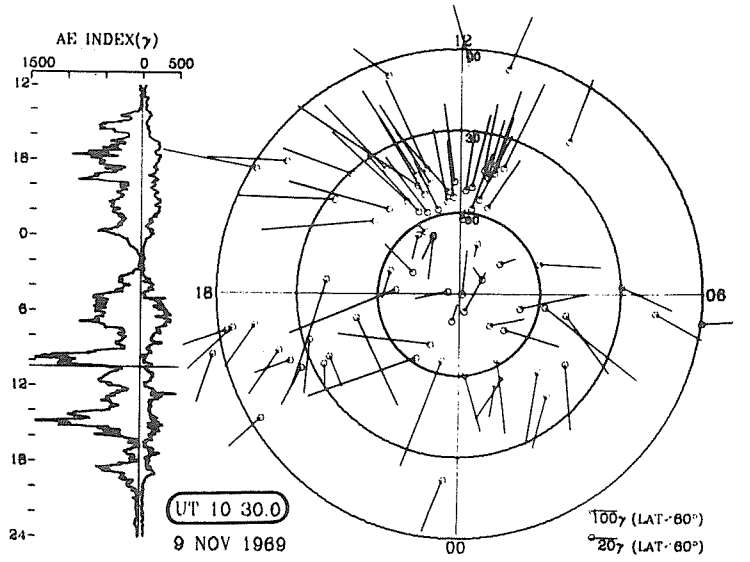
AE INDEX(γ)
1500
0
500
12
18
0
6
12
18
24
12
00
30
60
18
06
00
UT 10 30.0
9 NOV 1969
100γ (LAT<60°)
20γ (LAT<60°)

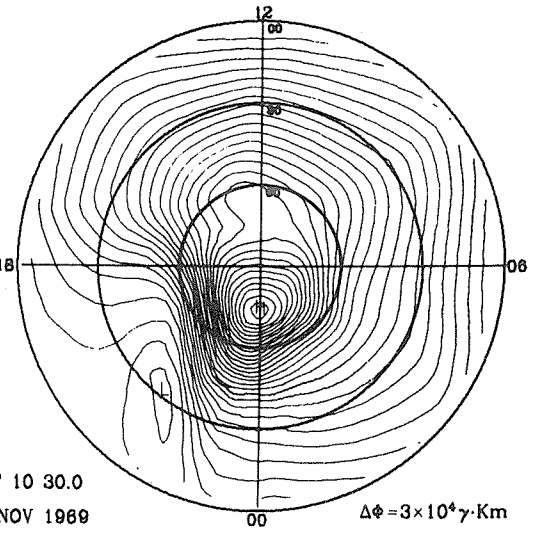
12
00
30
60
18
06
00
UT 10 30.0
9 NOV 1969
Δφ=3×10⁴γ·Km

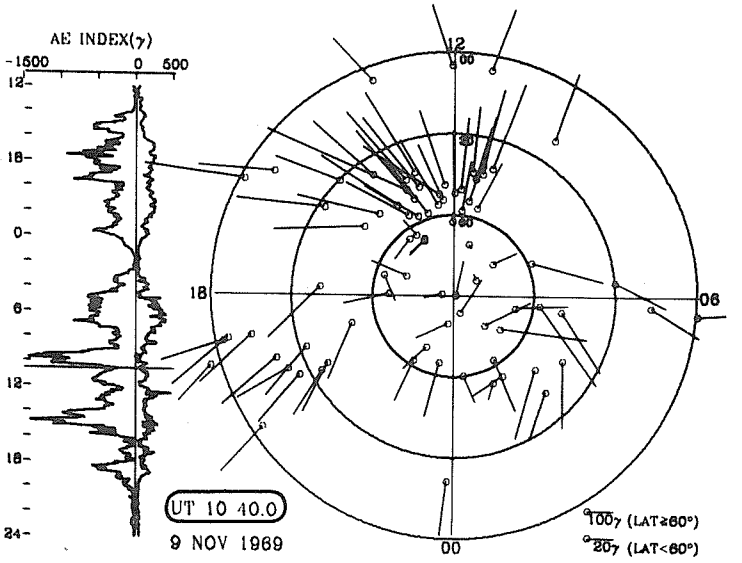
AE INDEX(γ)
1500
0
500
12
18
0
6
12
18
24
12
00
30
60
18
06
00
UT 10 40.0
9 NOV 1969
100γ (LAT≥60°)
20γ (LAT<60°)

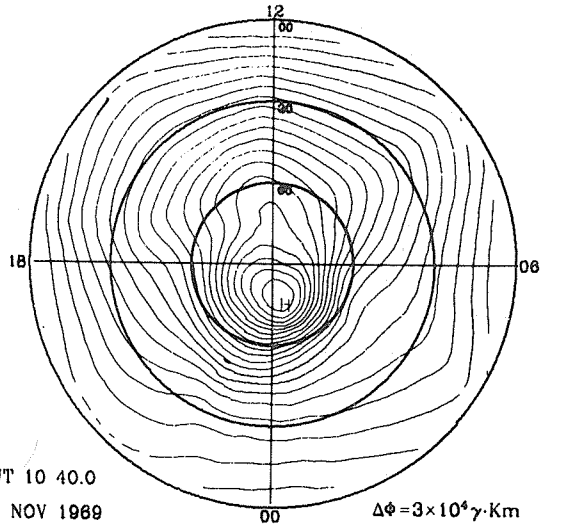
12
00
30
60
18
06
00
UT 10 40.0
9 NOV 1969
Δφ=3×10⁴γ·Km

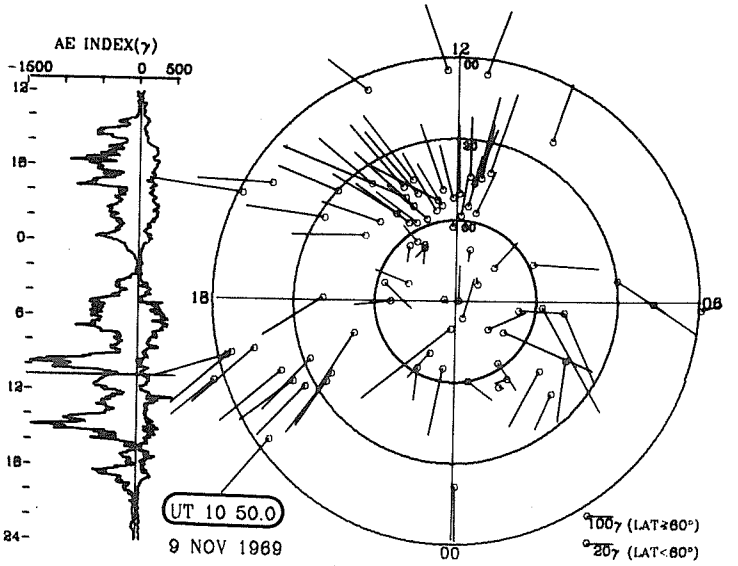
AE INDEX(γ)
1500
0
500
12
18
0
6
12
18
24
12
00
30
60
18
06
00
UT 10 50.0
9 NOV 1969
100γ (LAT≥60°)
20γ (LAT<60°)

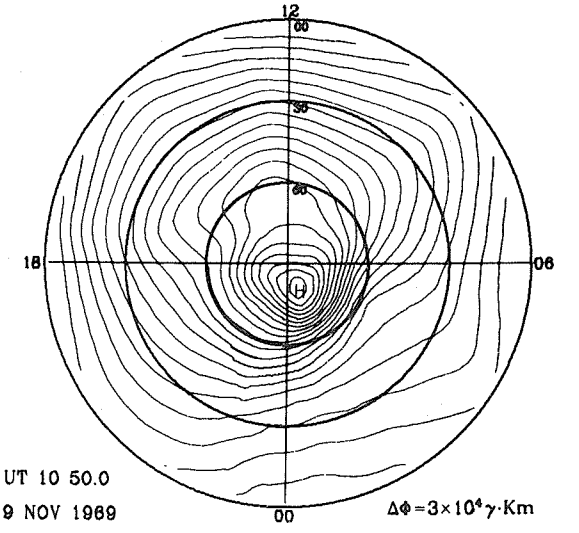
12
00
30
60
18
06
00
UT 10 50.0
9 NOV 1969
Δφ=3×10⁴γ·Km

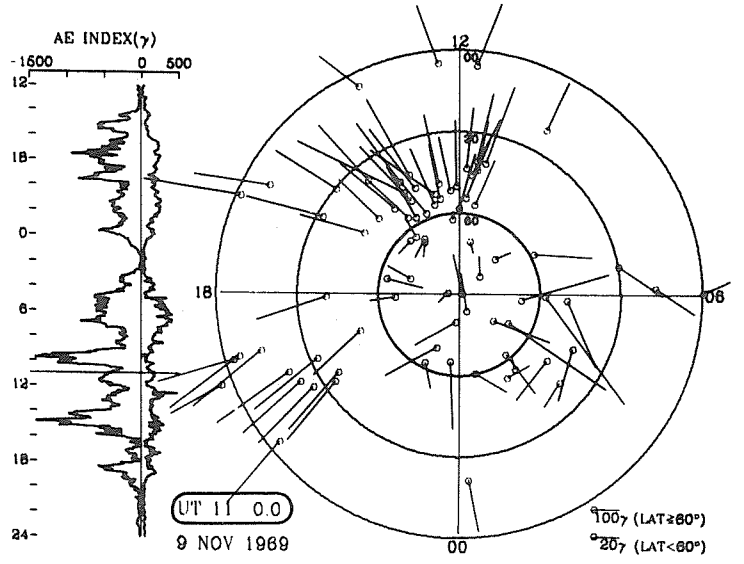
AE INDEX(γ)
-1600
0
500
12
18
0
6
12
18
24
12
00
18
06
00
30
60
UT 11 0.0
9 NOV 1969
100γ (LAT≥60°)
20γ (LAT<60°)

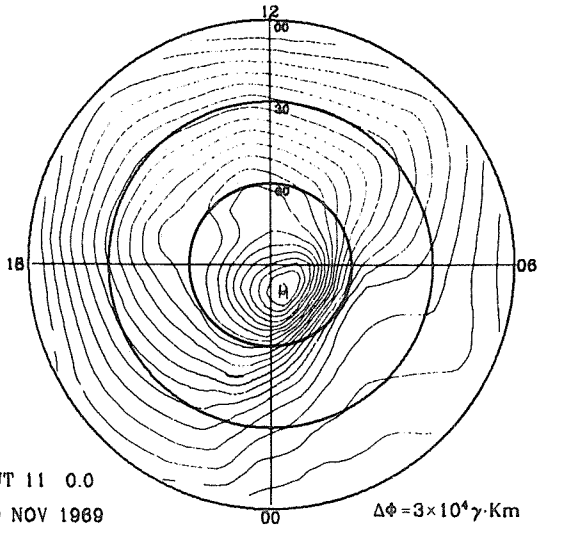
12
00
18
06
00
30
60
H
UT 11 0.0
9 NOV 1969
Δφ=3×10⁴γ·Km

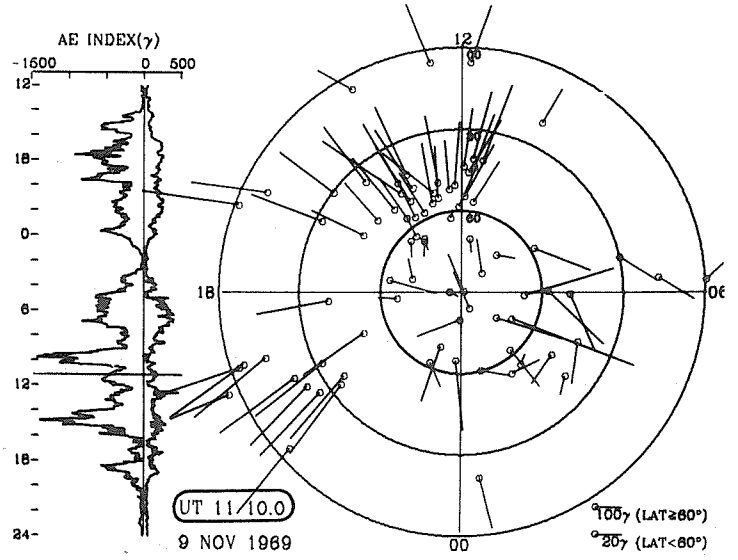
AE INDEX(γ)
-1600
0
500
12
18
0
6
12
18
24
12
00
18
06
00
30
60
UT 11 10.0
9 NOV 1969
100γ (LAT≥60°)
20γ (LAT<60°)

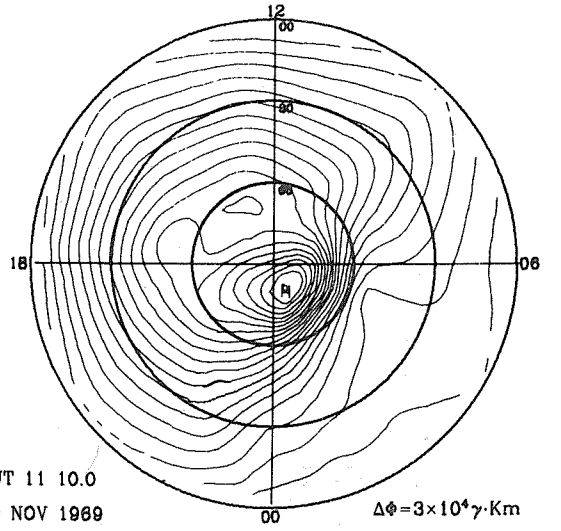
12
00
18
06
00
30
60
H
UT 11 10.0
9 NOV 1969
Δφ=3×10⁴γ·Km

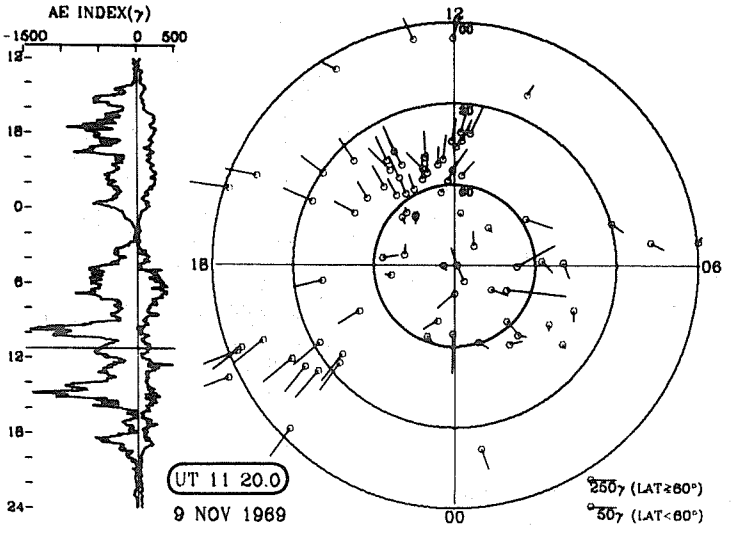
AE INDEX(γ)
-1600
0
500
12
18
0
6
12
18
24
12
00
18
06
00
30
60
UT 11 20.0
9 NOV 1969
250γ (LAT≥60°)
50γ (LAT<60°)

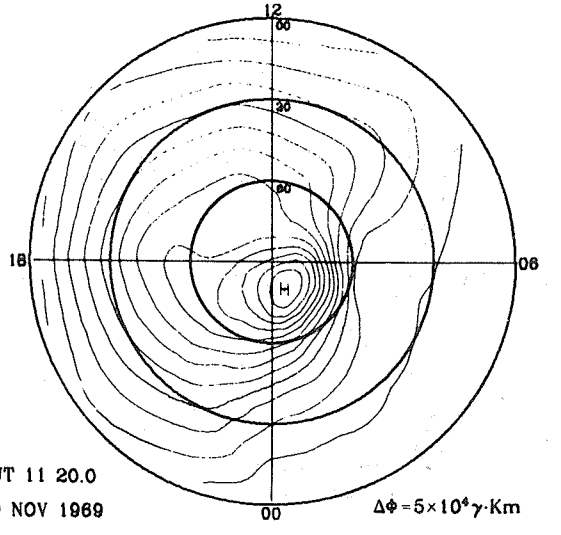
12
00
18
06
00
30
60
H
UT 11 20.0
9 NOV 1969
Δφ=5×10⁴γ·Km

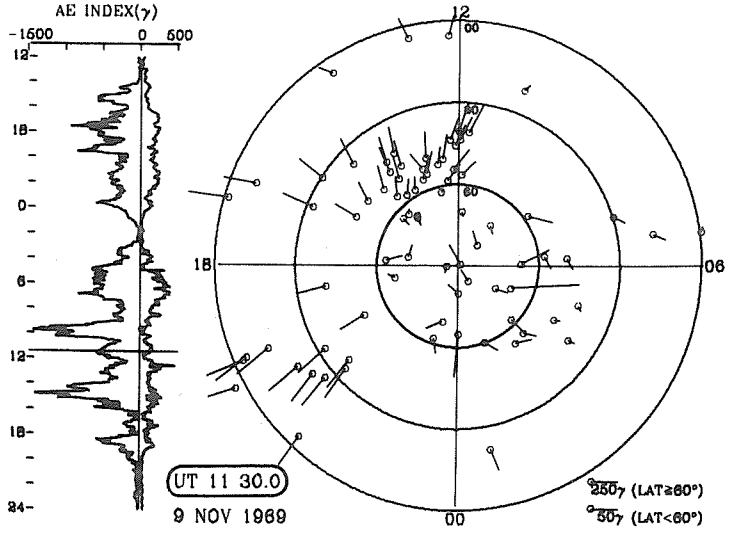
AE INDEX(γ)
-1600
0
600
12
18
0
6
12
18
24
12
00
30
60
18
06
00
UT 11 30.0
9 NOV 1969
250γ (LAT≥60°)
50γ (LAT<60°)

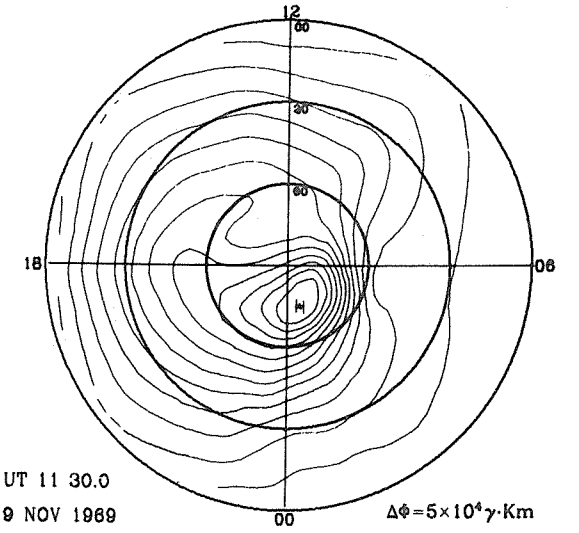
12
00
30
60
18
06
00
UT 11 30.0
9 NOV 1969
ΔΦ=5×10⁴γ·Km

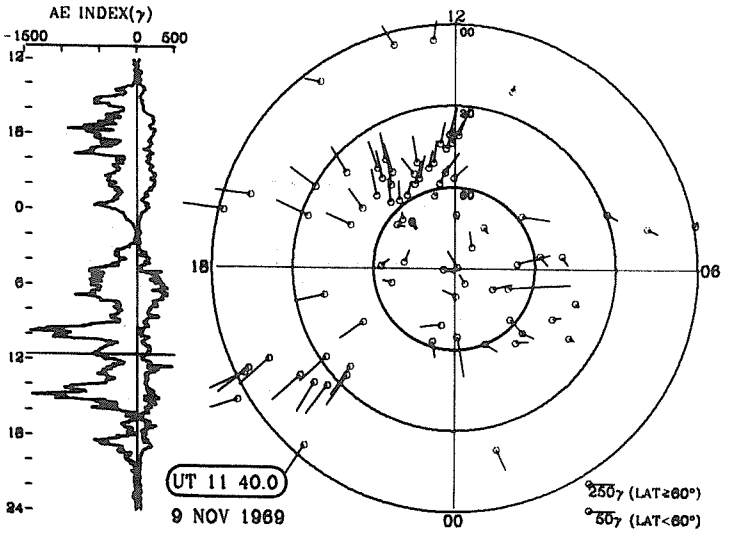
AE INDEX(γ)
-1600
0
600
12
18
0
6
12
18
24
12
00
30
60
18
06
00
UT 11 40.0
9 NOV 1969
250γ (LAT≥60°)
50γ (LAT<60°)

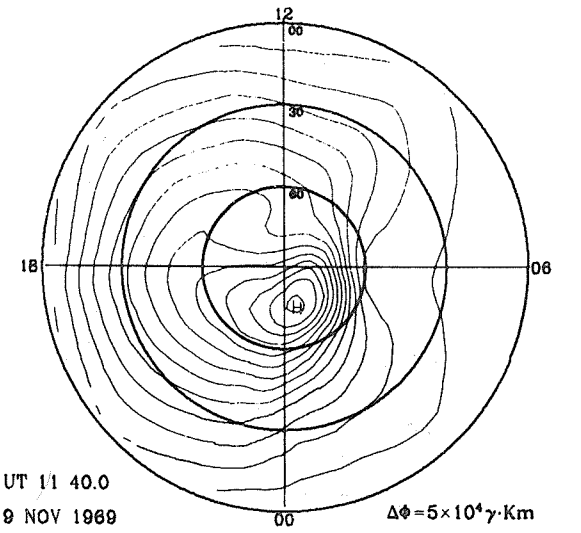
12
00
30
60
18
06
00
UT 11 40.0
9 NOV 1969
ΔΦ=5×10⁴γ·Km

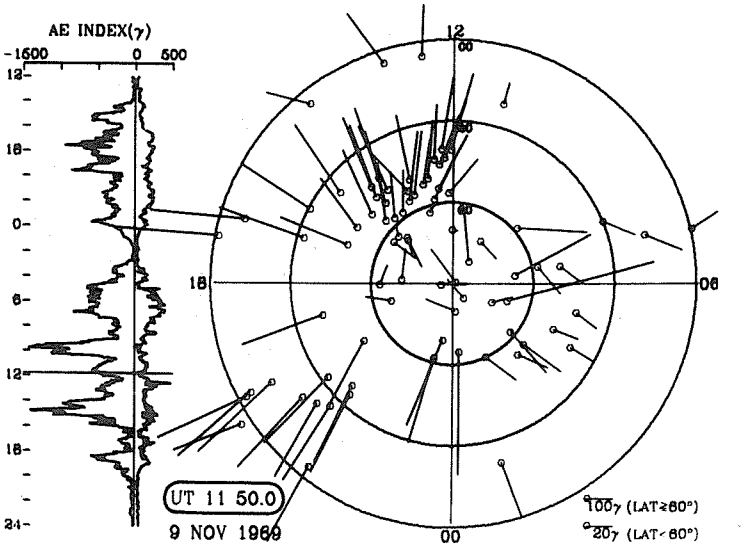
AE INDEX(γ)
-1600
0
600
12
18
0
6
12
18
24
12
00
30
60
18
06
00
UT 11 50.0
9 NOV 1969
100γ (LAT≥60°)
20γ (LAT<60°)

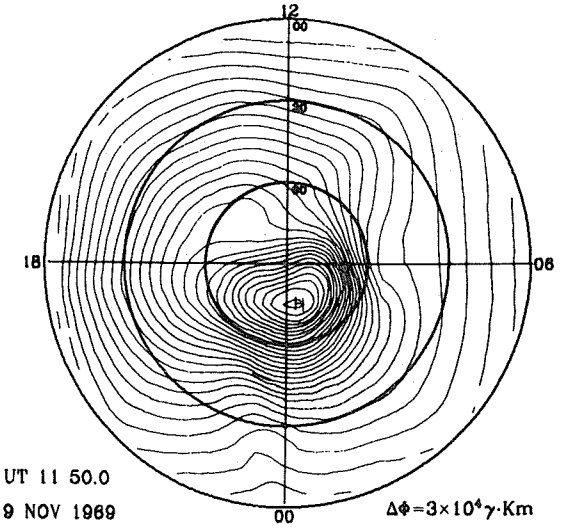
12
00
30
60
18
06
00
UT 11 50.0
9 NOV 1969
ΔΦ=3×10⁴γ·Km

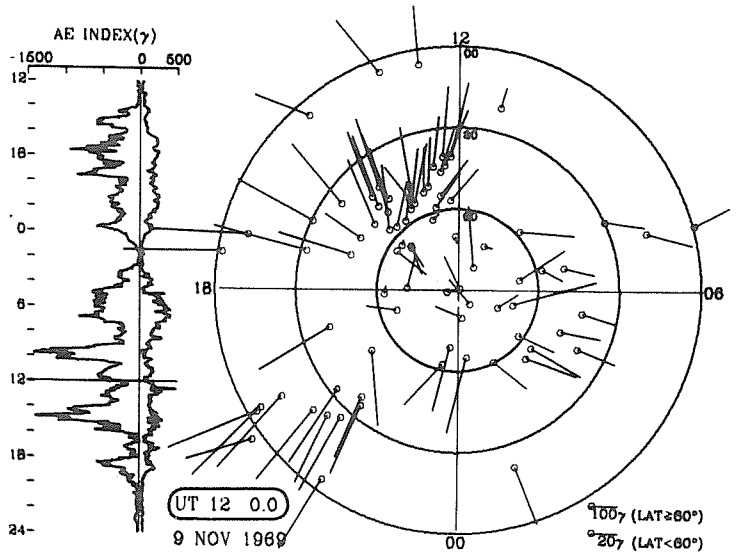
AE INDEX(γ)
-1500
0
500
12
18
0
6
12
18
24
12
00
18
06
30
60
UT 12 0.0
9 NOV 1969
100γ (LAT≥60°)
20γ (LAT<60°)

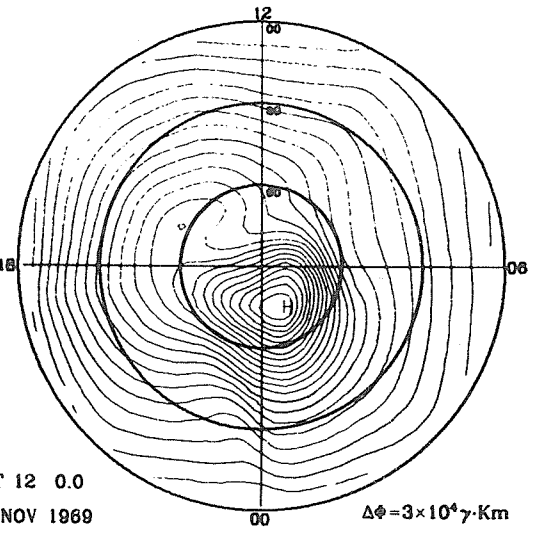
12
00
30
60
18
06
H
UT 12 0.0
9 NOV 1969
Δ𝚽=3×10⁴γ·Km

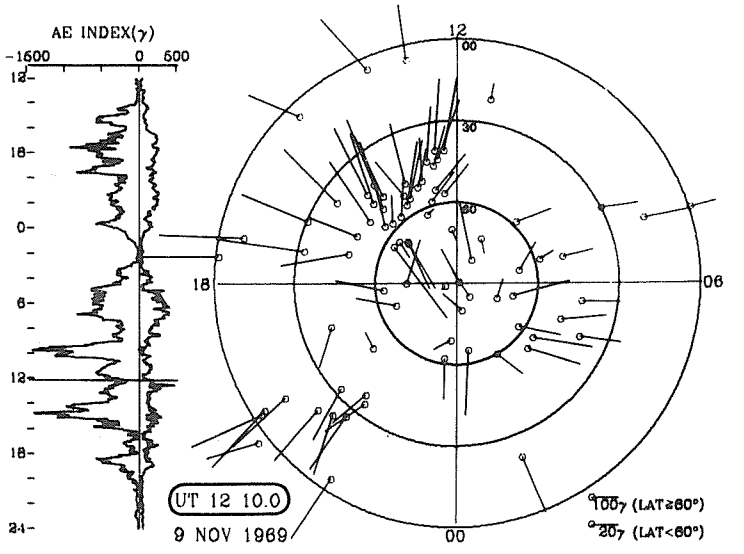
AE INDEX(γ)
-1500
0
500
12
18
0
6
12
18
24
12
00
18
06
30
60
UT 12 10.0
9 NOV 1969
100γ (LAT≥60°)
20γ (LAT<60°)

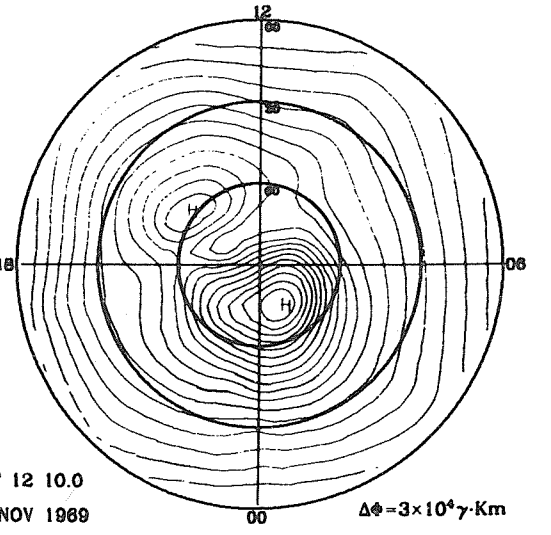
12
00
30
60
18
06
H
H
UT 12 10.0
9 NOV 1969
Δ𝚽=3×10⁴γ·Km

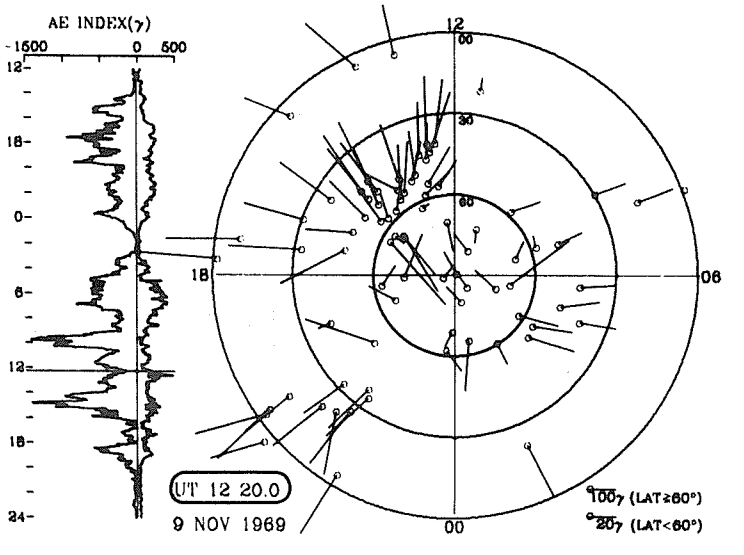
AE INDEX(γ)
-1500
0
500
12
18
0
6
12
18
24
12
00
18
06
30
60
UT 12 20.0
9 NOV 1969
100γ (LAT≥60°)
20γ (LAT<60°)

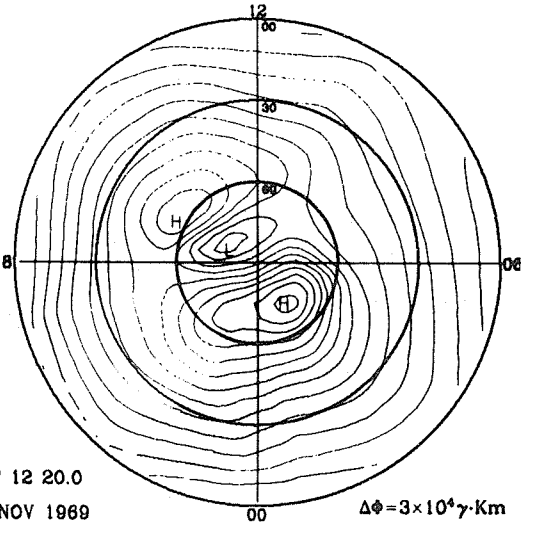
12
00
30
60
18
06
H
H
UT 12 20.0
9 NOV 1969
Δ𝚽=3×10⁴γ·Km

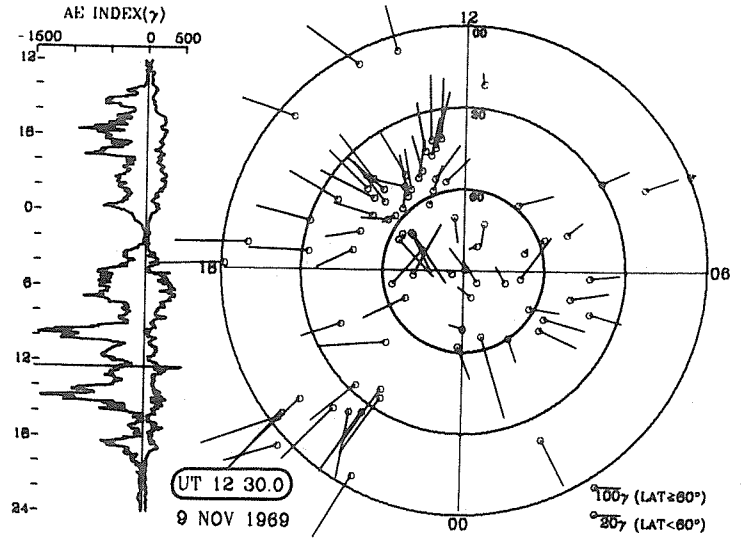
AE INDEX(γ)
-1500
0
500
12
18
0
6
12
18
24
12
00
30
60
18
06
00
UT 12 30.0
9 NOV 1969
100γ (LAT≥60°)
20γ (LAT<60°)

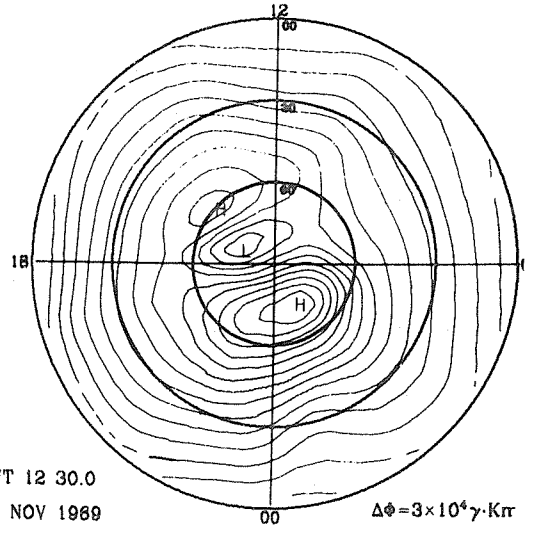
12
00
30
60
18
06
00
H
L
H
UT 12 30.0
9 NOV 1969
Δφ=3×10⁴γ·Km

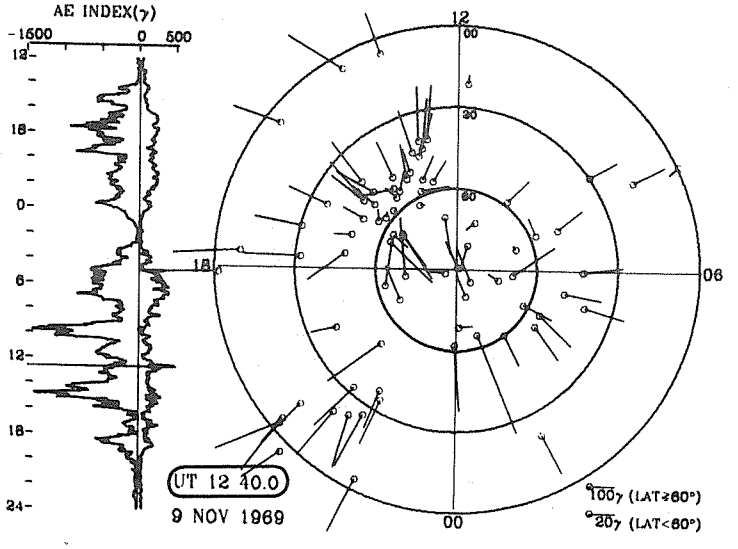
AE INDEX(γ)
-1500
0
500
12
18
0
6
12
18
24
12
00
30
60
18
06
00
UT 12 40.0
9 NOV 1969
100γ (LAT≥60°)
20γ (LAT<60°)

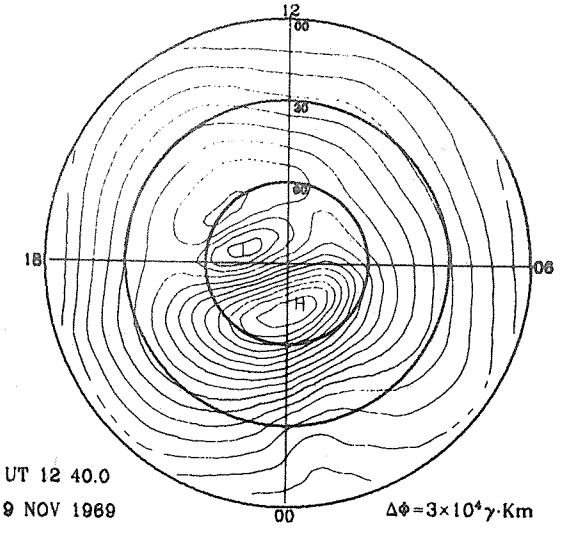
12
00
30
60
18
06
00
H
L
H
UT 12 40.0
9 NOV 1969
Δφ=3×10⁴γ·Km

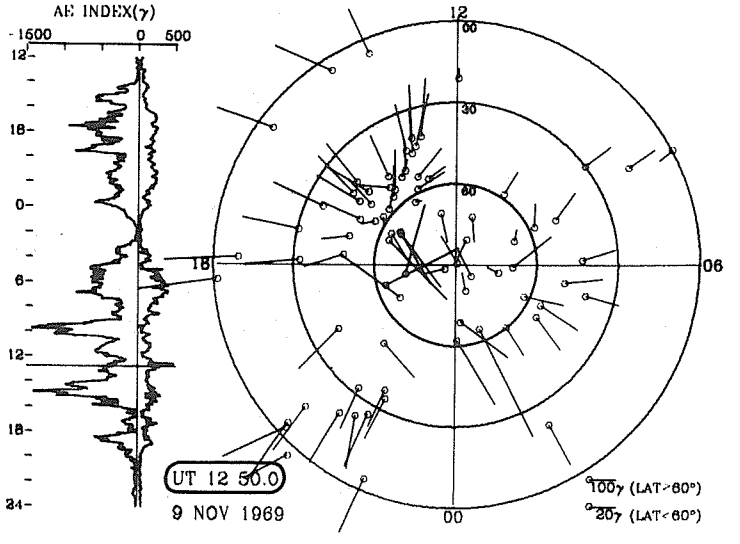
AE INDEX(γ)
-1500
0
500
12
18
0
6
12
18
24
12
00
30
60
18
06
00
UT 12 50.0
9 NOV 1969
100γ (LAT<60°)
20γ (LAT<60°)

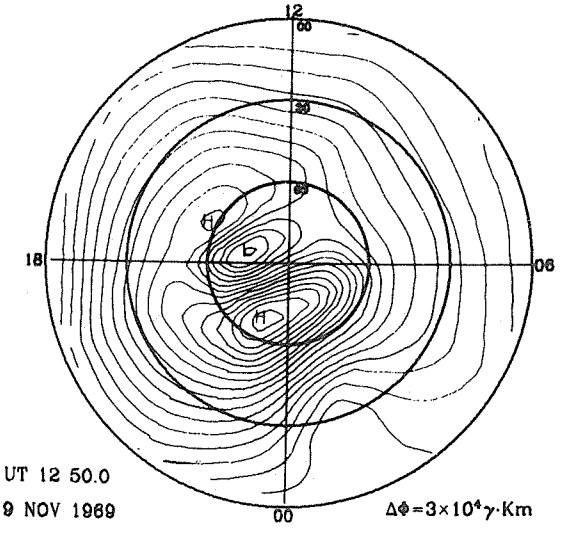
12
00
30
60
18
06
00
H
L
H
UT 12 50.0
9 NOV 1969
Δφ=3×10⁴γ·Km

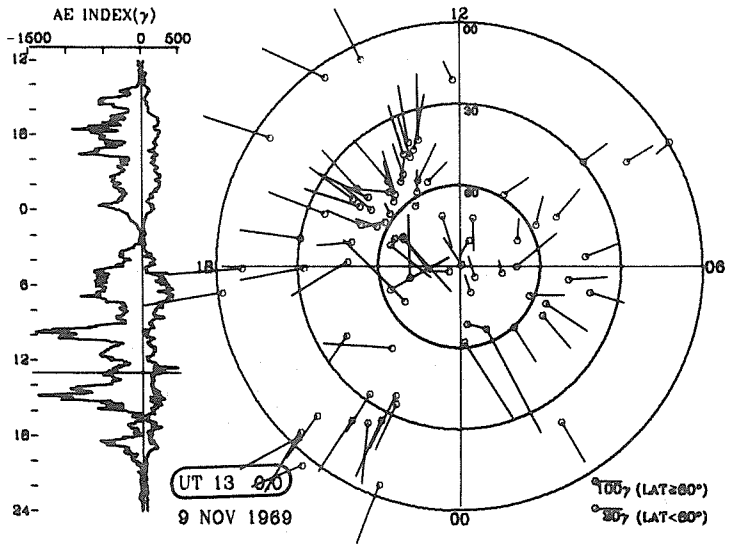
AE INDEX(γ)
-1500
0
500
12
18
0
6
12
18
24
12
00
30
60
18
06
00
UT 13 0.0
9 NOV 1969
100γ (LAT≥60°)
30γ (LAT<60°)

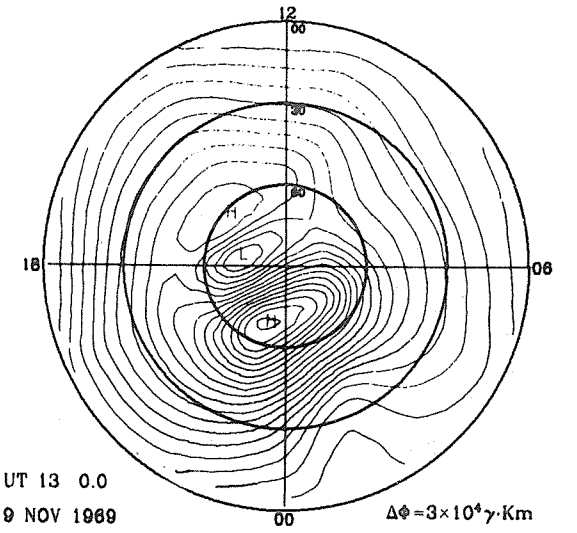
12
00
30
60
18
06
00
H
L
UT 13 0.0
9 NOV 1969
Δφ=3×10⁴γ·Km

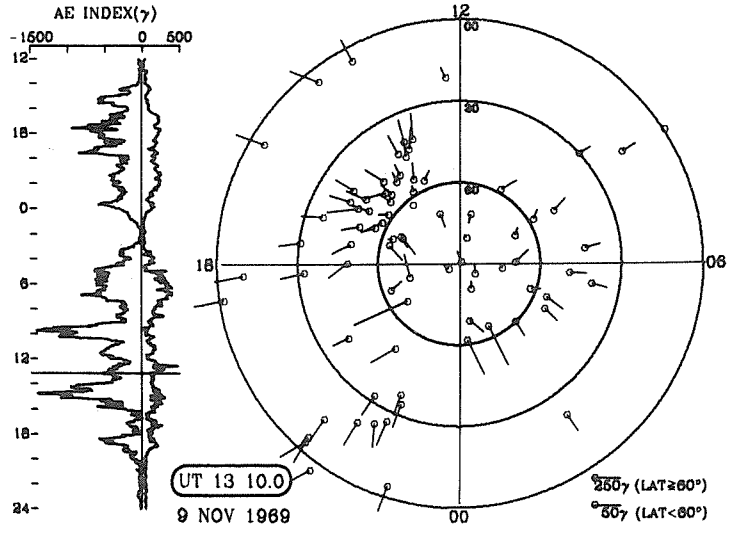
AE INDEX(γ)
-1500
0
500
12
18
0
6
12
18
24
12
00
30
60
18
06
00
UT 13 10.0
9 NOV 1969
250γ (LAT≥60°)
50γ (LAT<60°)

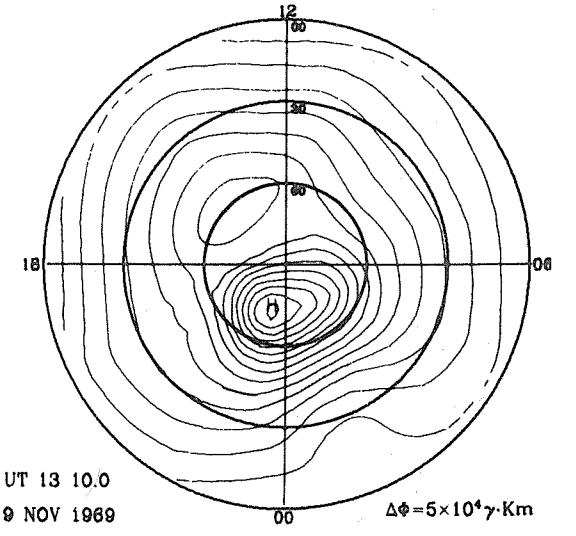
12
00
30
60
18
06
00
L
UT 13 10.0
9 NOV 1969
Δφ=5×10⁴γ·Km

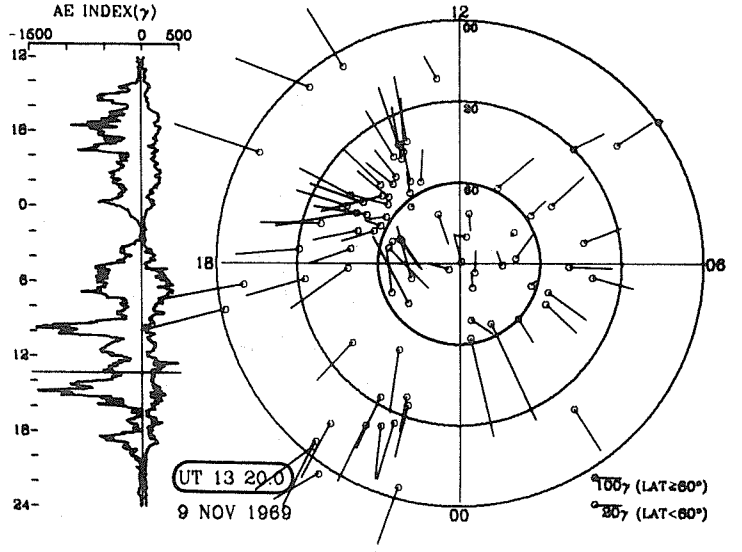
AE INDEX(γ)
-1500
0
500
12
18
0
6
12
18
24
12
00
30
60
18
06
00
UT 13 20.0
9 NOV 1969
100γ (LAT≥60°)
30γ (LAT<60°)

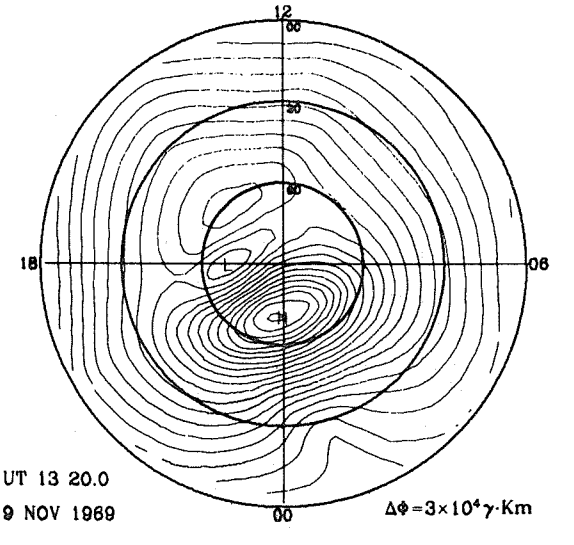
12
00
30
60
18
06
00
H
L
UT 13 20.0
9 NOV 1969
Δφ=3×10⁴γ·Km

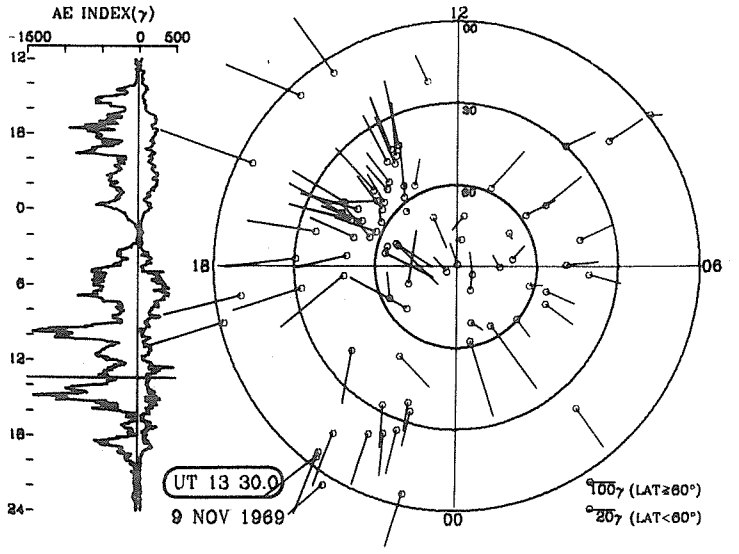
AE INDEX(γ)
-1600
0
500
12
18
0
6
12
18
24
12
00
30
60
18
06
00
UT 13 30.0
9 NOV 1969
100γ (LAT≥60°)
20γ (LAT<60°)

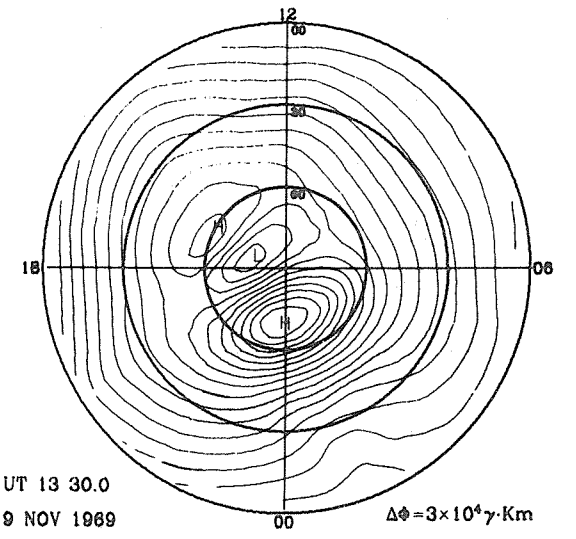
12
00
30
60
18
06
00
UT 13 30.0
9 NOV 1969
Δφ=3×10⁴γ·Km

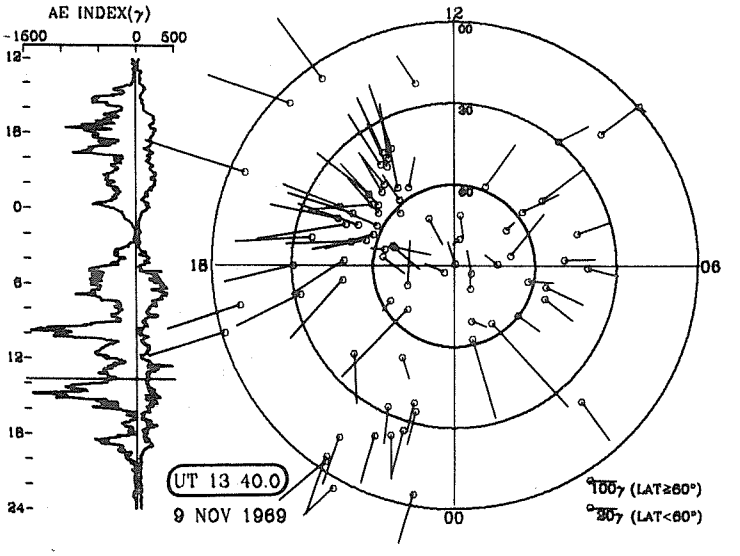
AE INDEX(γ)
-1600
0
500
12
18
0
6
12
18
24
12
00
30
60
18
06
00
UT 13 40.0
9 NOV 1969
100γ (LAT≥60°)
20γ (LAT<60°)

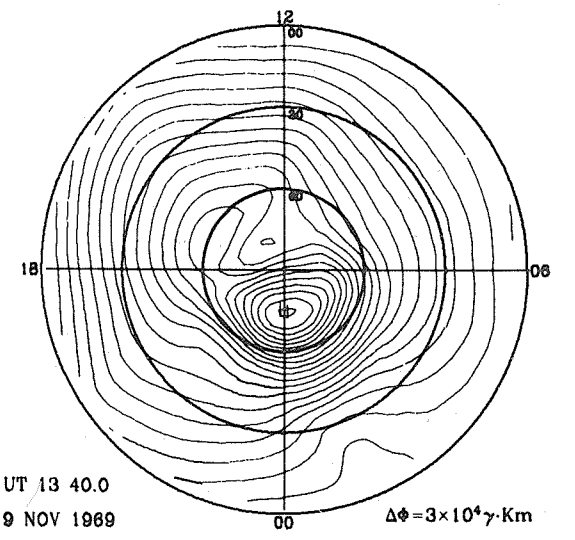
12
00
30
60
18
06
00
UT 13 40.0
9 NOV 1969
Δφ=3×10⁴γ·Km

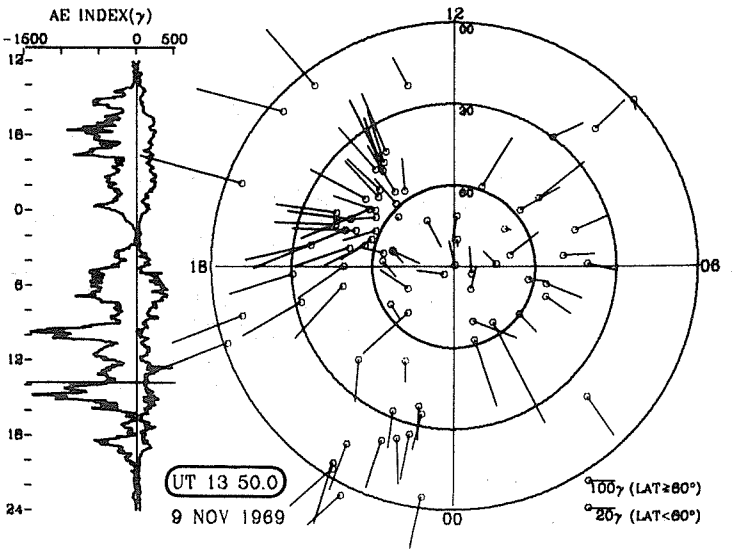
AE INDEX(γ)
-1600
0
500
12
18
0
6
12
18
24
12
00
30
60
18
06
00
UT 13 50.0
9 NOV 1969
100γ (LAT≥60°)
20γ (LAT<60°)

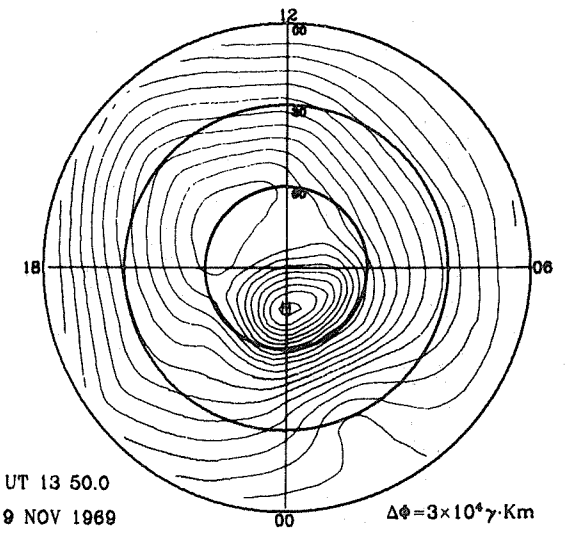
12
00
30
60
18
06
00
UT 13 50.0
9 NOV 1969
Δφ=3×10⁴γ·Km

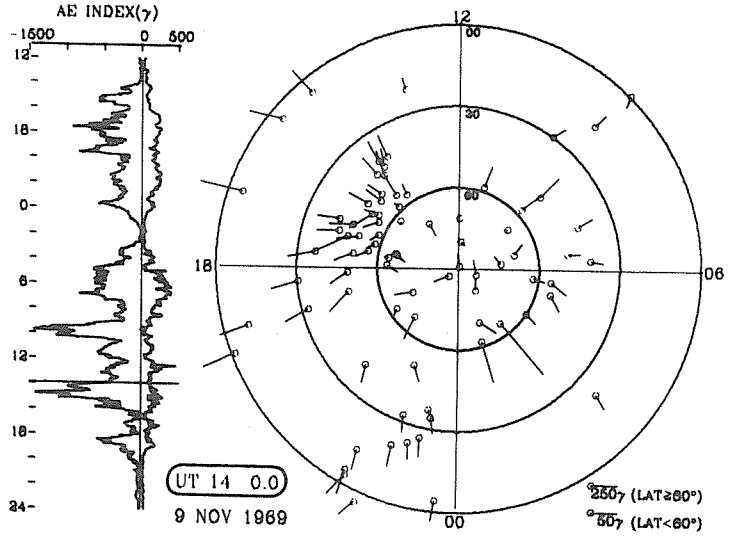
AE INDEX(γ)
-1500
0
500
12
18
0
6
12
18
24
12
00
30
60
18
06
00
UT 14 0.0
9 NOV 1969
250γ (LAT≥60°)
50γ (LAT<60°)

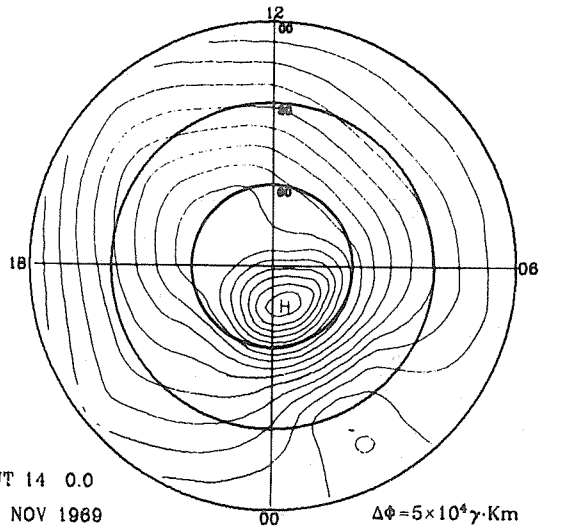
12
00
30
60
18
06
00
H
UT 14 0.0
9 NOV 1969
Δφ=5×10⁴γ·Km

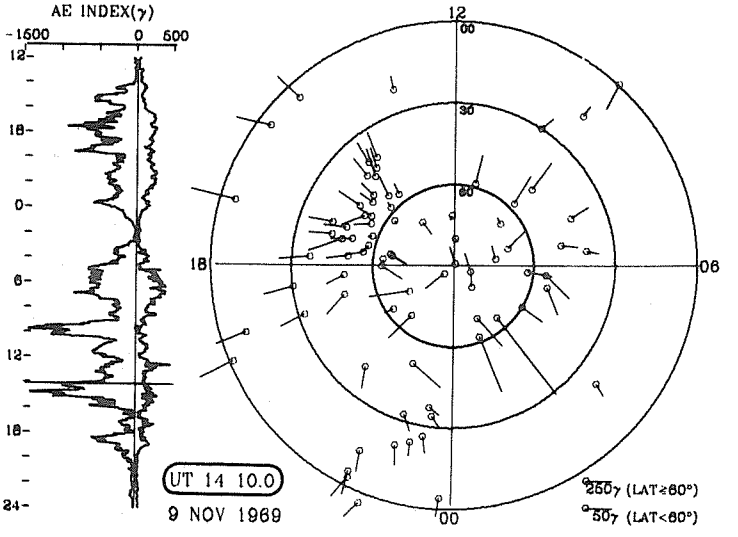
AE INDEX(γ)
-1500
0
500
12
18
0
6
12
18
24
12
00
30
60
18
06
00
UT 14 10.0
9 NOV 1969
250γ (LAT≥60°)
50γ (LAT<60°)

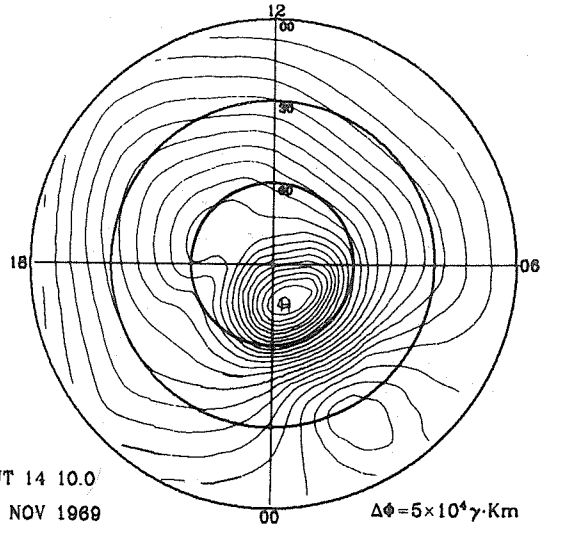
12
00
30
60
18
06
00
H
UT 14 10.0
9 NOV 1969
Δφ=5×10⁴γ·Km

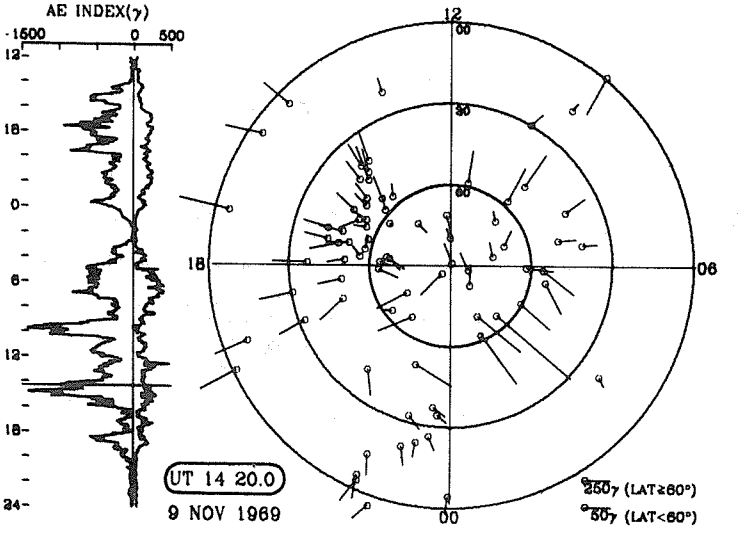
AE INDEX(γ)
-1500
0
500
12
18
0
6
12
18
24
12
00
30
60
18
06
00
UT 14 20.0
9 NOV 1969
250γ (LAT≥60°)
50γ (LAT<60°)

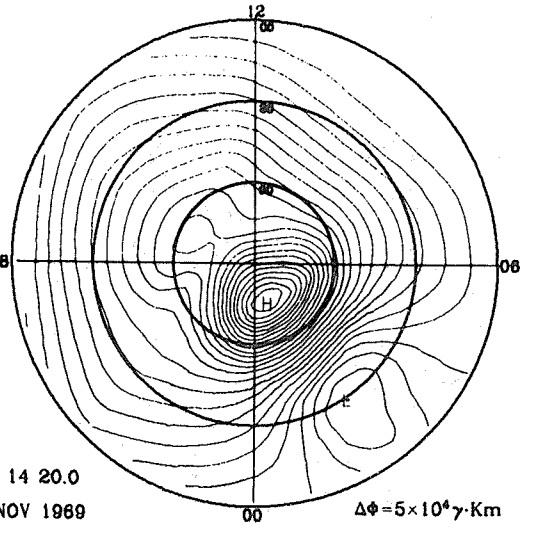
12
00
30
60
18
06
00
H
UT 14 20.0
9 NOV 1969
Δφ=5×10⁴γ·Km

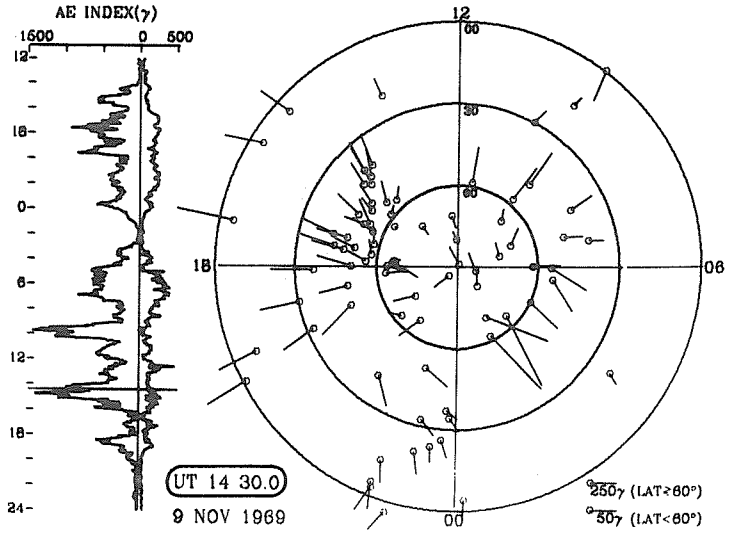
AE INDEX(γ)
1500
0
500
12
18
0
6
12
18
24
12
00
30
60
18
06
00
UT 14 30.0
9 NOV 1969
250γ (LAT≥60°)
50γ (LAT<60°)

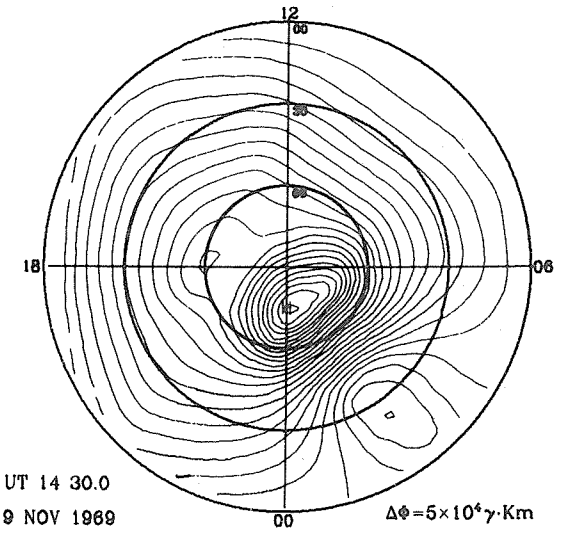
12
00
30
60
18
06
00
UT 14 30.0
9 NOV 1969
ΔΦ=5×10⁴γ·Km

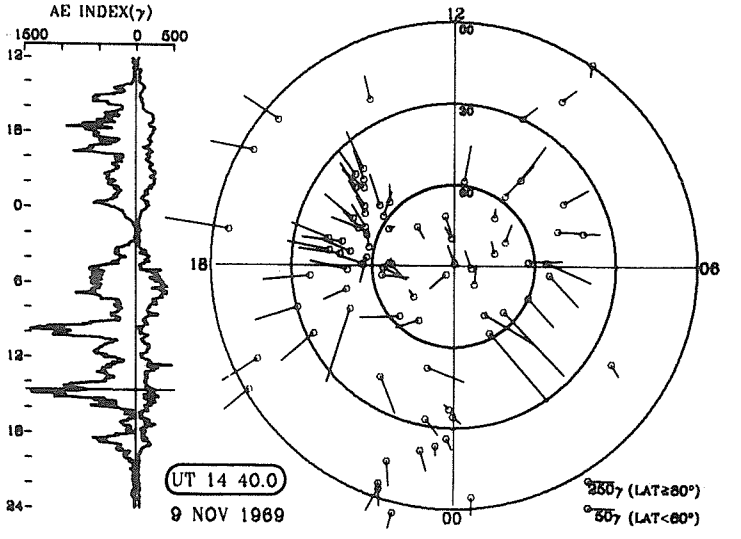
AE INDEX(γ)
1500
0
500
12
18
0
6
12
18
24
12
00
30
60
18
06
00
UT 14 40.0
9 NOV 1969
250γ (LAT≥60°)
50γ (LAT<60°)

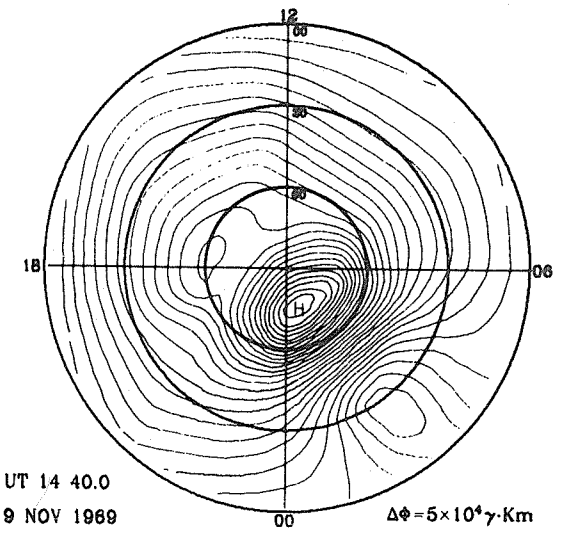
12
00
30
60
18
06
00
UT 14 40.0
9 NOV 1969
ΔΦ=5×10⁴γ·Km

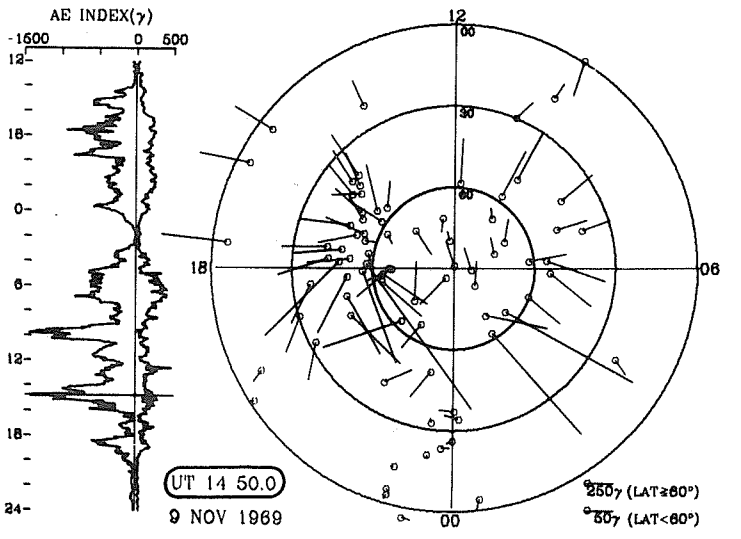
AE INDEX(γ)
1500
0
500
12
18
0
6
12
18
24
12
00
30
60
18
06
00
UT 14 50.0
9 NOV 1969
250γ (LAT≥60°)
50γ (LAT<60°)

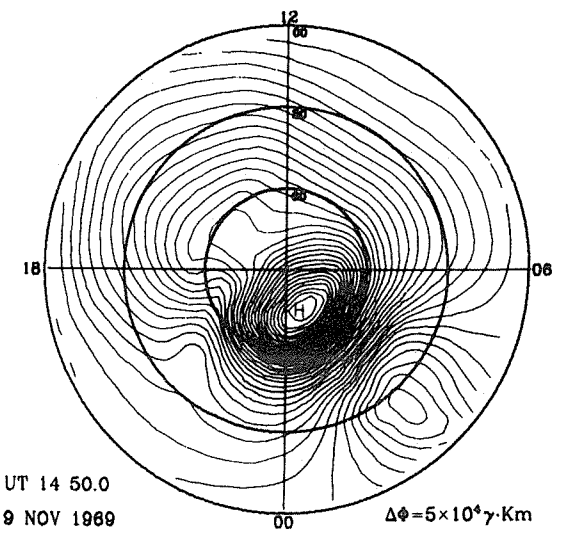
12
00
30
60
18
06
00
UT 14 50.0
9 NOV 1969
ΔΦ=5×10⁴γ·Km

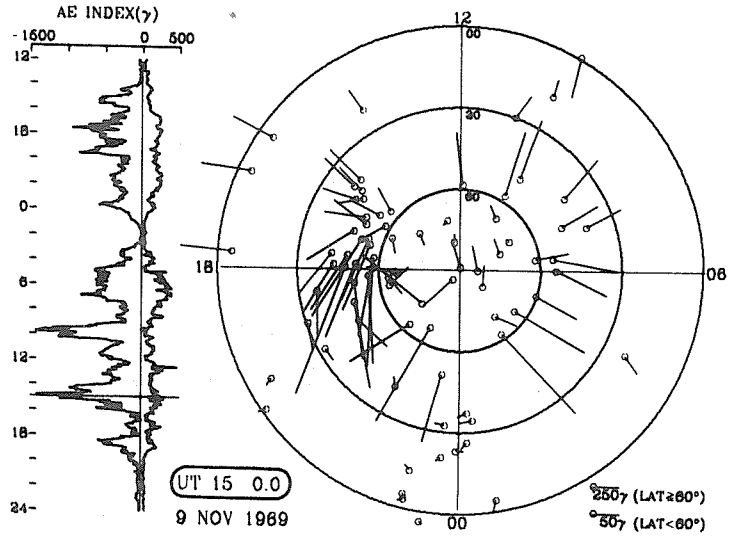
AE INDEX(γ)
-1500
0
500
12
18
0
6
12
18
24
12
00
30
60
18
06
00
UT 15 0.0
9 NOV 1969
250γ (LAT≥60°)
50γ (LAT<60°)

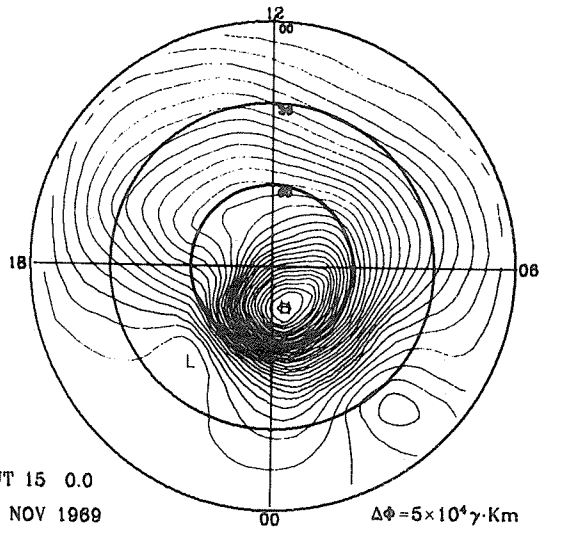
12
00
30
60
18
06
00
H
L
UT 15 0.0
9 NOV 1969
ΔΦ=5×10⁴γ·Km

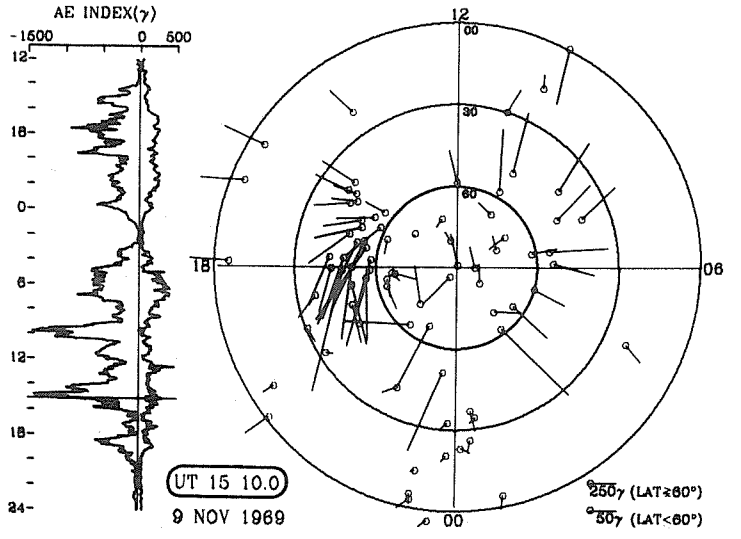
AE INDEX(γ)
-1500
0
500
12
18
0
6
12
18
24
12
00
30
60
18
06
00
UT 15 10.0
9 NOV 1969
250γ (LAT≥60°)
50γ (LAT<60°)

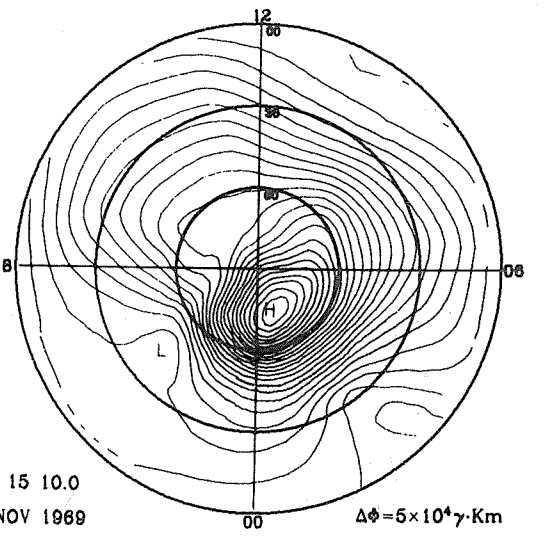
12
00
30
60
18
06
00
H
L
UT 15 10.0
9 NOV 1969
ΔΦ=5×10⁴γ·Km

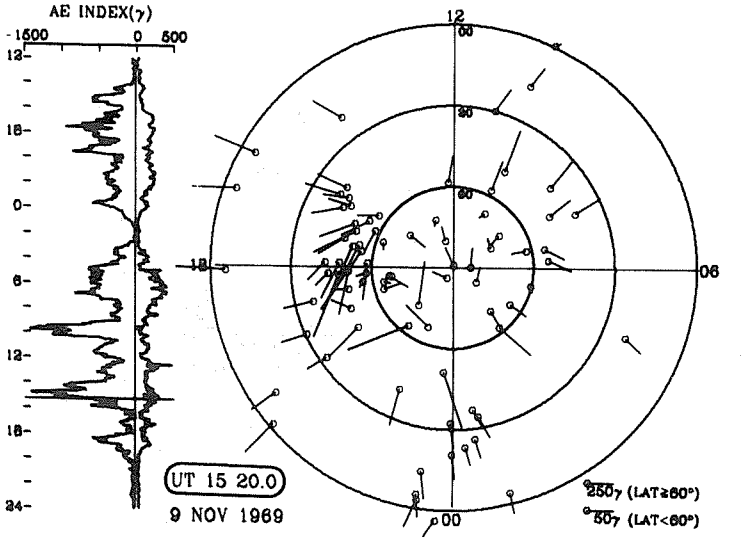
AE INDEX(γ)
-1500
0
500
12
18
0
6
12
18
24
12
00
30
60
18
06
00
UT 15 20.0
9 NOV 1969
250γ (LAT≥60°)
50γ (LAT<60°)

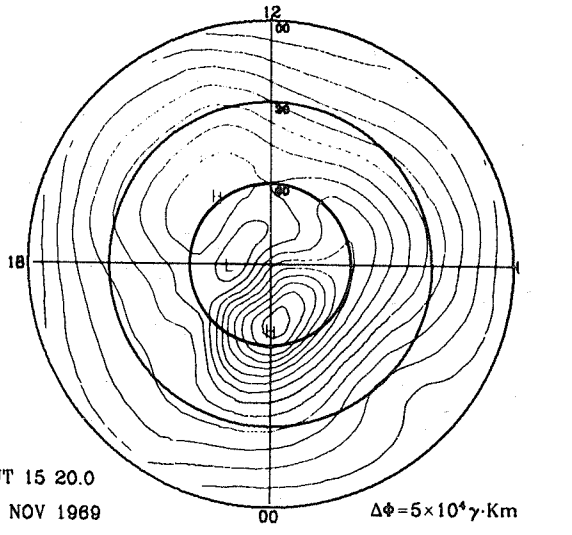
12
00
30
60
18
06
00
H
L
UT 15 20.0
9 NOV 1969
ΔΦ=5×10⁴γ·Km

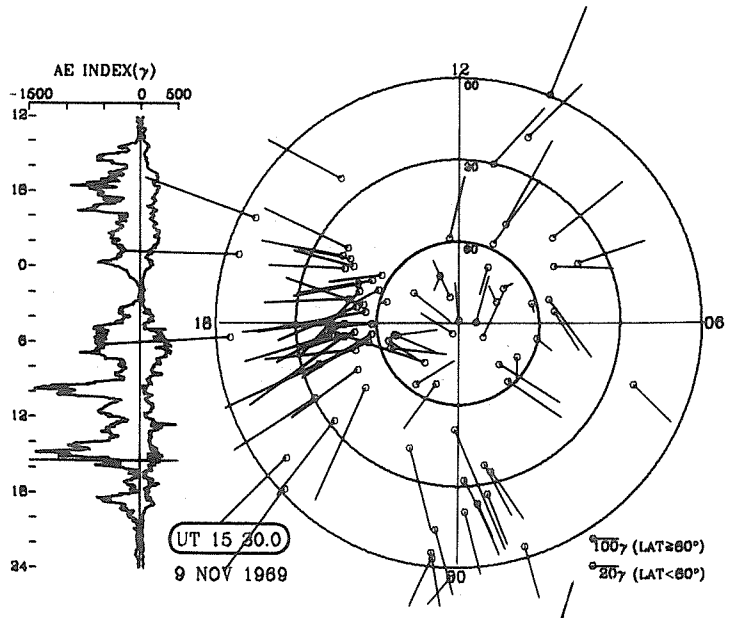
AE INDEX(γ)
-1600
0
500
12
18
0
6
12
18
24
12
00
30
60
18
06
00
UT 15 30.0
9 NOV 1969
100γ (LAT≥60°)
20γ (LAT<60°)

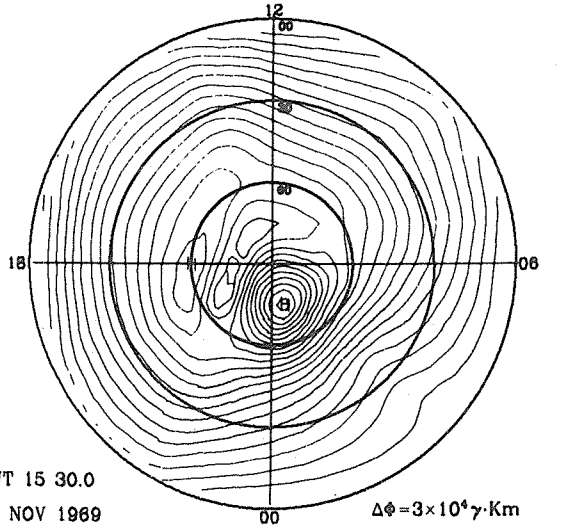
12
00
30
60
18
06
00
UT 15 30.0
9 NOV 1969
Δφ=3×10⁴γ·Km

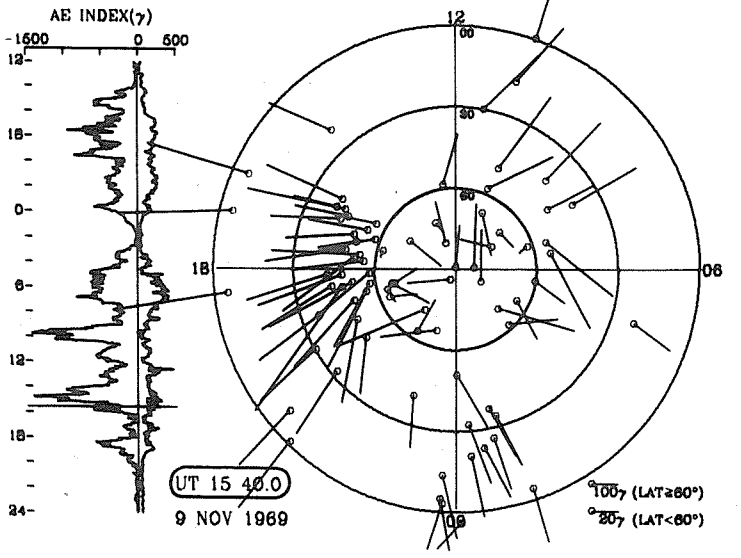
AE INDEX(γ)
-1600
0
500
12
18
0
6
12
18
24
12
00
30
60
18
06
00
UT 15 40.0
9 NOV 1969
100γ (LAT≥60°)
20γ (LAT<60°)

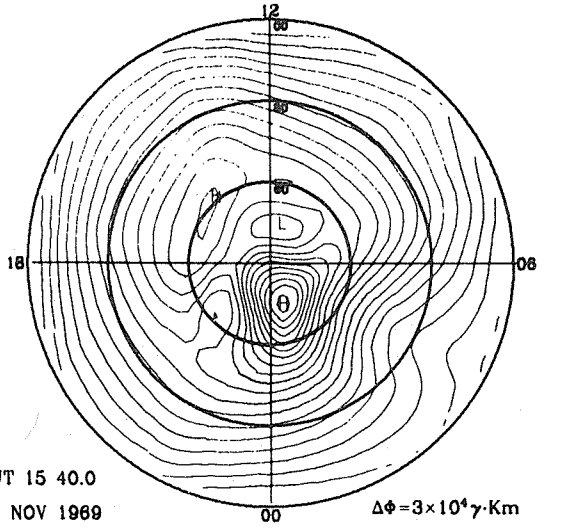
12
00
30
60
18
06
00
UT 15 40.0
9 NOV 1969
Δφ=3×10⁴γ·Km

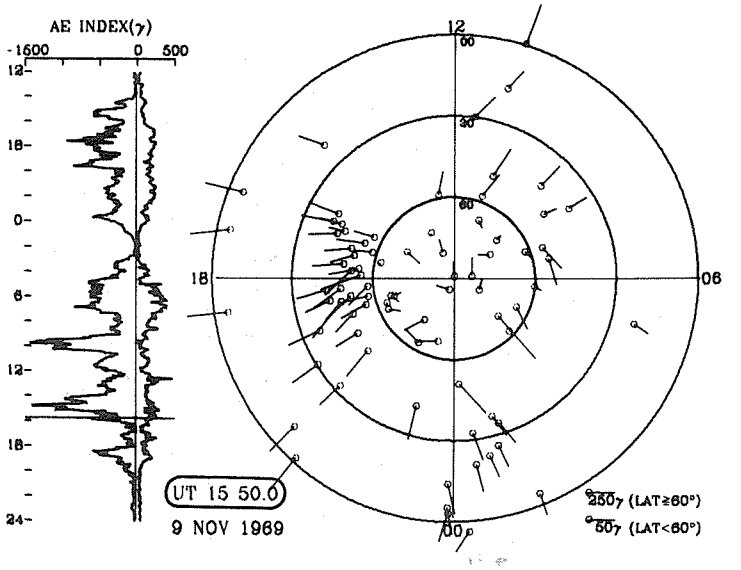
AE INDEX(γ)
-1600
0
500
12
18
0
6
12
18
24
12
00
30
60
18
06
00
UT 15 50.0
9 NOV 1969
250γ (LAT≥60°)
50γ (LAT<60°)

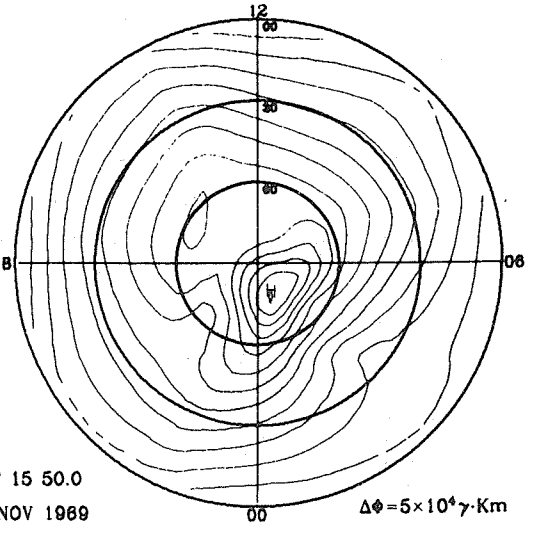
12
00
30
60
18
06
00
UT 15 50.0
9 NOV 1969
Δφ=5×10⁴γ·Km

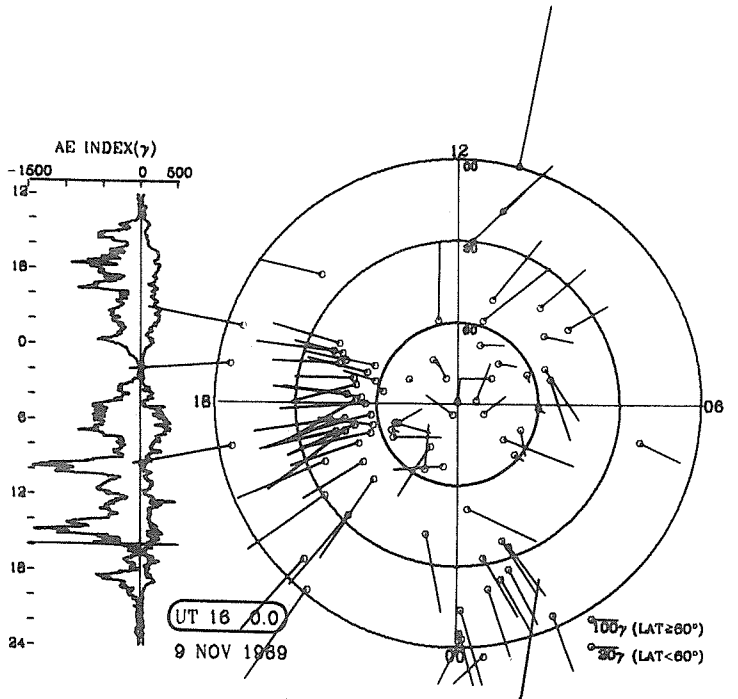
AE INDEX(γ)
-1500
0
500
12
18
0
6
12
18
24
12
00
30
60
18
06
00
UT 16 0.0
9 NOV 1969
100γ (LAT≥60°)
20γ (LAT<60°)

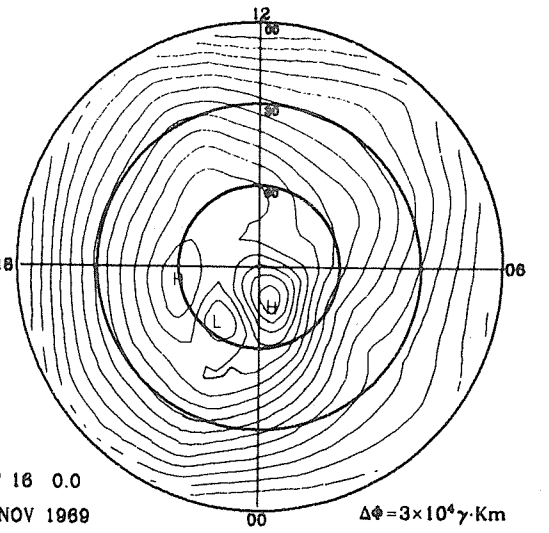
12
00
30
60
18
06
00
L
H
H
UT 16 0.0
9 NOV 1969
Δφ=3×10⁴γ·Km

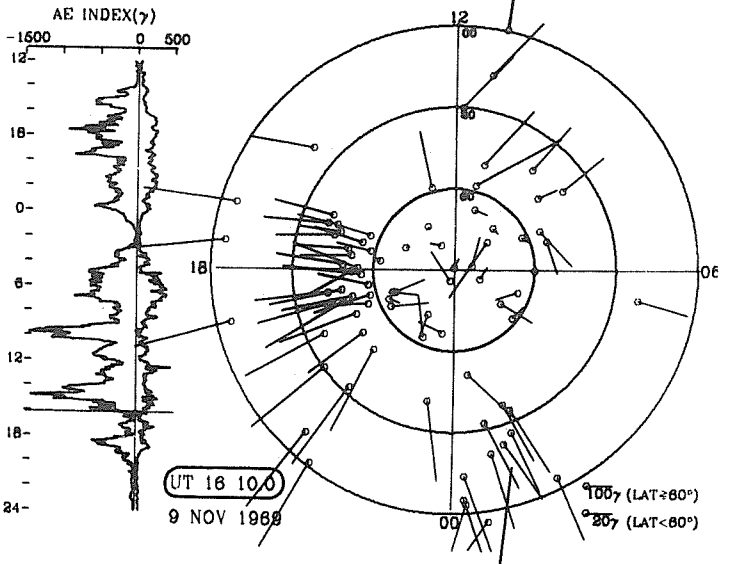
AE INDEX(γ)
-1500
0
500
12
18
0
6
12
18
24
12
00
30
60
18
06
00
UT 16 10.0
9 NOV 1969
100γ (LAT≥60°)
20γ (LAT<60°)

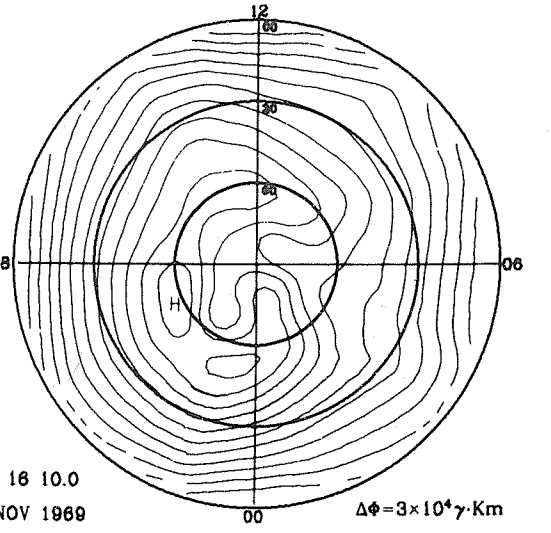
12
00
30
60
18
06
00
H
UT 16 10.0
9 NOV 1969
Δφ=3×10⁴γ·Km

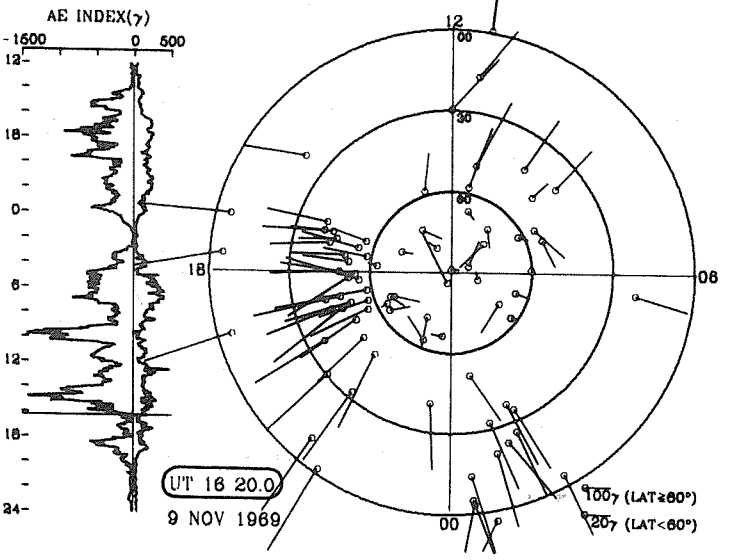
AE INDEX(γ)
-1500
0
500
12
18
0
6
12
18
24
12
00
30
60
18
06
00
UT 16 20.0
9 NOV 1969
100γ (LAT≥60°)
20γ (LAT<60°)

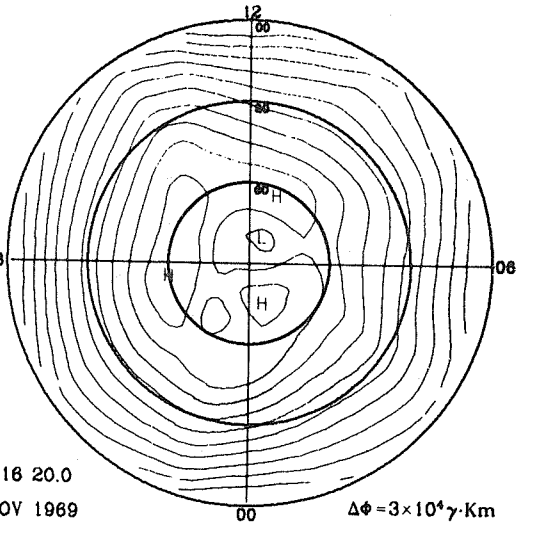
12
00
30
60
H
18
L
06
H
H
00
UT 16 20.0
9 NOV 1969
Δφ=3×10⁴γ·Km

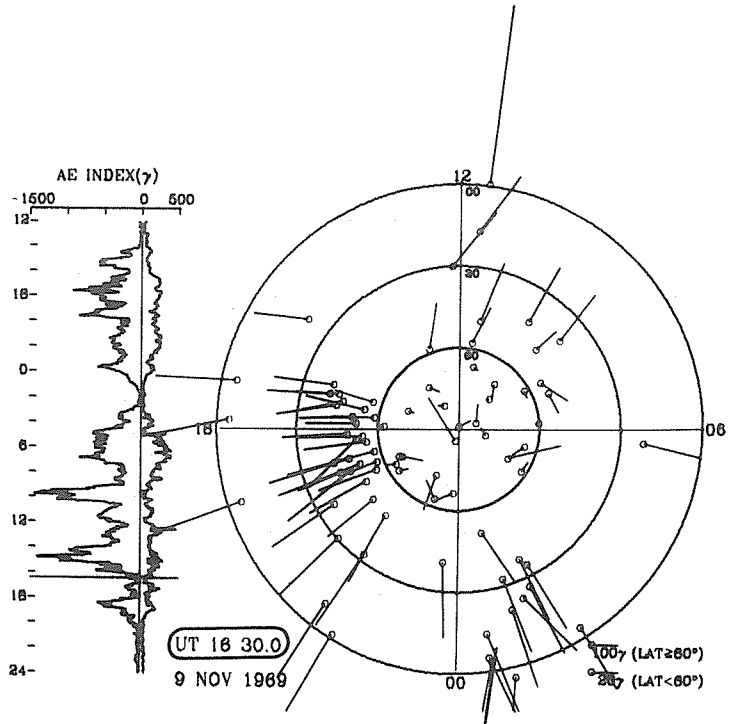
AE INDEX(γ)
-1500
0
500
12
18
0
6
12
18
24
12
00
30
60
18
06
00
UT 16 30.0
9 NOV 1969
100γ (LAT≥60°)
20γ (LAT<60°)

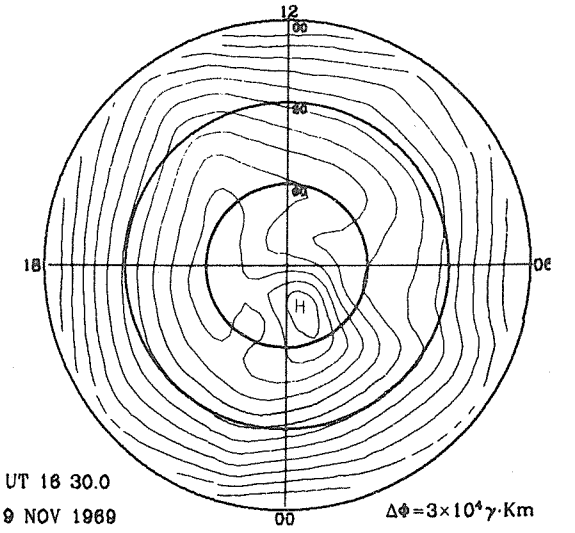
12
00
30
60
18
06
H
00
UT 16 30.0
9 NOV 1969
Δφ=3×10⁴γ·Km

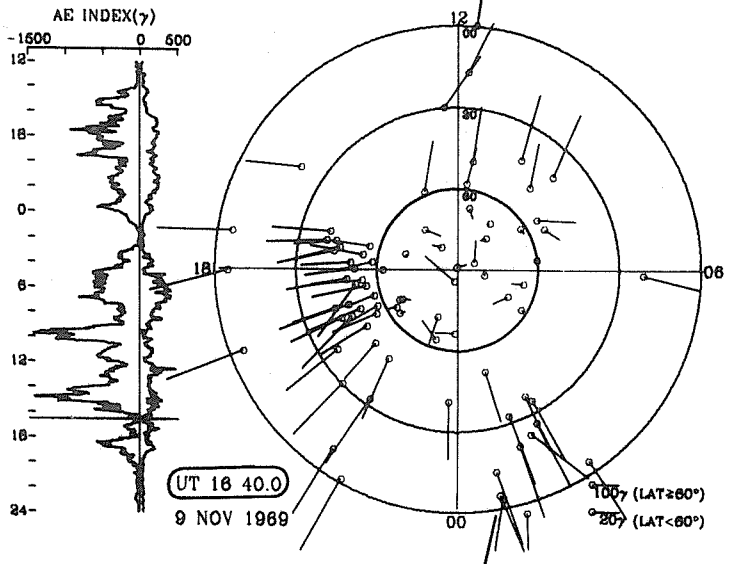
AE INDEX(γ)
-1500
0
500
12
18
0
6
12
18
24
12
00
30
60
18
06
00
UT 16 40.0
9 NOV 1969
100γ (LAT≥60°)
20γ (LAT<60°)

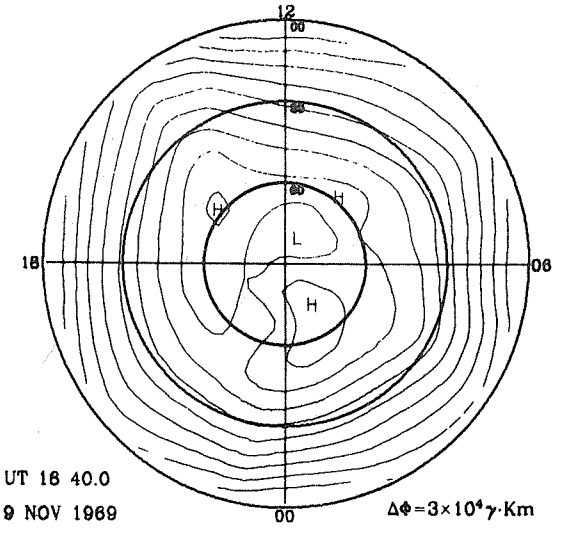
12
00
30
60
H
H
L
H
18
06
00
UT 16 40.0
9 NOV 1969
Δφ=3×10⁴γ·Km

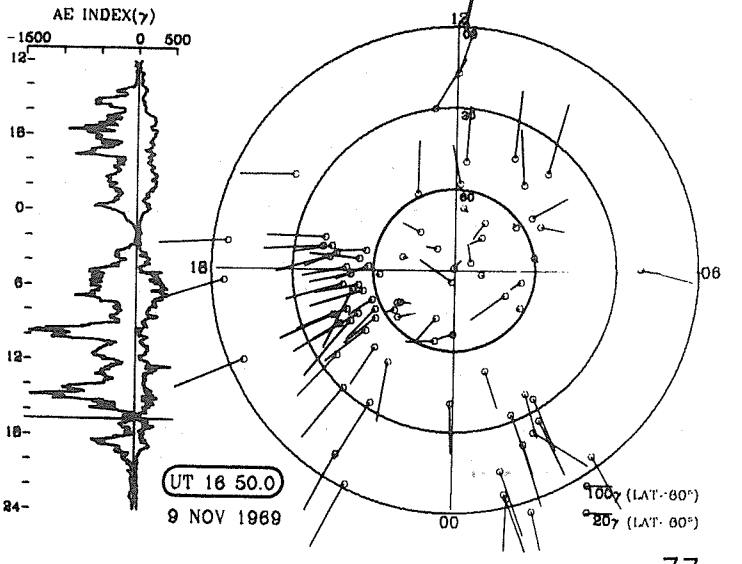
AE INDEX(γ)
-1500
0
500
12
18
0
6
12
18
24
12
00
30
60
18
06
00
UT 16 50.0
9 NOV 1969
100γ (LAT<60°)
20γ (LAT<60°)

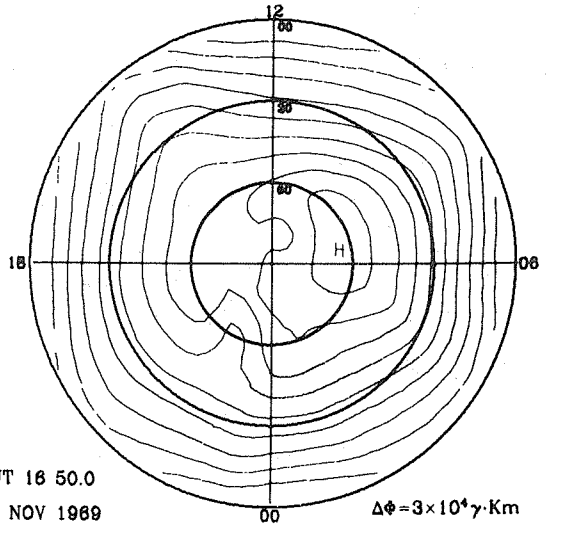
12
00
30
60
H
18
06
00
UT 16 50.0
9 NOV 1969
Δφ=3×10⁴γ·Km

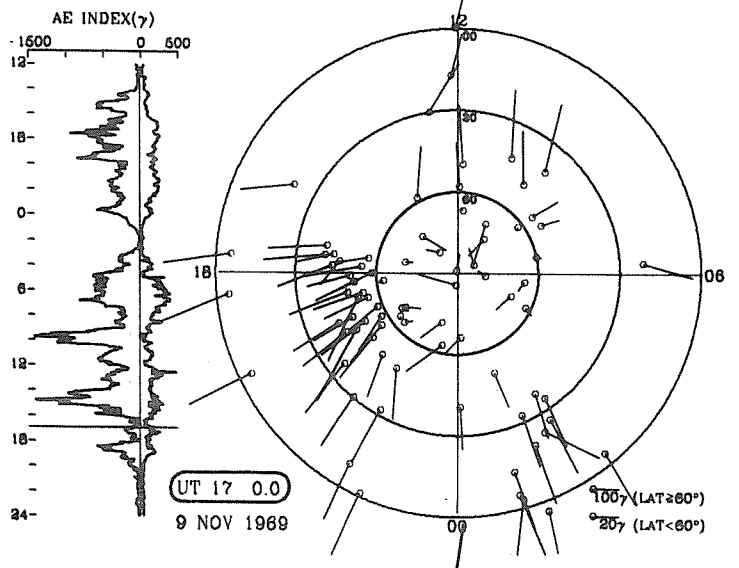
AE INDEX(γ)
-1500
0
500
12
18
0
6
12
18
24
12
00
30
60
18
06
00
UT 17 0.0
9 NOV 1969
100γ (LAT≥60°)
20γ (LAT<60°)

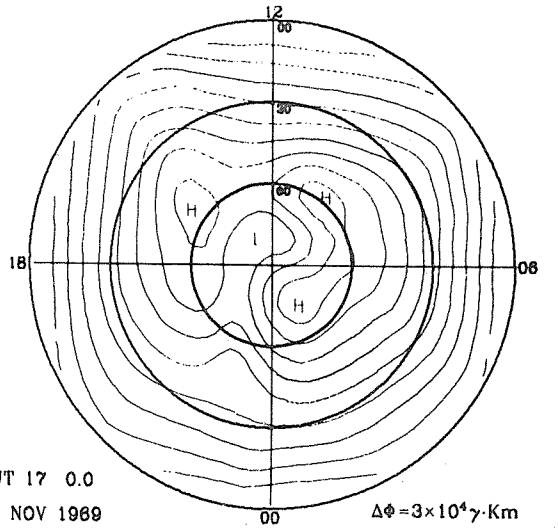
12
00
30
60
18
06
00
H
H
L
H
UT 17 0.0
9 NOV 1969
Δφ=3×10⁴γ·Km

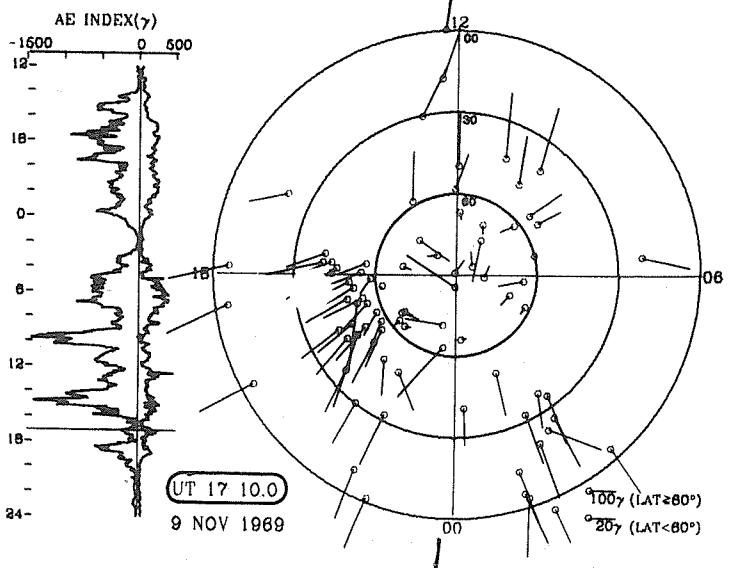
AE INDEX(γ)
-1500
0
500
12
18
0
6
12
18
24
12
00
30
60
18
06
00
UT 17 10.0
9 NOV 1969
100γ (LAT≥60°)
20γ (LAT<60°)

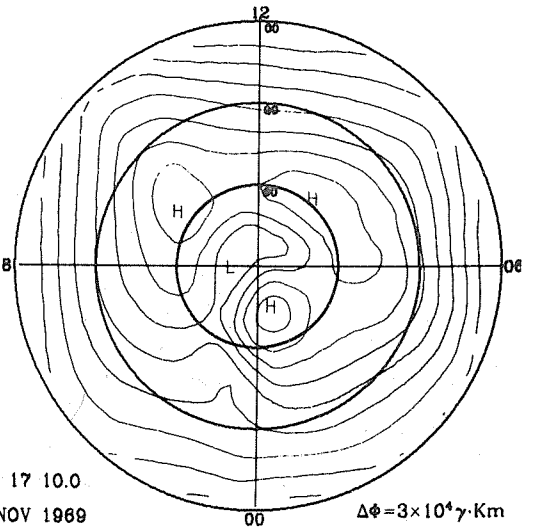
12
00
30
60
18
06
00
H
H
L
H
UT 17 10.0
9 NOV 1969
Δφ=3×10⁴γ·Km

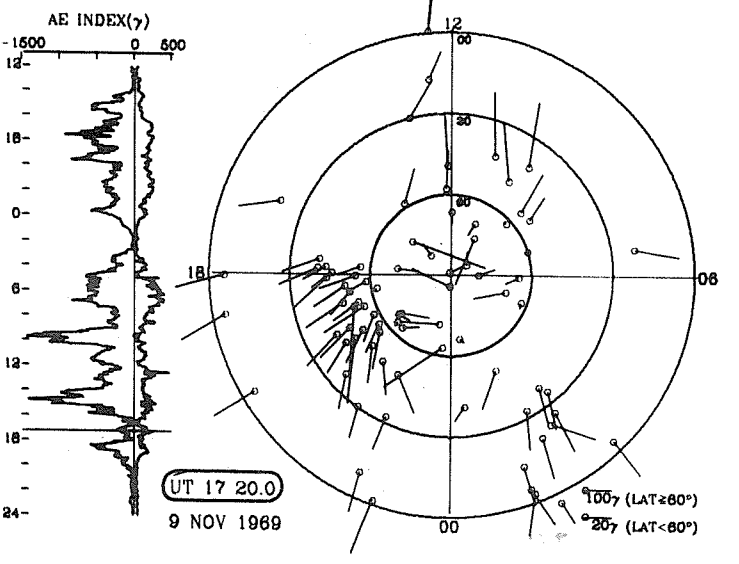
AE INDEX(γ)
-1500
0
500
12
18
0
6
12
18
24
12
00
30
60
18
06
00
UT 17 20.0
9 NOV 1969
100γ (LAT≥60°)
20γ (LAT<60°)

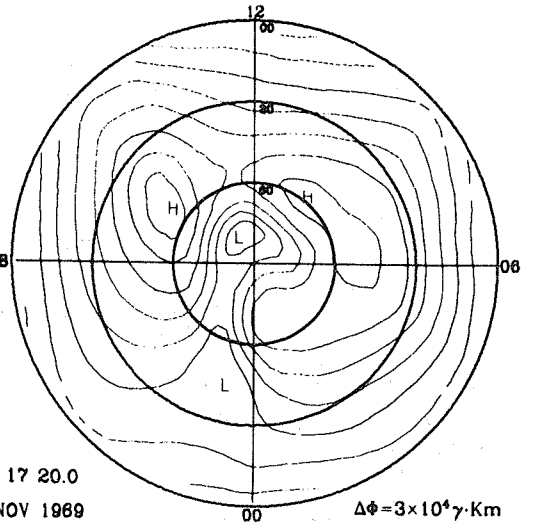
12
00
30
60
18
06
00
H
H
L
L
UT 17 20.0
9 NOV 1969
Δφ=3×10⁴γ·Km

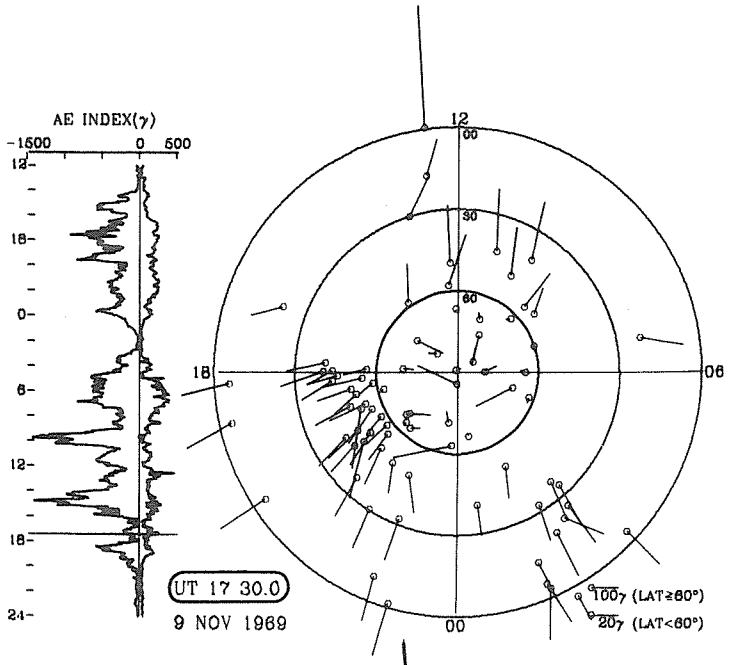
AE INDEX(γ)
-1500
0
500
12
18
0
6
12
18
24
12
00
30
60
18
06
00
UT 17 30.0
9 NOV 1969
100γ (LAT≥60°)
20γ (LAT<60°)

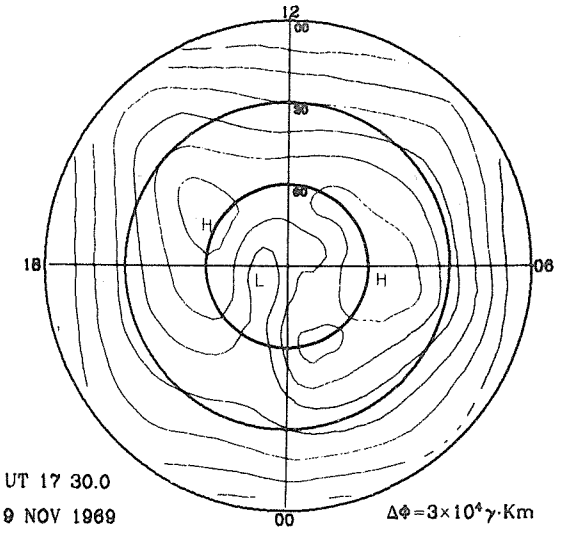
12
00
30
60
18
06
00
H
L
H
UT 17 30.0
9 NOV 1969
Δφ=3×10⁴γ·Km

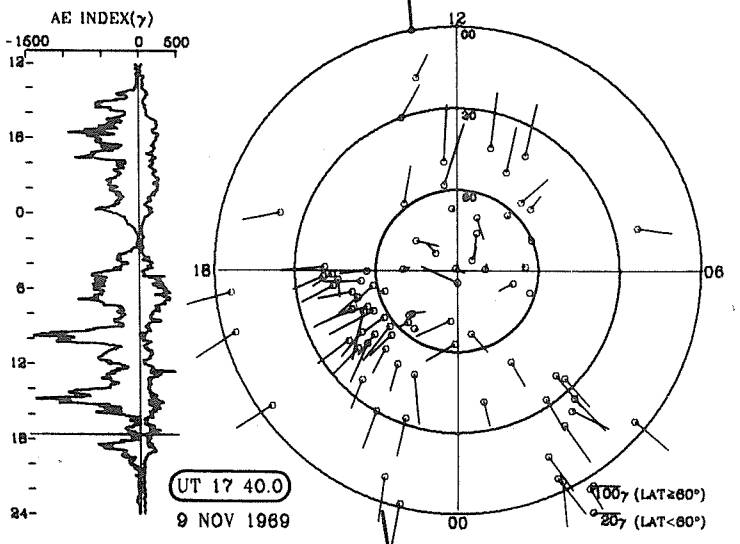
AE INDEX(γ)
-1500
0
500
12
18
0
6
12
18
24
12
00
30
60
18
06
00
UT 17 40.0
9 NOV 1969
100γ (LAT≥60°)
20γ (LAT<60°)

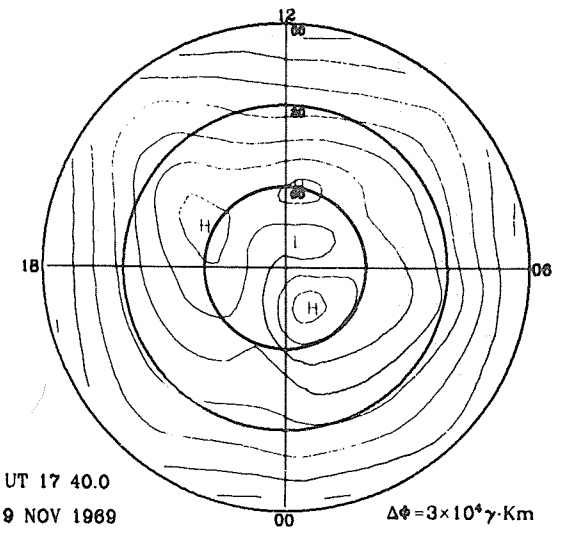
12
00
30
60
18
06
00
H
H
UT 17 40.0
9 NOV 1969
Δφ=3×10⁴γ·Km

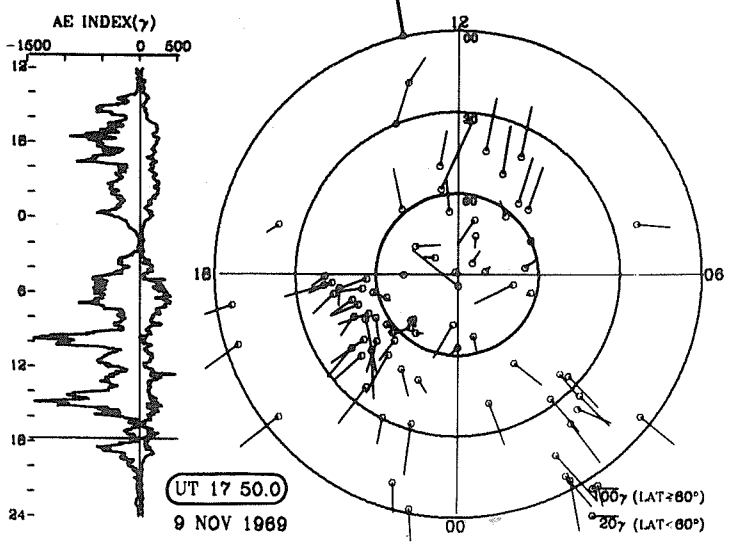
AE INDEX(γ)
-1500
0
500
12
18
0
6
12
18
24
12
00
30
60
18
06
00
UT 17 50.0
9 NOV 1969
100γ (LAT≥60°)
20γ (LAT<60°)

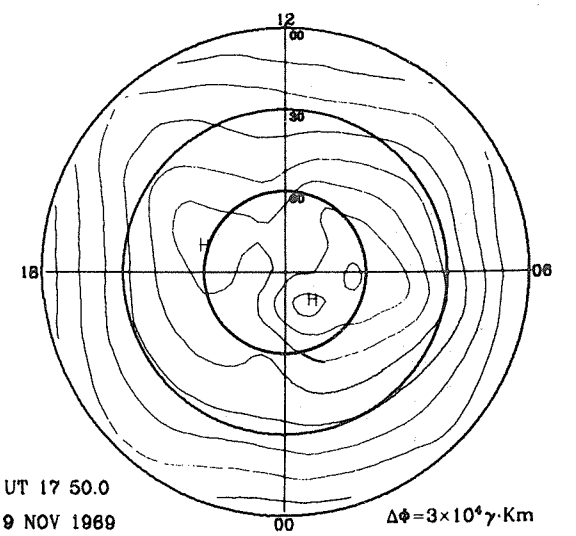
12
00
30
60
18
06
00
H
H
UT 17 50.0
9 NOV 1969
Δφ=3×10⁴γ·Km

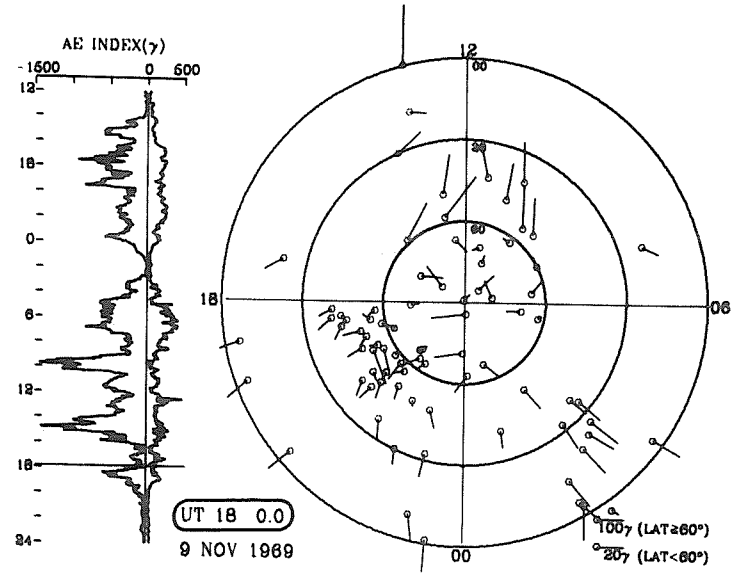
AE INDEX(γ)
-1500
0
500
12
18
0
6
12
18
24
12
00
30
60
18
06
00
UT 18 0.0
9 NOV 1969
100γ (LAT≥60°)
20γ (LAT<60°)

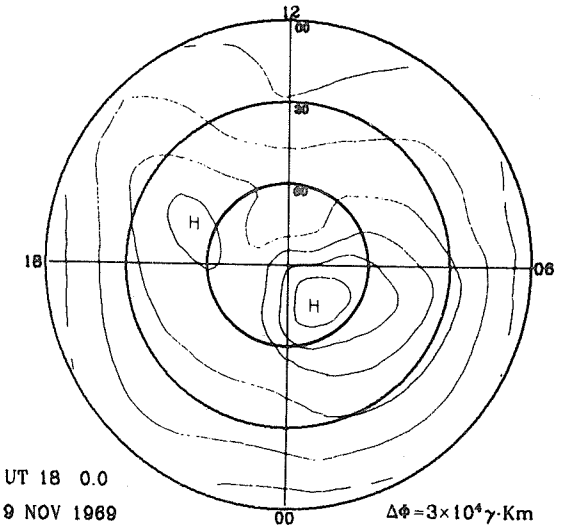
12
00
30
60
18
06
00
H
H
UT 18 0.0
9 NOV 1969
Δφ=3×10⁴γ·Km

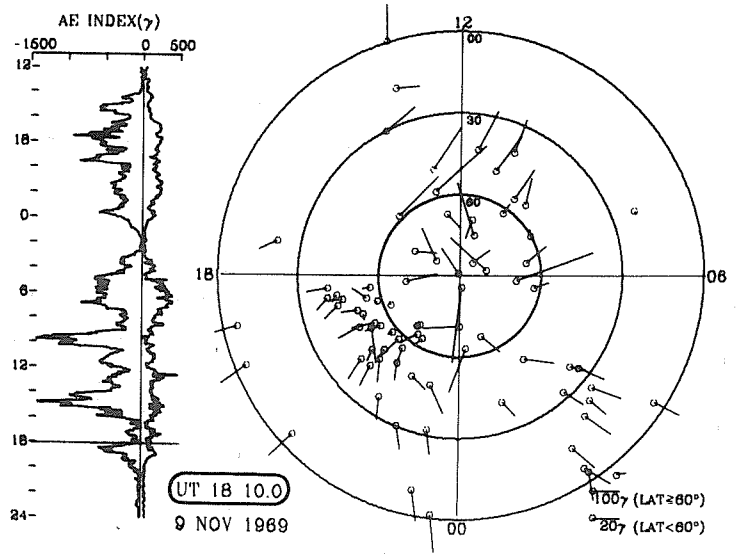
AE INDEX(γ)
-1500
0
500
12
18
0
6
12
18
24
12
00
30
60
18
06
00
UT 18 10.0
9 NOV 1969
100γ (LAT≥60°)
20γ (LAT<60°)

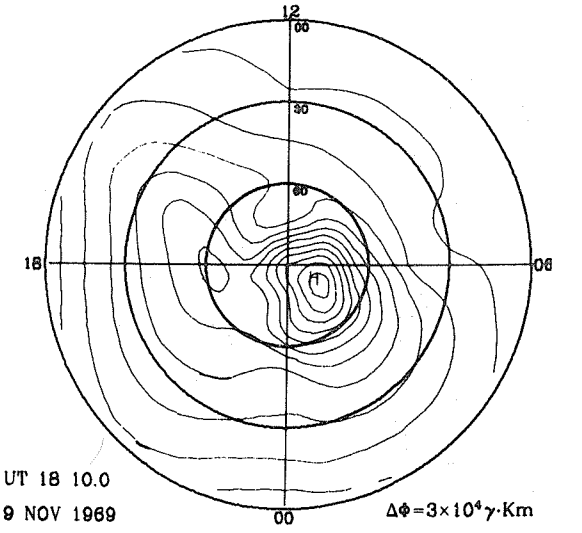
12
00
30
60
18
06
00
H
UT 18 10.0
9 NOV 1969
Δφ=3×10⁴γ·Km

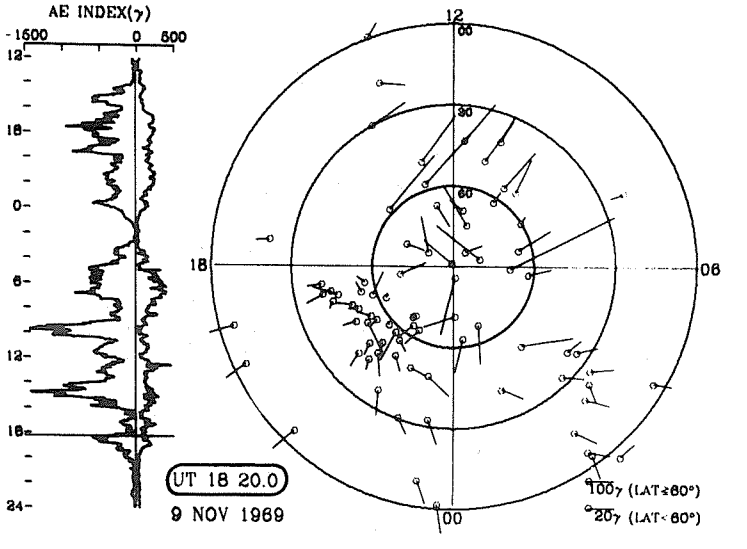
AE INDEX(γ)
-1500
0
500
12
18
0
6
12
18
24
12
00
30
60
18
06
00
UT 18 20.0
9 NOV 1969
100γ (LAT≥60°)
20γ (LAT<60°)

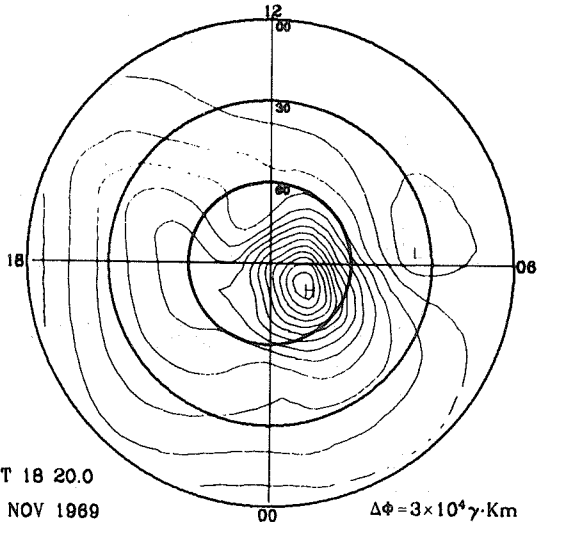
12
00
30
60
18
06
00
H
UT 18 20.0
9 NOV 1969
Δφ=3×10⁴γ·Km

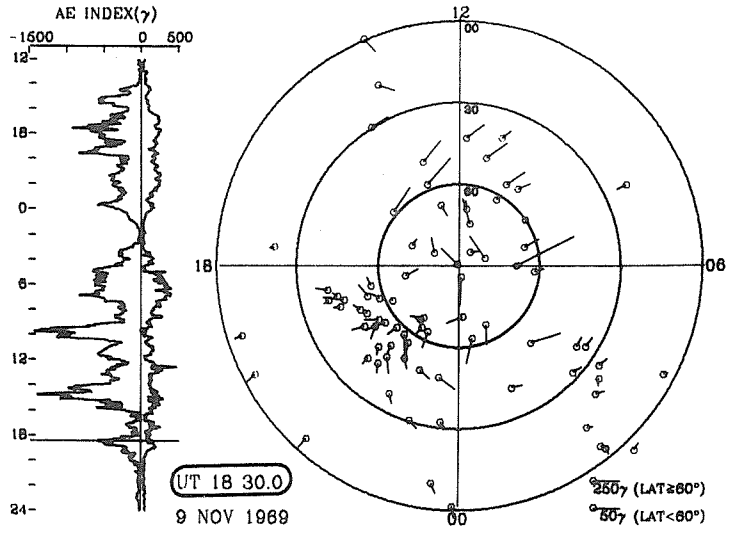
AE INDEX(γ)
-1500
0
500
12
18
0
6
12
18
24
12
00
30
60
18
06
00
UT 18 30.0
9 NOV 1969
250γ (LAT≥60°)
50γ (LAT<60°)

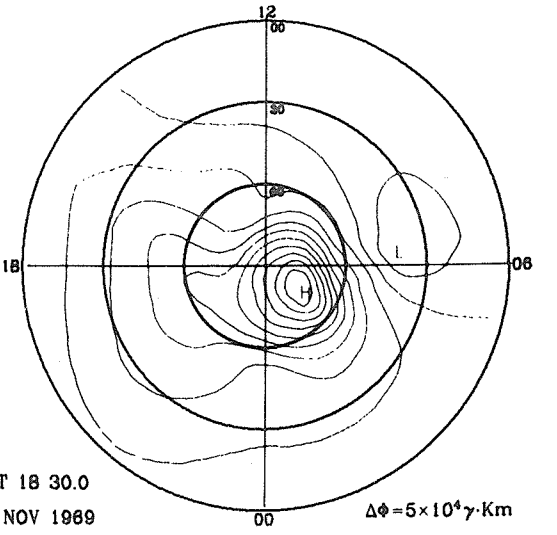
12
00
30
60
18
06
00
H
L
UT 18 30.0
9 NOV 1969
Δφ=5×10⁴γ·Km

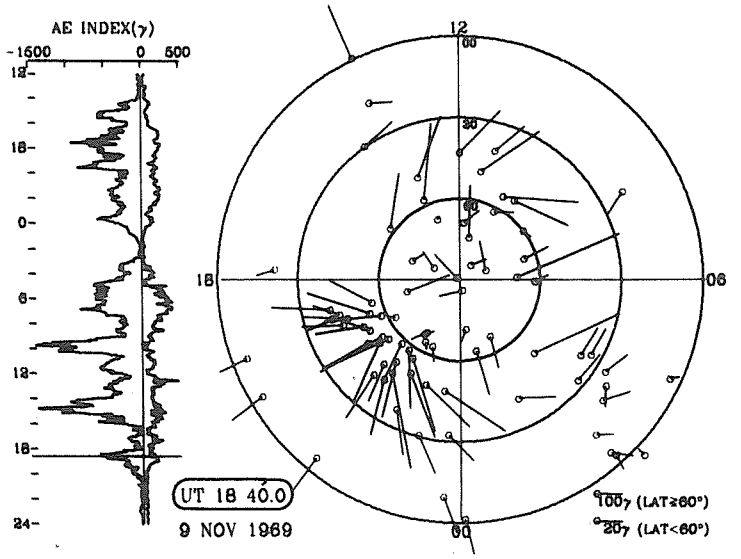
AE INDEX(γ)
-1500
0
500
12
18
0
6
12
18
24
12
00
30
60
18
06
00
UT 18 40.0
9 NOV 1969
100γ (LAT≥60°)
20γ (LAT<60°)

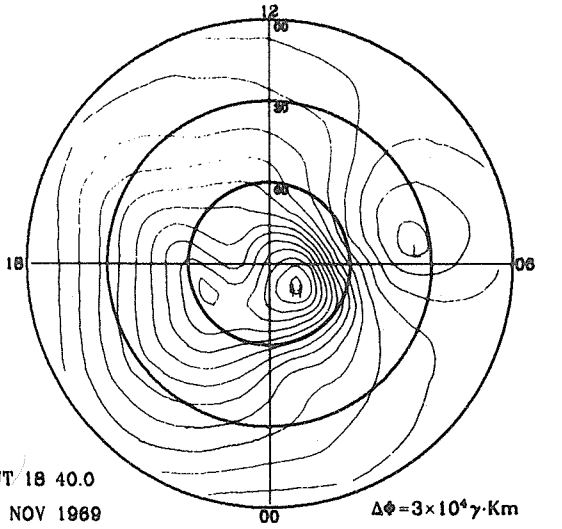
12
00
30
60
18
06
00
H
L
UT 18 40.0
9 NOV 1969
Δφ=3×10⁴γ·Km

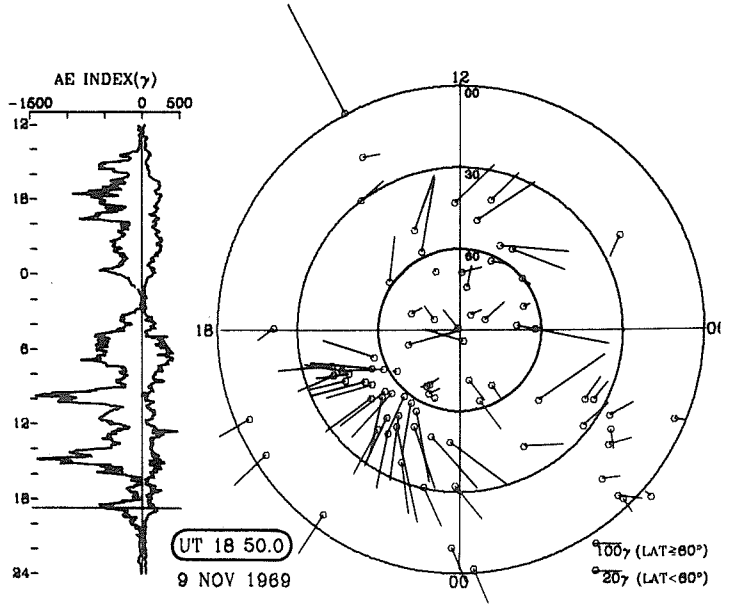
AE INDEX(γ)
-1500
0
500
12
18
0
6
12
18
24
12
00
30
60
18
06
00
UT 18 50.0
9 NOV 1969
100γ (LAT≥60°)
20γ (LAT<60°)

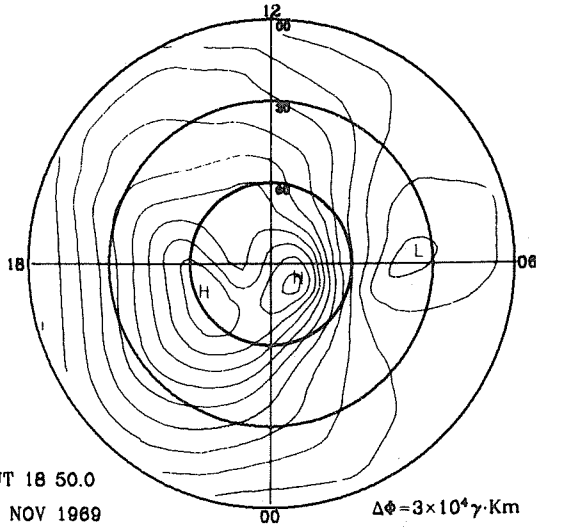
12
00
30
60
18
06
00
H
H
L
UT 18 50.0
9 NOV 1969
Δφ=3×10⁴γ·Km

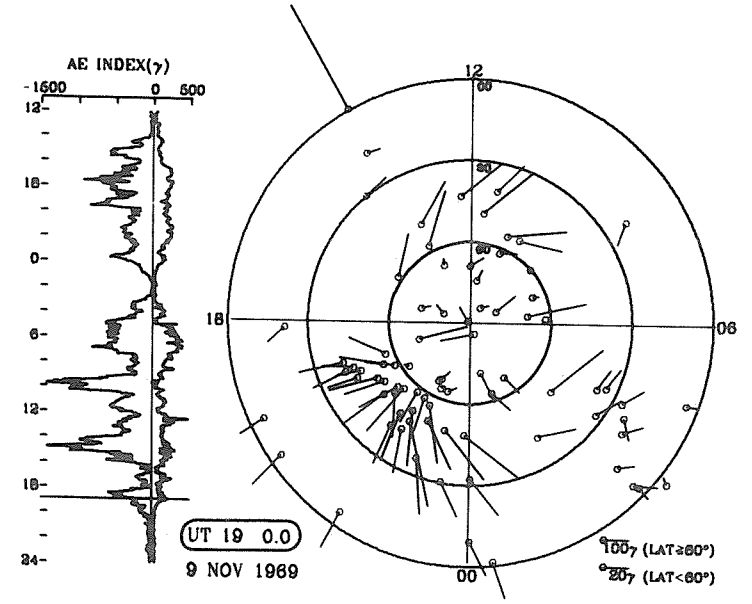
AE INDEX(γ)
-1500
0
500
12
18
0
6
12
18
24
12
00
30
60
18
06
00
UT 19 0.0
9 NOV 1969
100γ (LAT≥60°)
20γ (LAT<60°)

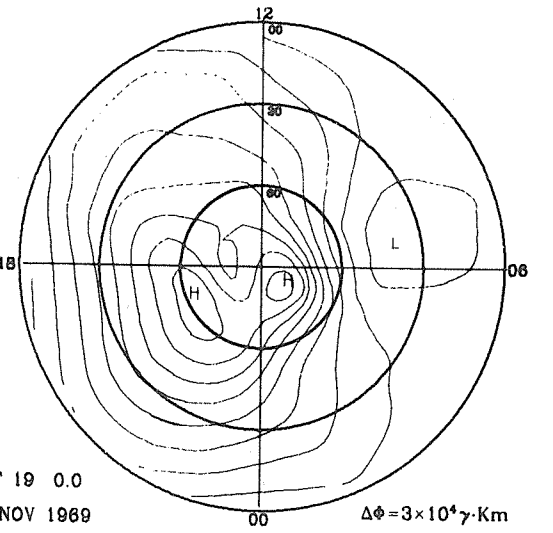
12
00
30
60
18
06
00
L
H
H
UT 19 0.0
9 NOV 1969
ΔΦ=3×10⁴γ·Km

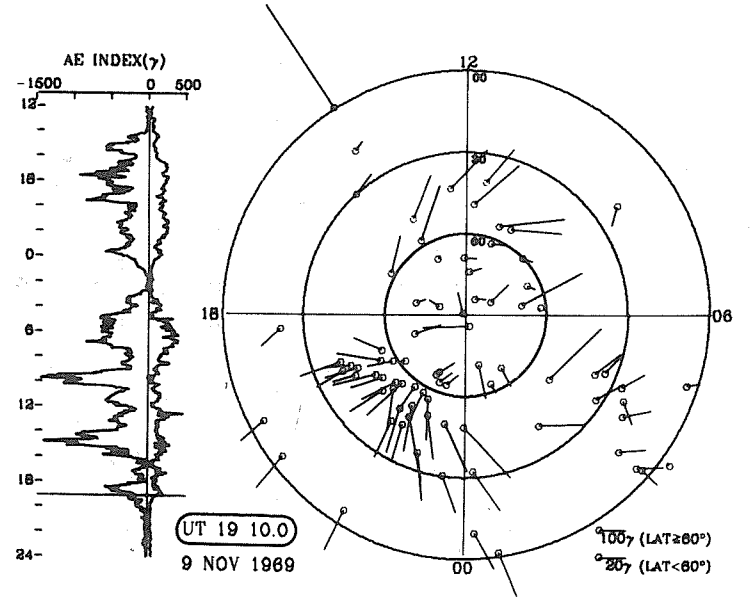
AE INDEX(γ)
-1500
0
500
12
18
0
6
12
18
24
12
00
30
60
18
06
00
UT 19 10.0
9 NOV 1969
100γ (LAT≥60°)
20γ (LAT<60°)

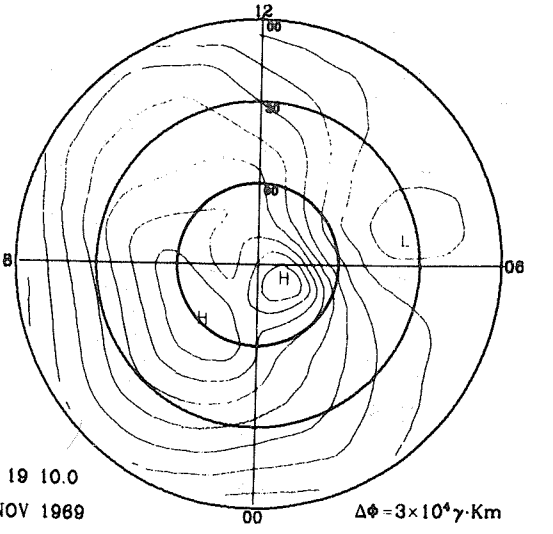
12
00
30
60
18
06
00
L
H
H
UT 19 10.0
9 NOV 1969
ΔΦ=3×10⁴γ·Km

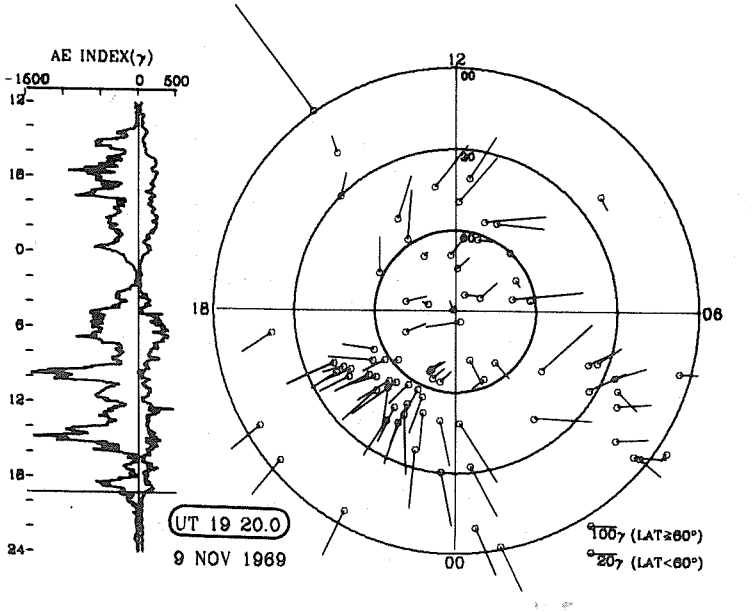
AE INDEX(γ)
-1500
0
500
12
18
0
6
12
18
24
12
00
30
60
18
06
00
UT 19 20.0
9 NOV 1969
100γ (LAT≥60°)
20γ (LAT<60°)

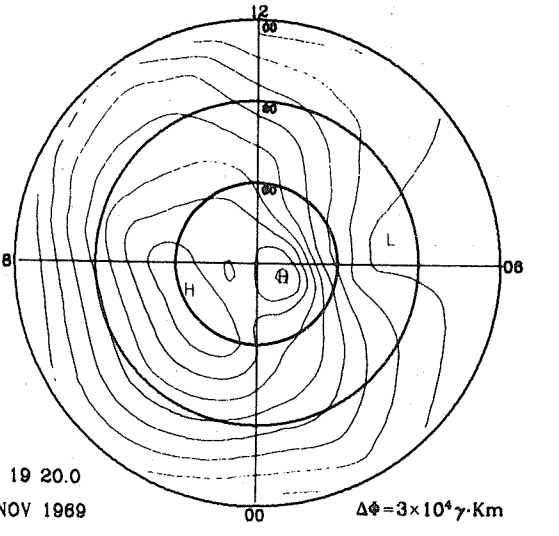
12
00
30
60
18
06
00
L
H
H
UT 19 20.0
9 NOV 1969
ΔΦ=3×10⁴γ·Km

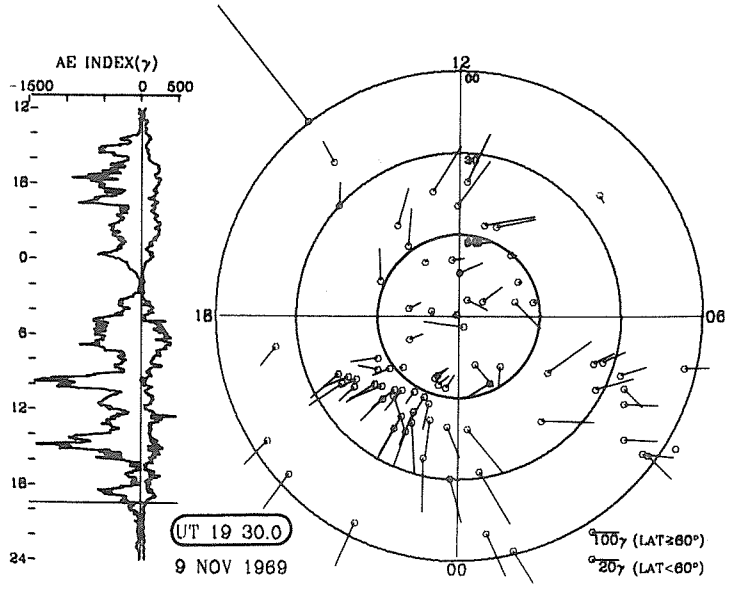
AE INDEX(γ)
-1500
0
500
12
18
0
6
12
18
24
12
00
30
60
18
06
00
UT 19 30.0
9 NOV 1969
100γ (LAT≥60°)
20γ (LAT<60°)

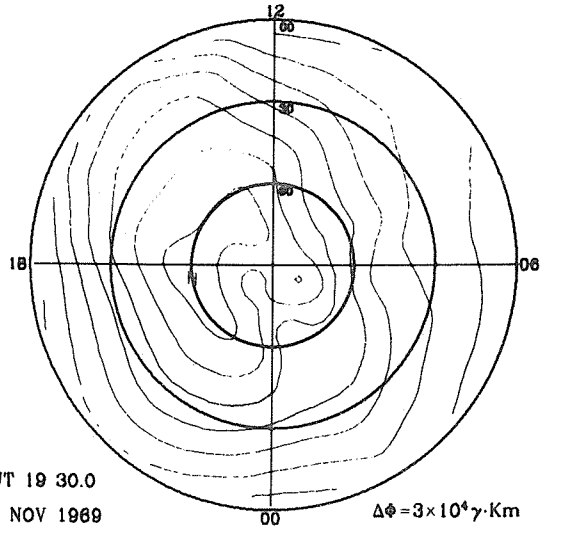
12
00
30
60
18
06
00
H
UT 19 30.0
9 NOV 1969
ΔΦ=3×10⁴γ·Km

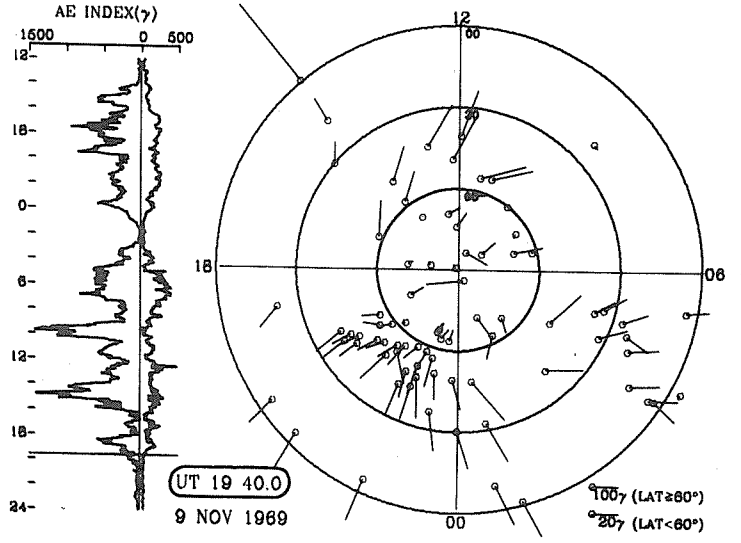
AE INDEX(γ)
-1500
0
500
12
18
0
6
12
18
24
12
00
30
60
18
06
00
UT 19 40.0
9 NOV 1969
100γ (LAT≥60°)
20γ (LAT<60°)

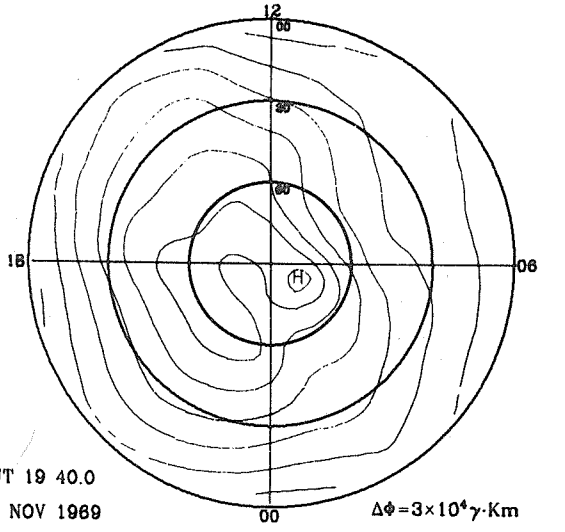
12
00
30
60
18
06
00
H
UT 19 40.0
9 NOV 1969
ΔΦ=3×10⁴γ·Km

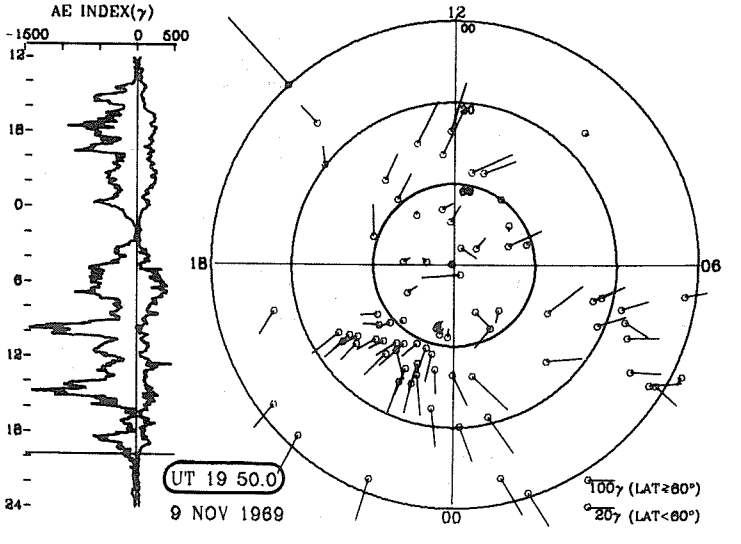
AE INDEX(γ)
-1500
0
500
12
18
0
6
12
18
24
12
00
30
60
18
06
00
UT 19 50.0
9 NOV 1969
100γ (LAT≥60°)
20γ (LAT<60°)

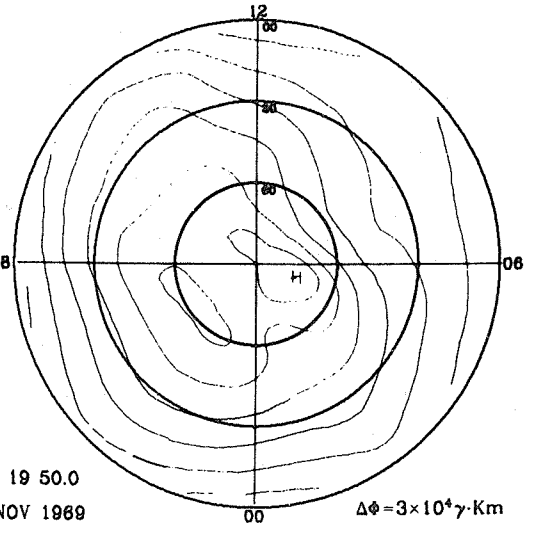
12
00
30
60
18
06
00
H
UT 19 50.0
9 NOV 1969
ΔΦ=3×10⁴γ·Km

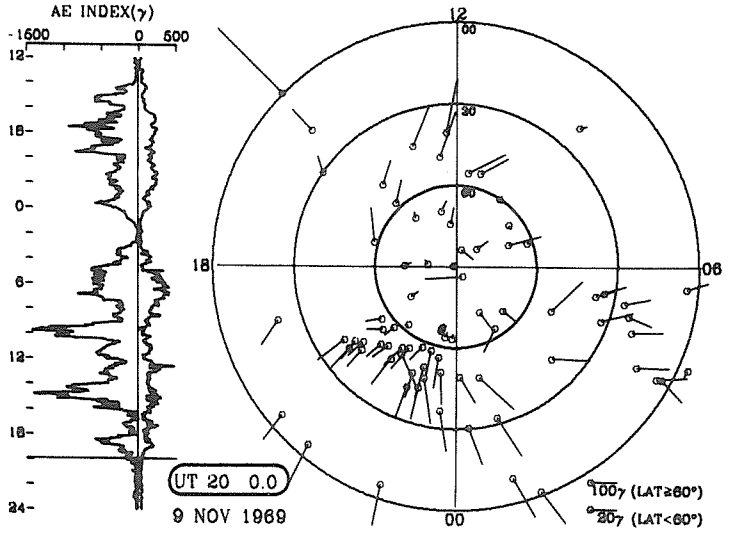
AE INDEX(γ)
-1600
0
500
12
18
0
6
12
18
24
12
00
30
60
18
06
00
UT 20 0.0
9 NOV 1969
100γ (LAT≥60°)
20γ (LAT<60°)

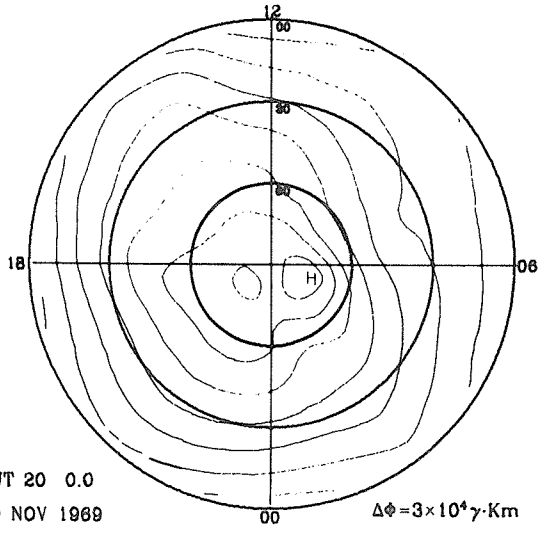
12
00
30
60
18
06
H
00
UT 20 0.0
9 NOV 1969
Δφ=3×10⁴γ·Km

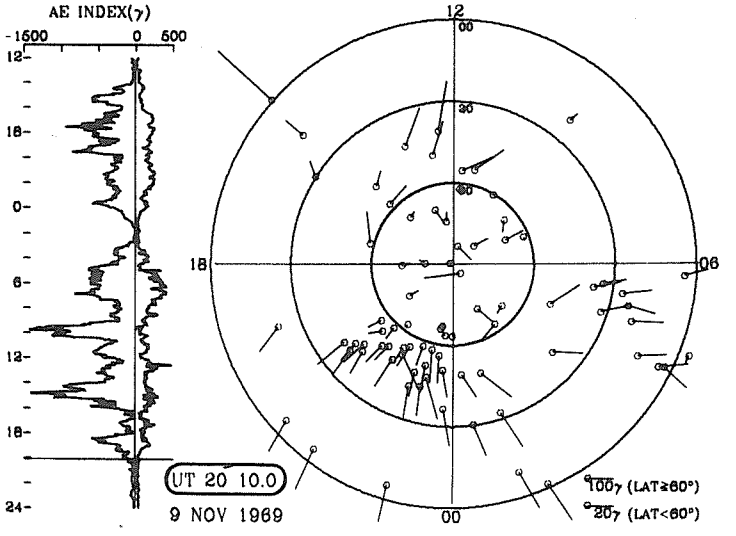
AE INDEX(γ)
-1600
0
500
12
18
0
6
12
18
24
12
00
30
60
18
06
00
UT 20 10.0
9 NOV 1969
100γ (LAT≥60°)
20γ (LAT<60°)

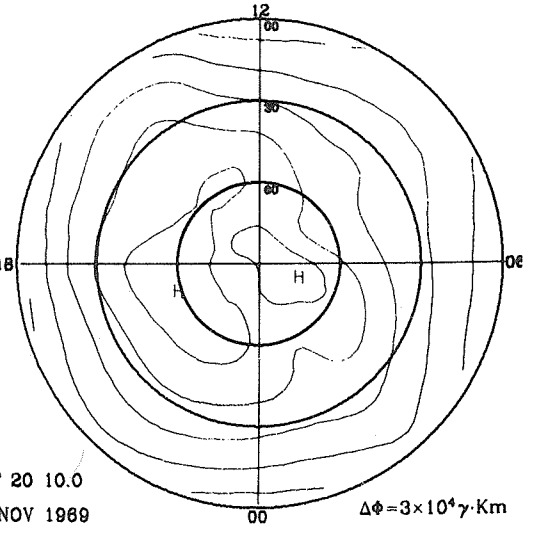
12
00
30
60
18
06
H
H
00
UT 20 10.0
9 NOV 1969
Δφ=3×10⁴γ·Km

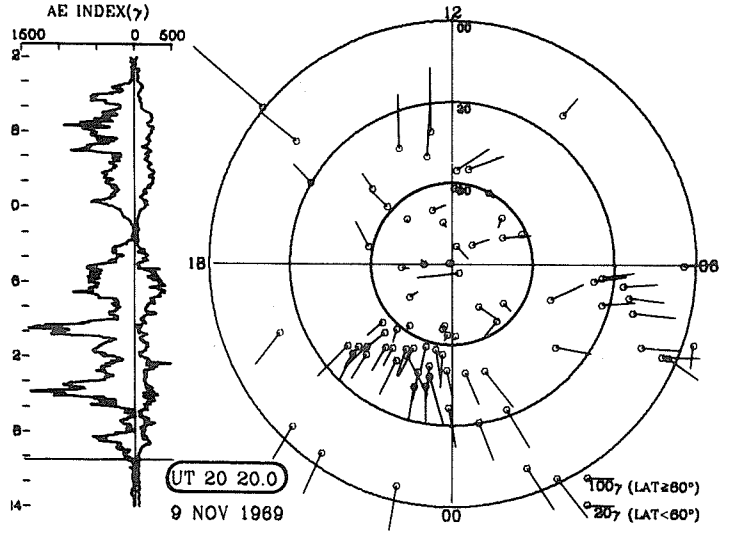
AE INDEX(γ)
1600
0
500
8
0
6
2
8
14
12
00
30
60
18
06
00
UT 20 20.0
9 NOV 1969
100γ (LAT≥60°)
20γ (LAT<60°)

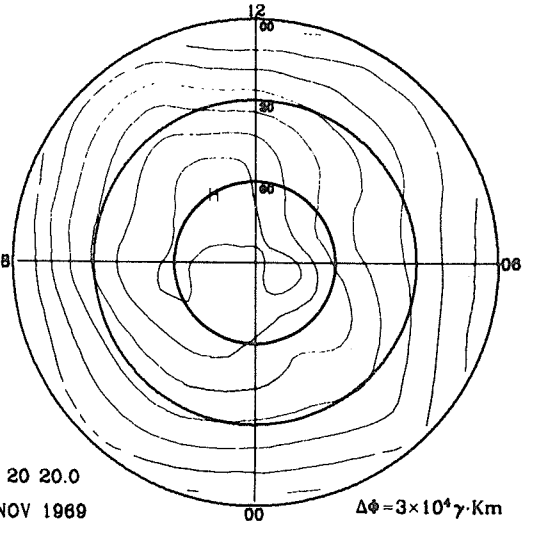
12
00
30
60
18
06
H
00
UT 20 20.0
9 NOV 1969
Δφ=3×10⁴γ·Km

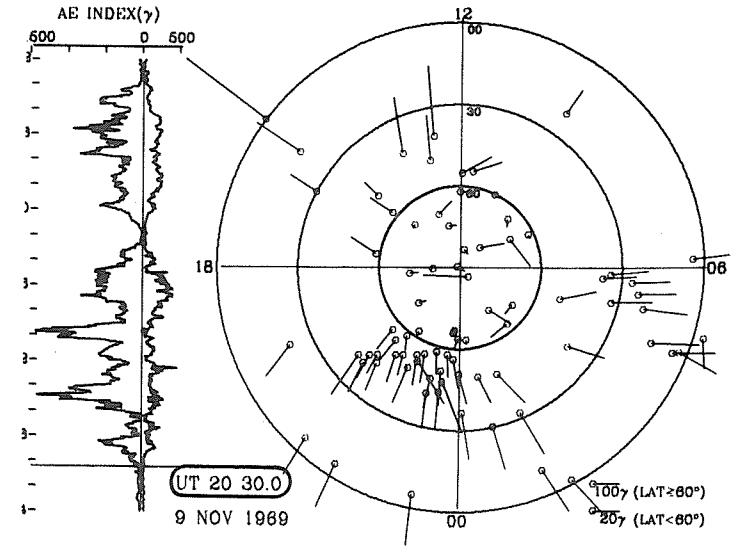
AE INDEX(γ)
600
0
600
12
00
30
60
18
06
00
UT 20 30.0
9 NOV 1969
100γ (LAT≥60°)
20γ (LAT<60°)

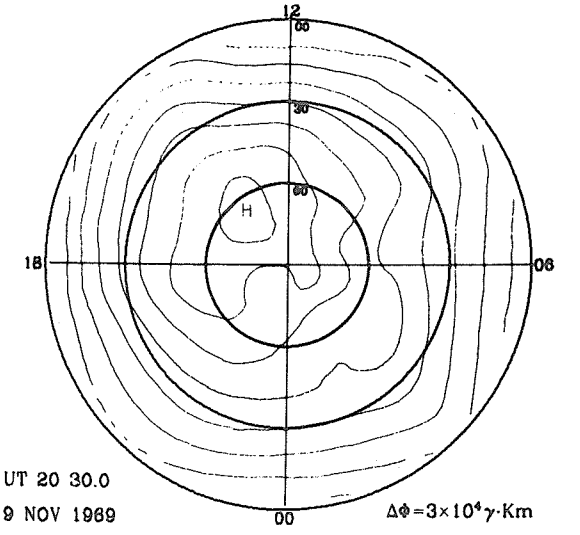
12
00
30
60
H
18
06
00
UT 20 30.0
9 NOV 1969
Δφ=3×10⁴γ·Km

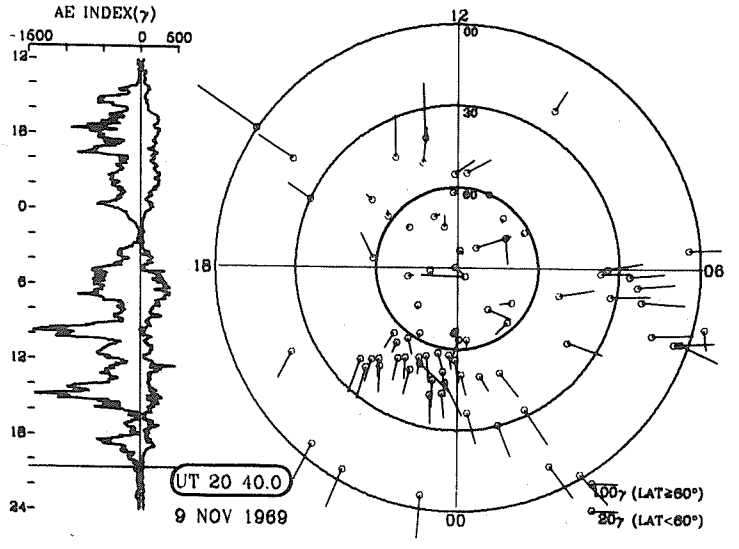
AE INDEX(γ)
1600
0
600
12
18
0
6
12
18
24
12
00
30
60
18
06
00
UT 20 40.0
9 NOV 1969
100γ (LAT≥60°)
20γ (LAT<60°)

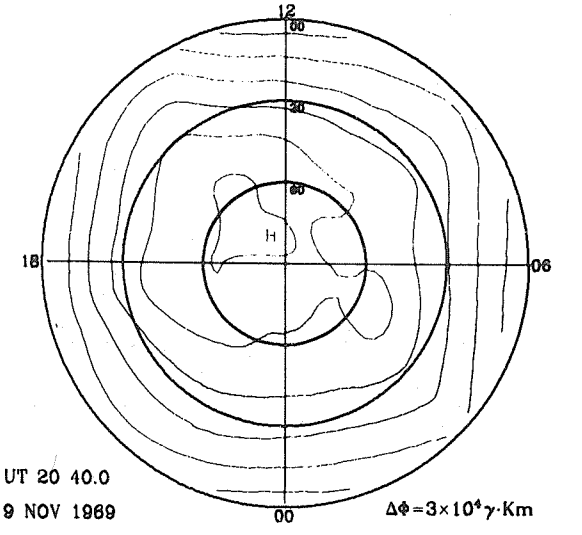
12
00
30
60
H
18
06
00
UT 20 40.0
9 NOV 1969
Δφ=3×10⁴γ·Km

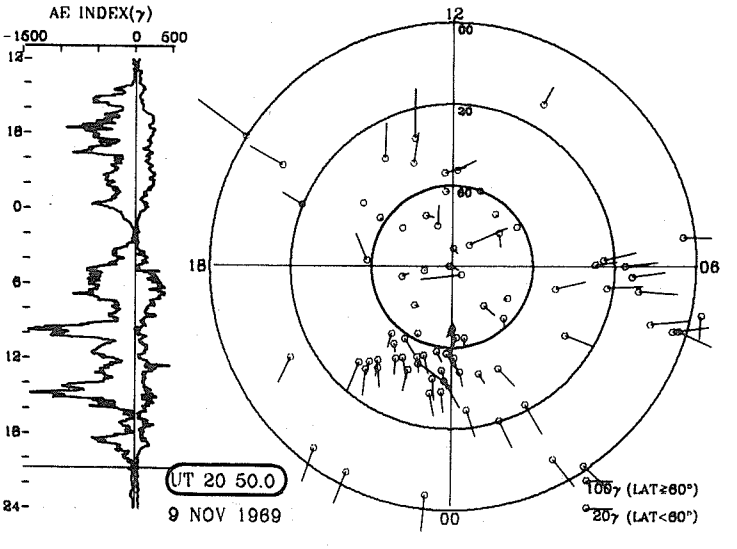
AE INDEX(γ)
1600
0
600
12
18
0
6
12
18
24
12
00
30
60
18
06
00
UT 20 50.0
9 NOV 1969
100γ (LAT≥60°)
20γ (LAT<60°)

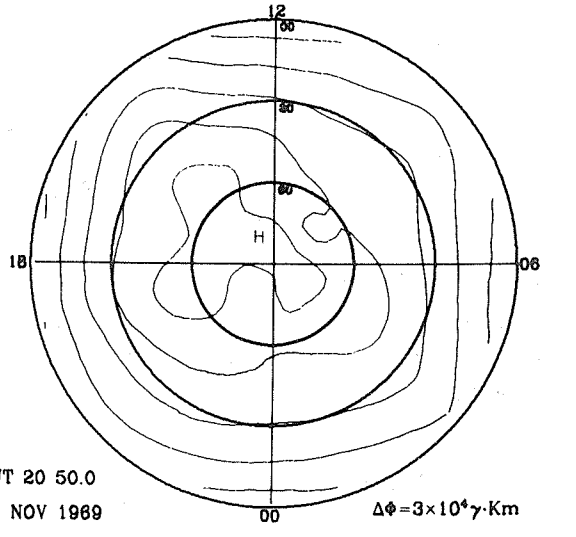
12
00
30
60
H
18
06
00
UT 20 50.0
9 NOV 1969
Δφ=3×10⁴γ·Km

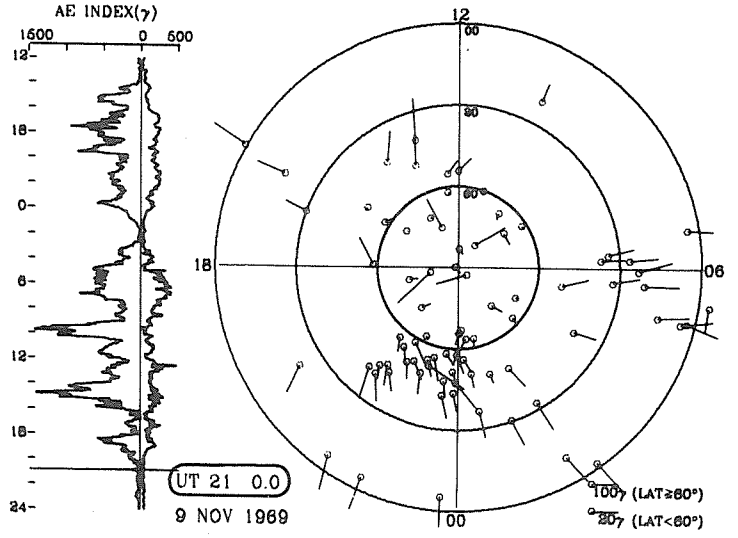
AE INDEX(γ)
1600
0
500
12
18
0
6
12
18
24
UT 21 0.0
9 NOV 1969
12
00
30
60
18
06
00
100γ (LAT≥60°)
20γ (LAT<60°)

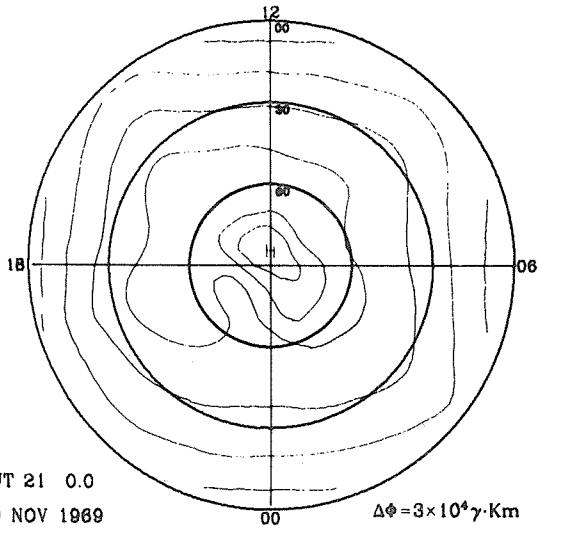
12
00
30
60
18
06
H
00
UT 21 0.0
9 NOV 1969
Δφ=3×10⁴γ·Km

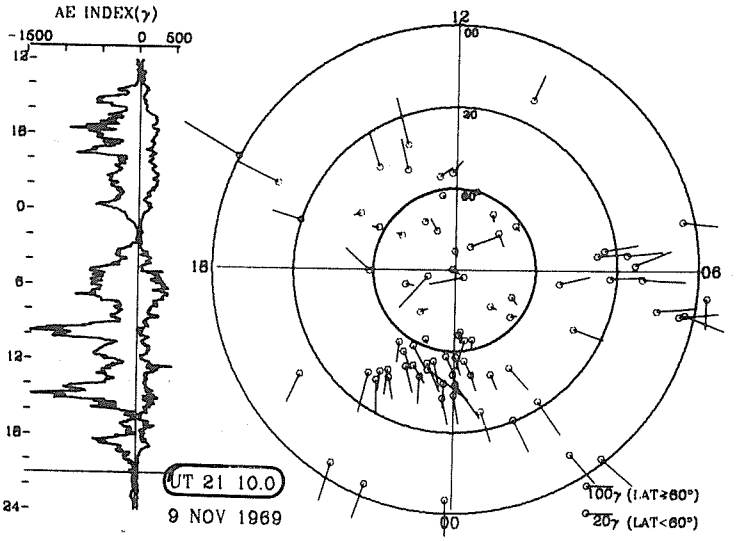
AE INDEX(γ)
-1600
0
500
12
18
0
6
12
18
24
UT 21 10.0
9 NOV 1969
12
00
30
60
18
06
00
100γ (LAT≥60°)
20γ (LAT<60°)

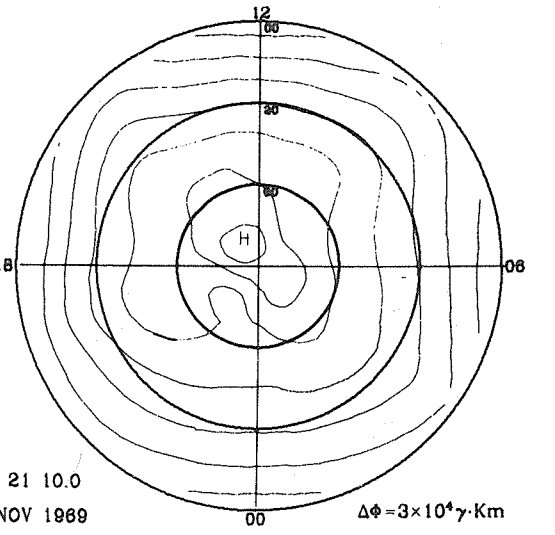
12
00
30
60
18
06
H
00
UT 21 10.0
9 NOV 1969
Δφ=3×10⁴γ·Km

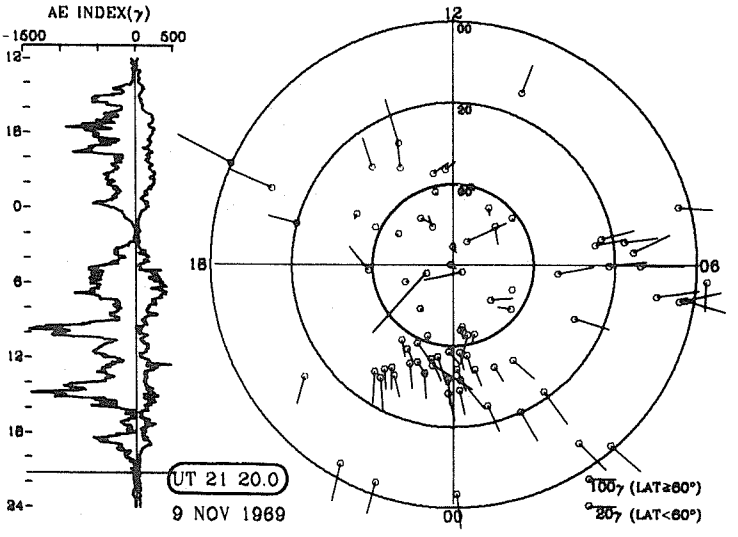
AE INDEX(γ)
-1600
0
500
12
18
0
6
12
18
24
UT 21 20.0
9 NOV 1969
12
00
30
60
18
06
00
100γ (LAT≥60°)
20γ (LAT<60°)

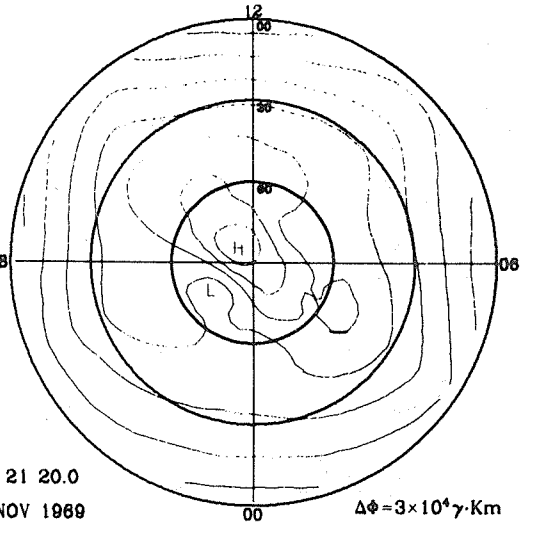
12
00
30
60
18
06
H
L
00
UT 21 20.0
9 NOV 1969
Δφ=3×10⁴γ·Km

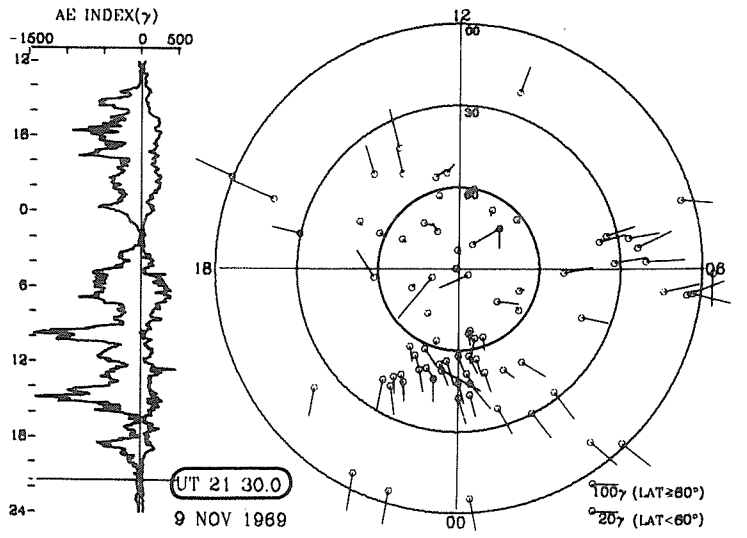
AE INDEX(γ)
-1500
0
500
UT 21 30.0
9 NOV 1969
100γ (LAT≥60°)
20γ (LAT<60°)

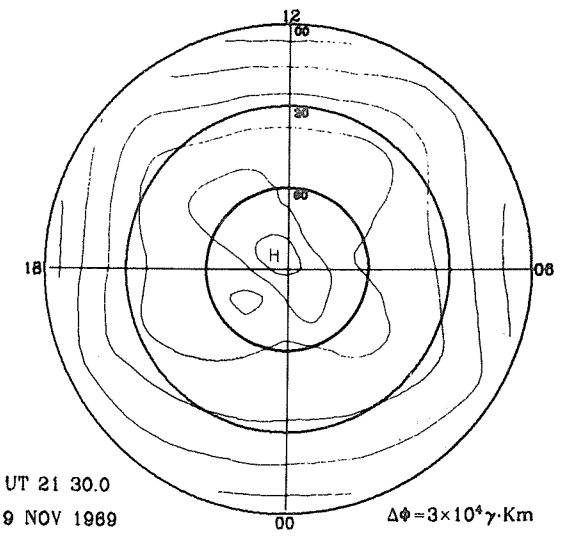
UT 21 30.0
9 NOV 1969
Δφ=3×10⁴γ·Km

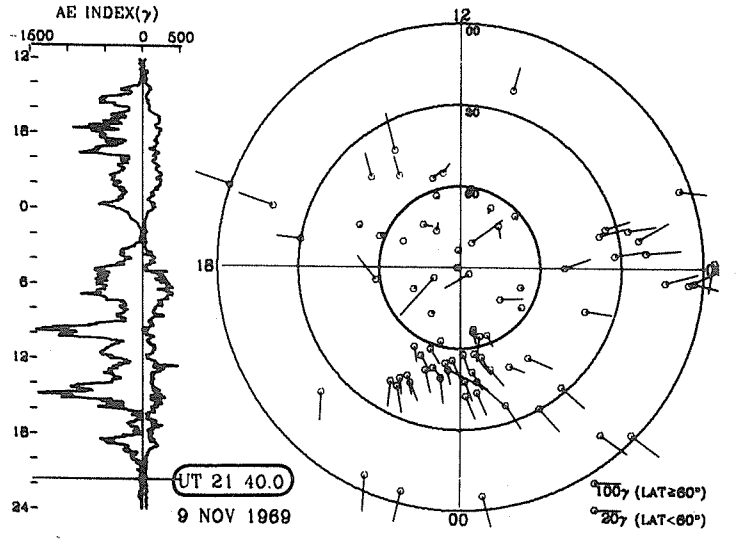
AE INDEX(γ)
-1500
0
500
UT 21 40.0
9 NOV 1969
100γ (LAT≥60°)
20γ (LAT<60°)

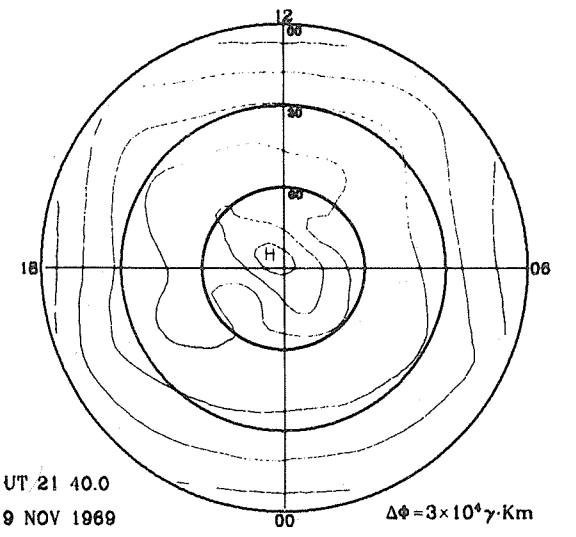
UT 21 40.0
9 NOV 1969
Δφ=3×10⁴γ·Km

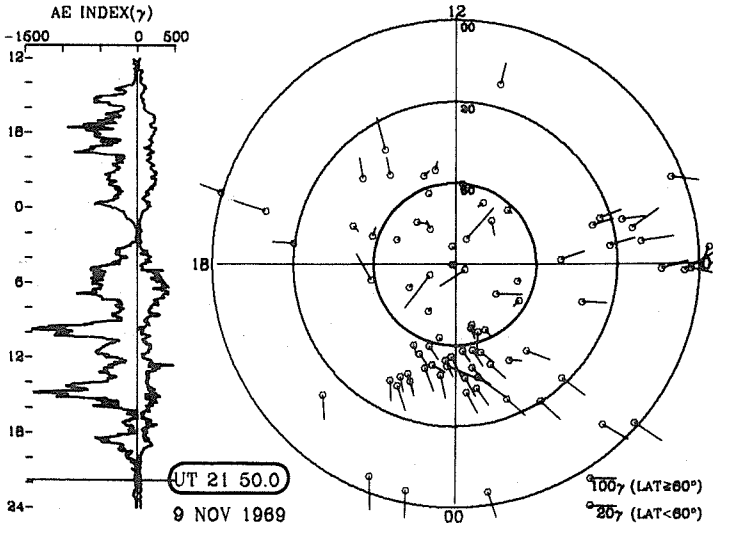
AE INDEX(γ)
-1500
0
500
UT 21 50.0
9 NOV 1969
100γ (LAT≥60°)
20γ (LAT<60°)

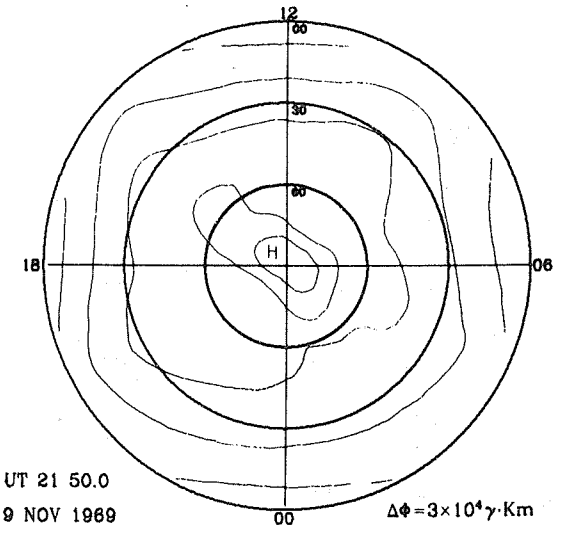
UT 21 50.0
9 NOV 1969
Δφ=3×10⁴γ·Km

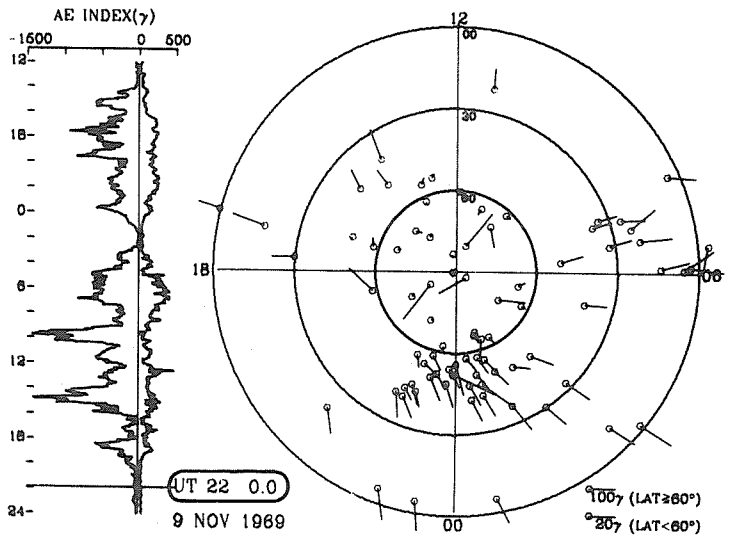
AE INDEX(γ)
-1600
0
500
12
18
0
6
12
18
24
UT 22 0.0
9 NOV 1969
12
00
30
60
18
06
00
100γ (LAT≥60°)
20γ (LAT<60°)

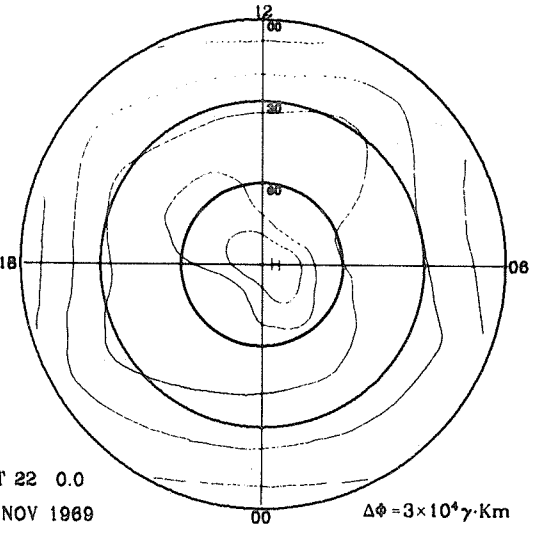
12
00
30
60
18
06
00
UT 22 0.0
9 NOV 1969
ΔΦ=3×10⁴γ·Km

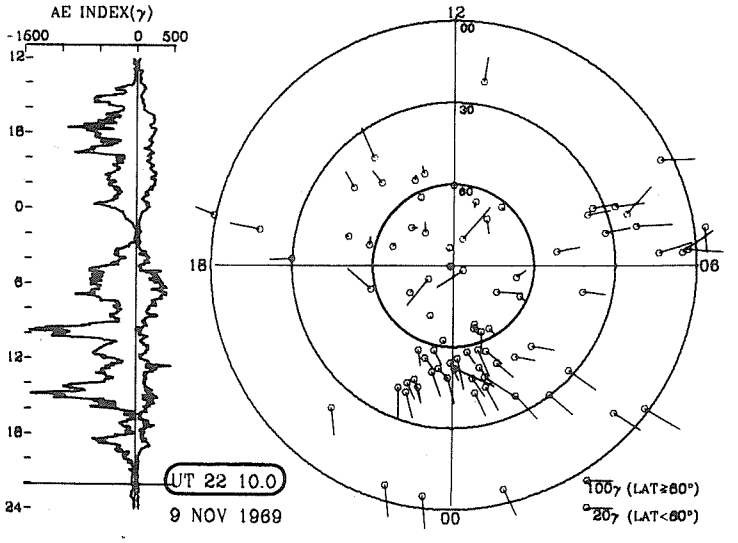
AE INDEX(γ)
-1600
0
500
12
18
0
6
12
18
24
UT 22 10.0
9 NOV 1969
12
00
30
60
18
06
00
100γ (LAT≥60°)
20γ (LAT<60°)

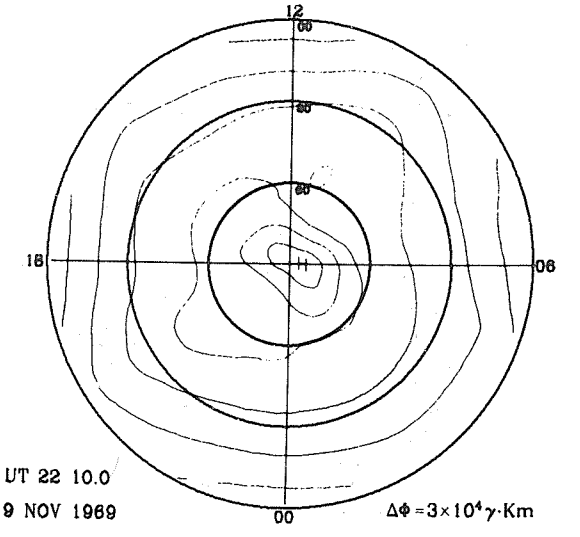
12
00
30
60
18
06
00
UT 22 10.0
9 NOV 1969
ΔΦ=3×10⁴γ·Km

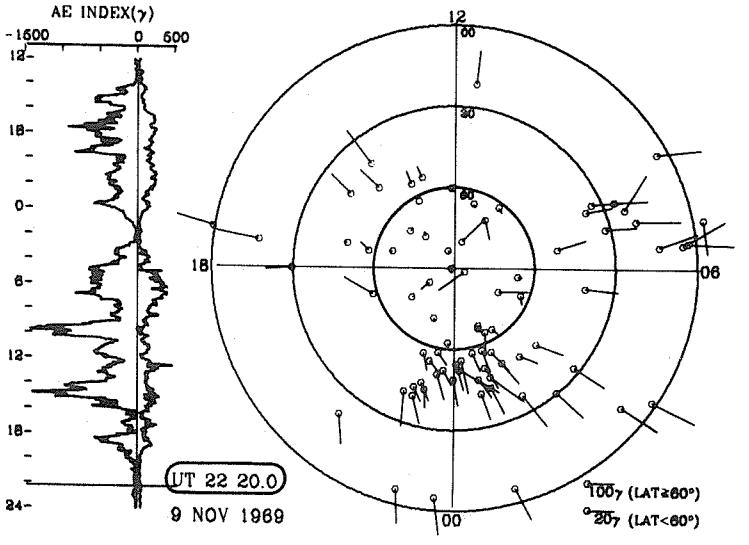
AE INDEX(γ)
-1600
0
500
12
18
0
6
12
18
24
UT 22 20.0
9 NOV 1969
12
00
30
60
18
06
00
100γ (LAT≥60°)
20γ (LAT<60°)

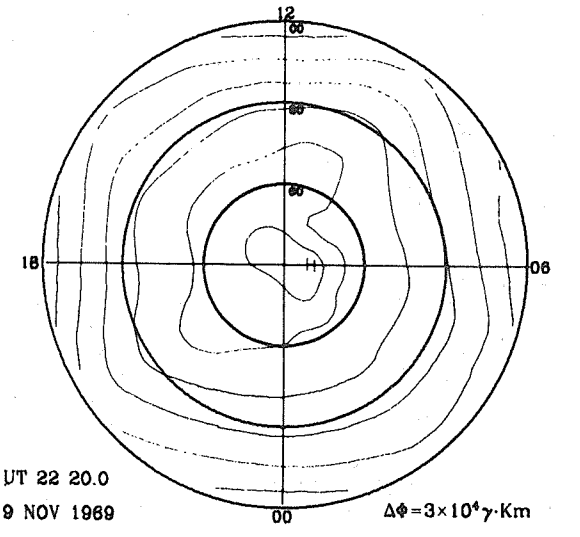
12
00
30
60
18
06
00
UT 22 20.0
9 NOV 1969
ΔΦ=3×10⁴γ·Km

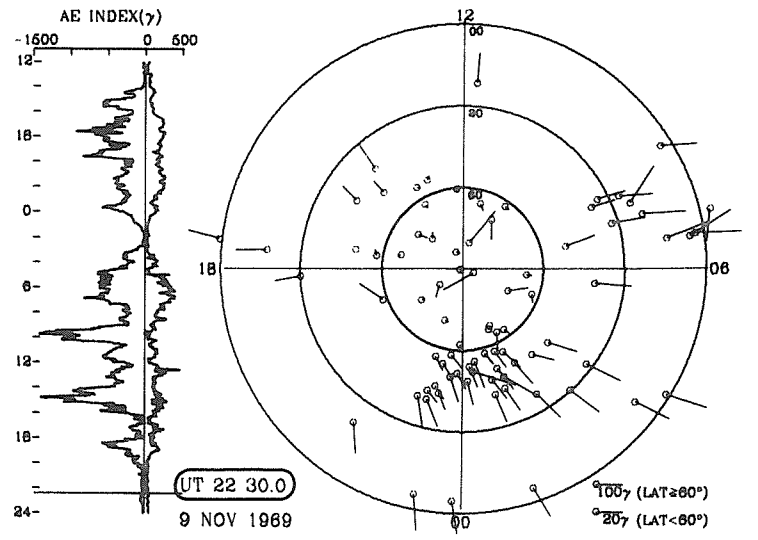
AE INDEX(γ)
-1600
0
500
UT 22 30.0
9 NOV 1969
100γ (LAT≥60°)
20γ (LAT<60°)

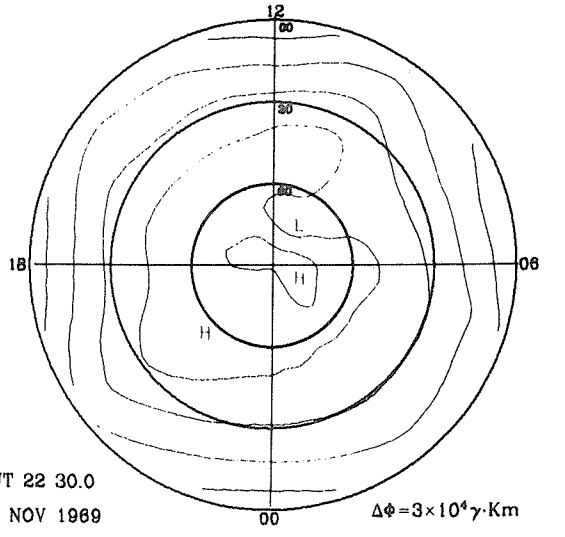
UT 22 30.0
9 NOV 1969
Δφ=3×10⁴γ·Km

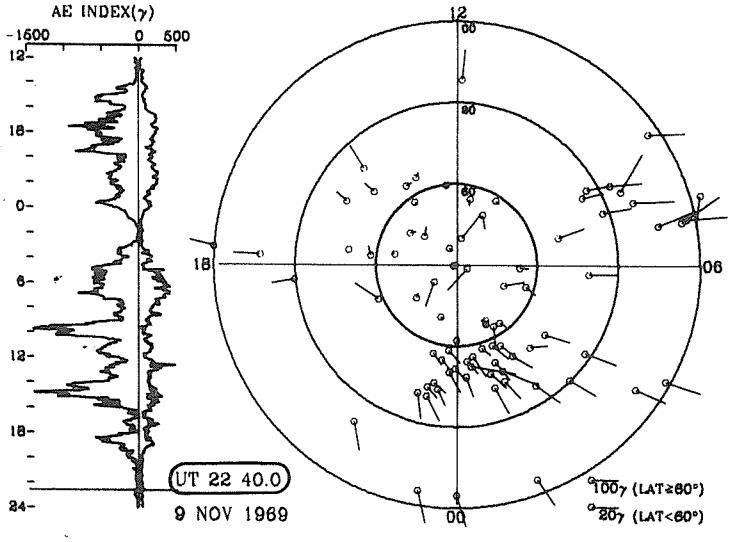
AE INDEX(γ)
-1600
0
500
UT 22 40.0
9 NOV 1969
100γ (LAT≥60°)
20γ (LAT<60°)

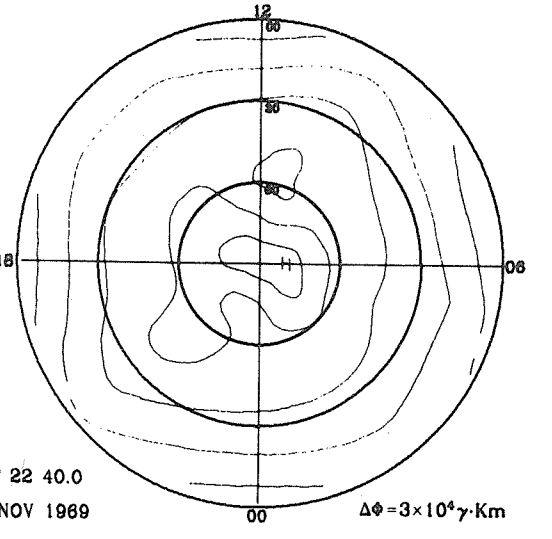
UT 22 40.0
9 NOV 1969
Δφ=3×10⁴γ·Km

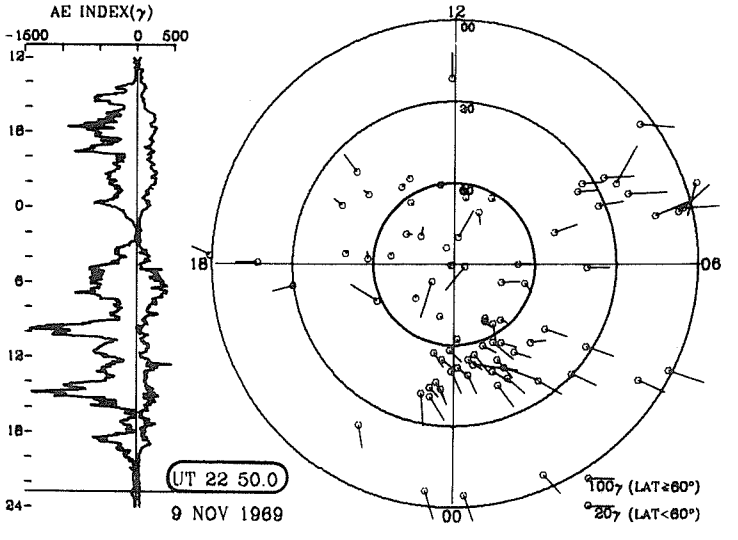
AE INDEX(γ)
-1600
0
500
UT 22 50.0
9 NOV 1969
100γ (LAT≥60°)
20γ (LAT<60°)

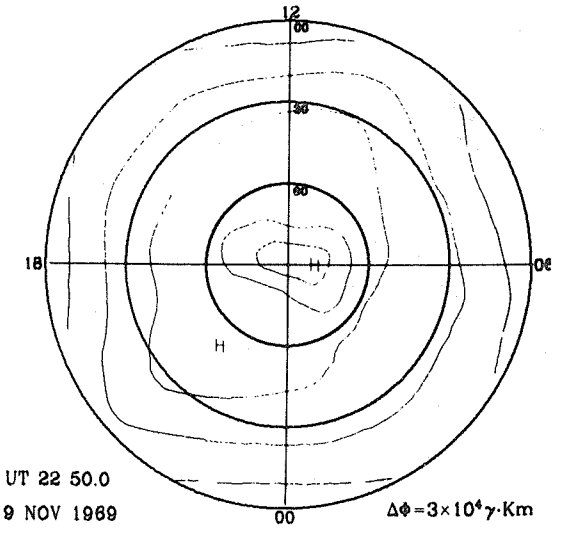
UT 22 50.0
9 NOV 1969
Δφ=3×10⁴γ·Km

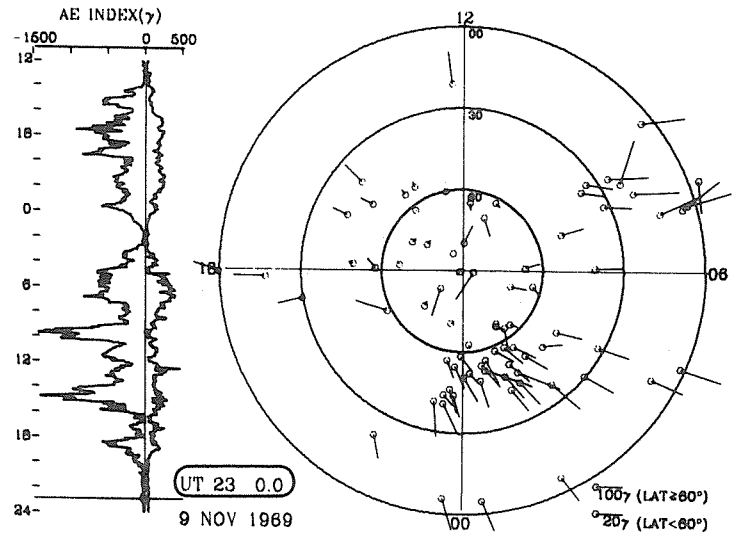
AE INDEX(γ)
-1500
0
500
UT 23 0.0
9 NOV 1969
100γ (LAT≥60°)
20γ (LAT<60°)

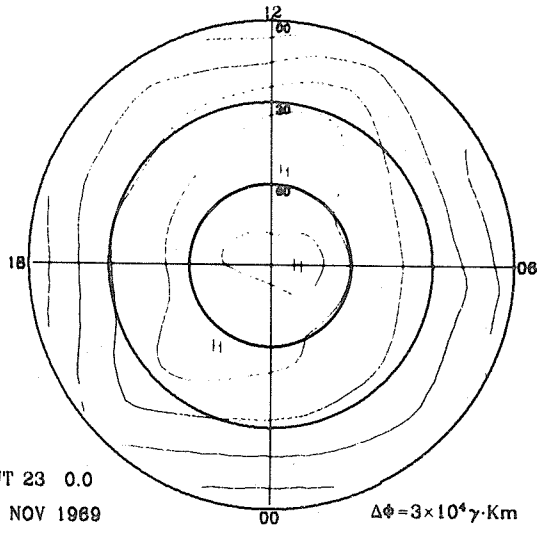
UT 23 0.0
9 NOV 1969
Δφ=3×10⁴γ·Km

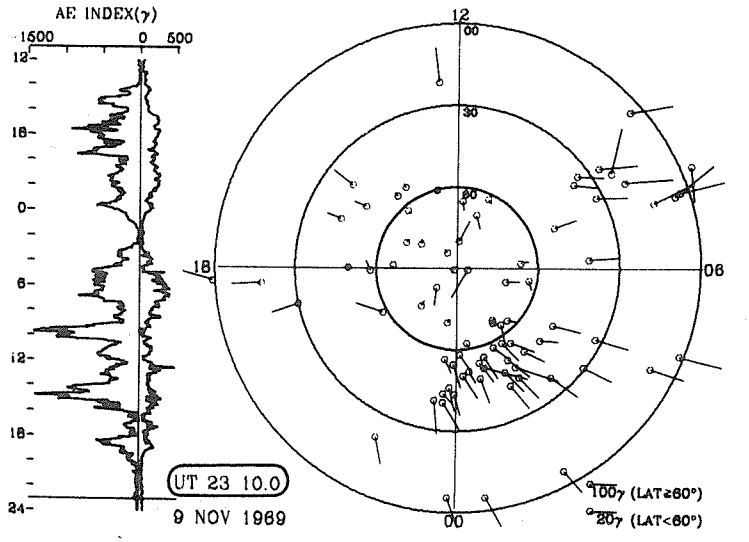
AE INDEX(γ)
-1500
0
500
UT 23 10.0
9 NOV 1969
100γ (LAT≥60°)
20γ (LAT<60°)

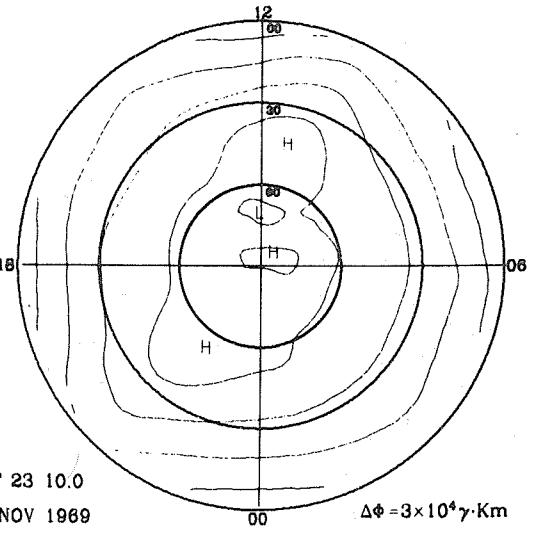
UT 23 10.0
9 NOV 1969
Δφ=3×10⁴γ·Km

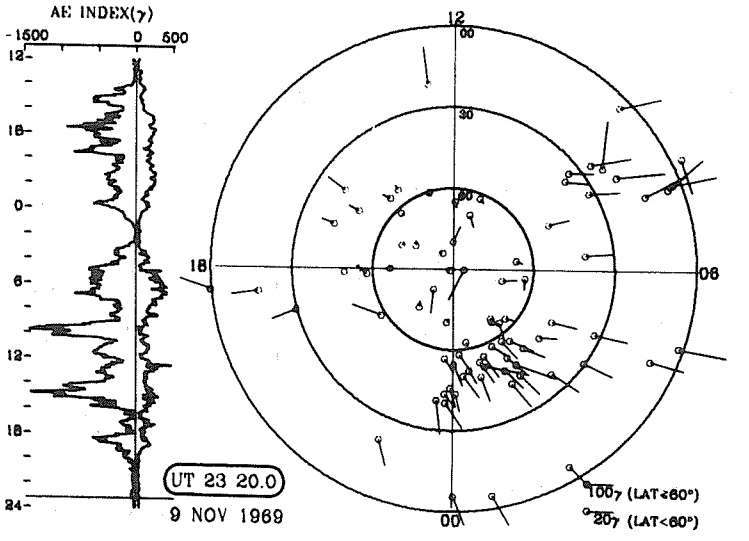
AE INDEX(γ)
-1500
0
500
UT 23 20.0
9 NOV 1969
100γ (LAT≥60°)
20γ (LAT<60°)

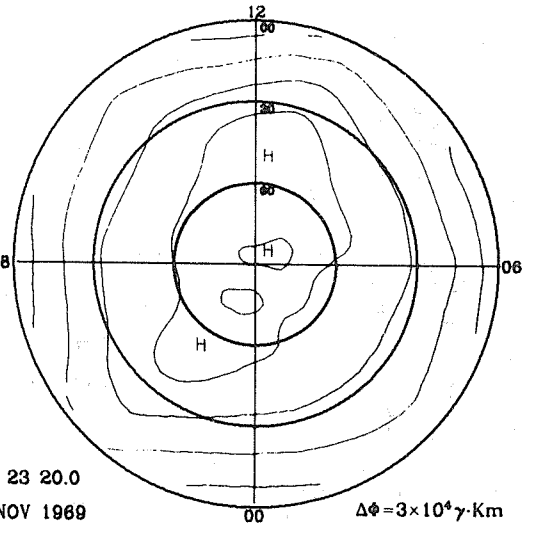
UT 23 20.0
9 NOV 1969
Δφ=3×10⁴γ·Km

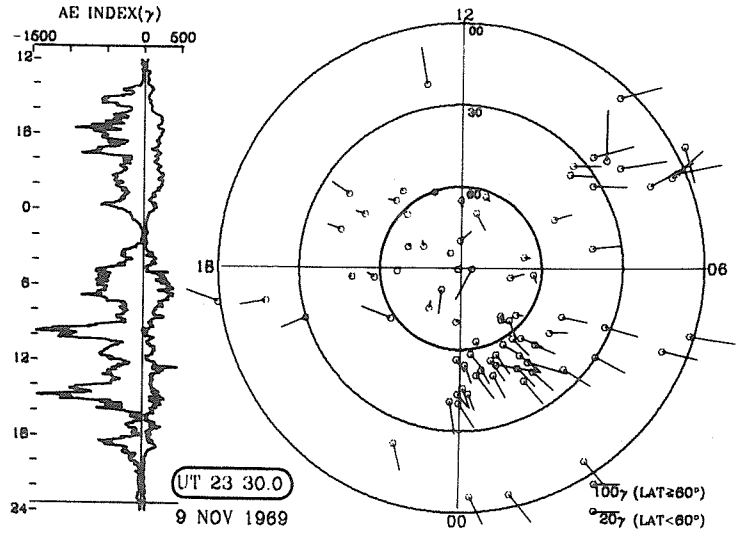
AE INDEX(γ)
-1600
0
500
12
18
0
6
12
18
24
12
00
30
60
18
06
00
UT 23 30.0
9 NOV 1969
100γ (LAT≥60°)
20γ (LAT<60°)

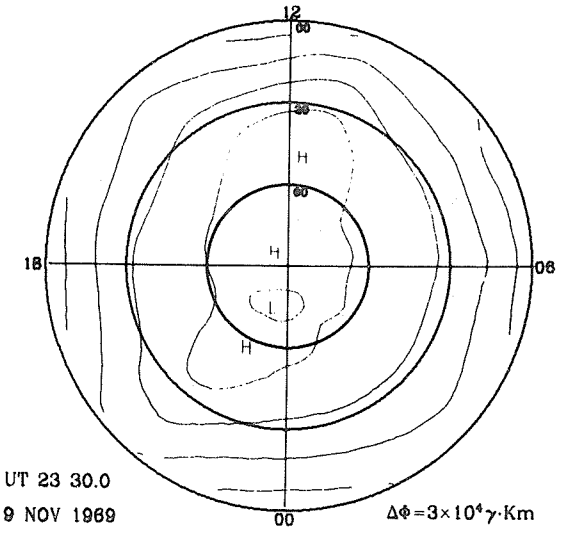
12
00
30
60
H
H
L
H
18
06
00
UT 23 30.0
9 NOV 1969
Δφ=3×10⁴γ·Km

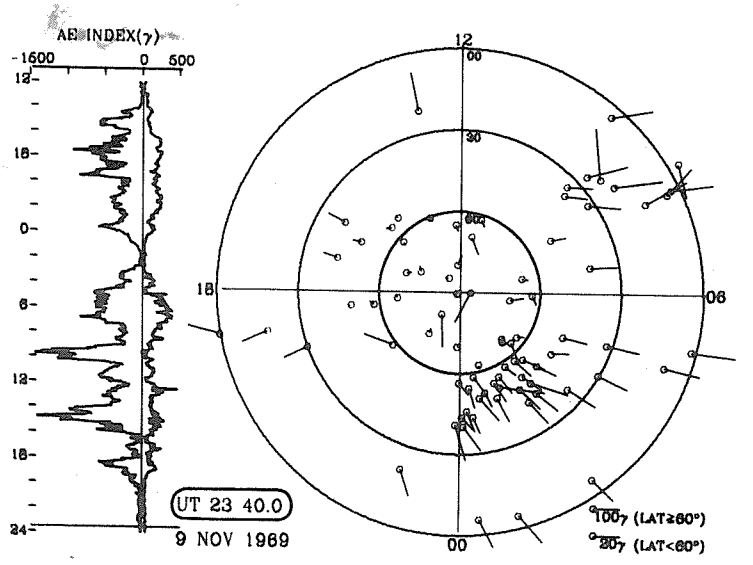
AE INDEX(γ)
-1600
0
500
12
18
0
6
12
18
24
12
00
30
60
18
06
00
UT 23 40.0
9 NOV 1969
100γ (LAT≥60°)
20γ (LAT<60°)

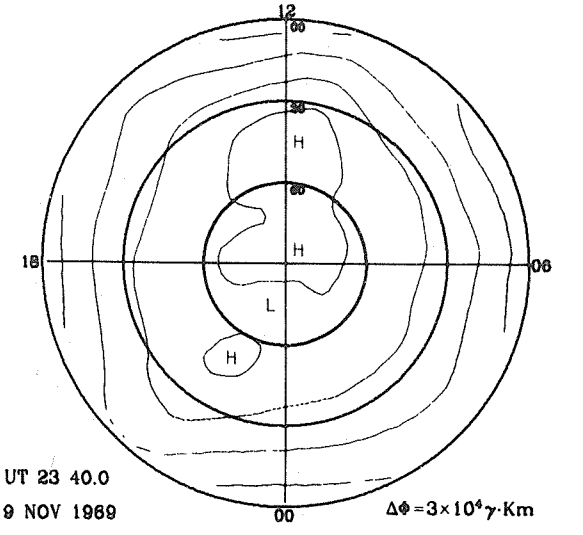
12
00
30
60
H
H
L
H
18
06
00
UT 23 40.0
9 NOV 1969
Δφ=3×10⁴γ·Km

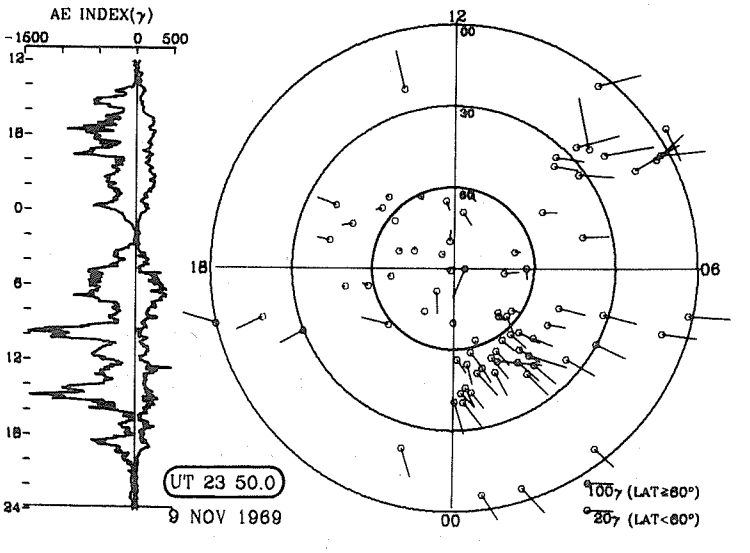
AE INDEX(γ)
-1600
0
500
12
18
0
6
12
18
24
12
00
30
60
18
06
00
UT 23 50.0
9 NOV 1969
100γ (LAT≥60°)
20γ (LAT<60°)

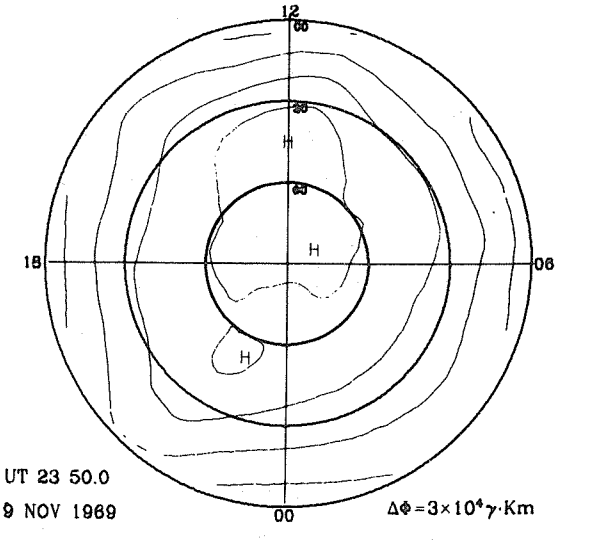
12
00
30
60
H
H
H
18
06
00
UT 23 50.0
9 NOV 1969
Δφ=3×10⁴γ·Km

UAG Series of Reports

Prepared by World Data Center A for Solar-Terrestrial Physics, NOAA, Boulder, Colorado, U.S.A.

These reports are for sale through the National Climatic Center, Federal Building, Asheville, NC 28801, Attn: Publications. Subscription price: $25.20 a year; $12.00 additional for foreign mailing; single copy price varies. These reports are issued on an irregular basis with 6 to 12 reports being issued each year. Therefore, in some years the single copy rate will be less than the subscription price, and in some years the single copy rate will be more than the subscription price. Make check or money order payable to: Department of Commerce, NOAA.

Some issues are now out of print and are available only on microfiche as indicated. Requests for microfiche should be sent to World Data Center A for Solar-Terrestrial Physics, NOAA, Boulder, Co 80302, with check or money order made payable to Department of Commerce, NOAA.

UAG-1 "IQSY Night Airglow Data", price $1.75.
UAG-2 "A Reevaluation of Solar Flares, 1964-1966", price 30 cents.
UAG-3 "Observations of Jupiter's Sporadic Radio Emission in the Range 7.6-41 MHz, 6 July 1966 through 8 September 1968", microfiche only, price 45 cents.
UAG-4 "Abbreviated Calendar Record 1966-1967", price $1.25.
UAG-5 "Data on Solar Event of May 23, 1967 and its Geophysical Effects", price 65 cents.

UAG-6 "International Geophysical Calendars 1957-1969", price 30 cents.
UAG-7 "Observations of the Solar Electron Corona: February 1964-January 1968", price 15 cents.
UAG-8 "Data on Solar-Geophysical Activity October 24-November 6, 1968", price (includes Parts 1 and 2) $1.75.
UAG-9 "Data on Cosmic Ray Event of November 18, 1968 and Associated Phenomena", price 55 cents.
UAG-10 "Atlas of Ionograms", price $1.50.

UAG-11 "Catalogue of Data on Solar-Terrestrial Physics" (now obsolete).
UAG-12 "Solar-Geophysical Activity Associated with the Major Geomagnetic Storm of March 8, 1970", price (includes Parts 1-3) $3.00.
UAG-13 "Data on the Solar Proton Event of November 2, 1969 through the Geomagnetic Storm of November 8-10, 1969", price 50 cents.
UAG-14 "An Experimental, Comprehensive Flare Index and Its Derivation for 'Major' Flares, 1955-1969", price 30 cents.
UAG-15 "Catalogue of Data on Solar-Terrestrial Physics" (now obsolete).

UAG-16 "Temporal Development of the Geographical Distribution of Auroral Absorption for 30 Substorm Events in each of IQSY (1964-65) and IASY (1969)", price 70 cents.
UAG-17 "Ionospheric Drift Velocity Measurements at Jicamarca, Peru (July 1967-March 1970)", microfiche only, price 45 cents.
UAG-18 "A Study of Polar Cap and Auroral Zone Magnetic Variations", price 20 cents.
UAG-19 "Reevaluation of Solar Flares 1967", price 15 cents.
UAG-20 "Catalogue of Data on Solar-Terrestrial Physics" (now obsolete).

UAG-21 "Preliminary Compilation of Data for Retrospective World Interval July 26 - August 14, 1972", price 70 cents.
UAG-22 "Auroral Electrojet Magnetic Activity Indices (AE) for 1970", price 75 cents.
UAG-23 "U.R.S.I. Handbook of Ionogram Interpretation and Reduction", price $1.75.
UAG-24 "Data on Solar-Geophysical Activity Associated with the Major Ground Level Cosmic Ray Events of 24 January and 1 September 1971", price (includes Parts 1 and 2) $2.00.
UAG-25 "Observations of Jupiter's Sporadic Radio Emission in the Range 7.6-41 MHz, 9 September 1968 through 9 December 1971", price 35 cents.

UAG-26 "Data Compilation for the Magnetospherically Quiet Periods February 19-23 and November 29 - December 3, 1970", price 70 cents.
UAG-27 "High Speed Streams in the Solar Wind", price 15 cents.
UAG-28 "Collected Data Reports on August 1972 Solar-Terrestrial Events", price (includes Parts 1-3) $4.50.
UAG-29 "Auroral Electrojet Magnetic Activity Indices AE (11) for 1968", price 75 cents.
UAG-30 "Catalogue of Data on Solar-Terrestrial Physics", price $1.75.

UAG-31 "Auroral Electrojet Magnetic Activity Indices AE (11) for 1969", by Joe Haskell Allen, Carl C. Abston and Leslie D. Morris, National Geophysical and Solar-Terrestrial Data Center, Environmental Data Service, February 1974, 142 pages, price 75 cents.

UAG-32 "Synoptic Radio Maps of the Sun at 3.3 mm for the Years 1967-1969", by Earle B. Mayfield and Kennon P. White III, San Fernando Observatory, Space Physics Laboratory and Fred I. Shimabukuro, Electronics Research Laboratory, Laboratory Operations, The Aerospace Corporation, El Segundo, California, 90245, April 1974, 26 pages, price 35 cents.

UAG-33 "Auroral Electrojet Magnetic Activity Indices AE(10) for 1967", by Joe Haskell Allen, Carl C. Abston and Leslie D. Morris, National Geophysical and Solar-Terrestrial Data Center, Environmental Data Service, May 1974, 142 pages, price 75 cents.

UAG-34 "Absorption Data for the IGY/IGC and IQSY", compiled and edited by A. H. Shapley, National Geophysical and Solar-Terrestrial Data Center, NOAA, Boulder, Colorado, U.S.A., W. R. Piggott, Science Research Council, Slough, U.K., and K. Rawer, Arbeitsgruppe für Physikalische Weltraumforschung, Freiburg, G.F.R., June 1974, 381 pages, price $2.00.

UAG-35 "Catalogue of Digital Geomagnetic Variation Data at World Data Center A for Solar-Terrestrial Physics", prepared by Environmental Data Service, NOAA, Boulder, Colorado, July 1974, 20 pages, price 20 cents.

UAG-36 "An Atlas of Extreme Ultraviolet Flashes of Solar Flares Observed Via Sudden Frequency Deviations During the ATM-SKYLAB Missions", by R. F. Donnelly and E. L. Berger, NOAA Space Environment Laboratory, Lt. J. D. Busman, NOAA Commissioned Corps, B. Henson, NASA Marshall Space Flight Center, T. B. Jones, University of Leicester, UK, G. M. Lerfald, NOAA Wave Propagation Laboratory, K. Najita, University of Hawaii, W. M. Retallack, NOAA Space Environment Laboratory, and W. J. Wagner, Sacramento Peak Observatory, October 1974, 95 pages, price 55 cents.

UAG-37 "Auroral Electrojet Magnetic Activity Indices AE(10) for 1966", by Joe Haskell Allen, Carl C. Abston and Leslie D. Morris, National Geophysical and Solar-Terrestrial Data Center, Environmental Data Service, December 1974, 142 pages, price 75 cents.

UAG-38 "Master Station List for Solar-Terrestrial Physics Data at WDC-A for Solar-Terrestrial Physics", by R. W. Buhmann, World Data Center A for Solar-Terrestrial Physics, Juan D. Roederer, University of Denver, Denver, Colorado, M. A. Shea and D. F. Smart, A.F.C.R.L., Hanscom AFB, Massachusetts, December 1974, 110 pages, price $1.60.

UAG-39 "Auroral Electrojet Magnetic Activity Indices AE(11) for 1971", by Joe Haskell Allen, Carl C. Abston and Leslie D. Morris, National Geophysical and Solar-Terrestrial Data Center, Environmental Data Service, February 1975, 144 pages, price $2.05.

UAG-40 "H-Alpha Synoptic Charts of Solar Activity For the Period of Skylab Observations, May, 1973-March, 1974", by Patrick S. McIntosh, NOAA Environmental Research Laboratory, February 1975, 32 pages, price 56 cents.

UAG-41 "H-Alpha Synoptic Charts of Solar Activity During the First Year of Solar Cycle 20 October, 1964 - August, 1965", by Patrick S. McIntosh, NOAA Environmental Research Laboratory, and Jerome T. Nolte, American Science and Engineering, Cambridge, Massachusetts, March 1975, 25 pages, price 48 cents.

UAG-42 "Observations of Jupiter's Sporadic Radio Emission in the Range 7.6-80 MHz 10 December 1971 through 21 March 1975", by James W. Warwick, George A. Dulk, and Anthony C. Riddle, Department of Astro-Geophysics, University of Colorado, Boulder, Colorado 80302, April 1975, 49 pages, price $1.15.

UAG-43 "Catalog of Observation Times of Ground-Based Skylab-Coordinated Solar Observing Programs", compiled by Helen E. Coffey, World Data Center A for Solar-Terrestrial Physics, May 1975, 159 pages, price $3.00.

UAG-44 "Synoptic Maps of Solar 9.1 cm Microwave Emission from June 1962 to August 1973", by Werner Graf and Ronald N. Bracewell, Radio Astronomy Institute, Stanford University, Stanford, California 94305, May 1975, 183 pages, price $2.55.

UAG-45 "Auroral Electrojet Magnetic Activity Indices AE(11) for 1972", by Joe Haskell Allen, Carl C. Abston and Leslie D. Morris, National Geophysical and Solar-Terrestrial Data Center, Environmental Data Service, May 1975, 144 pages, price $2.10.

UAG-46 "Interplanetary Magnetic Field Data 1963-1974", by Joseph H. King, National Space Science Data Center, NASA Goddard Space Flight Center, Greenbelt, Maryland 20771, June 1975, 382 pages, price $2.95.

UAG-47 "Auroral Electrojet Magnetic Activity Indices AE(11) for 1973", by Joe Haskell Allen, Carl C. Abston and Leslie D. Morris, National Geophysical and Solar-Terrestrial Data Center, Environmental Data Service, June 1975, 144 pages, price $2.10.

UAG-48A "Synoptic Observations of the Solar Corona during Carrington Rotations 1580-1596 (11 October 1971 - 15 January 1973)", [Reissue with quality images] by R. A. Howard, M. J. Koomen, D. J. Michels, R. Tousey, C. R. Detwiler, D. E. Roberts, R. T. Seal and J. D. Whitney, E. O. Hulbert Center for Space Research, NRL, Washington, D. C. 20375 and R. T. and S. F. Hansen, C. J. Garcia and E. Yasukawa, High Altitude Observatory, NCAR, Boulder, Colorado 80303, February 1976, 200 pages.

UAG-49 "Catalog of Standard Geomagnetic Variation Data", prepared by Environmental Data Service, NOAA, Boulder, Colorado, August 1975, 125 pages, price $1.85.

UAG-50 "High-Latitude Supplement to the URSI Handbook on Ionogram Interpretation and Reduction", by W. R. Piggott, British Antarctic Survey, c/o SRC, Appleton Laboratory, Ditton Park, Slough, England, October 1975, 292 pages, price $4.00.

UAG-51 "Synoptic Maps of Solar Coronal Hole Boundaries Derived from He II 304Å Spectroheliograms from the Manned Skylab Missions", by J. D. Bohlin and D. M. Rubenstein, E. O. Hulbert Center for Space Research, Naval Research Laboratory, Washington, D. C. 20375 U.S.A., November 1975, 30 pages, price 54 cents.

UAG-52 "Experimental Comprehensive Solar Flare Indices for Certain Flares, 1970-1974", compiled by Helen W. Dodson and E. Ruth Hedeman, McMath-Hulbert Observatory, The University of Michigan, 895 Lake Angelus Road North, Pontiac, Michigan 48055 U.S.A., November 1975, 27 pages, price 60 cents.

UAG-53 "Description and Catalog of Ionospheric F-Region Data, Jicamarca Radar Observatory (November 1966 - April 1969)", by W. L. Clark and T. E. Van Zandt, Aeronomy Laboratory, NOAA, Boulder, Colorado 80302 and J. P.McClure, University of Texas at Dallas, Dallas, Texas 75230, April 1976, 10 pages.

UAG-54 "Catalog of Ionosphere Vertical Soundings Data", prepared by Environmental Data Service, NOAA, Boulder, Colorado 80302, April 1976, 130 pages.

UAG-55 "Equivalent Ionospheric Current Representations by a New Method, Illustrated for 8-9 November 1969 Magnetic Disturbances", by Y. Kamide, Cooperative Institute for Research in Environmental Sciences, University of Colorado, Boulder, Colorado 80302 and Geophysical Institute, University of Alaska, Fairbanks, Alaska 99701, H. W. Kroehl, Data Studies Division, NOAA/EDS/NGSDC, Boulder, Colorado 80302, M. Kanamitsu, Advanced Study Program, National Center for Atmospheric Research, Boulder, Colorado 80303, J. H. Allen, Data Studies Division, NOAA/EDS/NGSDC, Boulder, Colorado 80302, and S.-I. Akasofu, Geophysical Institute, University of Alaska, Fairbanks, Alaska 99701, April 1976, 91 pages.

UAG-56 "Iso-intensity Contours of Ground Magnetic H Perturbations for the December 16-18, 1971 Geomagnetic Storm", by Y. Kamide, Cooperative Institute for Research in Environmental Sciences, University of Colorado, Boulder, Colorado 80302 and Geophysical Institute, University of Alaska, Fairbanks, Alaska 99701 (currently Guest worker at Data Studies Division, NOAA/EDS/NGSDC, Boulder, Colorado 80302), April 1976, 37 pages.

USCOMM-NOAA-ASHEVILLE--5-7-76--1150